

Measurement of $\psi(2S)$ production cross-sections in proton-proton collisions at $\sqrt{s} = 7$ and 13 TeV

Jibo He¹, Pei-Rong Li^{1,3}, Xiao-Rui Lyu¹, Wenbin Qian¹, Miroslav Saur¹, Dan Wang¹, Yangheng Zheng¹

Yuanning Gao², Yunlong Li², Zhenwei Yang², Shunan Zhang², Mingrui Zhao²

¹ University of Chinese Academy of Sciences, Beijing, China

² Tsinghua University, Beijing, China

³ Lanzhou University, Lanzhou, China

Abstract

Using a data sample with an integrated luminosity of 275 pb^{-1} collected by the LHCb detector in the LHC operations in 2015, production cross-sections of $\psi(2S)$ mesons in proton-proton collisions at a centre-of-mass energy $\sqrt{s} = 13 \text{ TeV}$ are measured. The double differential cross-sections for prompt $\psi(2S)$ mesons and $\psi(2S)$ mesons from b -hadron decays are determined as functions of the transverse momentum p_T and the rapidity y of the $\psi(2S)$ meson in the kinematic range $2 < p_T < 20 \text{ GeV}/c$ and $2.0 < y < 4.5$. The production cross-sections integrated over the kinematic coverage are

$$\sigma_p = 1.430 \pm 0.005 \text{ (stat)} \pm 0.099 \text{ (syst)} \mu\text{b}$$

for prompt $\psi(2S)$ mesons, and

$$\sigma_b = 0.426 \pm 0.002 \text{ (stat)} \pm 0.030 \text{ (syst)} \mu\text{b}$$

for $\psi(2S)$ mesons from secondary b -hadron weak decays. All results show reasonable agreement with theoretical calculations.

Contents

1	Introduction	4
2	Data and Monte Carlo samples	5
2.1	Data	5
2.2	Monte Carlo	6
2.3	The TISTOS issue	6
3	Candidate reconstruction and selection	6
3.1	Trigger and Turbo stream selection	6
3.2	Offline selection	7
4	Cross-section determination	8
5	Signal extraction	9
5.1	Determination of the prompt and detached signal yields	9
6	Efficiency determination	12
6.1	Geometrical acceptance	13
6.2	Reconstruction-selection efficiency	13
6.3	Muon identification efficiency	15
6.4	Trigger efficiency	16
6.5	Total efficiency	17
7	Systematic uncertainties	19
7.1	Signal extraction	19
7.1.1	Signal mass shape	19
7.1.2	Fit to t_z	19
7.2	Global event cuts	20
7.3	Trigger efficiency	21
7.4	Tracking efficiency	21
7.5	Offline selection efficiency of $\psi(2S)$ vertex fit	22
7.6	MuonID efficiency	22
7.7	p_T - y -spectrum	24
7.8	Polarization scenarios	25
7.9	Other systematic uncertainties	26
7.10	Summary of systematic uncertainties	26
8	Results	28
8.1	Fraction of $\psi(2S)$ -from- b	28
8.2	Comparison with theoretical models	30
8.3	Cross-section ratios between 13 TeV and 7 TeV	30
8.4	Calculations of the ratios of the $\psi(2S)$ and J/ψ cross-sections at 13 TeV	36
8.5	Measurement of the inclusive branching fraction $\mathcal{B}(b \rightarrow \psi(2S)X)$	38
8.6	Comparison with polarised results at 13 TeV	40
9	Conclusion	42

A	Tables of cross section results	43
B	Tables of the fit results in each kinematic bin	48
C	Efficiency tables	59
D	Fitting plots in each kinematic bin	66
E	$\psi(2S)$ production cross-section measurement at 7 TeV with 2011 data.	95
E.1	Data and Monte Carlo samples	95
E.2	Trigger	95
E.3	Offline selection	95
E.4	Signal extraction	96
E.5	Efficiencies	97
E.6	Summary of systematic uncertainties	99
E.7	Tables of cross-section results	101
E.8	Fraction of $\psi(2S)$ -from- b mesons	101
E.9	Systematic uncertainties between $\psi(2S)$ and J/ψ at 7 TeV	102
E.10	Measurement of the $\mathcal{B}(b \rightarrow \psi(2S)X)$ at 7 TeV	102
E.11	Comparison with polarised results at 7 TeV	103
F	Checks and comparisons with the 2010 results	110
G	Checks and corrections done for 2010 erratum	116
References		121

¹ Preface

² Version v4.4

³ Added new section G about checks and studies done in order to provide an erratum for
⁴ the published paper based on 2010 data.

⁵ Version v4.3

⁶ Added new section F about discrepancies between 2010 and 2011 data.

⁷ Version v4.2

⁸ Added new subsection 8.5 about computation of $\mathcal{B}(b \rightarrow \psi(2S)X)$. Old measurement of
⁹ total $b\bar{b}$ production cross-section is now excluded, as it isn't a part of paper anymore.

¹⁰ Version v4.1

¹¹ Fixed some typo. Add more details of 7TeV results.

¹² Version v4.0

¹³ In this version, we include the measurement of $\psi(2S)$ production cross-sections at 7 TeV
¹⁴ using the 2011 data sample, and the results are used to calculate the cross-section ratios
¹⁵ between 13 TeV and 7 TeV. In the comparison with the new measurement at 7 TeV, the
¹⁶ cancellation of the systematic uncertainties can be treated in a better way than what we
¹⁷ could do before. In addition, we can provide the ratio as a function of rapidity.

¹⁸ Since the selection $DLLmu > 2$ was applied in the stripping line for both the 7 TeV
¹⁹ sample, we replaced the original PID selection based on ProbNN in the 13 TeV analysis
²⁰ by this one. The results with these two different PID selections are consistent with each
²¹ other.

²² Version v3.2

²³ Theoretical calculation for ratios are add to compare with experimental measurement.

²⁴ Version v3.1

²⁵ We consider the suggestion from Matteo for some detailed sentence description.

²⁶ Version v3.0

²⁷ In this version note, we consider the suggestion from Liupan and Matteo. The efficiency
²⁸ for prompt $\psi(2S)$ and $\psi(2S)$ -from- b are updated using corresponding MC type instead of
²⁹ use one whole MC samples. Besides, the $b\bar{b}$ cross section in 4π region is provide.

³⁰ **Version v2.1**

³¹ In this version note, ratio with J/ψ at 13 TeV as function of y is added. The comparison
³² with NRQCD calculations are added. Beside, we also consider the suggestion from Liupan
³³ and Matteo.

³⁴ **Version v2.0**

³⁵ In this version note, we checked the efficiency consistency between “read from turbo line”
³⁶ and “combined from stand particle offline”. During this process, we found the mass window
³⁷ of $\psi(2S)$ [$(3566,3806) \text{ MeV}/c^2$] is necessary for MC sample. Then all the efficiency are
³⁸ renewed with the mass window requirement. And also there are some other updates are
³⁹ included, shown below. Consider all the comments above, the whole analysis is updated.

- ⁴⁰ 1. As suggested by Patrick and Andrii, p_T and y -dependent fractions of $\psi(2S)$ from b ,
⁴¹ F_b are added.
- ⁴² 2. Cross-section ratio between $\psi(2S)$ at 13TeV and 7TeV are added.
- ⁴³ 3. Cross-section ratio between $\psi(2S)$ and J/ψ at 13TeV are added.

⁴⁴ **Version v1.1**

⁴⁵ This version note is updated for new $\psi(2S)$ p_T range. As suggested by Vanya, the p_T is
⁴⁶ covered to $20 \text{ GeV}/c$. All the efficiencies and systematics are updated. For the results in
⁴⁷ all kinematic region, we correct the wrong result before(forget to multiply bin size of y).
⁴⁸ Besides, comparison with theoretical calculations are added.

⁴⁹ **Version v1.0**

⁵⁰ This version note is updated with new version MC sample(sim09b). All the efficiencies
⁵¹ and systematics are updated. And also there are some updates are included.

- ⁵² 1. Some sentences are changed according to Lucio’s and Sebastian’s comments.
- ⁵³ 2. For the systematic uncertainty which we referred J/ψ paper are finished based on
⁵⁴ our analysis.
- ⁵⁵ 3. More information is added in the Appendix.
- ⁵⁶ 4. The tracking MC/data correction table is updated using the one developed for
⁵⁷ sim09b version.
- ⁵⁸ 5. The PID efficiency table is updated as the binning scheme is not very appropriate.
- ⁵⁹ 6. For the production cross-section integrated over the kinematic coverage, we considered
⁶⁰ the correlation of different bin now.
- ⁶¹ 7. Comparison with theoretical calculations need to be updated in the future version.

62 Version v0.1

63 This is the first version of the analysis note based on sim09a MC sample. We use this
64 version to ask convener first check on analysis strategy.

65 1 Introduction

66 Study of heavy quarkonium production in proton-proton(pp) collisions is a subject of
67 interest and debate, which could provide important information to probe quantum chromo-
68 dynamics (QCD). The heavy quarkonium production involves the production of a heavy
69 quark pair, $Q\bar{Q}$, and the followed hadronization of the $Q\bar{Q}$ pair into the heavy quarkonium.
70 The first step can be calculated with perturbative QCD, while the latter is nonperturbative
71 and must be determined using experimental results as inputs. The physics process of
72 heavy quarkonium production probes both perturbative and non-perturbative energy
73 regions of QCD, which is helpful to test QCD models and to improve our understanding
74 of strong interactions. The Colour Singlet Model (CSM) calculations [1–7] require the
75 intermediate $Q\bar{Q}$ state is colourless and has the same J^{PC} quantum numbers as the final
76 state quarkonium. While in the nonrelativistic QCD (NRQCD) approach [8–10], interme-
77 diate $Q\bar{Q}$ states with all possible colour-spin-parity quantum numbers have probabilities
78 to transform into the desired quarkonium. The transition probabilities, described by
79 long distance matrix elements (LDME) in NRQCD, are nonperturbative and must be
80 determined by fitting experimental data. These matrix elements are supposed to be
81 universal, and their relative strength is ordered in powers of the velocity of heavy quarks,
82 v , in the rest frame of the heavy quarkonium. For perturbative expansions, only a few
83 matrix elements need to be taken into account for $\psi(2S)$ hadronic production, and the
84 NRQCD coincides with CSM when only the leading v term is considered.

85 The CSM calculation at the leading order (LO) underestimates the J/ψ and $\psi(2S)$
86 production cross-sections by more than one order of magnitude in the range of transverse
87 momentum (p_T) higher than the masses of the charmonia [11]. The correction at the
88 next-to-leading order (NLO) for the CSM changes the p_T behaviour at high p_T [12, 13],
89 and reduces the gap between predictions and experimental data significantly but still not
90 satisfactory. The NLO and the next-to-next-to-leading-order (NNLO) terms in the CSM
91 yielded predictions in better agreement with experimental data, which resurrected interest
92 for the colour-singlet framework. Besides, the predicted J/ψ polarisation changes from
93 transverse dominating at the LO to significantly longitudinal [14].

94 NRQCD, with the matrix elements determined by fitting the CDF data, can describe
95 the p_T -dependent J/ψ cross-section at CDF [15, 16]. These matrix elements can also well
96 describe the magnitude and the p_T dependence of quarkonium cross-sections measured
97 at the LHC [17–19], confirming the universality of these matrix elements. Despite the
98 success of NRQCD in describing quarkonium hadronic production cross-sections, the
99 predicted large transverse polarisation at high p_T [20–23] is not supported by experimental
100 results [24–30]. In one word, neither CSM nor NRQCD can model the polarisation
101 satisfactorily.

102 In high-energy proton-proton (pp) collisions, most charmonium states can be produced
103 1) directly from hard collisions of partons inside the protons, 2) through the feed-down
104 of higher states, or 3) via weak decays of b hadrons. The first two contributions cannot
105 be distinguished experimentally, which is referred to as prompt production; while the
106 third component could be separated from the prompt production using the decay vertex
107 information. For prompt J/ψ production the feed-down contribution is large, mostly
108 from radiative decays of χ_c ($J = 0, 1, 2$) mesons. This complicates the comparison
109 between theoretical calculations and experimental results. On the contrary, the feed-down
110 contribution to $\psi(2S)$ mesons is negligible [31], theoretical calculations can be directly

compared with measurements. This analysis studies the production of $\psi(2S)$ mesons in pp collisions at the LHC. The $\psi(2S)$ mesons from prompt production are abbreviated as "prompt $\psi(2S)$ ", while those from b -hadron decays are abbreviated as " $\psi(2S)$ -from- b ".

The $\psi(2S)$ differential production cross-section has been measured in $p\bar{p}$ collisions from Tevatron at $\sqrt{s} = 1.8$ TeV [11] and $\sqrt{s} = 1.96$ TeV [32]. With the LHC data in pp collisions at $\sqrt{s} = 7$ TeV, the $\psi(2S)$ differential production cross-section are also measured by CMS [33] and LHCb [34]. The $\psi(2S)$ polarisation was also measured by CDF [24] in $p\bar{p}$ collisions at 1.96 TeV, CMS [27] and LHCb [35] in pp collisions at 7 TeV. Theoretical calculations with NRQCD were compared with the measurements for prompt $\psi(2S)$ production. The production cross-sections of $\psi(2S)$ from b -hadron decays were compared to the calculation at Fixed Order plus Next-to-Leading Logarithms (FONLL) [36], which is a tool to calculate the heavy quark production cross-section. FONLL is able to describe both the integrated cross-sections and the p_T -dependence and y -dependence very well for $\psi(2S)$ from b -hadron decays.

This note describes details of the $\psi(2S)$ cross-section measurement in pp collisions at $\sqrt{s} = 13$ TeV, using the data collected in LHCb operations in 2015 corresponding to an integrated luminosity of 275 pb^{-1} . The measurements include the double differential production cross-sections of prompt $\psi(2S)$ and $\psi(2S)$ from b as functions of p_T and rapidity y , the fraction, F_b , of $\psi(2S)$ from b as a function of p_T and y , the integrated production cross-sections of prompt $\psi(2S)$ and $\psi(2S)$ from b with $2 \text{ GeV}/c < p_T < 20 \text{ GeV}/c$ and $2.0 < y < 4.5$. Due to the constrain of trigger requirement, the measurement in the region $p_T < 2 \text{ GeV}/c$ is not performed. The production cross-sections at 13 TeV are compared with those at 7 TeV. The latter are measured using the 2011 data sample with the same analysis strategy.

2 Data and Monte Carlo samples

2.1 Data

The study reported here uses pp collision data collected by the LHCb detector at a centre-of-mass energy of 13 TeV in 2015, corresponding to an integrated luminosity of $275 \pm 10 \text{ pb}^{-1}$. The data used in this analysis were collected using four different trigger configuration keys (TCKs)¹:

- 83.57 pb^{-1} with TCK 0x10600A2 MagDown;
- 60.00 pb^{-1} with TCK 0x10600A3 MagDown;
- 11.05 pb^{-1} with TCK 0x10800A2 MagDown;
- 48.56 pb^{-1} with TCK 0x10800A2 MagUp;
- 71.52 pb^{-1} with TCK 0x11400A8 MagUp.

In this analysis only muon triggers are used, which are identical for the TCKs used: 0x10600A2, 0x10600A3, 0x10800A2, and 0x11400A8.

¹ One TCK uniquely defines the sequence of algorithms, and cuts used by the trigger.

¹⁴⁸ **2.2 Monte Carlo**

¹⁴⁹ To study the efficiency, simulated samples with about 8 M events are generated. In
¹⁵⁰ the simulation, pp collisions are generated using PYTHIA [37] with a specific LHCb
¹⁵¹ configuration [38]. Decays of hadronic particles are described by EvtGen [39], in
¹⁵² which final state radiation is generated using PHOTOS [40]. The interaction of the
¹⁵³ generated particles with the detector and its response are implemented using the GEANT4
¹⁵⁴ toolkit [41, 42] as described in Ref. [43]. The prompt charmonium production is simulated
¹⁵⁵ in PYTHIA with contributions from both the leading order color-singlet and color-octet
¹⁵⁶ mechanisms [38, 44], and the charmonium is generated without polarization.

¹⁵⁷ **2.3 The TISTOS issue**

¹⁵⁸ For real data, this analysis use Turbo stream outputs, so it's fine. For Monte Carlo
¹⁵⁹ simulation we make the tuple file under DaVinci version "v42r6p1" which is already fixed
¹⁶⁰ this issue.

¹⁶¹ **3 Candidate reconstruction and selection**

¹⁶² **3.1 Trigger and Turbo stream selection**

¹⁶³ The reconstruction and preselection of the $\psi(2S)$ candidates for real data were based on
¹⁶⁴ the Turbo stream. The LHCb trigger system consists of three levels. The first level (L0)
¹⁶⁵ is designed to retain instreaming data rate from detector read-outs up to 1 MHz, at which
¹⁶⁶ the LHC bunch crossing rate is 40 MHz. The L0 triggered data is input to the first stage
¹⁶⁷ of the software trigger (HLT1), which then performs a partial event reconstruction to
¹⁶⁸ filter out potential interested signals in the inflow data. The second stage of the software
¹⁶⁹ trigger (HLT2) performs a full event reconstruction to further remove backgrounds. Our
¹⁷⁰ analysis is based on *L0DiMuon*, *Hlt1DiMuonHighMass* and *Hlt2DiMuonPsi2STurbo* and
the selections are summarised in Table 3.1.

Table 3.1: Summary of the trigger lines used in 13 TeV analysis.

trigger line	main cuts
<i>L0DiMuon</i>	$p_{T1} \times p_{T2} > 1.69(\text{GeV}/c)^2$, nSPDHits < 900
<i>Hlt1DiMuonHighMass</i>	$p > 6\text{ GeV}/c$ $p_T > 0.3\text{ GeV}/c$ vertex DOCA < 0.2 Track $\chi^2/\text{ndf} < 3$ vertex $\chi^2/\text{ndf} < 25$ Muon ID: isMuon $m_{\mu^+\mu^-} > 2.7\text{ GeV}/c^2$
<i>Hlt2DiMuonPsi2STurbo</i>	$ m_{\mu^+\mu^-} - m_{\psi(2S)} < 120\text{ MeV}/c^2$ $p_{T\psi(2S)} > 2000\text{ MeV}/c$

172 3.2 Offline selection

173 The offline selections are applied to $\psi(2S)$ candidates to reduce the combinatorial back-
 174 ground to a reasonable level and ensure the good quality of the signal-extraction fit.
 175 First, each event is required to have at least one primary vertex (PV) reconstructed, in
 176 order to utilize the decay time information. $\psi(2S)$ candidates are formed from pairs of
 177 opposite charged tracks reconstructed in the full tracking system (long tracks). To remove
 178 possible clone tracks, the Kullback-Leibler (KL) distance [45] between two particles is
 179 used to suppress duplicate particles created by the reconstruction. We require the ghost
 180 probability for each track (μ^+ and μ^-) to be less than 0.3. Both two tracks must have a
 181 transverse momentum p_T above 1200 MeV/ c , pass muon identification and have a good
 182 quality of the track fit ($\chi^2/\text{ndf} < 3$). The pseudorapidity of each muon is required to
 183 be in the range $2.0 < \eta < 4.9$. A Particle identification (PID) is performed to identify
 184 muon candidates ($\text{DLLmu} > 2$). The two muons are required to form a good vertex by
 185 restricting the vertex fit quality $\text{Prob}(\chi^2/\text{ndf}) > 0.5\%$.

186 The pseudo-proper time of the $\psi(2S)$ is defined as

$$t_z = \frac{(z_{\psi(2S)} - z_{\text{PV}}) \times m_{\psi(2S)}}{p_z}, \quad (3.1)$$

187 where $z_{\psi(2S)}$ is the z position of the $\psi(2S)$ decay vertex, z_{PV} that of the primary vertex.
 188 p_z the measured $\psi(2S)$ momentum along the beam axis z , and $m_{\psi(2S)}$ the known $\psi(2S)$
 189 mass [46]. This variable was found to give a good approximation of the b -hadron decay
 190 proper time: given that b -hadrons are not fully reconstructed, the $\psi(2S)$ momentum is
 191 used instead of the exact b -hadron momentum. For event with multiple PV reconstructed
 192 (PileUp), the $\psi(2S)$ candidate is associated to the PV with smallest χ^2_{IP} . t_z is calculated
 193 event by event with uncertainty with a maximum of 0.3 ps. In the analysis, it is required
 194 to be in the range $-10 < t_z < 10$ ps. Prompt $\psi(2S)$ and $\psi(2S)$ -from- b can be separated
 195 by the different behaviors in the pseudo-proper time t_z .

The full offline selection criteria are summarized in Table 3.2.

Table 3.2: Offline selection criteria for $\psi(2S) \rightarrow \mu^+ \mu^-$.

Quantity	Requirement
Track ghost probability	< 0.3
μ : p_T	> 1200 MeV/ c
μ : η	$2.0 < \eta < 4.9$
μ : track quality χ^2/ndf	< 3
μ : track PID	IsMuon and $\text{DLLmu} > 2$
$\psi(2S)$: Vertex $\text{Prob}(\chi^2/\text{ndf})$	> 0.5%
Pseudo proper time t_z	(−10, 10) ps
Uncertainty of t_z	< 0.3 ps
$\psi(2S)$: Mass Window	(3566,3806) MeV/ c^2
$\psi(2S)$: L0 Trigger On Signal	L0DiMuon
$\psi(2S)$: HLT1 Trigger On Signal	Hlt1DiMuonHighMass

197 4 Cross-section determination

198 The determination of the double-differential production cross-section requires knowledge
 199 of the numbers of prompt $\psi(2S)$ and $\psi(2S)$ from b -hadron decays in bins of the kinematic
 200 variables y and p_T . This is done by performing a simultaneous fit to the distributions of
 201 the dimuon invariant mass and the pseudo-proper time t_z in each kinematic bin. The
 202 t_z of promptly produced $\psi(2S)$ signals has zero lifetime, while the t_z distribution for
 203 $\psi(2S)$ from b -hadron decays is approximately exponential as seen from simulation. The
 204 pseudo-proper time t_z allows us to statistically separate the prompt $\psi(2S)$ from the $\psi(2S)$
 205 mesons created in decays of b -hadrons.

206 The double differential cross-section for prompt and $\psi(2S)$ from- b production in a
 207 given (p_T, y) bin is defined as

$$\frac{d^2\sigma}{dydp_T} = \frac{N(\psi(2S) \rightarrow \mu^+\mu^-)}{\mathcal{L} \times \varepsilon_{\text{tot}} \times k \cdot \mathcal{B}(\psi(2S) \rightarrow e^+e^-) \times \Delta y \times \Delta p_T}. \quad (4.1)$$

208 where

- 209 * $N(\psi(2S) \rightarrow \mu^+\mu^-)$ is either the number of prompt $\psi(2S)$ or $\psi(2S)$ from b -hadron
 210 signals reconstructed through the dimuon decay channel. They are obtained by the
 211 fits described in Sec. 5;
- 212 * \mathcal{L} is the integrated luminosity;
- 213 * ε_{tot} is the total efficiency in that particular $p_T - y$ bin, described in detail in Sec. 6;
- 214 * $k = 0.9939$ is the phase space factor to correct the difference between dielectron
 215 channel and dimuon channel. It is calculated as:

$$k = \frac{(m_{\psi(2S)}^2 + 2m_\mu^2) \cdot \sqrt{m_{\psi(2S)}^2 - 4m_\mu^2}}{(m_{\psi(2S)}^2 + 2m_e^2) \cdot \sqrt{m_{\psi(2S)}^2 - 4m_e^2}}. \quad (4.2)$$

216 The lepton universality is a reasonable assumption under the current statistical
 217 precisions;

- 218 * $\mathcal{B}(\psi(2S) \rightarrow e^+e^-) = (7.89 \pm 0.17) \times 10^{-3}$ is the branching fraction of the decay
 219 $\psi(2S) \rightarrow e^+e^-$, quoted from the PDG 2016 review [47]. The dielectron branching
 220 fraction is used since it has a much smaller uncertainty than the dimuon one;
- 221 * $\Delta p_T = 1 \text{ GeV}/c$ is the bin width of the $\psi(2S)$ transverse momentum;
- 222 * $\Delta y = 0.5$ is the bin width of the $\psi(2S)$ rapidity.

223 The following boundaries are used for the binning scheme of p_T and y of the $\psi(2S)$
 224 meson:

- 225 • p_T boundaries [GeV/c]: 2, 3, 4, 5, 6, 7, 8, 9, 10, 11, 12, 13, 14, 15, 16, 17, 18, 20;
- 226 • y boundaries: 2.0, 2.5, 3.0, 3.5, 4.0, 4.5.

227 In each bin, the efficiency ε_{tot} is assumed to be constant as a function of p_T and y in
 228 the small ranges, and thus a single number with corresponding uncertainty is provided.
 229 The efficiency for prompt $\psi(2S)$ and $\psi(2S)$ -from- b are calculated separately.

230 5 Signal extraction

231 The total number of $\psi(2S)$ signals is determined from an extended unbinned maximum
 232 likelihood fit to the invariant mass distribution of the selected $\psi(2S)$ candidates. In the
 233 fit the component of the background is modelled with an exponential function

$$f_{\text{bkg}}(m) = a_0 e^{-p_0 \cdot m}. \quad (5.1)$$

234 The signal component is described by the sum of two Crystal Ball (CB) functions [48].
 235 The CB function is defined as:

$$f_{\text{CB}}(m; \mu, \sigma, \alpha, n) = \begin{cases} \left(\frac{n}{|\alpha|}\right)^n e^{-\frac{1}{2}\alpha^2} \left(\frac{n}{|\alpha|} - |\alpha| - \frac{m-\mu}{\sigma}\right)^{-n} & \frac{m-\mu}{\sigma} < -|\alpha| \\ \exp\left(-\frac{1}{2}\left(\frac{m-\mu}{\sigma}\right)^2\right) & \frac{m-\mu}{\sigma} > -|\alpha|. \end{cases}, \quad (5.2)$$

236 which combines a Gaussian core (described by the parameters μ and σ) and one tail in
 237 left (described by the parameters α and n).

238 The tails in CB functions are used to model the radiative effects, which leads to more
 239 $\psi(2S)$ candidates with lower invariant masses. Not all parameters of the CB functions
 240 are free when fitting data. Some parameters are fixed or parameterized following the
 241 previous study of J/ψ production at 13 TeV [49], which have been well understood and
 242 also verified in the simulated $\psi(2S)$ sample. The two CB functions share one common
 243 mean value μ and have different widths σ_1 and σ_2 , which are parametrized from simulation
 244 as a linear function: $\sigma_2 = 25.7 + \sigma_1$. The fraction of the narrower CB function is fixed to
 245 0.96 from simulation. For the tail parameters, n is fixed to unity from physics [50], and α
 246 is parametrized from simulation as a function of the σ : $\alpha = 2.066 \pm 0.0085\sigma - 0.00011\sigma^2$,
 247 which applies to both CB functions. Therefore, there are merely two free parameters for
 248 the signal shape, μ and σ_1 .

249 The invariant mass fit is performed in each p_T and y bin of the $\psi(2S)$ candi-
 250 date. The parameters from one dimensional mass fit [μ_{mass} (mean value of narrower
 251 Gaussian), σ_{mass} (width of narrower Gaussian), n_{sig} (signal yields), n_{bkg} (background
 252 number), $1000 * p_0$ (parameter in exponential function)] are list in Appendix B.

253 5.1 Determination of the prompt and detached signal yields

254 To determine the signal yields of prompt $\psi(2S)$ and $\psi(2S)$ from b separately, the t_z
 255 distribution is used. In each kinematic bin, an unbinned extended maximum likelihood
 256 fit to the two-dimension distributions of invariant mass $m(\mu^+\mu^-)$ and t_z is performed to
 257 separate prompt $\psi(2S)$ from $\psi(2S)$ from b .

258 At the generator level, the t_z distribution of the prompt $\psi(2S)$ is a Dirac delta function,
 259 $\delta(t_z)$, while that of $\psi(2S)$ from b follows an exponential function as seen from simulation.
 260 For $\psi(2S)$ signals, the detector resolution is taken into account by convolving a resolution
 261 function, which is described by the sum of two Gaussian functions,

$$f_{\text{resolution}}(t_z; \mu, S_1, S_2, \beta) = \frac{\beta}{\sqrt{2\pi} S_1 \sigma} e^{-\frac{(t_z - \mu)^2}{2S_1^2 \sigma^2}} + \frac{1 - \beta}{\sqrt{2\pi} S_2 \sigma} e^{-\frac{(t_z - \mu)^2}{2S_2^2 \sigma^2}}. \quad (5.3)$$

262 The parameter σ is the event-by-event uncertainty of t_z , calculated by combining the
 263 estimated uncertainties of the $\psi(2S)$ decay vertex and the associated PV. Besids, S_1 and

²⁶⁴ S_2 are two scale factors to correct the non-perfect estimation of the t_z uncertainty, the
²⁶⁵ parameter μ is the bias of the t_z measurement, and β is the fraction of one of the two
²⁶⁶ Gaussians. In the fitting procedure all the resolution parameters are floated. The imperfect
²⁶⁷ modelling of the detector resolution will be studied as one source of systematic uncertainty.

²⁶⁸ It is possible that the reconstructed $\psi(2S)$ candidate is associated to a “wrong” PV.
²⁶⁹ This can happen either because the real PV that produces the $\psi(2S)$ candidate failed to
²⁷⁰ be reconstructed, and the candidate was associated to the nearest reconstructed PV in the
²⁷¹ event, or because a wrong PV is accidentally close to the $\psi(2S)$ candidate. For the latter
²⁷² case, the positions of the reconstructed and the true PV are correlated, which results in
²⁷³ a Gaussian-like t_z distribution with a width much larger than the detection resolution.
²⁷⁴ This effect can be described by adding a third Gaussian with much larger width than
²⁷⁵ the resolution function. However, it is found from simulation that including the wide
²⁷⁶ Gaussian in the resolution does not change the fitted parameters significantly because
²⁷⁷ the fraction of this component is quite small, $<= 1\%$ as seen from studies in Ref. [49].
²⁷⁸ Therefore, the third wide Gaussian is not used in the fit function. For the former case
²⁷⁹ that the true PV is not reconstructed, the true PV and wrongly associated PV are not
²⁸⁰ correlated, which results in a long tail in the t_z distribution that can be modelled using
²⁸¹ the next-event method. The next-event pseudo-proper time, t_z^{next} , for each candidate, is
²⁸² calculated combining the $\psi(2S)$ candidate with the closest PV of another (next) event as

$$t_z^{\text{next}} = \frac{(z_{\mu\mu} - z_{\text{PV}}^{\text{next}}) \times m_{\mu\mu}}{p_z}, \quad (5.4)$$

²⁸³ where $z_{\text{PV}}^{\text{next}}$ is the z -coordinate of the nearest PV of the next selected event. The tail
²⁸⁴ distribution is extract in each bin separately and not convolved with resolution functions
²⁸⁵ since the distribution is much wider than the resolution, and very smooth in the whole t_z
²⁸⁶ region. It should be noted that since the requirement of PV reconstruction is loose, using
²⁸⁷ at least 4 VELO tracks, the probability to reconstruct the true PV is very high ($> 99\%$).

²⁸⁸ The candidates in the mass sidebands, $3566 < m_{\mu^+\mu^-} < 3620 \text{ MeV}/c^2$ and $3750 <$
²⁸⁹ $m_{\mu^+\mu^-} < 3806 \text{ MeV}/c^2$, are used as the background control sample to model the t_z
²⁹⁰ distribution of the background. The background control sample consists of random
²⁹¹ combinations of muons from semi-leptonic b and c decays, which tend to produce positive
²⁹² t_z values, as well as mis-reconstructed tracks from decays-in-flight of kaons and pions,
²⁹³ which contribute both to positive and negative t_z values. The t_z distribution of the
²⁹⁴ background is therefore modelled with an empirical function, composed of a Dirac delta
²⁹⁵ function and five exponentials (three for positive t_z and two for negative t_z , with one
²⁹⁶ positive t_z and one negative sharing the same slope parameter). This function is convolved
²⁹⁷ with the sum of two Gaussian function as a resolution function, which has different
²⁹⁸ parameters as for signals,²,

$$\begin{aligned} f_{\text{background}} = & \left[(1 - f_1 - f_2 - f_3 - f_4) \delta(t_z) + \theta(t_z) \left(\frac{f_1}{\tau_1} e^{-t_z/\tau_1} + \frac{f_2}{\tau_2} e^{-t_z/\tau_2} \right) \right. \\ & \left. + \theta(-t_z) \frac{f_3}{\tau_3} e^{t_z/\tau_3} + \frac{f_4}{2\tau_4} e^{-|t_z|/\tau_4} \right] * \left(\frac{\beta'}{\sqrt{2\pi S'_1} \sigma} e^{-\frac{(t_z-\mu)^2}{2S'^2_1\sigma^2}} + \frac{1-\beta'}{\sqrt{2\pi S'_2} \sigma} e^{-\frac{(t_z-\mu)^2}{2S'^2_2\sigma^2}} \right). \end{aligned} \quad (5.5)$$

²The uncertainty on the background vertex is usually worse than that for the signal vertex.

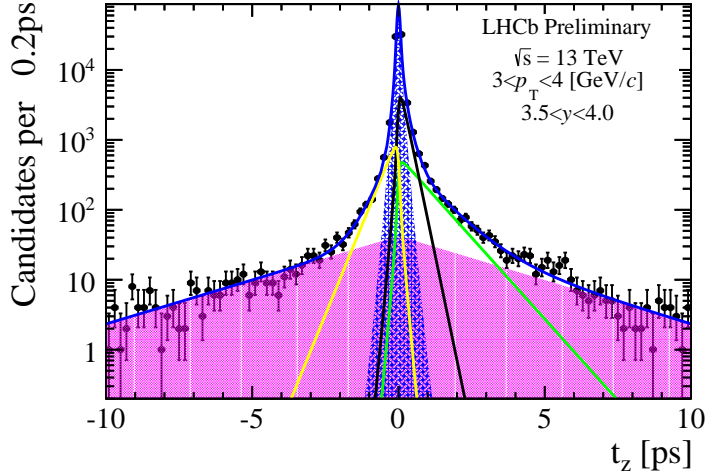


Figure 5.1: Distribution of t_z for the background $\psi(2S)$ in the kinematic bin $p_T \in [3, 4] \text{ GeV}/c$ and $y \in [3.5, 4.0]$.

299 The parameters in Eq. 5.5 are determined by fitting the t_z distribution of background
300 control sample defined above(bin by bin), and are fixed for the final fits. In Fig. 5.1, the t_z
301 distribution of the background in the kinematic range $p_T \in [3, 4] \text{ GeV}/c$ and $y \in [3.5, 4.0]$
302 is shown, superposed by a fit using Eq. 5.5. In Tables B.6, B.7, B.8, B.9 and B.10, all the
303 background parameters in t_z fits are given in each kinematic bin.

304 In total, the eventual function for the t_z fit is:

$$F_{t_z}(t_z; n_{\text{prompt}}, n_{\text{tail}}, n_{\text{bdecay}}, n_{\text{bkg}}, \mu, S_1, S_2, \beta, \tau_b) \\ = \left(n_{\text{prompt}} \delta(t_z) + \frac{n_{\text{bdecay}}}{\tau_b} e^{-t_z/\tau_b} \right) * f_{\text{resolution}}(t_z; \mu, S_1, S_2, \beta) + n_{\text{tail}} f_{\text{tail}}(t_z) + n_{\text{bkg}} f_{\text{background}}(t_z), \quad (5.6)$$

305 where n_{bkg} , n_{prompt} , n_{bdecay} and n_{tail} are the number of background, prompt $\psi(2S)$,
306 $\psi(2S)$ from b and wrong PV events, respectively. Because the requirement of the PV
307 reconstruction is loose, and the PV is not refitted by removing the VELO segments of
308 the muon tracks, it is reasonable to assume that prompt $\psi(2S)$ and $\psi(2S)$ from b have
309 equal probability to be assigned with a wrong PV. Therefore, the fractions of the prompt
310 $\psi(2S)$ and $\psi(2S)$ from b components in n_{tail} is equal to the fraction $\frac{n_{\text{prompt}}}{n_{\text{bdecay}}+n_{\text{prompt}}}$ and
311 $\frac{n_{\text{bdecay}}}{n_{\text{bdecay}}+n_{\text{prompt}}}$. It has been validated that the efficiencies for prompt $\psi(2S)$ and $\psi(2S)$
312 from b are almost the same which can be seen in Sec. 6.

313 The two-dimensional fit to the invariant mass and the lifetime in the kinematic range
314 $5 \text{ GeV}/c < p_T < 6 \text{ GeV}/c$ and $2.5 < y < 3.0$ is shown in Fig. 5.2. During the t_z -mass
315 combined fitting procedure, the parameters of mass signal shape(μ_{mass} , σ_{mass} , p_0) are
316 determined by previous one dimensional mass fit bin by bin and are fixed for the final
317 fits. The t_z -mass combine fitted value β (fraction of first Gaussian of signal resolution
318 function), $1000 * \mu_{t_z}$ (bias of t_z distribution), $S(1, 2)_{t_z}$ ($\sigma_{1,2}$ of first/second Gaussian
319 resolution function convolved with the t_z function), τ_b (effective b -hadron lifetime), n_{bkg} ,
320 n_{prompt} (number of prompt $\psi(2S)$), $n_{b-\text{decay}}$ (number of $\psi(2S)$ -from- b) and n_{tail} (number
321 of events in tail) are given in TablesB.1, B.2, B.3, B.4 and B.5.

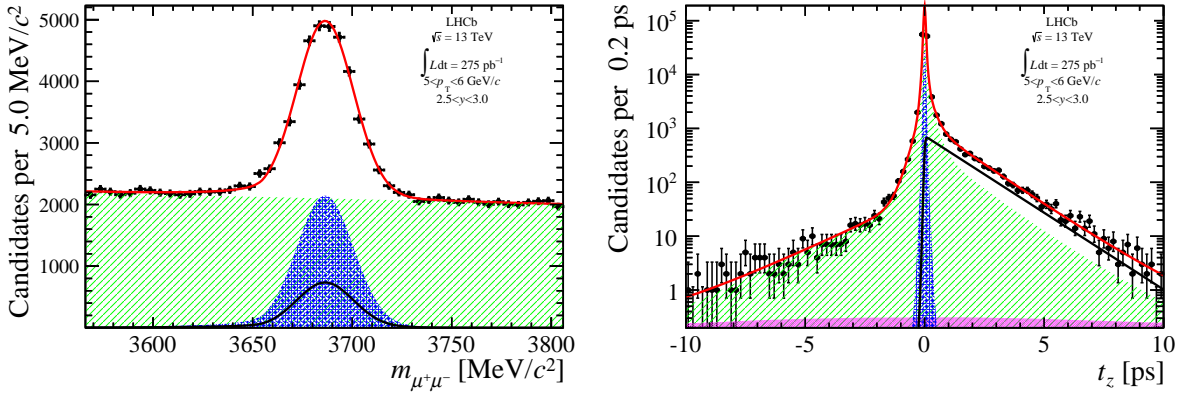


Figure 5.2: Invariant mass (left) and pseudo decay time (right) distributions for the kinematic bin $5 < p_T < 6 \text{ GeV}/c$, $2.5 < y < 3.0$, with fit results superimposed. The solid (red) line is the total fit function, the shaded (green) area corresponds to the background component. The prompt $\psi(2S)$ contribution is shown in cross-hatched area (blue), $\psi(2S)$ -from- b in a solid (black) line and the tail contribution due to the association of $\psi(2S)$ with the wrong PV is shown in full filled (magenta) area. The tail contribution is not visible in the invariant mass plot.

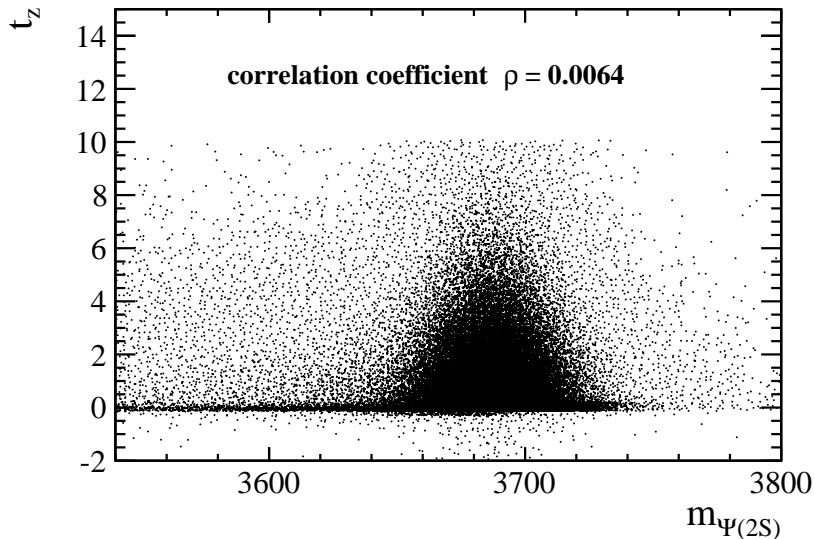


Figure 5.3: Dependency of $m_{\psi(2S)}$ on t_z .

322 The dependency of $m_{\psi(2S)}$ on t_z was studied (Fig. 5.3), the final correlation is found
 323 to be negligible on the level $\rho = 0.0064$.

324 6 Efficiency determination

325 The total efficiency ϵ_{tot} is expressed as the multiplication of the efficiencies of geometrical
 326 acceptance, the reconstruction-selection, the muon identification and the trigger:

$$\epsilon_{\text{tot}} = \epsilon_{\text{acc}} \times \epsilon_{\text{Reco\&Sel}} \times \epsilon_{\text{MuonID}} \times \epsilon_{\text{Trigger}}, \quad (6.1)$$

327 The efficiencies are calculated in each bin of $\psi(2S)$ p_T and y separately, using simulated

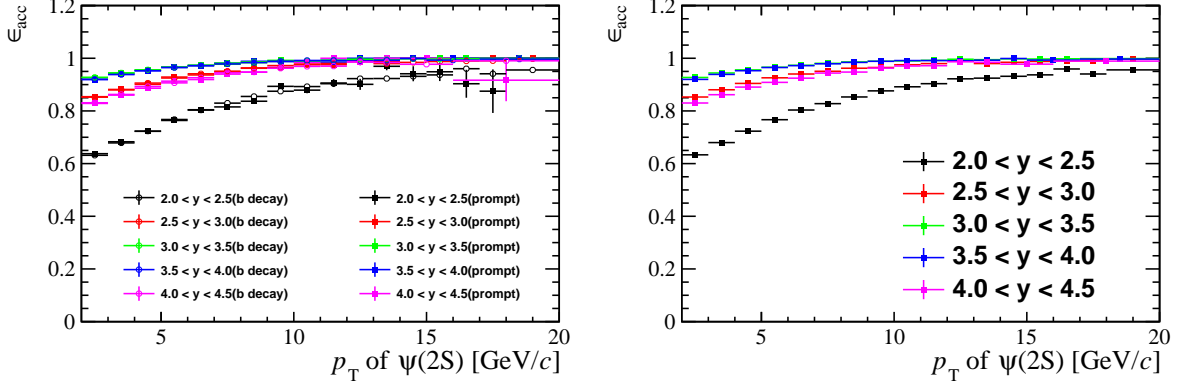


Figure 6.1: Geometrical acceptance ϵ_{acc} calculated using simulated events as a function of p_{T} in bins of y . The right figure shows the average between efficiency of prompt $\psi(2S)$ and $\psi(2S)$ from b .

samples that pass the truth match requirement. It is found that the truth-matching fail rate is around 0.4%, which is negligible compared to the statistical and systematic uncertainties.

In the simulated sample, the prompt $\psi(2S)$ and $\psi(2S)$ from b are separated using the MC truth information. For each efficiency, it is calculated independently for prompt $\psi(2S)$ and $\psi(2S)$ from b , and the average efficiency for both prompt $\psi(2S)$ and $\psi(2S)$ from b is also provided. The efficiency between prompt $\psi(2S)$ and $\psi(2S)$ from b shown consistency to some extent. The separate efficiency for prompt $\psi(2S)$ and $\psi(2S)$ from b are used to calculate final cross section.

6.1 Geometrical acceptance

The geometrical acceptance in each kinematic bin is defined as

$$\epsilon_{\text{acc}} \equiv \frac{\psi(2S) \text{ with both } \mu \text{ in LHCb acceptance}}{\text{Generated } \psi(2S)}. \quad (6.2)$$

The LHCb acceptance means the polar angle $[10, 400]$ mrad defined with respect to the direction of LHCb z -axis, before the effect of the magnetic field. The efficiency ϵ_{acc} is determined using a simulated sample at the generator level. In Fig. 6.1, the efficiency in each p_{T} and y bin of the $\psi(2S)$ meson is shown for prompt $\psi(2S)$ and $\psi(2S)$ from b , and is summarized in Tables C.1, C.2 and C.3 in Appendix C. The geometrical acceptances of prompt $\psi(2S)$ and $\psi(2S)$ from b , and the average over prompt $\psi(2S)$ and $\psi(2S)$ from b are shown in Fig. 6.1.

6.2 Reconstruction-selection efficiency

The reconstruction and selection efficiency in each kinematic bin is estimated as

$$\epsilon_{\text{Reco\&Sel}} \equiv \frac{\psi(2S) \text{ reconstructed and selected (w/o } \mu\text{ID)}}{\psi(2S) \text{ with both } \mu \text{ in LHCb acceptance}}. \quad (6.3)$$

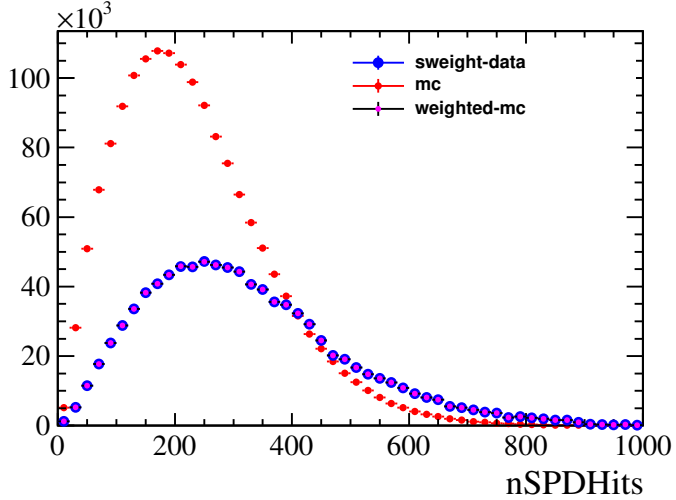


Figure 6.2: Distribution of the number of the SPD hits for (blue) data and (red) simulation for $\psi(2S)$.

348 It includes the efficiency of reconstructing the two muon tracks and the selection of the
 349 $\psi(2S)$ signals, with the selection criteria listed in Table 3.2 (excluding muon identification
 350 and the trigger).

351 Studies show that the tracking efficiency is slightly different between simulation and
 352 data. As a result, the reconstruction efficiency in simulation is corrected as a function
 353 of the kinematics of the two muons. When applying the efficiency correction we first
 354 reweighted the event multiplicity distribution in simulation to keep consistency with
 355 the data. As the J/ψ analysis [49], the number of the SPD hits is used to describe the
 356 multiplicity of the event. It is clearly shown in Fig. 6.2 that the distributions of the
 357 variable in data and Monte Carlo are different before the reweighting. The distribution
 358 of the number of the SPD hits after reweighting is also shown in Fig. 6.2. Here the
 359 distribution for data is obtained by subtracting the background using the sPlot technique
 360 with the invariant mass of $\psi(2S)$ mesons as the discriminant. All the offline selections
 361 except the PID and trigger selections are applied. The simulated samples are selected by
 362 all the offline selections except the PID and the trigger selections. Then the reconstruction
 363 efficiency is further corrected using the data-over-simulation single tracking efficiency ratio.
 364 The ratio of tracking efficiencies for a single track in data and simulation determined with
 365 the Long Tag-Probe method [51] is shown in Fig. 6.3, which was given by the tracking
 366 group. For a given event the correction factor is determined by multiplying the efficiency
 367 ratios for each of the tracks in the final state. Since the event multiplicity distribution
 368 of prompt $\psi(2S)$ and $\psi(2S)$ from b in simulation is quite similar compared to the event
 369 multiplicity difference between simulation and data, we assume prompt $\psi(2S)$ and $\psi(2S)$
 370 from b have the same efficiency corrections.

371 For each p_T and y bin, the efficiency of $\epsilon_{\text{Reco\&Sel}}$ is shown in Fig. 6.4, and summarized
 372 in Tables C.4, C.5 and C.6 in Appendix C for prompt $\psi(2S)$ and $\psi(2S)$ from b .

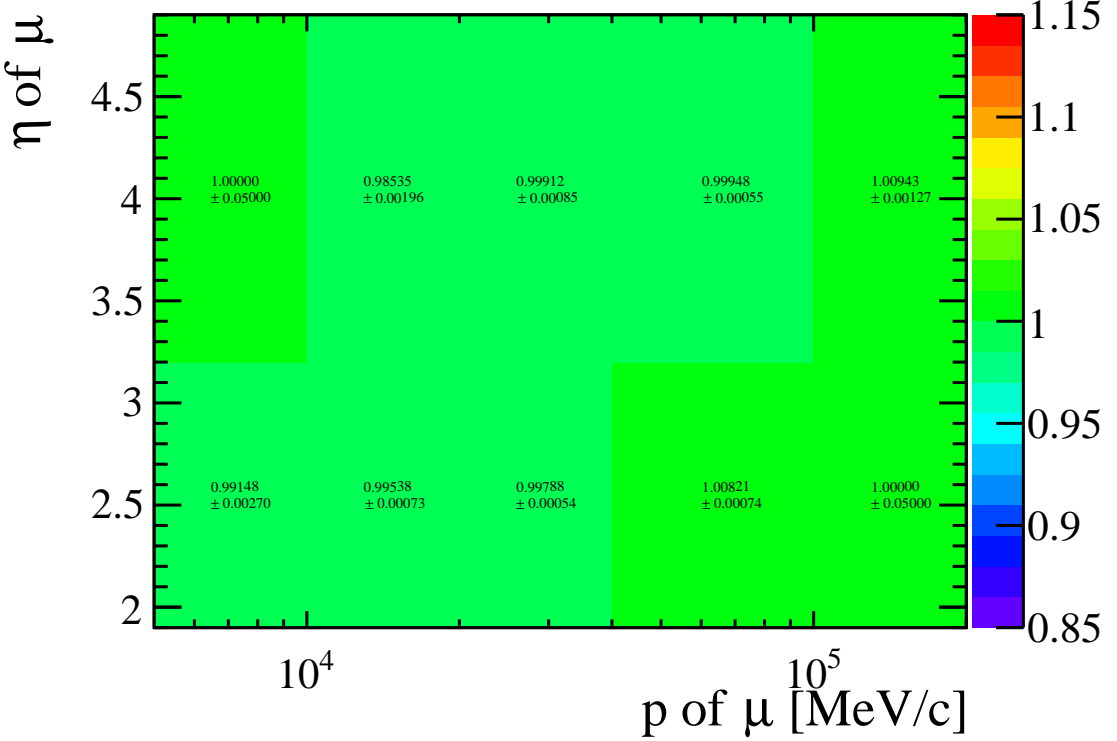


Figure 6.3: Tracking efficiency ratio between data and MC2015 simulation in bins of p_μ and η_μ of the muon.

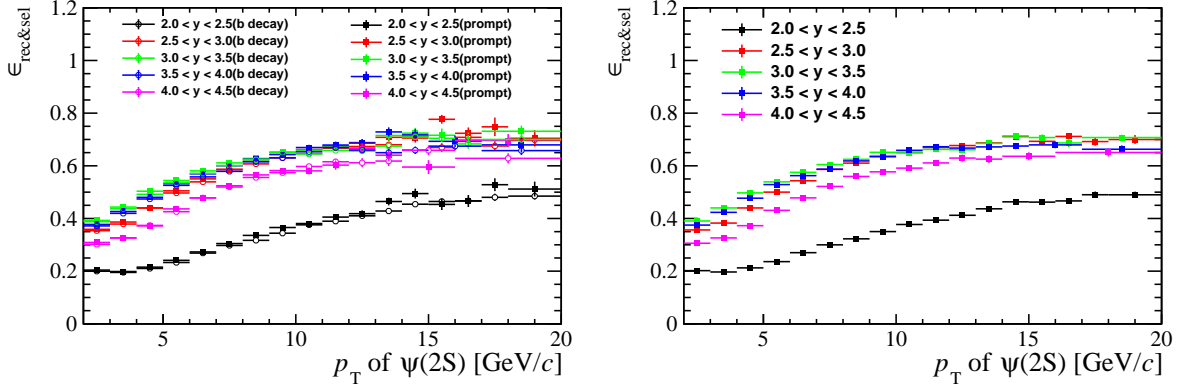


Figure 6.4: Reconstruction-Selection efficiency $\epsilon_{\text{Reco\&Sel}}$ calculated using simulated events as a function of p_T in bins of y . The right figure shows the average between efficiency of prompt $\psi(2S)$ and $\psi(2S)$ from b .

373 6.3 Muon identification efficiency

374 The muon identification requirement used in this analysis is IsMuon == 1&&DLLmu > 2.
 375 The efficiency of this requirement in each kinematic bin is given by The efficiency introduced
 376 by

$$\epsilon_{\text{MuonID}} \equiv \frac{\psi(2S) \text{ selected including } \mu\text{ID requirement}}{\psi(2S) \text{ reconstructed and selected (w/o } \mu\text{ID)}}. \quad (6.4)$$

377 The Muon ID efficiency is obtained using simulated samples, calibrated with the data

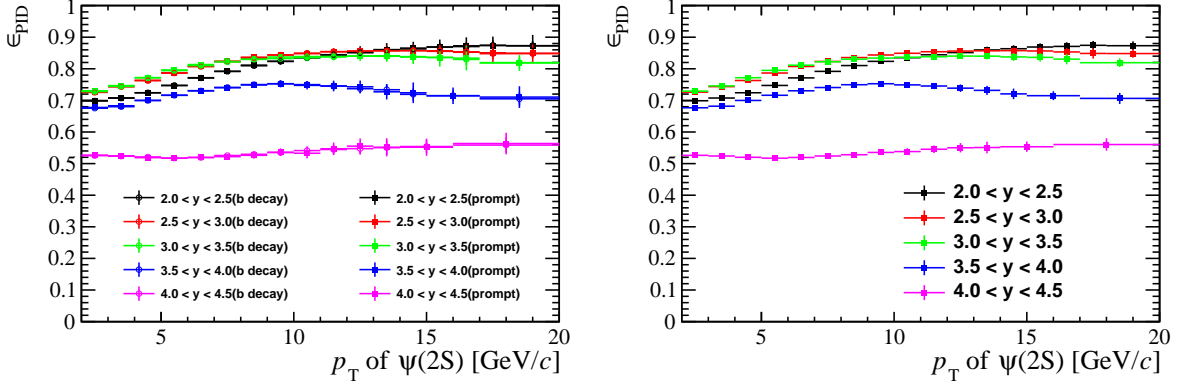


Figure 6.5: MuonID efficiency ϵ_{MuonID} calculated using simulated events as a function of p_T in bins of y . The right figure shows the average between efficiency of prompt $\psi(2S)$ and $\psi(2S)$ from b .

378 using the PIDCalib package. The full simulated samples used here are selected by all
 379 the selections except the muon ID and the trigger. The selected samples are the same
 380 with the ones used in the reconstruction and selection. As estimating the reconstruction
 381 and selection efficiency, we firstly reweight the nSPDhits in simulation according to the
 382 distribution of nSPDhits in data. The muon ID efficiency in each (p_T, y) bin of $\psi(2S)$
 383 mesons is then calculated by averaging the muon ID efficiency of each candidate in the
 384 bin, which is the product of the muon ID efficiencies of the two muons from the efficiency
 385 table, obtained from the PIDCalib package, according to their $(p, \eta, \text{nSPDhits})$ values.
 386 The formula is

$$\bar{\epsilon}(p_T, y) = \frac{\sum \epsilon_{\mu^+}(p_{\mu^+}, \eta_{\mu^+}, \text{nSPDhits}) \epsilon_{\mu^-}(p_{\mu^-}, \eta_{\mu^-}, \text{nSPDhits})}{N_{\text{res}\&\text{sel}}}. \quad (6.5)$$

387 where $\epsilon_{\mu^+}(p_{\mu^+}, \eta_{\mu^+}, \text{nSPDhits})$ and $\epsilon_{\mu^-}(p_{\mu^-}, \eta_{\mu^-}, \text{nSPDhits})$ are the muon ID efficiencies
 388 obtained from the efficiency table. The efficiency table we used here is from the calibration
 389 sample which contains J/ψ candidates taken in the same period and the average efficiency
 390 over the whole period is used. One 3-Dimensional efficiency table dedicated for the muon
 391 ID selection is obtained from this calibration sample in bins of the muon $(p, \eta, \text{nSPDhits})$
 392 using the tag-and-probe method. The MagDown and MagUp efficiencies are calculated
 393 separately. For the muon candidates whose $(p, \eta, \text{nSPDhits})$ are out of the range of the
 394 calibration sample, the value in the nearby bin is taken.

395 For each p_T and y bin, the efficiency of ϵ_{MuonID} is shown in Fig. 6.5, and summarized
 396 in Tables C.7 and C.8 in Appendix C for prompt $\psi(2S)$ and $\psi(2S)$ from b .

397 6.4 Trigger efficiency

398 The trigger efficiency in each kinematic bin is defined as

$$\epsilon_{\text{Trigger}} \equiv \frac{\psi(2S) \text{ triggered}}{\psi(2S) \text{ selected including } \mu\text{ID requirement}} \quad (6.6)$$

399 Here the triggers include both TOS requirement of L0DiMuon, Hlt1DiMuonHighMass and
 400 Hlt2DiMuonPsi2STurbo. Only L0DiMuon and Hlt1DiMuonHighMass contribute actually

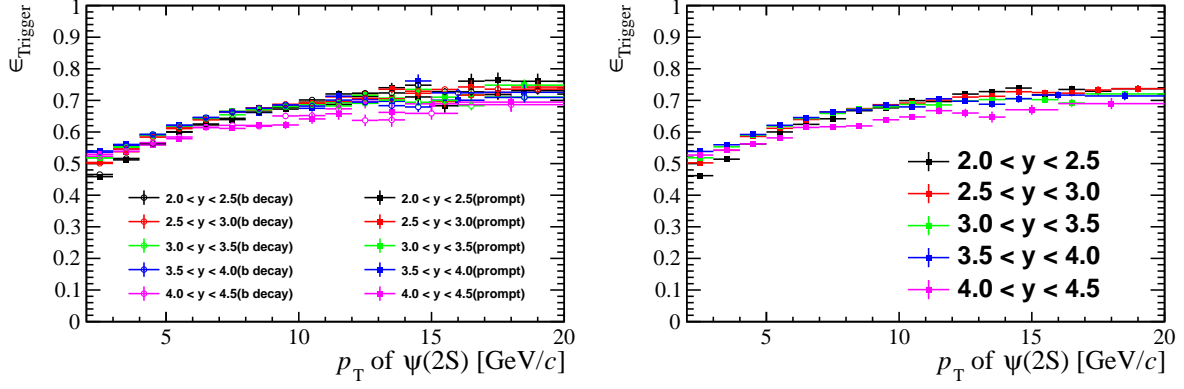


Figure 6.6: Trigger efficiency $\epsilon_{\text{Trigger}}$ calculated using simulated events as a function of p_T in bins of y . The right figure shows the average between efficiency of prompt $\psi(2S)$ and $\psi(2S)$ from b .

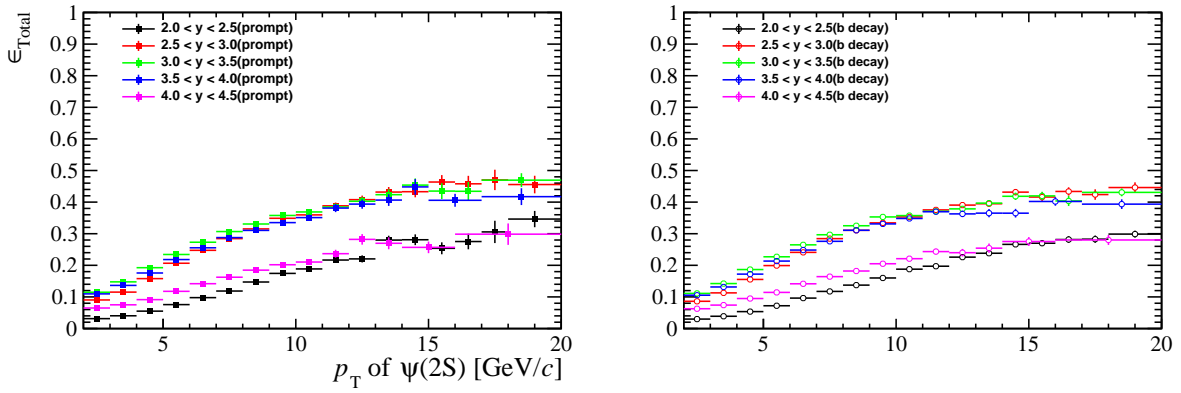


Figure 6.7: Total efficiency ϵ_{tot} calculated using simulated events as a function of p_T in bins of y are shown in the plot.

401 to the efficiency, because the `Hlt2DiMuonPsi2STurbo` is almost fully efficient due to the
 402 facts that the offline selections are tighter than those in `Hlt2DiMuonPsi2STurbo` and the
 403 same reconstruction procedure and tools are implemented online and offline. For each p_T
 404 and y bin, the efficiency of $\epsilon_{\text{Trigger}}$ is shown in Fig. 6.6, and summarized in Tables C.10,
 405 C.11 and C.12 in Appendix C for prompt $\psi(2S)$ and $\psi(2S)$ from b .

406 6.5 Total efficiency

407 The total efficiency ϵ_{tot} is shown in Fig. 6.7 for prompt $\psi(2S)$ and $\psi(2S)$ from b , and
 408 is summarized in Tables C.13 and C.14 in Appendix C. The ratio between efficiency of
 409 prompt $\psi(2S)$ and $\psi(2S)$ from b shown in Fig. 6.8 are almost unity which indicate that
 410 the prompt $\psi(2S)$ and $\psi(2S)$ from b have similar efficiency. The separate efficiency for
 411 prompt $\psi(2S)$ and $\psi(2S)$ from b are used to calculate final cross section.

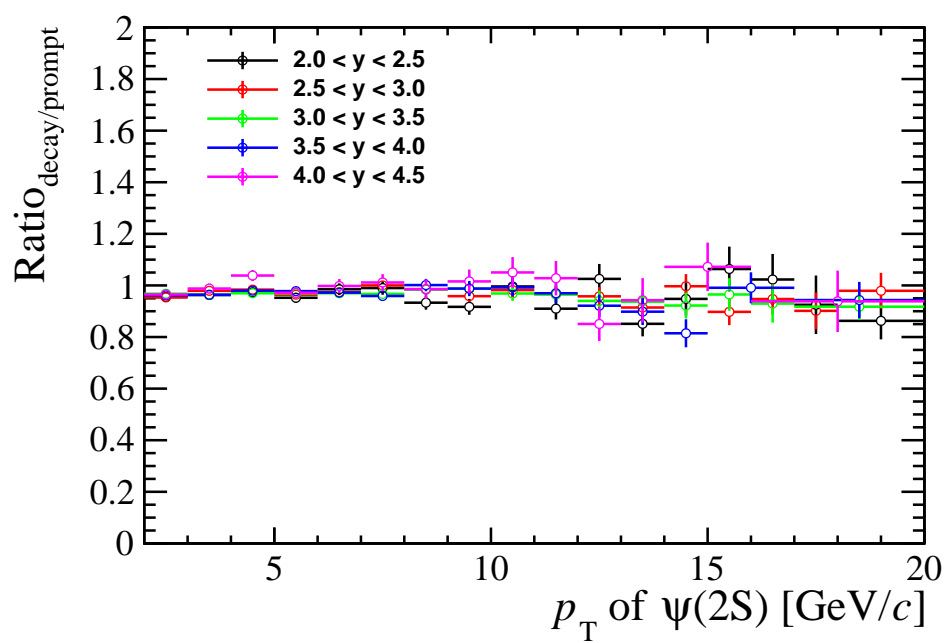


Figure 6.8: The ratio between efficiency of prompt $\psi(2S)$ and $\psi(2S)$ from b in different p_T and y bins.

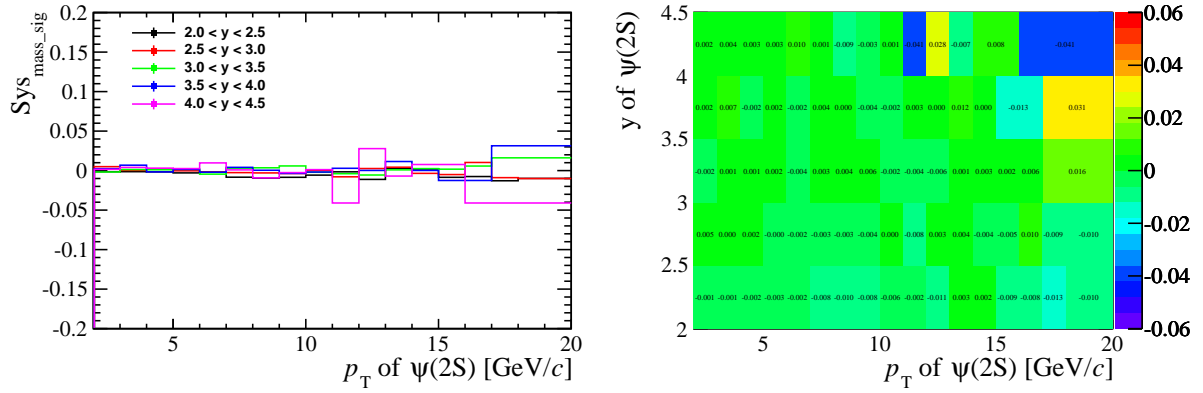


Figure 7.1: Systematic uncertainties due to the model of signal invariant mass distribution which calculated in different p_T and y bins.

412 7 Systematic uncertainties

413 The following sources of systematic uncertainties are considered.

414 7.1 Signal extraction

415 7.1.1 Signal mass shape

416 Using the sum of two Crystal Ball functions parametrized as described in Section 5 could
 417 bias the signal yields. For an alternative, the signal invariant mass is also fitted with the
 418 model which extracted from the kernel-estimated distribution from the simulated sample
 419 bin dependently. In order to account for the resolution difference between data and
 420 simulation, a Gaussian function (all the parameters are float during the fit procedure) is
 421 used to smear the shape of the signals. The study is performed in each kinematic bin,
 422 and the signal yields from the default fit and alternative fit are compared. The relative
 423 difference is about 0.0 – 4.1%, which is taken as the systematic uncertainty due to the
 424 model to describe the signal invariant mass distribution. The detailed results in each p_T
 425 and y bin is shown in Fig. 7.1.

426 7.1.2 Fit to t_z

427 There are several scenarios that could deviate the fitted b fraction from its true value:

- 428 • Imperfect modelling of the detector resolution of t_z . Since the shape of prompt
 429 $\psi(2S)$ is dominated by the resolution, a defective description of resolution could
 430 make the prompt $\psi(2S)$ distribution not fitted very well, and thus will affect the
 431 fitted fraction of $\psi(2S)$ from b . To study this effect, a third wide Gaussian is added
 432 to the resolution function. It is found that the difference of the fitted F_b between
 433 the default fit and the new fit is negligible.
- 434 • Systematic uncertainty related to the background description. In the nominal
 435 procedure, the cFit explicitly models the background distribution using the mass
 436 sidebands. As an alternative, the parameters of the t_z distribution for the background
 437 is obtained by the sPlot technique, and are fixed in the t_z fit. The change of the

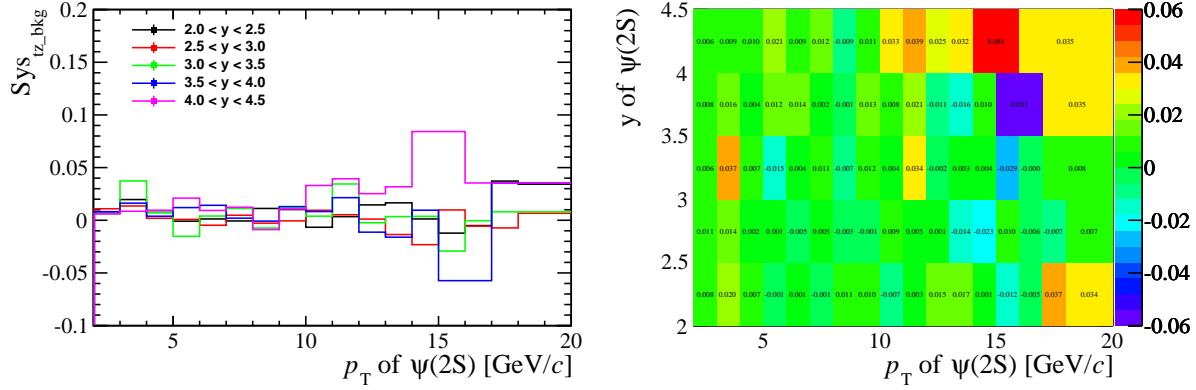


Figure 7.2: Systematic uncertainties due to the model of background t_z distribution.

fraction of $\psi(2S)$ from b is $0.0 - 8.4\%$. For each p_T and y bin, the detailed results is shown in Fig. 7.2.

- Systematic uncertainty due to the long tail of the t_z distribution. The nominal approach to describe the tail is the next-event method, defined in Section 5.1. An alternative approach is to describe the tail with an analytic function of a bifurcated exponential with equal slopes on the positive and negative sides. Here the slope parameter is left free in the t_z fit. The relative difference of the fitted F_b between the two fits is 0.1% , which is small due to the fact that the tail is rather small.

In total, the systematic uncertainty due to the t_z fit model is $0.1 - 8.4\%$.

7.2 Global event cuts

In the L0DiMuon trigger line, apart from the p_T cut, a cut on the number of the SPD hits ($nSPDhits < 900$) is applied to remove too busy events. As the $nSPDhits$ distribution in data is not well reproduced by simulation, this could lead to a systematic uncertainty. To evaluate such effect, the $nSPDhits$ distribution in the range $(0, 900)$ for data is fitted with two Γ -functions as shown in Fig. 7.3 for $\psi(2S)$ as the same method used in Ref. [52]. In the simulated sample, the cut efficiency is 99.98% .

The Γ -functions is defined below

$$f(x) = \frac{(\frac{x-\mu}{\beta})^{\gamma-1} \exp(-\frac{x-\mu}{\beta})}{\beta \Gamma(\gamma)} \quad x \geq \mu; \gamma, \beta > 0, \quad (7.1)$$

where γ is the shape parameter, μ is the location parameter, β is the scale parameter, and Γ is the gamma function which has the formula

$$\Gamma(a) = \int_0^\infty t^{a-1} e^{-t} dt. \quad (7.2)$$

Here, both the data and simulation samples have passed all the selections. For data, the distribution is obtained from the background-subtracted sample using the *sPlot* technique [53]. As a result, the efficiency of $nSPDhits < 900$ for $\psi(2S)$ mesons is 99.46% in data. The relative difference between data and simulation is 0.5% , which is taken as the systematic uncertainty due to global event cuts.

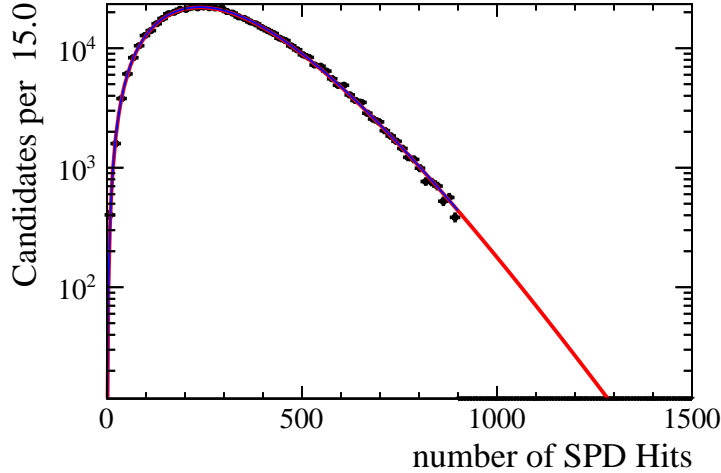


Figure 7.3: The nSPDhits distribution together with the fit result in data after background subtraction using the *sPlot* technique.

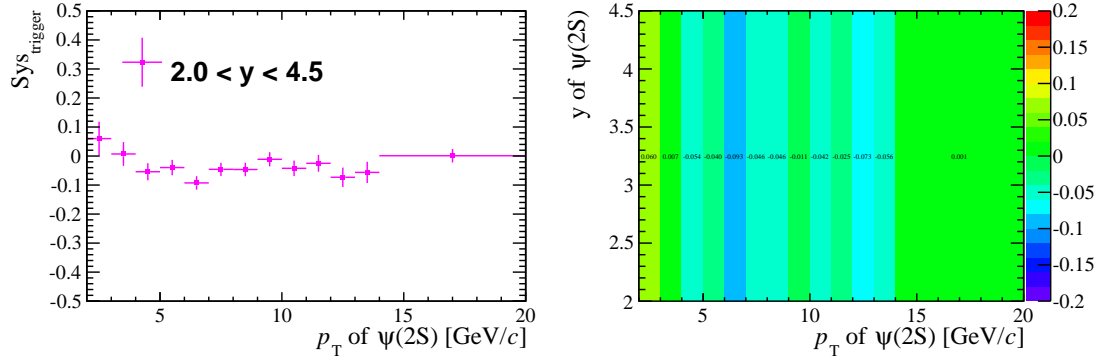


Figure 7.4: Systematic uncertainty of trigger requirement determined with the TisTos method.

462 7.3 Trigger efficiency

463 The trigger efficiency in simulation is cross-checked with data, and the difference be-
 464 tween simulation and data is quoted as the systematic uncertainty. For both L0DiMuon
 465 and Hlt1DiMuonHighMass the TisTos method is used to evaluate the efficiency for
 466 L0DiMuon&&Hlt1DiMuonHighMass both in simulation and data. We use L0Global and
 467 Hlt1Global as the TIS line. As the data sample size is limited by the number of the TIS
 468 events, we only consider the uncertainty in different p_T bins and assume the same value
 469 in different y bins. The relative efficiency difference (in absolute value) between data and
 470 simulation in each $\psi(2S)$ kinematic bin is quoted as the systematic uncertainty. Fig. 7.4
 471 show the systematic uncertainty obtained use TisTos method. The uncertainties vary
 472 between 0.1% and 9.3% depending on different kinematic bins for $\psi(2S)$ mesons.

473 7.4 Tracking efficiency

474 There are two sources of systematic uncertainties associated with the track reconstruction
 475 efficiency.

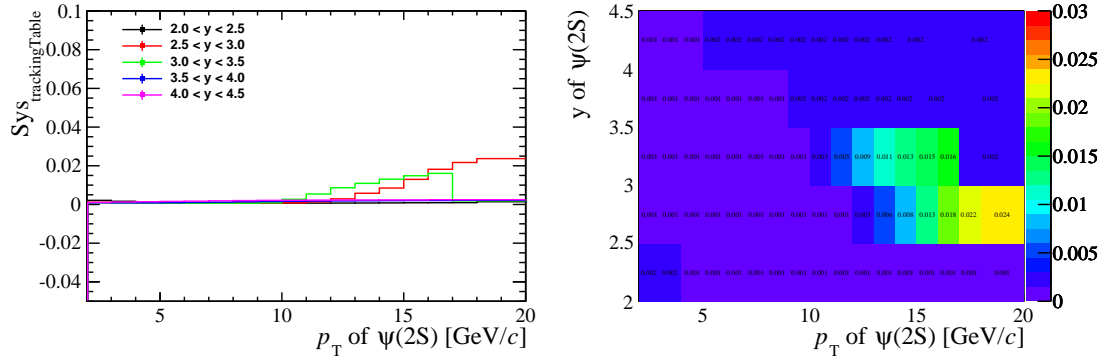


Figure 7.5: The relative difference for the $\epsilon_{\text{Reco\&Sel}}$ aroused by statistic uncertainty of correction table.

476 One is the statistical uncertainty of the ratios due to the limited sample size used to
 477 obtain the tracking correction table. This part could be obtained by toy studies: Two
 478 hundreds of experiments were performed where the efficiency for each bin in the p and η
 479 was sampled from Fig. 6.3 by Gaussian distributions with the corresponding central value
 480 as the mean and the uncertainty as the width; For each experiment, the reconstruction and
 481 selection efficiency of $\psi(2S)$ mesons in different bins could be obtained with the sampled
 482 efficiency correction table; Finally, using a gaussian function fit to the two hundreds of
 483 results of each $\psi(2S)$ kinematic bin and the sigma divided by the mean value of the fit
 484 result is quoted as the relative uncertainty. The relative uncertainty is around 0.1 – 2.4%
 485 depending on different bins as shown in Fig. 7.5.

486 Another one is the choice of event multiplicity variable. This systematic is provided
 487 by tracking group. The tracking experts indicate that choice of the multiplicity variable
 488 (nTracks, nSPDHits, or others) is relevant for deciding the systematics. They studied this
 489 effect and suggest 0.8% per track, as detailed in Ref. [54].

490 7.5 Offline selection efficiency of $\psi(2S)$ vertex fit

491 The systematic uncertainty related to selections on kinematic variables is treated as part
 492 of the uncertainty due to unknown spectrum and is studied in section 7.7. The selections
 493 on track quality and track ghost probability are very loose, and their effects are taken
 494 into account in the systematic uncertainty due to the track efficiency, as described in
 495 Section 7.4.

496 In previous studies differences in the efficiency of the vertex quality criteria between
 497 data and simulation were seen. In Fig. 7.6 a comparison between the $\psi(2S)$ vertex χ^2
 498 distribution for data and simulation simulation is shown. The nominal selection requires
 499 for the vertex fit probability $P(\chi^2/\text{ndf}) > 0.5\%$. The systematic uncertainty of the vertex
 500 fit quality cut is studied by comparing the cut efficiency in data and simulation. The
 501 relative change value of 0.4% is observed for the difference of the efficiencies between data
 502 and simulation, which is taken as a systematic uncertainty.

503 7.6 MuonID efficiency

504 The systematic uncertainty due to MuonID includes the following contributions:

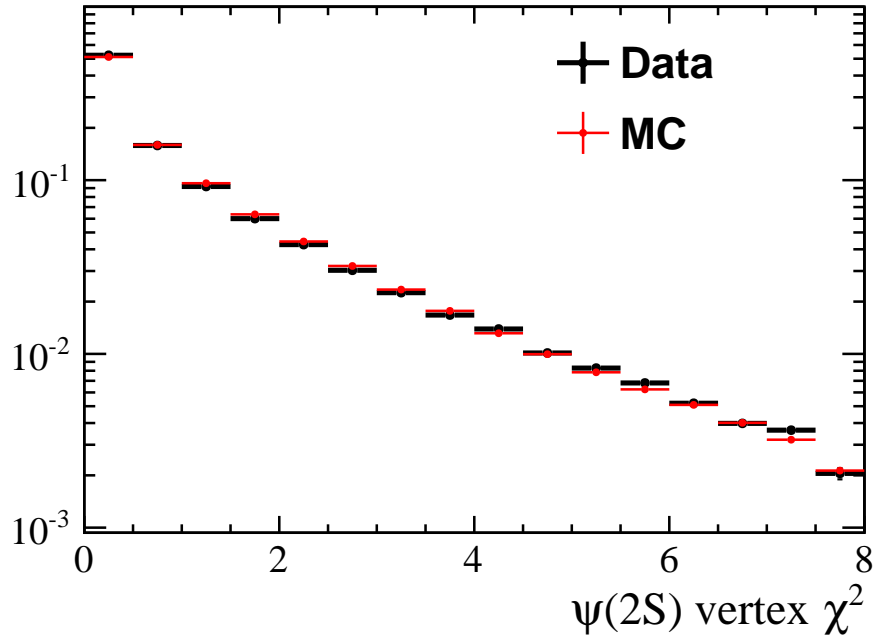


Figure 7.6: Vertex fit χ^2 distribution in data and simulation.

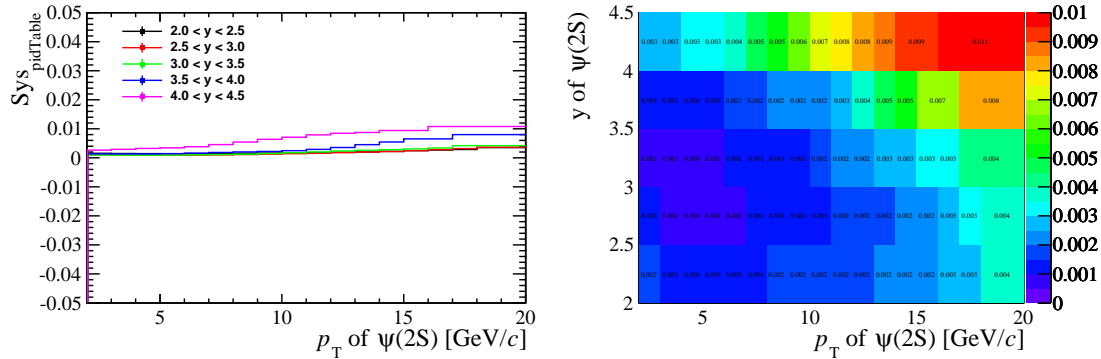


Figure 7.7: The relative difference for the ϵ_{MuonID} aroused by statistic uncertainty of correction table.

- The statistical uncertainty due to the finite size of the calibration sample. To estimate the systematic uncertainty due to the limited calibration sample size, we first generate two hundred tables of efficiencies from the original table, where the efficiency in each bin of each table is randomly sampled from a Gaussian distribution using the central value as the mean and the uncertainty as the width. Then, we use Eq. 6.5 to obtain two hundred efficiency values from the generated efficiency tables. Finally, we fit the distribution of the two hundred efficiencies with a Gaussian function. The ratio between the width and the mean value of the fitted Gaussian function is quoted as a systematic uncertainty, which is found to be 0.1 – 1.1% depending on different bins as shown in Fig. 7.7.
- Uncertainty due to binning scheme of the calibration sample, studied by varying the binning method in p_μ , η_μ and nSPDHits respectively. The default one and the

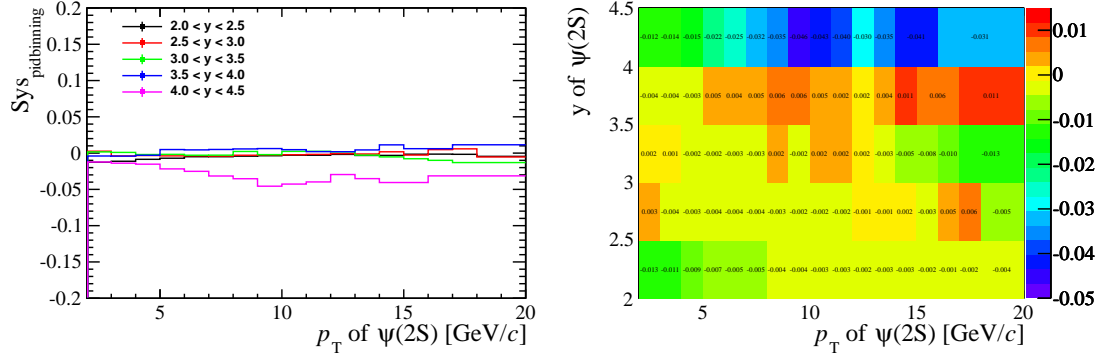


Figure 7.8: The relative difference for the ϵ_{MuonID} aroused by binning schemes.

two alternative binning schemes could be found below. The nominal binning scheme of the muon ID efficiency for muons we use to calculate the muon ID efficiency of $\psi(2S)$ mesons is defined:

- p_μ boundaries [GeV/c]: 3, 6, 8, 10, 12, 13, 14, 15, 16, 18, 20, 24, 28, 32, 40, 60, 70, 80, 90, 100, 200, 1000
- η boundaries: 2.0, 2.5, 3.0, 3.5, 4.0, 4.5, 4.9
- nSPDhits boundaries: 0, 200, 400, 1000.

One of the two alternative binning schemes is defined:

- p_μ boundaries [GeV/c]: 3, 7, 9, 11, 12, 13, 14, 15, 17, 19, 23, 27, 32, 40, 55, 65, 75, 85, 95, 150, 200, 1000
- η boundaries: 2.0, 2.4, 2.9, 3.4, 3.9, 4.4, 4.9
- nSPDhits boundaries: 0, 300, 500, 1000.

The other one binning schemes is defined:

- p_μ boundaries [GeV/c]: 3, 5.5, 7.5, 9.5, 11.5, 12.5, 13.5, 14.5, 15.5, 17.5, 19.5, 23.5, 27.5, 32, 38, 48, 58, 68, 78, 88, 98, 198, 1000
- η boundaries: 2.0, 2.6, 3.1, 3.6, 4.1, 4.6, 4.9
- nSPDhits boundaries: 0, 150, 480, 1000.

The maximum difference between the two new efficiency and the original efficiency is quoted as the systematic uncertainty. The relative uncertainty is around 0.1 – 4.6% depending on different bins as shown in Fig. 7.8.

The quadratic sum of the above components are quoted as the PID systematic uncertainty and is considered as correlated in all $\psi(2S)$ bins.

7.7 p_T - y -spectrum

The kinematic distributions of the $\psi(2S)$ mesons in data and simulation could be different even though we have binned in (p_T, y) . As the bin size is not infinitely small, the different

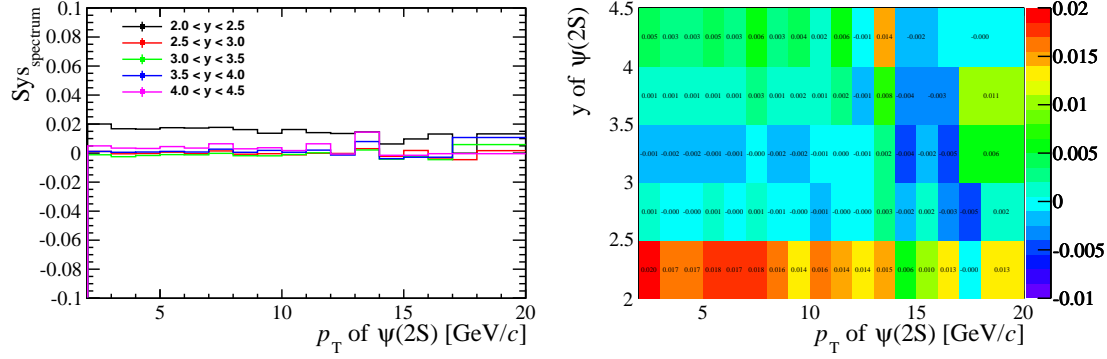


Figure 7.9: The relative systematic uncertainty due to the kinematic spectrum effects in each bin of p_T and y for $\psi(2S)$.

distribution in some (p_T, y) bin can still cause systematic effects. The p_T and y distribution of $\psi(2S)$ in simulation is weighted to that in the background-subtracted data, and the efficiency is evaluated again with the weighted kinematic distribution in each bin; the variation of the efficiencies is quoted as a systematic uncertainty. In Fig. 7.9, the spectrum systematic uncertainties for each bin are shown (before taking the absolute values).

7.8 Polarization scenarios

Extensive studies on the dimuon decay of J/ψ , $\psi(2S)$ and Υ mesons have shown that the total efficiency in the LHCb detector depends on the initial polarisation of the vector meson. The angular distribution of the muons is given by

$$\frac{dN}{d\cos \theta} = \frac{1 + \alpha \cos^2 \theta}{2 + 2 \cdot \alpha / 3}. \quad (7.3)$$

where θ is the angle between the μ^+ in the $\psi(2S)$ rest frame and the $\psi(2S)$ momentum direction in the laboratory frame. The value $\alpha = +1, -1, 0$ correspond to fully transverse, fully longitudinal, and zero polarisation, respectively. As the energy of the muons in the laboratory frame becomes very small when the muon is emitted backwards, the $\psi(2S)$ polarisation affects the energy distribution of the muons and therefore the detection efficiency.

The polarisation of $\psi(2S)$ mesons produced in pp collisions at $\sqrt{s} = 7$ TeV has been studied by LHCb [35]. There are no evidence of significant transverse or longitudinal polarisation observed for the region $2 \text{ GeV}/c < p_T < 15 \text{ GeV}/c$ and $2.0 < y < 4.5$. The CMS collaboration measured inclusive $\psi(2S)$ polarization in the p_T range $[14, 50] \text{ GeV}/c$ and $|y|$ in the range $[1.2, 1.5]$, the values of polarization are about 0 with the uncertainty of 0.1 for almost all the fiducial region [27]. Therefore, in this analysis the central values of the final results are obtained under the assumption of zero polarisation, while the systematic uncertainties are assigned by comparing the results with the polarisation parameter $\alpha = -0.2$, which is the typical value of $\psi(2S)$ polarization measured in the RUNI data. The unpolarised simulation sample is weighted according to Eq. 7.3, and all efficiencies are re-calculated. By comparing the new efficiencies and the nominal ones, the systematic uncertainties for $\psi(2S)$ mesons vary from 1.8% to 5.9% in different bins as shown in Fig. 7.10. As a result, in this analysis, we only make the cross-section

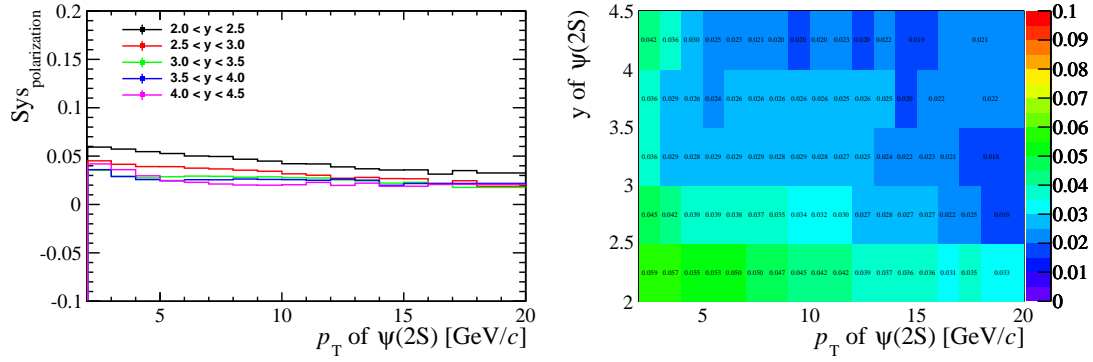


Figure 7.10: The relative difference for the ϵ_{tot} aroused by considering polarisation parameter $\alpha = -0.2$.

measurements assuming zero polarization and no systematic uncertainty is quoted on the cross-section related to this effect.

7.9 Other systematic uncertainties

- The uncertainty of $\mathcal{B}(\psi(2S) \rightarrow e^+e^-) = (7.89 \pm 0.17) \times 10^{-3}$ from PDG [47], is propagated to the cross-section measurement as 2.2% owing to the lepton universality.
- The relative uncertainty of the luminosity is 3.9%, which is propagated to the cross-section results.
- The limited size of the simulation sample used to determine the efficiencies is a source of systematic uncertainties. The uncertainties vary between 0.7% and 11.5% for prompt $\psi(2S)$ and vary between 0.8% and 5.7% for $\psi(2S)$ -from- b depending on the kinematic bins.
- A fraction of events are lost because of the QED radiative tail. The efficiency of the mass window is estimated using the simulated sample, and the imperfect modelling of the radiative decay is considered as a source of systematic uncertainty. This has been studied in previous analysis and the similar effect is expected. Therefore, as in previous RUN-II charmonium analysis ([49]) a value of 1% is quoted.

7.10 Summary of systematic uncertainties

In Table 7.1, the systematic uncertainties are summarized.

Table 7.1: Summary of the relative systematic uncertainties (%)

Quantity	Systematic uncertainty	Comment
Signal shape	0.0-4.1	Correlated between bins
Global event cuts(GECs)	0.5	Correlated between bins
Trigger	0.1-9.3	Correlated between bins
Tracking	(0.1-2.4) \oplus (2 \times 0.8)	Correlated between bins
Muon ID	(0.1-1.1) \oplus (0.1-4.6)	Correlated between bins
p_T - y -spectrum	0.0-2.0	Bin dependent
$\psi(2S)$ vertex fit	0.4	Correlated between bins
Radiative tail	1.0	Correlated between bins
Luminosity	3.9	Correlated between bins
$\mathcal{B}(\psi(2S) \rightarrow e^+e^-)$	2.2	Correlated between bins
simulated sample size	0.7-11.5(prompt $\psi(2S)$) 0.8-5.7($\psi(2S)$ -from- b)	Bin dependent
t_z fits	0.1-8.4	Only affects $\psi(2S)$ from b

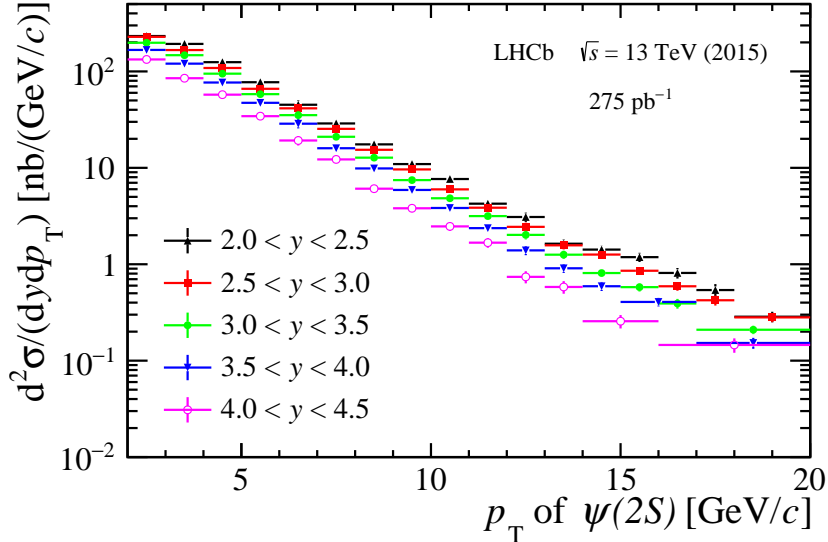


Figure 8.1: Differential cross-section for prompt $\psi(2S)$ in data as a function of p_T in bins of y , assuming that prompt $\psi(2S)$ are produced unpolarised. Statistical and systematic uncertainties are added in quadrature.

588 8 Results

589 With the signal yields determined from the fitting to dimuon invariant mass distributions,
 590 the efficiencies estimated from simulation and calibrated control sample, and the systematic
 591 uncertainties, the $\psi(2S)$ production cross-sections are measured. By integrating the
 592 double differential results over $p_T(y)$ one can obtain the single differential cross-section as
 593 functions of $y(p_T)$, which can be compared with theories. And also the total cross-sections
 594 can be obtained by integrating the double differential results over p_T and y bins.

595 The measured differential cross-sections for prompt $\psi(2S)$ and $\psi(2S)$ -from- b are shown
 596 in Figs. 8.1 and 8.2, respectively. Tables A.1 and A.2 in Appendix A give the measured
 597 double-differential cross-sections for prompt $\psi(2S)$ and $\psi(2S)$ -from- b in different (p_T, y)
 598 bins. The cross-sections results integrated over y or p_T are shown in Figs. 8.4 and Figs. 8.5,
 599 respectively.

600 The integrated cross-section for prompt $\psi(2S)$ and $\psi(2S)$ -from- b in the nominal
 601 kinematic range, summing over all kinematic bins, are:

$$\sigma_p = 1.430 \pm 0.005 \text{ (stat)} \pm 0.099 \text{ (syst)} \mu\text{b},$$

$$\sigma_b = 0.426 \pm 0.002 \text{ (stat)} \pm 0.030 \text{ (syst)} \mu\text{b},$$

602 where the first uncertainty is statistical and the second one systematic.

603 8.1 Fraction of $\psi(2S)$ -from- b

604 The fraction of $\psi(2S)$ -from- b production yields, $F_b = N_b/(N_b + N_p)$, which are corrected
 605 with the detection efficiencies for prompt $\psi(2S)$ and $\psi(2S)$ -from- b , is calculated in each
 606 kinematic bin. In Fig. 8.3 and Table 8.1, the fraction of $\psi(2S)$ -from- b in different kinematics
 607 bins are shown, where the uncertainties are dominated by statistical uncertainties and

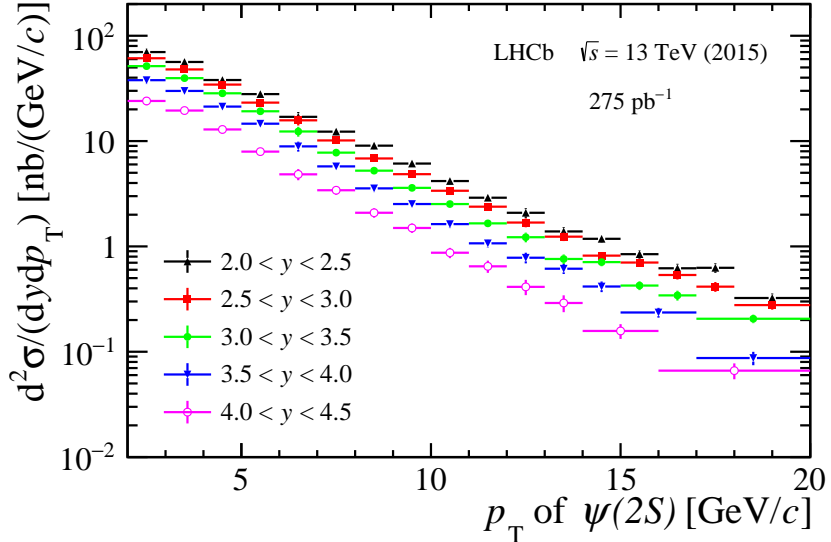


Figure 8.2: Differential cross-section for $\psi(2S)$ -from- b in data as a function of p_T for the various y bins, assuming that $\psi(2S)$ -from- b are produced unpolarised. Statistical and systematic uncertainties are added in quadrature.

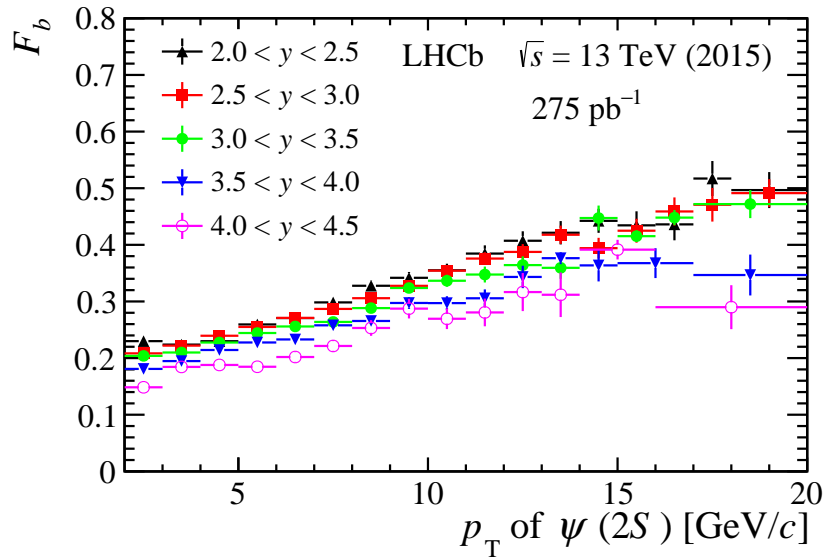


Figure 8.3: Fractions of $\psi(2S)$ -from- b in bins of $\psi(2S)$ p_T and y . The uncertainties are mainly from statistical ones and systematic uncertainties are negligible.

the systematic uncertainties are negligible ³. As we can see, the fraction F_b gradually increases as a function of p_T , especially for low rapidity y ; while in each specific p_T bin, F_b decreases with increasing y , which indicates that the b -hadrons are produced less forward than prompt $\psi(2S)$.

³ Only the systematic uncertainty due to the t_z background modelling contributes to the systematic uncertainty, and it is small enough to be neglected.

Table 8.1: The fraction of $\psi(2S)$ -from- b mesons (in %) in kinematic bins of the $\psi(2S)$ transverse momentum p_T and rapidity y . The uncertainties are mainly from statistical ones and systematic uncertainties are negligible.

p_T (GeV/c)	$2 < y < 2.5$	$2.5 < y < 3$	$3 < y < 3.5$	$3.5 < y < 4$	$4 < y < 4.5$
2-3	23.0 ± 0.6	20.8 ± 0.4	20.4 ± 0.4	18.1 ± 0.4	14.8 ± 0.5
3-4	22.4 ± 0.6	22.2 ± 0.4	21.0 ± 0.4	19.5 ± 0.4	18.4 ± 0.6
4-5	23.0 ± 0.6	23.9 ± 0.4	22.8 ± 0.4	21.4 ± 0.4	18.8 ± 0.7
5-6	25.9 ± 0.6	25.5 ± 0.4	24.4 ± 0.4	22.8 ± 0.5	18.5 ± 0.7
6-7	27.1 ± 0.7	27.1 ± 0.5	25.6 ± 0.5	23.3 ± 0.5	20.2 ± 1.0
7-8	29.8 ± 0.8	28.7 ± 0.5	26.4 ± 0.6	25.8 ± 0.7	22.1 ± 1.0
8-9	32.8 ± 0.9	30.6 ± 0.6	28.8 ± 0.7	26.6 ± 0.8	25.3 ± 1.4
9-10	34.2 ± 1.0	32.8 ± 0.8	32.4 ± 0.9	29.7 ± 1.0	28.7 ± 1.7
10-11	35.5 ± 1.2	35.4 ± 0.9	33.7 ± 1.1	29.7 ± 1.2	26.9 ± 1.8
11-12	38.5 ± 1.5	37.6 ± 1.1	34.8 ± 1.4	30.6 ± 1.6	28.1 ± 2.4
12-13	40.7 ± 1.7	38.7 ± 1.4	36.4 ± 1.5	34.3 ± 2.0	31.7 ± 3.4
13-14	42.1 ± 2.1	41.8 ± 1.6	35.9 ± 1.9	37.6 ± 1.0	31.2 ± 3.9
14-15	44.2 ± 2.1	39.4 ± 1.8	44.7 ± 2.2	36.4 ± 2.8	39.2 ± 1.7
15-16	43.4 ± 2.5	42.5 ± 2.1	41.5 ± 1.0	36.8 ± 2.6	—————
16-17	43.6 ± 2.8	45.9 ± 2.5	44.8 ± 1.3	—————	—————
17-18	51.7 ± 3.1	47.1 ± 3.0	—————	—————	—————
18-19	49.7 ± 3.2	49.1 ± 2.5	47.2 ± 2.5	34.7 ± 3.6	29.0 ± 3.9
19-20	—————	—————	—————	—————	—————

8.2 Comparison with theoretical models

The reported results are compared with the following theoretical models:

- NRQCD calculations [55] are compared for prompt $\psi(2S)$ cross-section as a function of transverse momentum integrated over y in the range $2 < y < 4.5$ in the left plot of Fig. 8.4. In the NRQCD calculations, only uncertainties associated with LDMEs are considered since it is the dominating uncertainty for absolute production cross-section predictions. Good agreement for $p_T > 7$ GeV/c is seen between NRQCD calculation and the measurement.
- FONLL calculations [36] are compared for $\psi(2S)$ -from- b cross-section as a function of transverse momentum integrated over y in the range $2 < y < 4.5$ in the right plot of Fig. 8.4. The $\psi(2S)$ -from- b cross-sections as functions of y integrated over p_T in the range $2 < p_T < 20$ GeV/c are also compared with FONLL calculations [56] for $\psi(2S)$ -from- b , as shown in right of Fig. 8.5. The FONLL calculation includes the uncertainties due to b -quark mass and renormalisation-factorisation scales for the prediction of absolute production cross-section. The calculation is consistent with our measurement.

8.3 Cross-section ratios between 13 TeV and 7 TeV

To compare the $\psi(2S)$ production cross-sections at 13 TeV with those at 7 TeV, we updated the production cross-sections of $\psi(2S)$ at 7 TeV with the 2011 data sample using the same

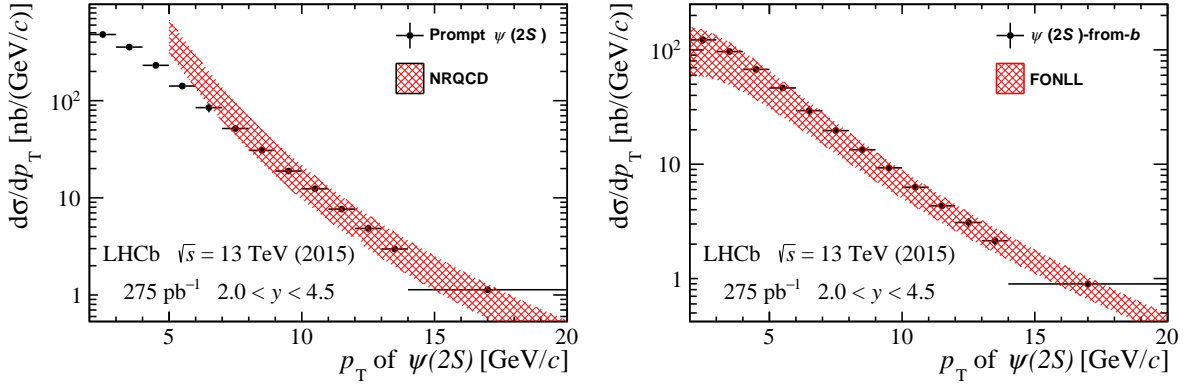


Figure 8.4: Differential cross-section as a function of p_T integrated over y between 2.0 and 4.5, (left) compared with the NRQCD calculation for prompt $\psi(2S)$ and (right) compared with the FONLL calculation for $\psi(2S)$ -from- b mesons.

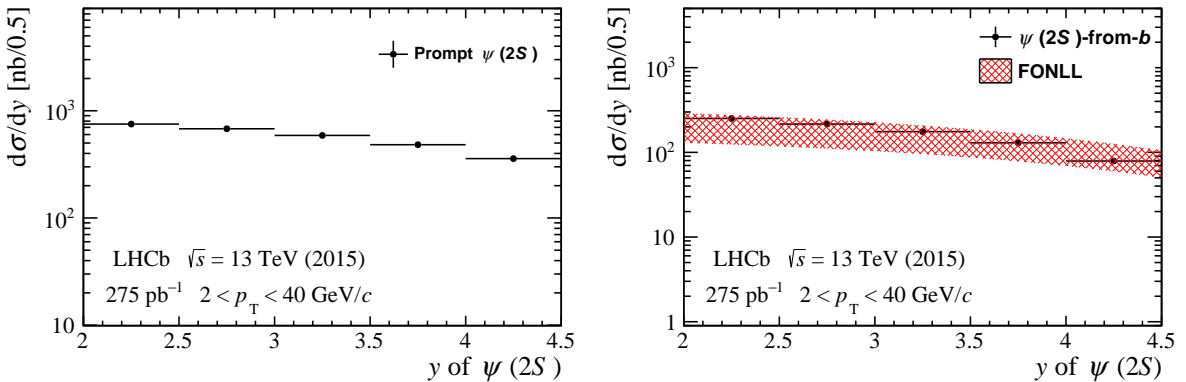


Figure 8.5: Differential cross-section as a function of y integrated over p_T between 2.0 and 20 GeV/c , (left) for prompt $\psi(2S)$ and (right) compared with the FONLL calculation for $\psi(2S)$ -from- b mesons.

analysis strategy. This allows us to provide the production ratio as a function of y ⁴. The details are presented in Appendix E. The production cross-section results are shown in Figs. 8.6, 8.7, 8.8 and 8.9. The corresponding values are listed in Tables 8.4 and 8.5.

The production ratio $R_{13/7} \equiv \sigma(13 \text{ TeV})/\sigma(7 \text{ TeV})$ is obtained as a function of p_T and y . In the ratio part of the systematic uncertainties cancel out. The correlations between the systematic uncertainties at 13 TeV and 7 TeV are considered as the following:

- $m_{\mu^+\mu^-}$ signal shape. Double CB functions are used to describe the $m_{\mu^+\mu^-}$ signal shape both in 13 TeV and 7 TeV measurements. This systematic uncertainty is correlated between the 13 TeV and 7 TeV analyses, however the correlation should not be 100%. So for a conservative estimation, we assume no correlation.
- Luminosity. The correlation of luminosity uncertainty between the 13 TeV and 7 TeV analyses is around 50% from the previous experience.

⁴ The production cross-section as a function of y was not measured in the analysis using the 2010 data sample [34].

Table 8.2: Differential cross-sections $d\sigma/dp_T$ (in nb/(GeV/c)) of prompt $\psi(2S)$ and $\psi(2S)$ -from- b mesons, integrated over y between 2.0 and 4.5. The first uncertainties are statistical and the second (third) are uncorrelated (correlated) systematic uncertainties amongst bins.

p_T (GeV/c)	Prompt $\psi(2S)$	$\psi(2S)$ -from- b
2-3	$479.94 \pm 3.97 \pm 3.08 \pm 37.31$	$122.26 \pm 1.38 \pm 0.91 \pm 9.56$
3-4	$356.19 \pm 2.69 \pm 2.29 \pm 17.79$	$96.62 \pm 1.02 \pm 0.66 \pm 5.27$
4-5	$231.12 \pm 1.64 \pm 1.56 \pm 16.92$	$67.47 \pm 0.71 \pm 0.45 \pm 4.95$
5-6	$141.52 \pm 0.98 \pm 1.04 \pm 8.99$	$46.43 \pm 0.49 \pm 0.34 \pm 2.98$
6-7	$84.84 \pm 0.65 \pm 0.68 \pm 8.92$	$29.40 \pm 0.35 \pm 0.21 \pm 3.10$
7-8	$51.72 \pm 0.44 \pm 0.48 \pm 3.52$	$19.68 \pm 0.26 \pm 0.16 \pm 1.34$
8-9	$30.80 \pm 0.30 \pm 0.32 \pm 2.11$	$13.38 \pm 0.20 \pm 0.12 \pm 0.92$
9-10	$18.87 \pm 0.22 \pm 0.23 \pm 0.99$	$9.29 \pm 0.16 \pm 0.08 \pm 0.49$
10-11	$12.39 \pm 0.17 \pm 0.18 \pm 0.82$	$6.29 \pm 0.12 \pm 0.07 \pm 0.42$
11-12	$7.65 \pm 0.13 \pm 0.13 \pm 0.44$	$4.33 \pm 0.10 \pm 0.05 \pm 0.26$
12-13	$4.84 \pm 0.11 \pm 0.10 \pm 0.43$	$3.09 \pm 0.08 \pm 0.04 \pm 0.28$
13-14	$2.98 \pm 0.07 \pm 0.06 \pm 0.23$	$2.14 \pm 0.06 \pm 0.03 \pm 0.17$
14-20	$1.13 \pm 0.02 \pm 0.02 \pm 0.06$	$0.90 \pm 0.02 \pm 0.01 \pm 0.05$

Table 8.3: Differential cross-sections $d\sigma/dy$ (in nb) of prompt $\psi(2S)$ and $\psi(2S)$ -from- b mesons, integrated over p_T between 2 and 20 GeV/c. The first uncertainties are statistical and the second (third) are uncorrelated (correlated) systematic uncertainties amongst bins.

y	Prompt $\psi(2S)$	$\psi(2S)$ -from- b
2.0-2.5	$751.4 \pm 7.7 \pm 7.6 \pm 51.8$	$251.2 \pm 2.8 \pm 2.3 \pm 17.6$
2.5-3.0	$679.1 \pm 4.6 \pm 2.4 \pm 46.7$	$215.9 \pm 1.6 \pm 0.7 \pm 15.0$
3.0-3.5	$588.7 \pm 3.7 \pm 2.0 \pm 40.4$	$175.8 \pm 1.4 \pm 0.6 \pm 12.7$
3.5-4.0	$482.3 \pm 2.9 \pm 1.9 \pm 33.2$	$129.6 \pm 1.2 \pm 0.5 \pm 9.1$
4.0-4.5	$357.8 \pm 2.8 \pm 2.3 \pm 25.6$	$79.0 \pm 1.4 \pm 0.5 \pm 5.7$

- Tracking. We assume the total tracking systematic uncertainty is 50% correlated.
- Vertexing. It is basically due to different distribution of $\psi(2S)$ vertex fit quality in MC simulations and data. We know that the MC simulations at 7 TeV and 13 TeV have similar distributions. Hence, it is reasonable to believe the consistent distributions for the two energy points in data. We assume 50% of the correlation between 13 TeV and 7 TeV data.
- Branching fraction. We use the same branching fraction value between 7 TeV and 13 TeV analyses. The correlation, therefore, is 100%, and the systematic uncertainty totally cancelled.
- MuonID. The systematic uncertainty of MuonID comes from two sources, the first class is the uncertainty of binning scheme, track multiplicity reweighting, the second source is the limited knowledge of muonID efficiency in data, which is given by the limited sample size of the MuonID calibration data. The first class is correlated among different analyses, while the second is uncorrelated. For a simple calculation, we assume MuonID systematic uncertainty 50% correlated.

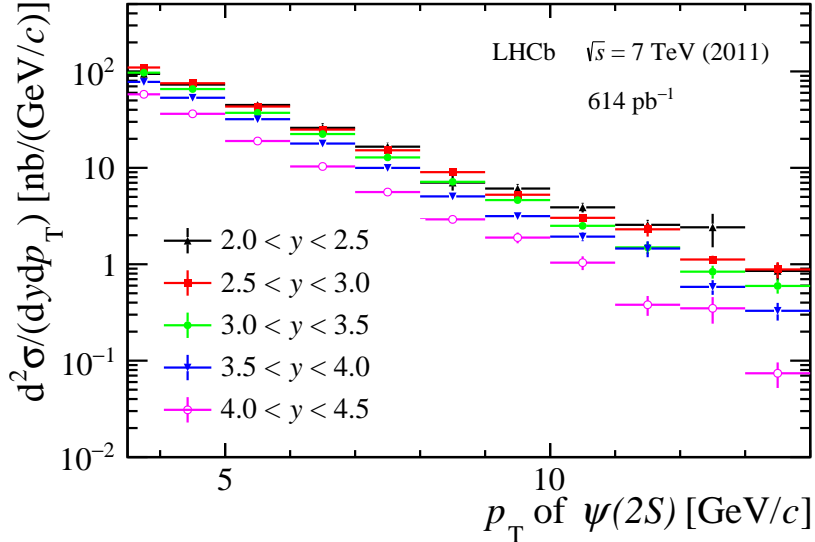


Figure 8.6: Differential cross-section for prompt $\psi(2S)$ in 2011 7 TeV data as a function of p_T in bins of y . Statistical and systematic uncertainties are added in quadrature.

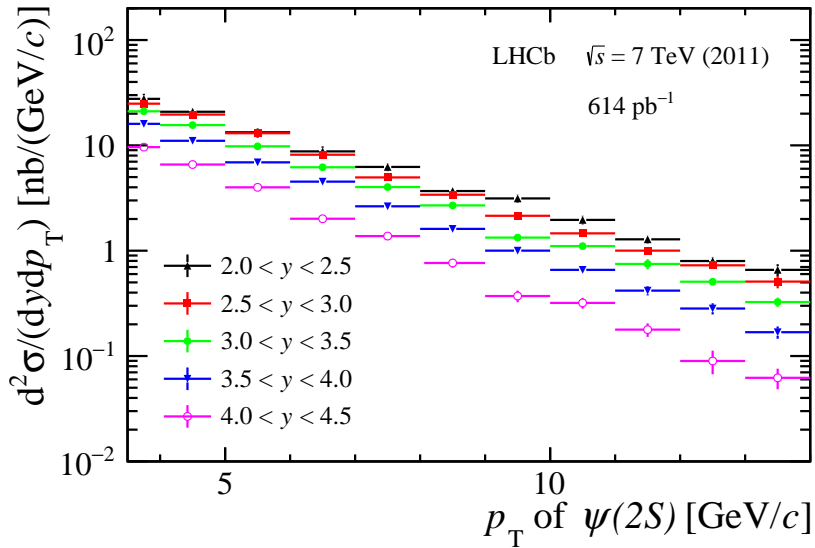


Figure 8.7: Differential cross-section for $\psi(2S)$ -from- b in 7 TeV data in 2011 as a function of p_T for the various y bins. Statistical and systematic uncertainties are added in quadrature.

- 658 • Trigger efficiency. The trigger systematic uncertainties are correlated between
 659 different analyses, and the remaining uncorrelated systematic uncertainties also
 660 exist. Due to variations of trigger requirements among different analyses, to be
 661 conservative, we assume the correlations are 50% between measurements at different
 662 energies.
- 663 • MC statistics. This is uncorrelated.
- 664 • Radiative tail. Both two analyses used similar models to describe radiative $\psi(2S)$
 665 decays, so this effect totally cancels (100% correlated) between different analysis.

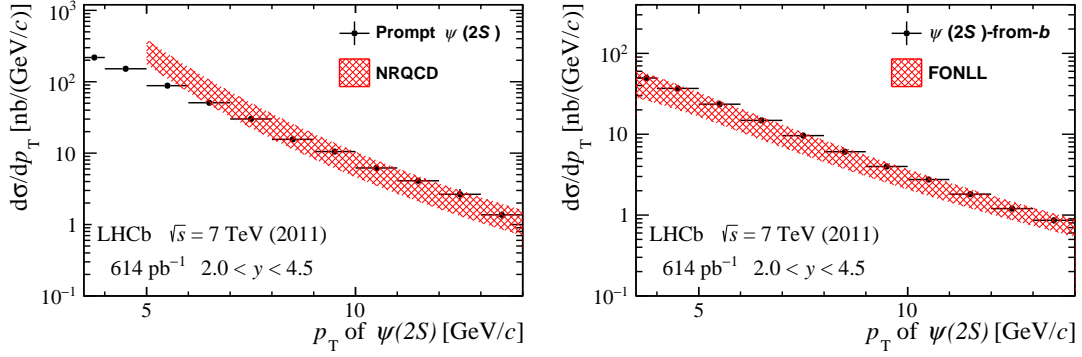


Figure 8.8: Differential cross-section as a function of p_T integrated over y between 2.0 and 4.5 in 7 TeV data in 2011, (left) compared with the NRQCD calculation for prompt $\psi(2S)$ and (right) compared with the FONLL calculation for $\psi(2S)$ -from- b mesons.

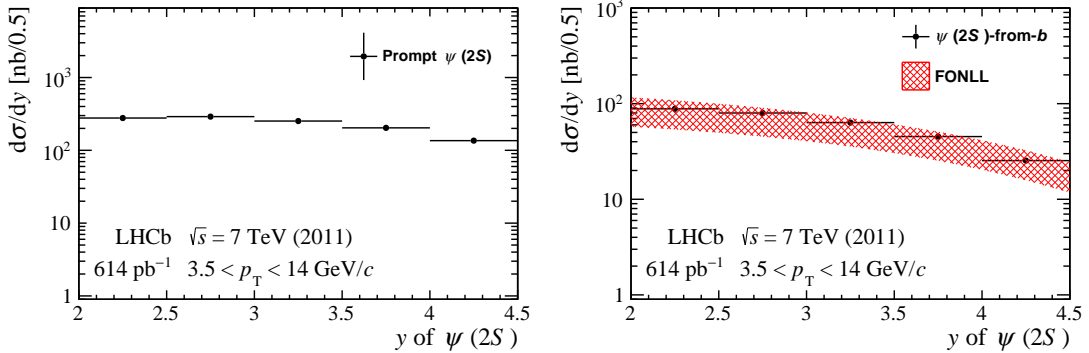


Figure 8.9: Differential cross-section as a function of y integrated over p_T between 3.5 and 14 GeV/c for 2011 7 TeV data, (left) for prompt $\psi(2S)$ and (right) compared with the FONLL calculation for $\psi(2S)$ -from- b mesons.

- 666 • p_T - y -spectrum. The relevant systematics are evaluated independent using different
667 MC samples for different analyses. So for a conservative estimation, we assume the
668 correlation is zero.
- 669 • Global event cuts (GEC). This uncertainty at 7 TeV is 0.45%, while that at 13 TeV
670 is 0.3%. For a conservative treatment, we take them as uncorrelated.
- 671 • t_z fit. This issue only affects the $\psi(2S)$ -from- b cross-section measurement. There
672 exist partial correlations between the different analyses, since the tail effects should
673 behave with some similarity. However, we also acknowledge they are not fully
674 correlated. To be conservative, its correlation is assumed to be uncorrelated.

675 Since the nominal results of both analyses take zero polarization assumption, the
676 polarization effect in the ratio is neglected.

677 In Figs. 8.10 and 8.11, the production cross-section ratio $R_{13/7}$ as a function of p_T
678 integrated over $2 < y < 4.5$ and the production cross-section ratio as a function of y
679 integrated over $3.5 < p_T < 14$ between the 13 TeV and 7 TeV measurements are given for
680 prompt $\psi(2S)$ and $\psi(2S)$ -from- b , taking into account the correlations of various systematic
681 uncertainties as discussed above. The numerical results are also given in Tables 8.6 and 8.7.

Table 8.4: Differential cross-sections $d\sigma/dp_T$ (in nb/(GeV/c)) of prompt $\psi(2S)$ and $\psi(2S)$ -from- b mesons, integrated over y between 2.0 and 4.5 for 2011 7 TeV data. The first uncertainties are statistical and the second (third) are uncorrelated (correlated) systematic uncertainties amongst bins.

p_T (GeV/c)	Prompt $\psi(2S)$	$\psi(2S)$ -from- b
3.5-4	$218.52 \pm 1.61 \pm 3.38 \pm 11.61$	$49.61 \pm 0.70 \pm 0.91 \pm 3.34$
4-5	$151.91 \pm 0.78 \pm 2.39 \pm 7.05$	$36.83 \pm 0.35 \pm 0.60 \pm 1.97$
5-6	$88.13 \pm 0.47 \pm 1.51 \pm 4.94$	$23.52 \pm 0.24 \pm 0.50 \pm 1.55$
6-7	$50.77 \pm 0.30 \pm 0.99 \pm 2.92$	$14.83 \pm 0.16 \pm 0.24 \pm 0.95$
7-8	$30.10 \pm 0.21 \pm 0.73 \pm 1.45$	$9.62 \pm 0.12 \pm 0.18 \pm 0.52$
8-9	$15.59 \pm 0.12 \pm 0.65 \pm 0.74$	$6.08 \pm 0.09 \pm 0.11 \pm 0.32$
9-10	$10.52 \pm 0.10 \pm 0.38 \pm 0.47$	$3.99 \pm 0.07 \pm 0.11 \pm 0.24$
10-11	$6.20 \pm 0.08 \pm 0.25 \pm 0.30$	$2.75 \pm 0.05 \pm 0.07 \pm 0.16$
11-12	$4.10 \pm 0.06 \pm 0.27 \pm 0.24$	$1.81 \pm 0.04 \pm 0.04 \pm 0.12$
12-13	$2.65 \pm 0.06 \pm 0.46 \pm 0.15$	$1.20 \pm 0.03 \pm 0.03 \pm 0.08$
13-14	$1.37 \pm 0.03 \pm 0.12 \pm 0.11$	$0.86 \pm 0.03 \pm 0.04 \pm 0.07$

Table 8.5: Differential cross-sections $d\sigma/dy$ (in nb) of prompt $\psi(2S)$ and $\psi(2S)$ -from- b mesons, integrated over p_T between 3.5 and 14 GeV/c for the 2011 7 TeV data. The first uncertainties are statistical and the second (third) are uncorrelated (correlated) systematic uncertainties amongst bins.

y	Prompt $\psi(2S)$	$\psi(2S)$ -from- b
2.0-2.5	$230.5 \pm 2.0 \pm 6.3 \pm 15.7$	$74.5 \pm 0.9 \pm 1.8 \pm 5.8$
2.5-3.0	$235.4 \pm 1.1 \pm 2.3 \pm 13.1$	$67.4 \pm 0.5 \pm 0.4 \pm 4.4$
3.0-3.5	$203.9 \pm 0.8 \pm 1.6 \pm 8.5$	$52.8 \pm 0.4 \pm 0.3 \pm 2.5$
3.5-4.0	$164.6 \pm 0.7 \pm 1.7 \pm 6.8$	$37.3 \pm 0.3 \pm 0.3 \pm 1.6$
4.0-4.5	$106.9 \pm 0.7 \pm 1.6 \pm 4.2$	$20.6 \pm 0.3 \pm 0.3 \pm 1.0$

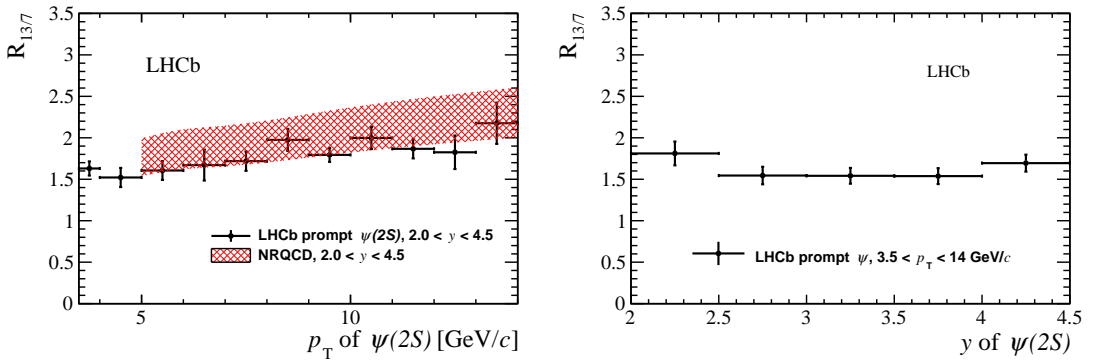


Figure 8.10: Ratio of differential cross-sections between the 13 TeV and 7 TeV measurements as a function of (left) p_T integrated over y , (right) y integrated over p_T for prompt $\psi(2S)$. Theoretical calculations of NRQCD [55] are compared to prompt $\psi(2S)$ mesons on the left side.

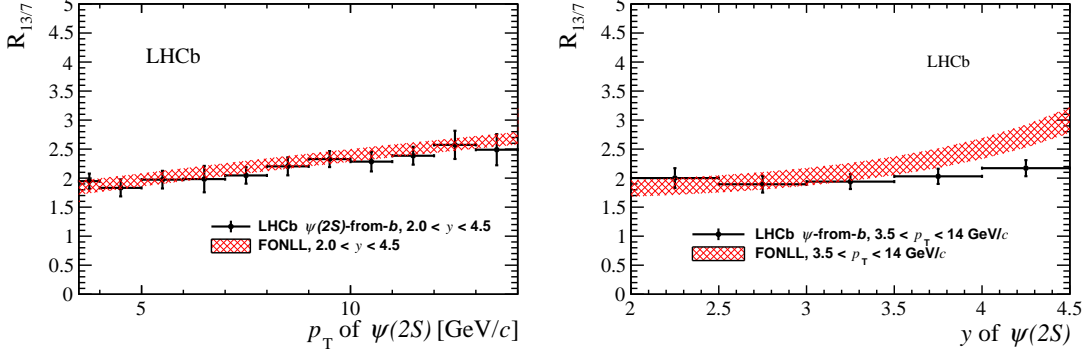


Figure 8.11: Ratio of differential cross-sections between the 13 TeV and the 7 TeV measurements as a function of (left) p_T integrated over y , (right) y integrated over p_T for $\psi(2S)$ -from- b . Theoretical FONLL calculations [56] are compared to the measured $\psi(2S)$ -from- b ratio.

Table 8.6: The ratio of cross-sections between measurements at 13 TeV and 7 TeV in different bins of p_T and integrated over y for $\psi(2S)$ from prompt productions and b -decays. The Statistical and systematic uncertainties are added in quadrature.

p_T (GeV/c)	Prompt $\psi(2S)$	$\psi(2S)$ -from- b
3.5-4	1.63 ± 0.09	1.95 ± 0.13
4-5	1.52 ± 0.12	1.83 ± 0.15
5-6	1.61 ± 0.11	1.97 ± 0.15
6-7	1.67 ± 0.19	1.98 ± 0.23
7-8	1.72 ± 0.12	2.05 ± 0.14
8-9	1.97 ± 0.13	2.20 ± 0.15
9-10	1.79 ± 0.08	2.33 ± 0.14
10-11	2.00 ± 0.13	2.28 ± 0.17
11-12	1.87 ± 0.12	2.39 ± 0.15
12-13	1.83 ± 0.20	2.57 ± 0.24
13-14	2.18 ± 0.25	2.49 ± 0.27

8.4 Calculations of the ratios of the $\psi(2S)$ and J/ψ cross-sections at 13 TeV

We make a comparison of our results with the J/ψ cross-section measurements in pp collisions at a centre-of-mass energy of 13 TeV [49]. To calculate their ratios, we need to

Table 8.7: The ratio of cross-sections between measurements at 13 TeV and 7 TeV in different bins of y and integrated over p_T for $\psi(2S)$ from prompt productions and b -decays. The Statistical and systematic uncertainties are added in quadrature.

y	Prompt $\psi(2S)$	$\psi(2S)$ -from- b
2.0-2.5	1.81 ± 0.14	2.00 ± 0.17
2.5-3.0	1.54 ± 0.11	1.89 ± 0.14
3.0-3.5	1.54 ± 0.10	1.94 ± 0.13
3.5-4.0	1.54 ± 0.10	2.03 ± 0.13
4.0-4.5	1.69 ± 0.10	2.17 ± 0.14

686 evaluate the correlations of various sources of systematic uncertainties between this two
687 analyses. The correlations are treated according the following rules:

- 688 • Signal mass shape. In this two analysis, both of them used two CB function to
689 describe the signal mass shape. This systematic uncertainty is correlated between
690 $\psi(2S)$ analysis and J/ψ analysis. We assume the correlation is 100%.
- 691 • Luminosity. The correlation of luminosity uncertainty between $\psi(2S)$ analysis and
692 J/ψ resulting the correlation 100% as we all used 2015 data. The uncertainty 3.9%
693 are the common value provided by the luminosity group.
- 694 • Tracking. We assume the tracking systematic uncertainty is correlated. Since the
695 same tracking environment is used and data are taken in same year, there should be
696 correlated between two analysis.
- 697 • Vertexing. This is due to different distribution of $\psi(2S)$ vertex fit quality in
698 simulation and data. We noticed that the J/ψ simulation and this analysis have
699 a similar distribution, and the value is almost same. We assume they are totally
700 correlated between $\psi(2S)$ and J/ψ analysis.
- 701 • Branching fraction. The systematic uncertainty between the two analysis is totally
702 uncorrelated.
- 703 • MuonID. The systematic uncertainty of MuonID comes from two sources, the first
704 class is the uncertainty of binning scheme, track multiplicity reweighting, the second
705 source is the limited knowledge of muonID efficiency in data, which is given by the
706 limited sample size of the MuonID calibration data. The first class is correlated
707 among different analyses, while the second is uncorrelated. We assume MuonID
708 systematic uncertainty is uncorrelated.
- 709 • Trigger efficiency. The trigger requirements in this two analysis is different. The
710 systematic uncertainties due to the trigger efficiencies are considered to be fully
711 uncorrelated.
- 712 • Simulated sample size. This is Uncorrelated.
- 713 • Radiative tail. This effect can be cancelled as this two analysis cite the same value
714 in same place.
- 715 • p_T - y -spectrum. The numbers are evaluated independent using different simulated
716 samples for different analyses and also J/ψ analysis didn't consider this effect. So
717 for a conservative estimation, we assume the correlation is zero.
- 718 • Global event cuts (GEC). This is taken as uncorrelated as J/ψ analysis didn't have
719 this effect.
- 720 • t_z fit. This only affects the $\psi(2S)$ from b cross-section. We assume they are fully
721 correlated between the different analyses, since they use same methods to estimate
722 the uncertainties.

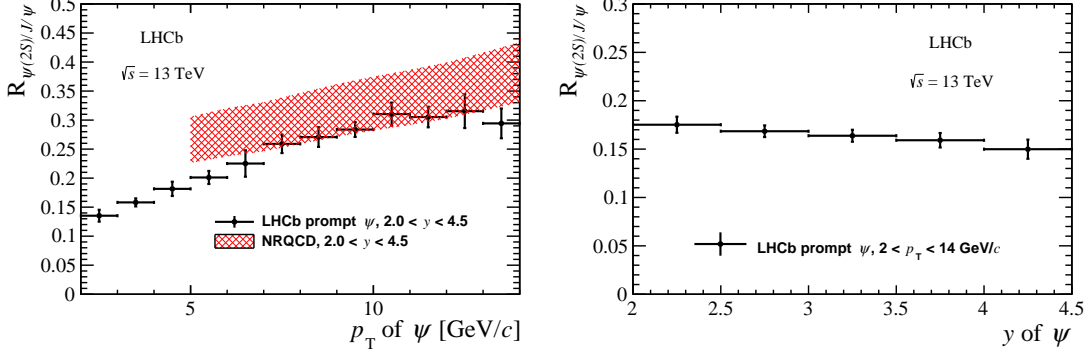


Figure 8.12: Ratio of differential cross-sections between $\psi(2S)$ and J/ψ measurement as a function of (left) p_T integrated over y , (right) y integrated over p_T for prompt $\psi(2S)$. Theoretical calculations of NRQCD [55] are compared to prompt $\psi(2S)$ mesons on the left side.

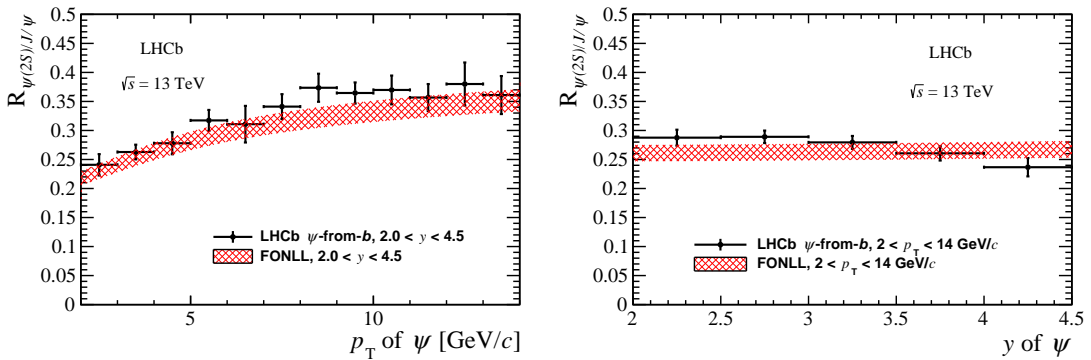


Figure 8.13: Ratio of differential cross-sections between $\psi(2S)$ and J/ψ measurement as a function of (left) p_T integrated over y , (right) y integrated over p_T for $\psi(2S)$ from b . Theoretical FONLL calculations [56] are compared to the measured $\psi(2S)$ -from- b ratio.

In Figs. 8.12 and 8.13, cross-section ratio as a function of p_T (y) integrated over $2 < y < 4.5$ ($2 < p_T < 14$) between $\psi(2S)$ analysis and J/ψ analysis at 13 TeV are given for prompt productions and b -decay-productions, taking into account the correlations of various systematic uncertainties as discussed above. The detailed numbers are given in Tables 8.8 and 8.9.

8.5 Measurement of the inclusive branching fraction $\mathcal{B}(b \rightarrow \psi(2S)X)$

The reported results of $\sigma(\psi(2S)\text{-from-}b, 13 \text{ TeV})$, in combination with the previous results about J/ψ production [49], can be used to determine the inclusive branching fraction $\mathcal{B}(b \rightarrow \psi(2S)X)$. To achieve this, both results must be extrapolated to the full phase space, as they are measured only for a limited range of phase space. The extrapolation factors for two decay channels, $\alpha_{4\pi}(\psi(2S))$ and $\alpha_{4\pi}(J/\psi)$, are determined using the LHCb-tuned Pythia 8 [57] (Pythia 6 [37] for J/ψ measurement). The factors $\alpha_{4\pi}(\psi(2S))$ and $\alpha_{4\pi}(J/\psi)$ are found to be 7.29 and 5.20, respectively. All $\alpha_{4\pi}$ factors, obtained by Pythia or by FONLL, are listed in Tab. 8.10. In the ratio of the two factors, $\xi \equiv \frac{\alpha_{4\pi}(\psi(2S))}{\alpha_{4\pi}(J/\psi)} = 1.402$, most of the theoretical uncertainties are expected to be cancelled. Although, additional

Table 8.8: The ratio of cross-sections between measurements of $\psi(2S)$ and J/ψ at 13 TeV in different bins of p_T and integrated over y for prompt productions and b -decay-productions. The Statistical and systematic uncertainties are added in quadrature.

p_T (GeV/c)	Prompt production	from- b -decay
2-3	0.14 ± 0.01	0.24 ± 0.02
3-4	0.16 ± 0.01	0.26 ± 0.01
4-5	0.18 ± 0.01	0.28 ± 0.02
5-6	0.20 ± 0.01	0.32 ± 0.02
6-7	0.23 ± 0.02	0.31 ± 0.03
7-8	0.26 ± 0.02	0.34 ± 0.02
8-9	0.27 ± 0.02	0.37 ± 0.02
9-10	0.28 ± 0.01	0.36 ± 0.02
10-11	0.31 ± 0.02	0.37 ± 0.02
11-12	0.31 ± 0.02	0.36 ± 0.02
12-13	0.32 ± 0.03	0.38 ± 0.04
13-14	0.29 ± 0.03	0.36 ± 0.03

Table 8.9: The ratio of cross-sections between measurements of $\psi(2S)$ and J/ψ at 13 TeV in different bins of y and integrated over p_T for prompt productions and b -decay-productions. The Statistical and systematic uncertainties are added in quadrature.

y	Prompt production	from- b -decay
2.0-2.5	0.18 ± 0.01	0.29 ± 0.01
2.5-3.0	0.17 ± 0.01	0.29 ± 0.01
3.0-3.5	0.16 ± 0.01	0.28 ± 0.01
3.5-4.0	0.16 ± 0.01	0.26 ± 0.01
4.0-4.5	0.15 ± 0.01	0.24 ± 0.02

⁷³⁹ uncertainty, arising from additional model uncertainties, equal to 3 % can be assigned to
⁷⁴⁰ the ξ parameter. With the definition of the ratio ξ , it follows

$$\frac{\mathcal{B}(b \rightarrow \psi(2S)X)}{\mathcal{B}(b \rightarrow J/\psi X)} = \xi \frac{\sigma(\psi(2S)\text{-from-}b, 13 \text{ TeV})}{\sigma(J/\psi\text{-from-}b, 13 \text{ TeV}).} \quad (8.1)$$

⁷⁴¹ By inserting the value $\sigma(J/\psi\text{-from-}b, 13 \text{ TeV}) = 2.25 \pm 0.01(\text{stat}) \pm 0.14(\text{syst})$ and the
⁷⁴² value of ξ , it gives

$$\frac{\mathcal{B}(b \rightarrow \psi(2S)X)}{\mathcal{B}(b \rightarrow J/\psi X)} = 0.265 \pm 0.002(\text{stat}) \pm 0.015(\text{syst}) \pm 0.006(\text{BF}),$$

⁷⁴³ where possible correlations between uncertainties originates from $\psi(2S)\text{-from-}b$ and
⁷⁴⁴ $J/\psi\text{-from-}b$, respectively, are taken into account as what is done in Section 8.4. The last
⁷⁴⁵ uncertainty originates from the uncertainty of the branching fractions $\mathcal{B}(\psi(2S) \rightarrow e^+e^-)$
⁷⁴⁶ and $\mathcal{B}(J/\psi \rightarrow \mu^+\mu^-)$. Using the known value $\mathcal{B}(b \rightarrow J/\psi X) = (1.16 \pm 0.10) \times 10^{-2}$ [31],
⁷⁴⁷ one obtains

$$\mathcal{B}(b \rightarrow \psi(2S)X) = (3.08 \pm 0.02(\text{stat}) \pm 0.18(\text{syst}) \pm 0.27(\text{BF})) \times 10^{-3}.$$

748 The $\mathcal{B}(b \rightarrow J/\psi X)$ uncertainty dominates the total uncertainty originates from branching
 749 fractions. This result is in agreement with the world-average value [31], while succeeding
 750 the previous measurement done reported by the LHCb [34] with significantly improved
 751 statistical uncertainty.

	$\psi(2S)$	J/ψ	$\xi [-]$
Pythia 8 (J/ψ : 6)	7.288	5.079	1.435
Pythia 6	N/A	5.200	1.402*
FONLL CTEQ6.6	6.993	4.961	1.410
NNPDF30_nlo_as_0118	6.838	4.907	1.394

Table 8.10: List of $\alpha_{4\pi}$ parameters and their ratios obtained from Pythia and FONLL using different PDFs (CTEQ6.6, NNPDF30_nlo_as_011) for 13 TeV. Pythia 6 was used in order to obtain $\alpha_{4\pi}$ of J/ψ . * The ratio is done with respect to $\alpha_{4\pi}(\psi(2S))$ obtained via Pythia 8

752 8.6 Comparison with polarised results at 13 TeV

753 In order to further studies about possible polarisation of $\psi(2S)$, cross-section measure-
 754 ment was done also with polarisation based on polarisation measurements at 7 TeV [35].
 755 Polarisation factor, based on aforementioned measurement, was calculated for every bin,
 756 no global factor was assigned. Results, single differential cross-section as function of p_T
 757 (y) is shown at the Table 8.11 (8.12). Only the polarisation parameter λ_{theta} is taken as
 758 non-zero.

759 Results are compatible with the results obtained under the assumption of no polarisa-
 760 tion (shown at the Table 8.2, 8.3), where the largest deviations can be seen for high p_T
 761 bins, where the largest relative change between measurements is up to 4.3 %, still much
 762 smaller than total systematic uncertainty.

Table 8.11: Differential cross-sections $d\sigma/dp_T$ (in nb/(GeV/c)) of prompt $\psi(2S)$ and $\psi(2S)$ -from- b mesons, integrated over y between 2.0 and 4.5. The first uncertainties are statistical and the second (third) are uncorrelated (correlated) systematic uncertainties amongst bins.

p_T (GeV/c)	Prompt $\psi(2S)$	$\psi(2S)$ -from- b
2-3	$479.34 \pm 3.96 \pm 3.07 \pm 37.26$	$122.10 \pm 1.38 \pm 0.91 \pm 9.55$
3-4	$355.82 \pm 2.69 \pm 2.29 \pm 17.77$	$96.52 \pm 1.02 \pm 0.66 \pm 5.26$
4-5	$230.87 \pm 1.63 \pm 1.56 \pm 16.90$	$67.40 \pm 0.71 \pm 0.45 \pm 4.95$
5-6	$141.70 \pm 0.98 \pm 1.05 \pm 9.00$	$46.49 \pm 0.49 \pm 0.34 \pm 2.99$
6-7	$84.95 \pm 0.65 \pm 0.68 \pm 8.93$	$29.44 \pm 0.35 \pm 0.21 \pm 3.10$
7-8	$52.34 \pm 0.45 \pm 0.49 \pm 3.56$	$19.92 \pm 0.26 \pm 0.17 \pm 1.36$
8-9	$31.15 \pm 0.31 \pm 0.33 \pm 2.14$	$13.54 \pm 0.20 \pm 0.12 \pm 0.93$
9-10	$19.10 \pm 0.22 \pm 0.23 \pm 1.00$	$9.41 \pm 0.16 \pm 0.08 \pm 0.50$
10-11	$11.81 \pm 0.16 \pm 0.17 \pm 0.78$	$6.00 \pm 0.11 \pm 0.06 \pm 0.40$
11-12	$7.34 \pm 0.12 \pm 0.12 \pm 0.42$	$4.14 \pm 0.09 \pm 0.05 \pm 0.25$
12-13	$4.63 \pm 0.11 \pm 0.09 \pm 0.41$	$2.97 \pm 0.08 \pm 0.04 \pm 0.27$
13-14	$2.87 \pm 0.07 \pm 0.06 \pm 0.22$	$2.06 \pm 0.06 \pm 0.03 \pm 0.16$
14-20	$1.09 \pm 0.02 \pm 0.02 \pm 0.06$	$0.86 \pm 0.02 \pm 0.01 \pm 0.05$

Table 8.12: Differential cross-sections $d\sigma/dy$ (in nb) of prompt $\psi(2S)$ and $\psi(2S)$ -from- b mesons, integrated over p_T between 2 and 20 GeV/c. The first uncertainties are statistical and the second (third) are uncorrelated (correlated) systematic uncertainties amongst bins.

y	Prompt $\psi(2S)$	$\psi(2S)$ -from- b
2.0-2.5	$750.3 \pm 7.6 \pm 7.6 \pm 51.7$	$250.6 \pm 2.8 \pm 2.3 \pm 17.6$
2.5-3.0	$678.7 \pm 4.6 \pm 2.4 \pm 46.7$	$215.6 \pm 1.6 \pm 0.7 \pm 15.0$
3.0-3.5	$588.4 \pm 3.7 \pm 2.0 \pm 40.3$	$175.7 \pm 1.4 \pm 0.6 \pm 12.7$
3.5-4.0	$481.9 \pm 2.9 \pm 1.9 \pm 33.2$	$129.5 \pm 1.2 \pm 0.5 \pm 9.1$
4.0-4.5	$357.6 \pm 2.8 \pm 2.3 \pm 25.6$	$78.9 \pm 1.4 \pm 0.5 \pm 5.7$

763 9 Conclusion

764 The production cross-sections of $\psi(2S)$ mesons in proton-proton collisions at a centre-
765 of-mass energy $\sqrt{s} = 13\text{ TeV}$ are reported with a data sample corresponding to an
766 integrated luminosity of $275 \pm 11\text{ pb}^{-1}$, collected by the LHCb detector in 2015. The
767 double differential cross-sections, as functions of p_{T} and y of the $\psi(2S)$ meson in the
768 range of $2 < p_{\text{T}} < 20\text{ GeV}/c$ and $2.0 < y < 4.5$, are determined for prompt $\psi(2S)$ mesons
769 and $\psi(2S)$ mesons from b -hadron decays. The measured prompt $\psi(2S)$ production cross-
770 section as a function of transverse momentum is in good agreement at high p_{T} region
771 with theoretical calculations in the NRQCD framework. Theoretical predictions based
772 on the FONLL calculations describe well the measured cross-sections for $\psi(2S)$ mesons
773 from b -hadron decays. An updated measurement of $\psi(2S)$ production cross-sections at
774 7 TeV is performed using the 2011 data sample. The results between 13 TeV and 7 TeV
775 are compared. They show reasonable agreement with the theoretical calculated ratios.

776 **A** Tables of cross section results

Table A.1: Double differential production cross-section in nb (GeV/c) for prompt $\psi(2S)$ mesons in bins of (p_T, y). The first uncertainties are statistical, the second are the uncorrelated systematic uncertainties shared between bins and the last are the correlated systematic uncertainties.

p_T (GeV/c)	$2 < y < 2.5$	$2.5 < y < 3$	$3 < y < 3.5$	$3.5 < y < 4$	$4 < y < 4.5$
2-3	$232.86 \pm 5.80 \pm 5.39 \pm 18.24$	$228.46 \pm 3.53 \pm 1.65 \pm 17.70$	$198.36 \pm 2.86 \pm 1.34 \pm 15.33$	$167.07 \pm 2.19 \pm 1.30 \pm 12.93$	$133.13 \pm 1.99 \pm 1.62 \pm 10.42$
3-4	$192.93 \pm 3.96 \pm 4.02 \pm 9.74$	$166.62 \pm 2.36 \pm 1.27 \pm 8.22$	$147.39 \pm 1.90 \pm 1.07 \pm 7.25$	$120.42 \pm 1.49 \pm 0.96 \pm 6.00$	$85.03 \pm 1.42 \pm 1.09 \pm 4.37$
4-5	$124.73 \pm 2.38 \pm 2.70 \pm 9.15$	$108.56 \pm 1.41 \pm 0.88 \pm 7.92$	$94.79 \pm 1.09 \pm 0.74 \pm 6.90$	$76.73 \pm 0.93 \pm 0.68 \pm 5.59$	$57.41 \pm 1.00 \pm 0.82 \pm 4.28$
5-6	$77.27 \pm 1.46 \pm 1.78 \pm 4.89$	$66.05 \pm 0.82 \pm 0.59 \pm 4.16$	$58.12 \pm 0.65 \pm 0.52 \pm 3.65$	$47.25 \pm 0.44 \pm 0.48 \pm 2.98$	$34.35 \pm 0.66 \pm 0.58 \pm 2.29$
6-7	$45.13 \pm 0.91 \pm 1.11 \pm 4.73$	$41.43 \pm 0.53 \pm 0.43 \pm 4.34$	$35.20 \pm 0.43 \pm 0.37 \pm 3.69$	$28.70 \pm 0.39 \pm 0.36 \pm 3.01$	$19.22 \pm 0.47 \pm 0.38 \pm 2.08$
7-8	$28.87 \pm 0.62 \pm 0.77 \pm 1.95$	$25.38 \pm 0.35 \pm 0.32 \pm 1.70$	$21.00 \pm 0.30 \pm 0.27 \pm 1.41$	$15.97 \pm 0.27 \pm 0.25 \pm 1.07$	$12.23 \pm 0.32 \pm 0.31 \pm 0.91$
8-9	$17.52 \pm 0.42 \pm 0.49 \pm 1.19$	$15.39 \pm 0.25 \pm 0.24 \pm 1.04$	$12.75 \pm 0.22 \pm 0.20 \pm 0.86$	$9.86 \pm 0.20 \pm 0.19 \pm 0.67$	$6.08 \pm 0.21 \pm 0.18 \pm 0.47$
9-10	$10.94 \pm 0.29 \pm 0.34 \pm 0.56$	$9.63 \pm 0.18 \pm 0.18 \pm 0.48$	$7.46 \pm 0.16 \pm 0.14 \pm 0.38$	$5.90 \pm 0.15 \pm 0.15 \pm 0.30$	$3.81 \pm 0.16 \pm 0.14 \pm 0.26$
10-11	$7.66 \pm 0.23 \pm 0.28 \pm 0.50$	$5.98 \pm 0.14 \pm 0.13 \pm 0.39$	$4.84 \pm 0.13 \pm 0.11 \pm 0.31$	$3.83 \pm 0.12 \pm 0.11 \pm 0.25$	$2.47 \pm 0.11 \pm 0.11 \pm 0.19$
11-12	$4.25 \pm 0.16 \pm 0.17 \pm 0.23$	$3.86 \pm 0.11 \pm 0.10 \pm 0.21$	$3.16 \pm 0.10 \pm 0.09 \pm 0.17$	$2.37 \pm 0.09 \pm 0.08 \pm 0.13$	$1.67 \pm 0.10 \pm 0.09 \pm 0.13$
12-13	$3.09 \pm 0.13 \pm 0.16 \pm 0.27$	$2.44 \pm 0.13 \pm 0.07 \pm 0.21$	$2.02 \pm 0.08 \pm 0.07 \pm 0.18$	$1.39 \pm 0.07 \pm 0.06 \pm 0.12$	$0.74 \pm 0.06 \pm 0.05 \pm 0.07$
13-14	$1.63 \pm 0.09 \pm 0.08 \pm 0.12$	$1.57 \pm 0.07 \pm 0.06 \pm 0.12$	$1.26 \pm 0.06 \pm 0.05 \pm 0.09$	$0.91 \pm 0.05 \pm 0.04 \pm 0.07$	$0.58 \pm 0.06 \pm 0.04 \pm 0.05$
14-15	$1.42 \pm 0.08 \pm 0.08 \pm 0.07$	$1.26 \pm 0.06 \pm 0.05 \pm 0.06$	$0.81 \pm 0.05 \pm 0.04 \pm 0.04$	$0.59 \pm 0.04 \pm 0.04 \pm 0.03$	$0.26 \pm 0.03 \pm 0.02 \pm 0.02$
15-16	$1.18 \pm 0.08 \pm 0.09 \pm 0.06$	$0.86 \pm 0.05 \pm 0.04 \pm 0.04$	$0.58 \pm 0.04 \pm 0.03 \pm 0.03$	$0.41 \pm 0.03 \pm 0.02 \pm 0.02$	
16-17	$0.81 \pm 0.06 \pm 0.07 \pm 0.04$	$0.59 \pm 0.04 \pm 0.03 \pm 0.03$	$0.39 \pm 0.03 \pm 0.03 \pm 0.02$		
17-18	$0.54 \pm 0.05 \pm 0.06 \pm 0.03$	$0.42 \pm 0.03 \pm 0.03 \pm 0.02$			
18-19	$0.29 \pm 0.02 \pm 0.02 \pm 0.01$	$0.28 \pm 0.02 \pm 0.02 \pm 0.02$	$0.21 \pm 0.01 \pm 0.01 \pm 0.01$	$0.15 \pm 0.01 \pm 0.01 \pm 0.01$	$0.15 \pm 0.01 \pm 0.02 \pm 0.01$
19-20					

Table A.2: Double differential production cross-section in nb (GeV/c) for $\psi(2S)$ -from- b mesons in bins of (p_T, y) . The first uncertainties are statistical, the second are the uncorrelated systematic uncertainties shared between bins and the last are the correlated systematic uncertainties.

p_T (GeV/c)	$2 < y < 2.5$	$2.5 < y < 3$	$3 < y < 3.5$	$3.5 < y < 4$	$4 < y < 4.5$
2-3	69.99 \pm 1.94 \pm 1.65 \pm 5.51	61.15 \pm 1.14 \pm 0.48 \pm 4.78	51.47 \pm 0.97 \pm 0.40 \pm 3.99	37.86 \pm 0.87 \pm 0.35 \pm 2.95	24.04 \pm 0.94 \pm 0.36 \pm 1.89
3-4	56.37 \pm 1.45 \pm 1.17 \pm 3.05	47.89 \pm 0.83 \pm 0.36 \pm 2.45	39.58 \pm 0.70 \pm 0.31 \pm 2.45	29.92 \pm 0.64 \pm 0.27 \pm 1.57	19.49 \pm 0.70 \pm 0.29 \pm 1.01
4-5	37.99 \pm 1.00 \pm 0.78 \pm 2.80	34.38 \pm 0.58 \pm 0.25 \pm 2.51	28.42 \pm 0.48 \pm 0.21 \pm 2.08	21.25 \pm 0.45 \pm 0.19 \pm 1.55	12.89 \pm 0.50 \pm 0.20 \pm 0.97
5-6	27.93 \pm 0.72 \pm 0.60 \pm 1.77	23.18 \pm 0.40 \pm 0.18 \pm 1.46	19.18 \pm 0.34 \pm 0.15 \pm 1.24	14.62 \pm 0.24 \pm 0.14 \pm 0.94	7.94 \pm 0.35 \pm 0.14 \pm 0.56
6-7	16.99 \pm 0.49 \pm 0.37 \pm 1.78	15.74 \pm 0.29 \pm 0.13 \pm 1.65	12.33 \pm 0.24 \pm 0.11 \pm 1.29	8.91 \pm 0.22 \pm 0.10 \pm 0.94	4.83 \pm 0.25 \pm 0.09 \pm 0.52
7-8	12.29 \pm 0.37 \pm 0.28 \pm 0.83	10.14 \pm 0.21 \pm 0.09 \pm 0.68	7.77 \pm 0.18 \pm 0.08 \pm 0.53	5.75 \pm 0.17 \pm 0.07 \pm 0.39	3.41 \pm 0.18 \pm 0.08 \pm 0.26
8-9	9.05 \pm 0.29 \pm 0.20 \pm 0.62	6.84 \pm 0.16 \pm 0.07 \pm 0.46	5.24 \pm 0.14 \pm 0.06 \pm 0.36	3.56 \pm 0.13 \pm 0.05 \pm 0.24	2.09 \pm 0.13 \pm 0.05 \pm 0.16
9-10	6.12 \pm 0.22 \pm 0.13 \pm 0.32	4.85 \pm 0.13 \pm 0.06 \pm 0.24	3.60 \pm 0.11 \pm 0.05 \pm 0.19	2.53 \pm 0.10 \pm 0.04 \pm 0.13	1.50 \pm 0.10 \pm 0.05 \pm 0.10
10-11	4.17 \pm 0.16 \pm 0.11 \pm 0.27	3.38 \pm 0.11 \pm 0.05 \pm 0.22	2.52 \pm 0.09 \pm 0.04 \pm 0.16	1.63 \pm 0.08 \pm 0.03 \pm 0.11	0.87 \pm 0.06 \pm 0.03 \pm 0.07
11-12	2.90 \pm 0.13 \pm 0.07 \pm 0.16	2.38 \pm 0.09 \pm 0.04 \pm 0.13	1.66 \pm 0.08 \pm 0.03 \pm 0.11	1.07 \pm 0.06 \pm 0.03 \pm 0.06	0.65 \pm 0.06 \pm 0.03 \pm 0.06
12-13	2.09 \pm 0.11 \pm 0.06 \pm 0.19	1.68 \pm 0.07 \pm 0.03 \pm 0.15	1.22 \pm 0.06 \pm 0.03 \pm 0.11	0.78 \pm 0.05 \pm 0.02 \pm 0.07	0.41 \pm 0.05 \pm 0.02 \pm 0.04
13-14	1.39 \pm 0.08 \pm 0.04 \pm 0.11	1.24 \pm 0.06 \pm 0.03 \pm 0.09	0.76 \pm 0.05 \pm 0.02 \pm 0.06	0.61 \pm 0.04 \pm 0.02 \pm 0.05	0.29 \pm 0.04 \pm 0.02 \pm 0.03
14-15	1.18 \pm 0.07 \pm 0.04 \pm 0.06	0.82 \pm 0.05 \pm 0.02 \pm 0.04	0.71 \pm 0.05 \pm 0.02 \pm 0.04	0.42 \pm 0.04 \pm 0.02 \pm 0.02	0.16 \pm 0.02 \pm 0.01 \pm 0.02
15-16	0.84 \pm 0.06 \pm 0.03 \pm 0.04	0.70 \pm 0.05 \pm 0.02 \pm 0.04	0.42 \pm 0.03 \pm 0.01 \pm 0.03	0.24 \pm 0.02 \pm 0.01 \pm 0.02	0.07 \pm 0.01 \pm 0.00 \pm 0.01
16-17	0.62 \pm 0.05 \pm 0.02 \pm 0.03	0.54 \pm 0.04 \pm 0.02 \pm 0.03	0.34 \pm 0.03 \pm 0.01 \pm 0.02		
17-18	0.63 \pm 0.05 \pm 0.03 \pm 0.04	0.41 \pm 0.03 \pm 0.02 \pm 0.02			
18-19	0.32 \pm 0.03 \pm 0.01 \pm 0.02	0.28 \pm 0.02 \pm 0.01 \pm 0.02	0.21 \pm 0.01 \pm 0.01 \pm 0.01	0.09 \pm 0.01 \pm 0.00 \pm 0.01	
19-20					

Table A.3: Double differential production cross-section in nb (GeV/c) for prompt $\psi(2S)$ mesons in bins of (p_T, y) . The first uncertainties are statistical, the second are the uncorrelated systematic uncertainties shared between bins and the last are the correlated systematic uncertainties. Results under the assumption of polarisation.

p_T (GeV/c)	$2 < y < 2.5$	$2.5 < y < 3$	$3 < y < 3.5$	$3.5 < y < 4$	$4 < y < 4.5$
2-3	$232.31 \pm 5.79 \pm 5.38 \pm 18.19$	$228.28 \pm 3.52 \pm 1.65 \pm 17.68$	$198.17 \pm 2.86 \pm 1.34 \pm 15.32$	$166.90 \pm 2.19 \pm 1.30 \pm 12.92$	$133.02 \pm 1.99 \pm 1.62 \pm 10.41$
3-4	$192.59 \pm 3.95 \pm 4.01 \pm 9.72$	$166.51 \pm 2.36 \pm 1.27 \pm 8.21$	$147.27 \pm 1.90 \pm 1.07 \pm 7.25$	$120.32 \pm 1.48 \pm 0.96 \pm 6.00$	$84.96 \pm 1.42 \pm 1.09 \pm 4.36$
4-5	$124.50 \pm 2.38 \pm 2.70 \pm 9.13$	$108.48 \pm 1.41 \pm 0.88 \pm 7.91$	$94.71 \pm 1.09 \pm 0.74 \pm 6.90$	$76.68 \pm 0.93 \pm 0.68 \pm 5.59$	$57.37 \pm 1.00 \pm 0.82 \pm 4.28$
5-6	$77.42 \pm 1.46 \pm 1.79 \pm 4.90$	$66.14 \pm 0.82 \pm 0.59 \pm 4.16$	$58.18 \pm 0.66 \pm 0.52 \pm 3.66$	$47.30 \pm 0.44 \pm 0.48 \pm 2.98$	$34.37 \pm 0.66 \pm 0.58 \pm 2.29$
6-7	$45.21 \pm 0.91 \pm 1.12 \pm 4.74$	$41.49 \pm 0.53 \pm 0.43 \pm 4.35$	$35.24 \pm 0.43 \pm 0.37 \pm 3.69$	$28.73 \pm 0.39 \pm 0.36 \pm 3.01$	$19.23 \pm 0.47 \pm 0.39 \pm 2.08$
7-8	$29.35 \pm 0.64 \pm 0.79 \pm 1.98$	$25.69 \pm 0.36 \pm 0.33 \pm 1.72$	$21.21 \pm 0.30 \pm 0.27 \pm 1.42$	$16.12 \pm 0.27 \pm 0.25 \pm 1.08$	$12.32 \pm 0.32 \pm 0.31 \pm 0.91$
8-9	$17.80 \pm 0.42 \pm 0.50 \pm 1.21$	$15.57 \pm 0.25 \pm 0.24 \pm 1.05$	$12.88 \pm 0.22 \pm 0.20 \pm 0.87$	$9.94 \pm 0.20 \pm 0.19 \pm 0.67$	$6.12 \pm 0.22 \pm 0.19 \pm 0.47$
9-10	$11.11 \pm 0.30 \pm 0.34 \pm 0.56$	$9.75 \pm 0.19 \pm 0.19 \pm 0.49$	$7.54 \pm 0.16 \pm 0.14 \pm 0.38$	$5.96 \pm 0.15 \pm 0.15 \pm 0.30$	$3.84 \pm 0.16 \pm 0.14 \pm 0.26$
10-11	$7.19 \pm 0.21 \pm 0.26 \pm 0.47$	$5.72 \pm 0.13 \pm 0.13 \pm 0.37$	$4.64 \pm 0.12 \pm 0.11 \pm 0.30$	$3.68 \pm 0.11 \pm 0.10 \pm 0.24$	$2.39 \pm 0.10 \pm 0.11 \pm 0.19$
11-12	$4.02 \pm 0.15 \pm 0.16 \pm 0.22$	$3.70 \pm 0.10 \pm 0.09 \pm 0.20$	$3.05 \pm 0.10 \pm 0.09 \pm 0.17$	$2.28 \pm 0.09 \pm 0.08 \pm 0.13$	$1.63 \pm 0.10 \pm 0.09 \pm 0.13$
12-13	$2.92 \pm 0.13 \pm 0.14 \pm 0.26$	$2.34 \pm 0.12 \pm 0.07 \pm 0.21$	$1.94 \pm 0.08 \pm 0.06 \pm 0.17$	$1.35 \pm 0.07 \pm 0.05 \pm 0.12$	$0.73 \pm 0.06 \pm 0.05 \pm 0.07$
13-14	$1.56 \pm 0.08 \pm 0.08 \pm 0.12$	$1.51 \pm 0.06 \pm 0.05 \pm 0.11$	$1.22 \pm 0.06 \pm 0.05 \pm 0.09$	$0.88 \pm 0.05 \pm 0.04 \pm 0.07$	$0.56 \pm 0.06 \pm 0.04 \pm 0.05$
14-15	$1.36 \pm 0.08 \pm 0.08 \pm 0.07$	$1.21 \pm 0.06 \pm 0.05 \pm 0.06$	$0.78 \pm 0.05 \pm 0.03 \pm 0.04$	$0.58 \pm 0.04 \pm 0.03 \pm 0.03$	$0.25 \pm 0.03 \pm 0.02 \pm 0.02$
15-16	$1.13 \pm 0.07 \pm 0.08 \pm 0.06$	$0.83 \pm 0.04 \pm 0.04 \pm 0.04$	$0.56 \pm 0.03 \pm 0.03 \pm 0.03$	$0.39 \pm 0.03 \pm 0.02 \pm 0.02$	$0.14 \pm 0.01 \pm 0.02 \pm 0.01$
16-17	$0.77 \pm 0.06 \pm 0.07 \pm 0.04$	$0.57 \pm 0.04 \pm 0.03 \pm 0.03$	$0.38 \pm 0.03 \pm 0.03 \pm 0.02$		
17-18	$0.51 \pm 0.04 \pm 0.06 \pm 0.03$	$0.41 \pm 0.03 \pm 0.03 \pm 0.02$			
18-19	$0.28 \pm 0.02 \pm 0.02 \pm 0.01$	$0.27 \pm 0.02 \pm 0.02 \pm 0.02$	$0.20 \pm 0.01 \pm 0.01 \pm 0.01$	$0.15 \pm 0.01 \pm 0.01 \pm 0.01$	
19-20					

Table A.4: Double differential production cross-section in nb (GeV/c) for $\psi(2S)$ -from- b mesons in bins of (p_T, y) . The first uncertainties are statistical, the second are the uncorrelated systematic uncertainties shared between bins and the last are the correlated systematic uncertainties. Results under the assumption of polarisation.

p_T (GeV/c)	$2 < y < 2.5$	$2.5 < y < 3$	$3 < y < 3.5$	$3.5 < y < 4$	$4 < y < 4.5$
2-3	$69.82 \pm 1.94 \pm 1.64 \pm 5.50$	$61.11 \pm 1.14 \pm 0.48 \pm 4.78$	$51.43 \pm 0.97 \pm 0.40 \pm 3.99$	$37.82 \pm 0.87 \pm 0.35 \pm 2.94$	$24.01 \pm 0.94 \pm 0.36 \pm 1.89$
3-4	$56.26 \pm 1.45 \pm 1.17 \pm 3.05$	$47.85 \pm 0.83 \pm 0.36 \pm 2.45$	$39.55 \pm 0.70 \pm 0.31 \pm 2.44$	$29.90 \pm 0.64 \pm 0.27 \pm 1.57$	$19.47 \pm 0.70 \pm 0.29 \pm 1.01$
4-5	$37.93 \pm 1.00 \pm 0.78 \pm 2.80$	$34.35 \pm 0.58 \pm 0.25 \pm 2.51$	$28.40 \pm 0.48 \pm 0.21 \pm 2.08$	$21.24 \pm 0.45 \pm 0.19 \pm 1.55$	$12.88 \pm 0.50 \pm 0.20 \pm 0.97$
5-6	$27.98 \pm 0.72 \pm 0.60 \pm 1.77$	$23.22 \pm 0.40 \pm 0.18 \pm 1.46$	$19.20 \pm 0.34 \pm 0.15 \pm 1.24$	$14.64 \pm 0.24 \pm 0.14 \pm 0.94$	$7.95 \pm 0.35 \pm 0.14 \pm 0.56$
6-7	$17.02 \pm 0.49 \pm 0.37 \pm 1.78$	$15.76 \pm 0.29 \pm 0.13 \pm 1.65$	$12.35 \pm 0.24 \pm 0.11 \pm 1.29$	$8.91 \pm 0.22 \pm 0.10 \pm 0.94$	$4.84 \pm 0.25 \pm 0.09 \pm 0.53$
7-8	$12.49 \pm 0.37 \pm 0.29 \pm 0.84$	$10.26 \pm 0.21 \pm 0.09 \pm 0.69$	$7.84 \pm 0.18 \pm 0.08 \pm 0.53$	$5.80 \pm 0.17 \pm 0.08 \pm 0.39$	$3.44 \pm 0.18 \pm 0.08 \pm 0.26$
8-9	$9.19 \pm 0.29 \pm 0.21 \pm 0.63$	$6.92 \pm 0.17 \pm 0.07 \pm 0.47$	$5.29 \pm 0.14 \pm 0.06 \pm 0.36$	$3.59 \pm 0.13 \pm 0.05 \pm 0.24$	$2.10 \pm 0.13 \pm 0.05 \pm 0.16$
9-10	$6.22 \pm 0.22 \pm 0.14 \pm 0.32$	$4.91 \pm 0.13 \pm 0.06 \pm 0.25$	$3.63 \pm 0.11 \pm 0.05 \pm 0.19$	$2.55 \pm 0.10 \pm 0.05 \pm 0.13$	$1.51 \pm 0.10 \pm 0.05 \pm 0.10$
10-11	$3.94 \pm 0.15 \pm 0.10 \pm 0.26$	$3.23 \pm 0.10 \pm 0.04 \pm 0.21$	$2.43 \pm 0.09 \pm 0.04 \pm 0.16$	$1.57 \pm 0.08 \pm 0.03 \pm 0.10$	$0.84 \pm 0.06 \pm 0.03 \pm 0.07$
11-12	$2.75 \pm 0.13 \pm 0.07 \pm 0.15$	$2.28 \pm 0.08 \pm 0.03 \pm 0.13$	$1.59 \pm 0.07 \pm 0.03 \pm 0.10$	$1.03 \pm 0.06 \pm 0.03 \pm 0.06$	$0.63 \pm 0.06 \pm 0.03 \pm 0.06$
12-13	$1.98 \pm 0.10 \pm 0.05 \pm 0.18$	$1.62 \pm 0.06 \pm 0.03 \pm 0.14$	$1.18 \pm 0.06 \pm 0.03 \pm 0.10$	$0.75 \pm 0.05 \pm 0.02 \pm 0.07$	$0.40 \pm 0.05 \pm 0.02 \pm 0.04$
13-14	$1.32 \pm 0.08 \pm 0.04 \pm 0.10$	$1.19 \pm 0.06 \pm 0.02 \pm 0.09$	$0.74 \pm 0.05 \pm 0.02 \pm 0.06$	$0.60 \pm 0.04 \pm 0.02 \pm 0.05$	$0.28 \pm 0.04 \pm 0.02 \pm 0.03$
14-15	$1.13 \pm 0.07 \pm 0.03 \pm 0.06$	$0.79 \pm 0.05 \pm 0.02 \pm 0.04$	$0.69 \pm 0.04 \pm 0.02 \pm 0.04$	$0.40 \pm 0.04 \pm 0.02 \pm 0.02$	$0.15 \pm 0.02 \pm 0.01 \pm 0.02$
15-16	$0.80 \pm 0.06 \pm 0.03 \pm 0.04$	$0.68 \pm 0.04 \pm 0.02 \pm 0.03$	$0.41 \pm 0.03 \pm 0.01 \pm 0.02$	$0.23 \pm 0.02 \pm 0.01 \pm 0.02$	$0.06 \pm 0.01 \pm 0.00 \pm 0.01$
16-17	$0.59 \pm 0.05 \pm 0.02 \pm 0.03$	$0.52 \pm 0.04 \pm 0.02 \pm 0.03$	$0.33 \pm 0.03 \pm 0.01 \pm 0.02$		
17-18	$0.60 \pm 0.05 \pm 0.02 \pm 0.04$	$0.40 \pm 0.03 \pm 0.02 \pm 0.02$			
18-19	$0.31 \pm 0.03 \pm 0.01 \pm 0.02$	$0.27 \pm 0.02 \pm 0.01 \pm 0.02$	$0.20 \pm 0.01 \pm 0.01 \pm 0.01$		
19-20					

777 B Tables of the fit results in each kinematic bin

778 For each kinematic bin of $\psi(2S)$ candidates, the mass fitted value of μ_{mass} (mean
779 value of narrower Gaussian), σ_{mass} (width of narrower Gaussian), n_{sig} (signal yields),
780 n_{bkg} (background number), $1000p_0$ (parameter in exponential function) and t_z -mass com-
781 bine fitted value β (fraction of first Gaussian of signal resolution function), $1000\mu_{t_z}$ (bias
782 of t_z distribution), $S(1, 2)_{t_z}$ ($\sigma_{1,2}$ of first/second Gaussian resolution function convolved
783 with the t_z function), τ_b (effective b -hadron lifetime), n_{bkg} , n_{prompt} (number of prompt
784 $\psi(2S)$), $n_{b-decay}$ (number of $\psi(2S)$ -from- b) and n_{tail} (number of events in tail) are given
785 in Tables B.1-B.5.

786 For each kinematic bin of $\psi(2S)$ candidates, the tzbkg fitted value of , β (fraction
787 of first Gaussian of background resolution function), $1000\mu_{tzbkg}$ (bias of background t_z
788 distribution), $S(1, 2)_{tzbkg}$ ($\sigma'_{1,2}$ correct factor of first/second Gaussian resolution function
789 which will be convolved with the t_z background function), $\tau_{1,2,3,4}$ (exponentials parameters),
790 $f_{1,2,3,4}$ (fraction of each exponentials component), are given in Tables B.6-B.10.

Table B.1: The parameters of the invariant mass and t_z fit, including the fitted yields and the shape parameters for different p_T bins in the rapidity bin $2.0 < y < 2.5$.

parameters	p_T (GeV/c)						
	2-3	3-4	4-5	5-6	6-7	7-8	8-9
μ_{mass}	3687.4 ± 0.4	3687.4 ± 0.3	3687.4 ± 0.3	3687.1 ± 0.3	3687.3 ± 0.3	3686.6 ± 0.3	3687.2 ± 0.3
σ_{mass}	12.9 ± 0.4	13.4 ± 0.3	13.4 ± 0.3	13.7 ± 0.3	13.5 ± 0.3	14.7 ± 0.3	15.1 ± 0.4
n_{sg}	13454 ± 381	13169 ± 304	11178 ± 230	9346 ± 181	7076 ± 141	5622 ± 116	4354 ± 94
n_{btg}	282562 ± 644	154568 ± 484	80491 ± 349	42746 ± 257	22851 ± 189	11831 ± 140	6415 ± 105
$1000 * p_0$	-0.36 ± 0.03	-0.57 ± 0.04	-0.60 ± 0.05	-0.51 ± 0.07	-0.52 ± 0.10	-0.37 ± 0.14	-0.51 ± 0.19
$1000 * \mu_{tz}$	-9.6 ± 1.2	-6.2 ± 1.0	-4.8 ± 1.0	-5.7 ± 0.9	-1.9 ± 0.9	-2.3 ± 0.9	-0.6 ± 1.0
$S1_{tz}$	1.81 ± 0.11	1.30 ± 0.06	1.10 ± 0.04	1.22 ± 0.08	1.45 ± 0.22	1.57 ± 0.20	1.44 ± 0.34
$S2_{tz}$	0.65 ± 0.04	0.61 ± 0.06	0.51 ± 0.12	0.69 ± 0.11	0.85 ± 0.10	0.82 ± 0.07	0.94 ± 0.13
β_{tz}	0.38 ± 0.05	0.62 ± 0.08	0.89 ± 0.06	0.69 ± 0.14	0.38 ± 0.20	0.37 ± 0.13	0.33 ± 0.33
τ_b	1.59 ± 0.04	1.58 ± 0.04	1.54 ± 0.04	1.49 ± 0.04	1.50 ± 0.04	1.41 ± 0.04	1.41 ± 0.04
n_{prompt}	10535 ± 262	10273 ± 211	8530 ± 163	6919 ± 131	5158 ± 104	3935 ± 85	2927 ± 69
n_{decay}	3109 ± 86	2953 ± 76	2556 ± 67	2424 ± 62	1914 ± 55	1674 ± 50	1426 ± 45
n_{tail}	0 ± 2	0 ± 3	8 ± 6	0 ± 2	0 ± 2	0 ± 2	3 ± 3
parameters	11-12	12-13	13-14	14-15	15-16	16-17	17-18
	3687.2 ± 0.5	3686.8 ± 0.6	3687.0 ± 0.7	3688.0 ± 0.8	3687.4 ± 0.9	3686.7 ± 1.2	3688.5 ± 1.5
μ_{mass}	15.6 ± 0.5	16.7 ± 0.6	15.3 ± 0.7	16.6 ± 0.8	16.8 ± 0.9	19.4 ± 1.3	20.0 ± 1.8
σ_{mass}	1666 ± 52	1290 ± 47	876 ± 38	790 ± 35	573 ± 30	433 ± 26	368 ± 27
n_{sg}	1425 ± 50	1006 ± 44	692 ± 35	454 ± 30	353 ± 26	206 ± 22	221 ± 24
n_{btg}	-0.83 ± 0.40	-0.51 ± 0.48	-1.31 ± 0.57	-0.64 ± 0.71	-0.26 ± 0.78	-0.00 ± 0.76	-0.00 ± 0.38
$1000 * p_0$	-1.5 ± 1.2	-2.3 ± 1.5	-3.0 ± 1.6	3.3 ± 1.9	-1.6 ± 2.3	0.4 ± 2.5	-1.0 ± 2.7
$1000 * \mu_{tz}$	1.81 ± 0.38	3.28 ± 1.03	2.28 ± 0.50	1.77 ± 0.38	1.61 ± 0.22	1.55 ± 0.19	1.72 ± 0.67
$S1_{tz}$	0.89 ± 0.06	1.09 ± 0.05	0.90 ± 0.08	0.90 ± 0.17	0.85 ± 0.28	0.69 ± 0.32	1.04 ± 0.21
$S2_{tz}$	0.19 ± 0.11	0.05 ± 0.04	0.21 ± 0.09	0.42 ± 0.24	0.70 ± 0.24	0.79 ± 0.19	0.29 ± 0.37
β_{tz}	1.41 ± 0.06	1.45 ± 0.07	1.37 ± 0.09	1.59 ± 0.10	1.48 ± 0.11	1.36 ± 0.11	1.41 ± 0.12
τ_b	1027 ± 38	766 ± 33	508 ± 27	440 ± 25	328 ± 21	246 ± 18	180 ± 16
n_{prompt}	642 ± 29	526 ± 26	370 ± 23	349 ± 21	252 ± 18	191 ± 16	193 ± 16
n_{decay}	0 ± 1	0 ± 1	0 ± 4	0 ± 1	0 ± 1	3 ± 3	0 ± 1
n_{tail}							0 ± 2
parameters	18-20						

Table B.2: The parameters of the invariant mass and t_z fit, including the fitted yields and the shape parameters for different p_T bins in the rapidity bin $2.5 < y < 3.0$.

parameters	p_T (GeV/c)									
	2-3	3-4	4-5	5-6	6-7	7-8	8-9	9-10	10-11	
μ_{mass}	3686.5 ± 0.2	3686.5 ± 0.2	3686.6 ± 0.2	3686.4 ± 0.2	3686.0 ± 0.2	3685.6 ± 0.2	3685.8 ± 0.2	3685.4 ± 0.3	3685.9 ± 0.4	
σ_{mass}	13.0 ± 0.3	13.2 ± 0.2	13.8 ± 0.2	14.2 ± 0.2	14.9 ± 0.2	14.8 ± 0.2	14.7 ± 0.2	15.2 ± 0.3	15.7 ± 0.4	
n_{sig}	34711 ± 639	31628 ± 507	27597 ± 390	21737 ± 281	16482 ± 208	11679 ± 154	7998 ± 120	5647 ± 97	3822 ± 80	
n_{bkg}	747512 ± 1057	457670 ± 827	233199 ± 598	100765 ± 397	42137 ± 262	18860 ± 176	9470 ± 126	5007 ± 94	2950 ± 74	
$1000 * p_0$	-0.49 ± 0.02	-0.65 ± 0.02	-0.52 ± 0.03	-0.37 ± 0.05	-0.34 ± 0.07	-0.42 ± 0.11	-0.63 ± 0.15	-0.54 ± 0.21	-0.54 ± 0.28	
$1000 * \mu_{tz}$	-6.7 ± 0.8	-5.7 ± 0.7	-5.5 ± 0.6	-2.6 ± 0.5	-1.9 ± 0.5	-2.9 ± 0.5	-2.1 ± 0.6	-1.3 ± 0.6	-0.8 ± 0.8	
$S1_{tz}$	1.70 ± 0.07	1.25 ± 0.05	1.37 ± 0.10	1.25 ± 0.06	1.32 ± 0.09	1.45 ± 0.09	1.30 ± 0.08	1.53 ± 0.13	1.69 ± 0.63	
$S2_{tz}$	0.73 ± 0.03	0.63 ± 0.05	0.79 ± 0.05	0.73 ± 0.08	0.72 ± 0.07	0.79 ± 0.05	0.79 ± 0.08	0.81 ± 0.07	1.07 ± 0.08	
β_{tz}	0.42 ± 0.04	0.61 ± 0.07	0.43 ± 0.11	0.65 ± 0.12	0.56 ± 0.12	0.47 ± 0.09	0.57 ± 0.14	0.45 ± 0.12	0.13 ± 0.21	
τ_b	1.62 ± 0.03	1.57 ± 0.03	1.47 ± 0.02	1.52 ± 0.03	1.47 ± 0.03	1.45 ± 0.03	1.42 ± 0.03	1.36 ± 0.04	1.51 ± 0.05	
n_{prompt}	27779 ± 429	24621 ± 349	20961 ± 272	16197 ± 200	11986 ± 152	8337 ± 116	5551 ± 90	3807 ± 73	2465 ± 58	
n_{decay}	7257 ± 135	7023 ± 122	6605 ± 112	5543 ± 96	4458 ± 83	3352 ± 69	2445 ± 58	1854 ± 50	1353 ± 42	
n_{tail}	0 ± 4	28 ± 19	35 ± 19	29 ± 15	12 ± 10	37 ± 10	0 ± 2	0 ± 3	0 ± 3	
parameters	11-12	12-13	13-14	14-15	15-16	16-17	17-18	18-20		
	3685.5 ± 0.4	3685.4 ± 0.5	3685.7 ± 0.6	3686.0 ± 0.7	3684.7 ± 0.8	3687.0 ± 1.0	3684.0 ± 1.2	3684.9 ± 1.0		
μ_{mass}	15.8 ± 0.4	16.3 ± 0.5	15.5 ± 0.6	16.9 ± 0.7	17.2 ± 0.7	17.6 ± 0.9	17.6 ± 1.3	18.2 ± 0.9		
σ_{mass}	2689 ± 64	1862 ± 54	1286 ± 45	982 ± 38	744 ± 33	545 ± 29	399 ± 26	536 ± 28		
n_{sig}	1743 ± 56	1152 ± 47	814 ± 39	501 ± 31	364 ± 27	269 ± 23	222 ± 22	239 ± 22		
n_{bkg}	-0.00 ± 0.18	-0.94 ± 0.45	-1.45 ± 0.53	-0.00 ± 0.56	-1.22 ± 0.80	-0.92 ± 0.93	-0.16 ± 1.54	-1.20 ± 0.99		
$1000 * p_0$	-1.8 ± 0.9	-1.0 ± 0.9	-3.1 ± 1.2	0.6 ± 1.4	-0.7 ± 1.6	-0.4 ± 1.6	1.0 ± 2.0	-0.7 ± 1.5		
$1000 * \mu_{tz}$	2.05 ± 0.61	1.16 ± 0.22	1.62 ± 0.63	1.62 ± 0.20	1.39 ± 0.11	1.44 ± 0.33	1.90 ± 0.50	1.02 ± 0.11		
$S1_{tz}$	1.04 ± 0.06	0.99 ± 5.45	0.97 ± 0.18	0.84 ± 0.12	0.56 ± 0.19	0.74 ± 0.18	0.82 ± 0.15	0.43 ± 0.84		
$S2_{tz}$	0.12 ± 0.10	0.99 ± 0.50	0.26 ± 0.36	0.48 ± 0.16	0.81 ± 0.12	0.49 ± 0.28	0.37 ± 0.20	0.94 ± 0.69		
β_{tz}	1.35 ± 0.05	1.52 ± 0.06	1.42 ± 0.07	1.33 ± 0.08	1.37 ± 0.09	1.49 ± 0.11	1.35 ± 0.11	1.45 ± 0.10		
τ_b	1673 ± 47	1110 ± 58	752 ± 32	597 ± 28	429 ± 23	293 ± 20	212 ± 17	270 ± 18		
n_{prompt}	1006 ± 36	736 ± 29	539 ± 26	388 ± 22	317 ± 20	249 ± 18	188 ± 16	261 ± 18		
n_{decay}	5 ± 5	9 ± 4	0 ± 3	0 ± 4	0 ± 1	0 ± 3	2 ± 2	0 ± 2		
n_{tail}										

Table B.3: The parameters of the invariant mass and t_z fit, including the fitted yields and the shape parameters for different p_T bins in the rapidity bin $3.0 < y < 3.5$.

parameters	p_T (GeV/c)								
	2-3	3-4	4-5	5-6	6-7	7-8	8-9	9-10	
μ_{mass}	3685.9 ± 0.3	3685.9 ± 0.2	3685.7 ± 0.2	3685.6 ± 0.2	3685.0 ± 0.2	3684.8 ± 0.2	3685.1 ± 0.3	3685.1 ± 0.3	3685.1 ± 0.3
σ_{mass}	15.1 ± 0.3	14.8 ± 0.2	15.1 ± 0.2	15.4 ± 0.2	16.3 ± 0.2	16.3 ± 0.2	16.5 ± 0.3	16.6 ± 0.4	16.6 ± 0.4
n_{sig}	37056 ± 653	34400 ± 527	29059 ± 372	21639 ± 254	15215 ± 189	10136 ± 140	6745 ± 110	4398 ± 87	
n_{bkg}	675557 ± 1032	426766 ± 818	178380 ± 536	67390 ± 332	27263 ± 218	12245 ± 148	6150 ± 108	3336 ± 80	
$1000 * p_0$	-0.54 ± 0.02	-0.55 ± 0.02	-0.37 ± 0.03	-0.44 ± 0.06	-0.32 ± 0.09	-0.18 ± 0.14	-0.49 ± 0.19	-0.66 ± 0.26	
$1000 * \mu_{tz}$	-5.1 ± 0.7	-4.5 ± 0.6	-3.1 ± 0.5	-3.6 ± 0.4	-3.2 ± 0.4	-3.2 ± 0.5	-2.6 ± 0.6	-3.4 ± 0.7	
$S1_{tz}$	1.28 ± 0.05	1.68 ± 0.07	1.62 ± 0.07	1.32 ± 0.06	0.80 ± 0.05	1.67 ± 0.16	3.73 ± 0.71	1.73 ± 0.32	
$S2_{tz}$	0.61 ± 0.03	0.74 ± 0.02	0.76 ± 0.02	0.74 ± 0.04	1.45 ± 0.12	0.86 ± 0.03	0.99 ± 0.02	0.93 ± 0.05	
β_{tz}	0.57 ± 0.05	0.34 ± 0.04	0.34 ± 0.04	0.50 ± 0.08	0.63 ± 0.10	0.24 ± 0.07	0.06 ± 0.02	0.18 ± 0.10	
τ_b	1.58 ± 0.03	1.54 ± 0.03	1.50 ± 0.03	1.42 ± 0.03	1.47 ± 0.03	1.44 ± 0.04	1.49 ± 0.04	1.43 ± 0.04	
n_{prompt}	29642 ± 428	27653 ± 356	22462 ± 258	16332 ± 184	11262 ± 138	7448 ± 106	4788 ± 83	2966 ± 64	
n_{bdecay}	7567 ± 143	7272 ± 129	6610 ± 112	5278 ± 93	3876 ± 77	2670 ± 63	1940 ± 53	1420 ± 44	
n_{tail}	4 ± 75	100 ± 10	24 ± 26	15 ± 20	10 ± 12	11 ± 8	0 ± 5	7 ± 5	
parameters	10-11	11-12	12-13	13-14	14-15	15-16	16-17	17-20	
	3685.4 ± 0.4	3684.1 ± 0.6	3685.1 ± 0.7	3685.0 ± 0.8	3686.9 ± 1.0	3682.5 ± 1.1	3687.0 ± 1.5	3684.1 ± 1.2	
μ_{mass}	17.8 ± 0.4	18.6 ± 0.5	18.9 ± 0.7	17.2 ± 0.7	19.1 ± 1.0	17.4 ± 1.0	20.1 ± 1.3	21.7 ± 1.2	
σ_{mass}	2971 ± 70	2003 ± 57	1380 ± 48	905 ± 37	711 ± 34	455 ± 27	320 ± 23	577 ± 32	
n_{sig}	1855 ± 61	1222 ± 50	757 ± 41	567 ± 33	379 ± 29	264 ± 23	206 ± 20	332 ± 28	
n_{bkg}	-0.71 ± 0.36	-0.19 ± 0.43	-1.43 ± 0.56	-0.70 ± 0.64	-1.32 ± 0.79	-0.05 ± 7.15	-1.27 ± 1.06	-0.67 ± 0.85	
$1000 * p_0$	-3.0 ± 0.8	-1.3 ± 0.9	-3.0 ± 1.2	-1.7 ± 1.3	2.7 ± 1.6	-1.3 ± 1.2	-1.4 ± 0.8	-2.1 ± 1.7	
$1000 * \mu_{tz}$	5.51 ± 1.10	8.05 ± 2.18	1.68 ± 0.40	2.78 ± 1.28	2.58 ± 0.85	0.97 ± 0.08	1.02 ± 9.33	1.41 ± 0.19	
$S1_{tz}$	1.03 ± 0.02	1.03 ± 0.03	0.93 ± 0.10	0.99 ± 0.05	1.01 ± 0.07	0.96 ± 7.53	1.01 ± 0.05	0.64 ± 0.19	
$S2_{tz}$	0.04 ± 0.01	0.04 ± 0.01	0.27 ± 0.21	0.05 ± 0.05	0.08 ± 0.07	0.99 ± 0.57	0.01 ± 0.55	0.62 ± 0.21	
β_{tz}	1.36 ± 0.05	1.47 ± 0.07	1.44 ± 0.08	1.35 ± 0.09	1.51 ± 0.10	1.09 ± 0.07	1.47 ± 0.05	1.19 ± 0.08	
τ_b	1972 ± 52	1326 ± 43	878 ± 34	579 ± 28	392 ± 23	266 ± 16	178 ± 13	305 ± 21	
n_{prompt}	1001 ± 37	670 ± 31	503 ± 26	325 ± 21	316 ± 20	189 ± 14	144 ± 12	272 ± 19	
n_{bdecay}	0 ± 1	3 ± 3	0 ± 1	2 ± 2	2 ± 2	6 ± 2	1 ± 1	0 ± 1	
n_{tail}									

Table B.4: The parameters of the invariant mass and t_z fit, including the fitted yields and the shape parameters for different p_T bins in the rapidity bin $3.5 < y < 4.0$.

parameters	p_T (GeV/c)								
	2-3	3-4	4-5	5-6	6-7	7-8	8-9	9-10	
μ_{mass}	3686.2 ± 0.3	3685.6 ± 0.2	3685.3 ± 0.2	3685.1 ± 0.2	3684.8 ± 0.3	3685.2 ± 0.3	3685.0 ± 0.4	3685.0 ± 0.5	
σ_{mass}	16.2 ± 0.3	16.8 ± 0.3	18.1 ± 0.3	18.8 ± 0.3	19.7 ± 0.3	19.8 ± 0.3	20.2 ± 0.4	21.9 ± 0.5	
n_{sig}	28161 ± 454	24872 ± 367	20223 ± 277	15512 ± 202	10612 ± 153	6750 ± 114	4458 ± 91	2963 ± 72	
n_{bkg}	269418 ± 669	158229 ± 518	69020 ± 354	27926 ± 230	11796 ± 157	5804 ± 109	3090 ± 83	1548 ± 62	
$1000 * p_0$	-0.58 ± 0.03	-0.52 ± 0.04	-0.40 ± 0.06	-0.42 ± 0.09	-0.72 ± 0.14	-0.31 ± 0.20	-0.60 ± 0.28	-0.82 ± 0.40	
$1000 * \mu_{tz}$	-1.6 ± 0.7	-0.8 ± 0.6	-1.8 ± 0.5	-0.7 ± 0.1	-0.7 ± 0.5	-0.7 ± 0.6	-1.2 ± 0.7	-0.9 ± 0.8	
$S_{1_{tz}}$	1.34 ± 0.07	1.24 ± 0.09	1.62 ± 0.12	0.03 ± 5.01	1.60 ± 0.13	1.37 ± 0.13	1.25 ± 0.09	1.89 ± 0.28	
$S_{2_{tz}}$	0.71 ± 0.04	0.74 ± 0.06	0.81 ± 0.03	1.01 ± 0.00	0.86 ± 0.03	0.83 ± 0.07	0.67 ± 0.10	0.85 ± 0.05	
β_{tz}	0.47 ± 0.07	0.49 ± 0.13	0.26 ± 0.05	0.00 ± 0.01	0.25 ± 0.06	0.43 ± 0.15	0.64 ± 0.14	0.23 ± 0.08	
τ_b	1.55 ± 0.03	1.57 ± 0.03	1.50 ± 0.03	1.44 ± 0.01	1.44 ± 0.04	1.42 ± 0.04	1.37 ± 0.05	1.42 ± 0.06	
n_{prompt}	22975 ± 302	20038 ± 247	15768 ± 191	11725 ± 108	8125 ± 111	5000 ± 84	3266 ± 66	2080 ± 53	
n_{decay}	5082 ± 117	4845 ± 103	4310 ± 91	3572 ± 60	2467 ± 62	1737 ± 51	1181 ± 42	880 ± 36	
n_{tail}	49 ± 27	0 ± 20	60 ± 29	35 ± 6	0 ± 5	0 ± 5	0 ± 5	0 ± 2	
parameters	10-11	11-12	12-13	13-14	14-15	15-17	17-20		
	3684.9 ± 0.7	3685.2 ± 0.8	3685.0 ± 1.1	3686.2 ± 1.3	3686.9 ± 1.7	3686.8 ± 1.7	3687.2 ± 2.0		
μ_{mass}	23.1 ± 0.7	22.5 ± 0.8	23.5 ± 1.1	23.5 ± 1.4	23.9 ± 1.8	26.9 ± 1.6	22.4 ± 2.3		
σ_{mass}	1977 ± 60	1318 ± 47	821 ± 39	581 ± 32	400 ± 28	473 ± 31	262 ± 24		
n_{sig}	897 ± 50	540 ± 38	424 ± 34	273 ± 27	210 ± 25	231 ± 27	215 ± 23		
n_{bkg}	-0.51 ± 0.54	-1.67 ± 0.70	-0.00 ± 0.93	-2.62 ± 0.99	-0.20 ± 1.47	-2.27 ± 1.12	-0.00 ± 0.70		
$1000 * p_0$	-0.2 ± 0.9	1.2 ± 1.1	-0.2 ± 1.4	0.6 ± 0.5	2.0 ± 2.3	0.4 ± 1.8	1.0 ± 2.0		
$1000 * \mu_{tz}$	1.72 ± 0.52	4.17 ± 2.22	2.13 ± 1.41	1.00 ± 7.84	1.39 ± 0.26	1.05 ± 0.06	5.36 ± 7.01		
$S_{1_{tz}}$	0.95 ± 0.06	1.01 ± 0.04	0.93 ± 0.06	0.97 ± 0.02	0.84 ± 0.50	5.45 ± 1.82	0.95 ± 0.07		
$S_{2_{tz}}$	0.11 ± 0.11	0.05 ± 0.03	0.04 ± 0.08	0.02 ± 0.97	0.77 ± 0.78	0.95 ± 0.03	0.00 ± 0.01		
β_{tz}	1.57 ± 0.08	1.23 ± 0.07	1.42 ± 0.10	1.64 ± 0.04	1.61 ± 0.16	1.47 ± 0.12	1.33 ± 0.16		
τ_b	1385 ± 42	913 ± 35	541 ± 27	363 ± 19	254 ± 18	306 ± 21	174 ± 16		
n_{prompt}	585 ± 28	402 ± 24	283 ± 20	215 ± 15	145 ± 14	177 ± 15	93 ± 12		
n_{decay}	1 ± 3	0 ± 1	0 ± 1	7 ± 3	0 ± 1	0 ± 1	0 ± 0		
n_{tail}									

Table B.5: The parameters of the invariant mass and t_z fit, including the fitted yields and the shape parameters for different p_T bins in the rapidity bin $4.0 < y < 4.5$.

parameters	p_T (GeV/c)								
	2-3	3-4	4-5	5-6	6-7	7-8	8-9		
μ_{mass}	3684.5 ± 0.4	3684.5 ± 0.4	3685.1 ± 0.4	3685.7 ± 0.5	3685.6 ± 0.6	3685.5 ± 0.8	3685.1 ± 1.0		
σ_{mass}	19.3 ± 0.4	20.2 ± 0.4	21.7 ± 0.4	22.1 ± 0.5	24.9 ± 0.7	26.6 ± 0.8	26.4 ± 1.1		
n_{sig}	12153 ± 229	9137 ± 182	7392 ± 149	5466 ± 119	3684 ± 98	2679 ± 79	1544 ± 62		
n_{bkg}	44127 ± 290	23495 ± 218	13147 ± 167	6812 ± 124	3370 ± 96	1746 ± 73	1077 ± 58		
$1000 * p_0$	-0.51 ± 0.07	-0.77 ± 0.10	-0.66 ± 0.13	-0.51 ± 0.19	-0.70 ± 0.27	-0.20 ± 0.39	-0.47 ± 0.49		
$1000 * \mu_{tz}$	-4.3 ± 1.0	-1.1 ± 1.0	-0.2 ± 1.0	1.0 ± 0.9	4.6 ± 1.1	3.0 ± 1.2	4.0 ± 1.6		
$S1_{tz}$	1.44 ± 0.10	1.46 ± 0.21	1.26 ± 0.09	2.10 ± 0.29	1.89 ± 1.99	1.42 ± 0.32	1.22 ± 0.28		
$S2_{tz}$	0.79 ± 0.05	0.88 ± 0.06	0.75 ± 0.10	0.88 ± 0.04	0.99 ± 0.18	0.95 ± 0.15	0.81 ± 0.96		
β_{tz}	0.45 ± 0.09	0.29 ± 0.16	0.64 ± 0.16	0.20 ± 0.06	0.13 ± 0.54	0.38 ± 0.37	0.81 ± 0.89		
τ_b	1.56 ± 0.06	1.47 ± 0.05	1.33 ± 0.06	1.44 ± 0.06	1.33 ± 0.07	1.46 ± 0.08	1.56 ± 0.10		
n_{prompt}	10299 ± 154	7399 ± 124	5945 ± 104	4438 ± 86	2923 ± 72	2084 ± 54	1152 ± 41		
n_{decay}	1795 ± 70	1674 ± 60	1376 ± 53	1004 ± 44	740 ± 38	593 ± 31	390 ± 24		
n_{tail}	34 ± 13	23 ± 12	36 ± 15	5 ± 10	19 ± 10	16 ± 8	2 ± 3		
parameters	9-10	10-11	11-12	12-13	13-14	14-16	16-20		
μ_{mass}	3684.1 ± 1.3	3684.1 ± 1.4	3689.4 ± 2.4	3687.4 ± 2.4	3690.1 ± 3.3	3688.5 ± 4.5	3688.2 ± 6.3		
σ_{mass}	30.2 ± 1.5	27.5 ± 1.5	36.5 ± 2.6	29.3 ± 2.8	31.6 ± 3.4	35.8 ± 5.1	47.4 ± 35.2		
n_{sig}	1084 ± 53	718 ± 41	546 ± 43	295 ± 29	212 ± 25	208 ± 34	228 ± 68		
n_{bkg}	559 ± 48	448 ± 37	225 ± 39	199 ± 27	145 ± 24	223 ± 35	117 ± 67		
$1000 * p_0$	-0.00 ± 0.96	-0.00 ± 1.45	-2.72 ± 1.43	-0.00 ± 0.63	-1.90 ± 1.50	-1.10 ± 1.22	-2.68 ± 2.99		
$1000 * \mu_{tz}$	3.9 ± 1.9	3.6 ± 1.4	5.5 ± 2.4	4.6 ± 3.4	-1.0 ± 1.9	10.5 ± 3.8	2.5 ± 3.5		
$S1_{tz}$	1.28 ± 0.14	1.03 ± 0.07	2.03 ± 0.89	1.40 ± 0.23	0.07 ± 0.05	1.10 ± 0.13	1.21 ± 0.32		
$S2_{tz}$	0.74 ± 0.25	1.03 ± 6.89	1.03 ± 0.11	0.73 ± 0.24	1.00 ± 0.09	0.17 ± 0.09	1.21 ± 0.50		
β_{tz}	0.74 ± 0.26	0.99 ± 0.59	0.13 ± 0.17	0.65 ± 0.28	0.04 ± 0.04	0.91 ± 0.08	0.62 ± 0.40		
τ_b	1.30 ± 0.09	1.33 ± 0.09	1.37 ± 0.14	1.38 ± 0.17	1.70 ± 0.25	1.23 ± 0.21	1.15 ± 0.17		
n_{prompt}	773 ± 33	523 ± 23	393 ± 24	203 ± 17	147 ± 14	126 ± 16	158 ± 16		
n_{decay}	312 ± 22	193 ± 14	153 ± 15	94 ± 12	67 ± 10	80 ± 11	68 ± 10		
n_{tail}	7 ± 5	3 ± 2	5 ± 4	0 ± 1	0 ± 2	0 ± 2	0 ± 0		

Table B.6: The parameters of the t_z background fit for different p_T bins in the rapidity bin $2.0 < y < 2.5$.

parameters	p_T (GeV/c)							
	2-3	3-4	4-5	5-6	6-7	7-8	8-9	9-10
τ_1	0.70 ± 0.03	0.98 ± 0.09	1.49 ± 0.11	1.44 ± 0.13	1.19 ± 0.13	1.54 ± 0.14	1.72 ± 0.29	5.42 ± 7.15
τ_2	0.09 ± 0.00	0.22 ± 0.02	0.24 ± 0.01	0.23 ± 0.03	0.24 ± 0.04	0.22 ± 0.04	0.45 ± 0.12	0.32 ± 0.15
τ_3	1.97 ± 0.15	3.86 ± 1.37	1.29 ± 0.44	2.71 ± 1.05	2.15 ± 0.75	1.51 ± 0.51	10.00 ± 9.92	0.73 ± 0.20
τ_4	0.04 ± 0.00	0.34 ± 0.03	0.27 ± 0.03	0.35 ± 0.05	0.26 ± 0.05	0.23 ± 0.05	0.62 ± 0.13	0.02 ± 0.01
f_1	0.030 ± 0.002	0.020 ± 0.003	0.019 ± 0.002	0.030 ± 0.003	0.050 ± 0.007	0.069 ± 0.007	0.060 ± 0.021	0.087 ± 0.019
f_2	0.159 ± 0.007	0.073 ± 0.003	0.078 ± 0.004	0.071 ± 0.006	0.075 ± 0.011	0.091 ± 0.013	0.090 ± 0.020	0.064 ± 0.021
f_3	0.004 ± 0.001	0.001 ± 0.000	0.003 ± 0.002	0.004 ± 0.001	0.007 ± 0.003	0.012 ± 0.006	0.000 ± 0.000	0.045 ± 0.017
f_4	0.146 ± 0.019	0.012 ± 0.001	0.020 ± 0.002	0.020 ± 0.003	0.041 ± 0.009	0.046 ± 0.010	0.029 ± 0.006	0.400 ± 0.289
-4.5 ± 0.6	-4.7 ± 0.3	-3.6 ± 0.4	-3.2 ± 0.5	-1.6 ± 0.7	-1.9 ± 0.9	-0.5 ± 1.2	13.1 ± 2.7	11.9 ± 2.6
$1000 * \mu_{tzbk}$	5.65 ± 0.23	2.69 ± 0.10	2.11 ± 0.10	2.58 ± 0.16	2.64 ± 0.40	2.11 ± 0.40	3.36 ± 0.43	5.29 ± 0.88
$S1_{tzbk}$	1.08 ± 0.01	1.07 ± 0.01	0.99 ± 0.02	1.05 ± 0.02	1.08 ± 0.03	1.03 ± 0.07	1.12 ± 0.05	1.14 ± 0.06
$S2_{tzbk}$	0.06 ± 0.00	0.16 ± 0.01	0.27 ± 0.03	0.21 ± 0.02	0.19 ± 0.03	0.28 ± 0.10	0.24 ± 0.04	0.17 ± 0.04
parameters	11-12	12-13	13-14	14-15	15-16	16-17	17-18	18-20
τ_1	1.11 ± 0.12	0.22 ± 0.05	0.14 ± 0.05	1.01 ± 0.14	0.99 ± 0.15	0.90 ± 0.17	1.27 ± 0.29	1.54 ± 0.27
τ_2	0.03 ± 0.01	1.66 ± 0.32	1.80 ± 0.27	5.00 ± 1.14	4.29 ± 1.46	0.02 ± 1.14	0.10 ± 0.04	0.02 ± 0.01
τ_3	0.81 ± 0.39	1.20 ± 0.55	0.67 ± 0.53	7.05 ± 3.83	0.63 ± 1.92	8.04 ± 3.34	5.74 ± 4.13	0.42 ± 9.71
τ_4	0.02 ± 0.01	0.11 ± 0.04	0.03 ± 0.01	0.18 ± 0.08	0.24 ± 0.09	0.54 ± 0.22	0.11 ± 0.03	0.42 ± 0.29
f_1	0.186 ± 0.021	0.195 ± 0.035	0.136 ± 0.048	0.265 ± 0.033	0.286 ± 0.040	0.304 ± 0.048	0.299 ± 0.056	0.309 ± 0.044
f_2	0.300 ± 0.294	0.125 ± 0.028	0.224 ± 0.031	0.000 ± 0.011	0.000 ± 0.010	0.000 ± 0.050	0.300 ± 0.026	0.257 ± 0.257
f_3	0.038 ± 0.025	0.032 ± 0.017	0.021 ± 0.017	0.000 ± 0.000	0.000 ± 0.128	0.000 ± 0.000	0.000 ± 0.000	0.000 ± 0.000
f_4	0.400 ± 0.386	0.109 ± 0.038	0.400 ± 0.274	0.057 ± 0.033	0.099 ± 0.043	0.067 ± 0.027	0.213 ± 0.053	0.024 ± 0.017
$1000 * \mu_{tzbk}$	3.7 ± 4.9	6.1 ± 3.2	16.1 ± 6.0	0.5 ± 4.6	7.1 ± 4.1	-0.3 ± 3.9	-7.1 ± 4.2	-0.8 ± 8.2
$S1_{tzbk}$	6.53 ± 2.05	0.60 ± 0.40	6.87 ± 1.27	9.69 ± 2.13	2.87 ± 0.86	1.30 ± 0.17	4.97 ± 7.05	2.47 ± 0.75
$S2_{tzbk}$	1.14 ± 0.14	1.32 ± 0.25	1.04 ± 0.19	1.66 ± 0.15	0.82 ± 0.17	0.36 ± 0.26	0.46 ± 0.12	0.74 ± 0.14
β_{tzbk}	0.14 ± 0.04	0.19 ± 0.25	0.16 ± 0.06	0.00 ± 0.06	0.52 ± 0.13	0.80 ± 0.13	0.00 ± 0.11	0.27 ± 0.16

Table B.7: The parameters of the t_z background fit for different p_T bins in the rapidity bin $2.5 < y < 3.0$.

parameters	p_T (GeV/c)							
	2-3	3-4	4-5	5-6	6-7	7-8	8-9	9-10
τ_1	0.61 ± 0.02	0.89 ± 0.05	0.95 ± 0.08	1.19 ± 0.08	1.21 ± 0.08	0.24 ± 0.04	0.23 ± 0.04	1.36 ± 0.13
τ_2	0.07 ± 0.00	0.20 ± 0.01	0.22 ± 0.02	0.24 ± 0.02	0.21 ± 0.02	1.49 ± 0.10	1.54 ± 0.14	0.18 ± 0.06
τ_3	1.89 ± 0.07	2.42 ± 0.19	2.26 ± 0.16	2.10 ± 0.20	2.94 ± 0.80	10.00 ± 6.23	1.75 ± 0.63	2.26 ± 0.98
τ_4	0.04 ± 0.00	0.36 ± 0.02	0.32 ± 0.02	0.26 ± 0.02	0.30 ± 0.03	0.43 ± 0.06	0.22 ± 0.03	0.26 ± 0.06
f_1	0.035 ± 0.001	0.021 ± 0.002	0.025 ± 0.003	0.028 ± 0.003	0.060 ± 0.005	0.091 ± 0.011	0.131 ± 0.014	0.140 ± 0.016
f_2	0.187 ± 0.005	0.072 ± 0.002	0.064 ± 0.003	0.081 ± 0.004	0.077 ± 0.008	0.074 ± 0.007	0.093 ± 0.010	0.108 ± 0.025
f_3	0.006 ± 0.000	0.005 ± 0.001	0.011 ± 0.001	0.012 ± 0.002	0.007 ± 0.002	0.000 ± 0.000	0.011 ± 0.005	0.012 ± 0.006
f_4	0.167 ± 0.012	0.019 ± 0.001	0.025 ± 0.002	0.045 ± 0.003	0.042 ± 0.005	0.034 ± 0.007	0.063 ± 0.012	0.062 ± 0.017
$1000 * \mu_{tz bkg}$	-4.5 ± 0.4	-4.5 ± 0.2	-4.1 ± 0.2	-3.4 ± 0.3	-2.7 ± 0.5	-1.6 ± 0.7	-1.1 ± 1.0	-0.4 ± 1.5
$S1_{tz bkg}$	5.60 ± 0.12	2.71 ± 0.06	2.90 ± 0.09	2.62 ± 0.12	3.16 ± 0.22	4.03 ± 0.46	2.75 ± 0.35	3.62 ± 0.65
$S2_{tz bkg}$	1.02 ± 0.01	1.05 ± 0.01	1.07 ± 0.01	1.04 ± 0.02	1.11 ± 0.02	1.17 ± 0.03	1.09 ± 0.06	1.12 ± 0.09
$\beta_{tz bkg}$	0.07 ± 0.00	0.19 ± 0.01	0.20 ± 0.01	0.25 ± 0.01	0.22 ± 0.02	0.22 ± 0.02	0.30 ± 0.05	0.25 ± 0.05
parameters	11-12	12-13	13-14	14-15	15-16	16-17	17-18	18-20
τ_1	0.13 ± 0.05	0.03 ± 0.01	0.14 ± 0.06	1.50 ± 0.00	1.14 ± 0.19	0.17 ± 5.63	1.67 ± 0.49	0.42 ± 0.58
τ_2	1.57 ± 0.17	1.40 ± 0.14	1.61 ± 0.24	0.14 ± 0.07	5.00 ± 4.80	1.38 ± 0.25	0.25 ± 0.12	1.67 ± 0.33
τ_3	10.00 ± 9.37	10.00 ± 8.25	9.90 ± 2.25	3.61 ± 4.03	0.07 ± 0.06	0.69 ± 0.42	3.58 ± 4.02	0.04 ± 0.03
τ_4	0.09 ± 0.06	0.02 ± 0.01	0.28 ± 0.08	0.20 ± 0.05	0.37 ± 0.17	4.75 ± 4.19	0.06 ± 0.02	0.04 ± 0.16
f_1	0.144 ± 0.034	0.400 ± 0.396	0.170 ± 0.056	0.200 ± 0.035	0.390 ± 0.053	0.000 ± 0.015	0.212 ± 0.064	0.058 ± 0.058
f_2	0.189 ± 0.021	0.247 ± 0.022	0.215 ± 0.032	0.160 ± 0.044	0.022 ± 0.026	0.283 ± 0.046	0.214 ± 0.065	0.300 ± 0.294
f_3	0.006 ± 0.004	0.000 ± 0.000	0.000 ± 0.003	0.000 ± 0.004	0.085 ± 0.142	0.054 ± 0.033	0.000 ± 0.000	0.241 ± 0.256
f_4	0.070 ± 0.037	0.266 ± 0.330	0.058 ± 0.023	0.096 ± 0.025	0.046 ± 0.025	0.000 ± 0.007	0.162 ± 0.081	0.010 ± 0.174
$1000 * \mu_{tz bkg}$	-0.3 ± 2.8	-6.1 ± 7.0	-2.5 ± 3.2	-1.2 ± 3.0	-3.8 ± 3.5	1.0 ± 3.8	4.8 ± 5.1	-2.9 ± 4.3
$S1_{tz bkg}$	10.00 ± 1.76	5.93 ± 0.65	1.03 ± 0.19	1.03 ± 0.44	2.63 ± 1.56	3.76 ± 1.61	1.68 ± 1.54	6.84 ± 2.57
$S2_{tz bkg}$	1.35 ± 0.09	0.88 ± 0.19	3.00 ± 1.15	1.20 ± 0.71	0.92 ± 0.24	1.16 ± 0.25	1.13 ± 0.41	1.13 ± 0.28
$\beta_{tz bkg}$	0.08 ± 0.05	0.27 ± 0.05	0.71 ± 0.13	0.59 ± 0.59	0.33 ± 0.23	0.26 ± 0.16	0.23 ± 0.62	0.14 ± 0.17

Table B.8: The parameters of the t_z background fit for different p_T bins in the rapidity bin $3.0 < y < 3.5$.

parameters	p_T (GeV/c)								
	2-3	3-4	4-5	5-6	6-7	7-8	8-9	9-10	
τ_1	0.18 ± 0.01	0.46 ± 0.02	0.26 ± 0.03	1.34 ± 0.09	0.18 ± 0.03	0.27 ± 0.05	0.16 ± 0.03	1.18 ± 0.08	
τ_2	0.76 ± 0.04	0.06 ± 0.00	1.00 ± 0.09	0.26 ± 0.02	1.14 ± 0.08	1.56 ± 0.12	1.38 ± 0.10	4.65 ± 1.07	
τ_3	2.84 ± 0.18	1.84 ± 0.04	3.14 ± 0.33	3.80 ± 0.79	4.20 ± 1.29	3.11 ± 1.93	3.50 ± 2.00	0.25 ± 0.11	
τ_4	0.38 ± 0.01	0.04 ± 0.00	0.50 ± 0.04	0.40 ± 0.03	0.32 ± 0.04	0.42 ± 0.10	0.24 ± 0.03	1.57 ± 1.13	
f_1	0.096 ± 0.002	0.041 ± 0.002	0.054 ± 0.004	0.042 ± 0.004	0.087 ± 0.010	0.094 ± 0.013	0.118 ± 0.018	0.189 ± 0.014	
f_2	0.030 ± 0.002	0.164 ± 0.008	0.030 ± 0.004	0.072 ± 0.005	0.083 ± 0.006	0.099 ± 0.010	0.137 ± 0.011	0.000 ± 0.008	
f_3	0.005 ± 0.000	0.027 ± 0.001	0.013 ± 0.002	0.009 ± 0.002	0.008 ± 0.002	0.006 ± 0.004	0.006 ± 0.003	0.080 ± 0.033	
f_4	0.021 ± 0.001	0.157 ± 0.013	0.023 ± 0.001	0.032 ± 0.003	0.037 ± 0.006	0.029 ± 0.007	0.069 ± 0.010	0.004 ± 0.005	
$1000 * \mu_{tzbk}$	-2.7 ± 0.2	-3.7 ± 0.5	-4.0 ± 0.2	-3.5 ± 0.3	-3.2 ± 0.6	-3.1 ± 0.8	-2.6 ± 1.1	1.8 ± 1.3	
$S1_{tzbk}$	2.67 ± 0.05	5.16 ± 0.12	3.81 ± 0.09	3.73 ± 0.15	3.82 ± 0.30	4.64 ± 0.53	0.91 ± 0.07	1.11 ± 0.07	
$S2_{tzbk}$	1.04 ± 0.01	1.05 ± 0.01	1.12 ± 0.01	1.13 ± 0.01	1.15 ± 0.03	1.24 ± 0.04	2.34 ± 0.24	4.18 ± 0.51	
β_{tzbk}	0.19 ± 0.01	0.13 ± 0.00	0.22 ± 0.01	0.24 ± 0.01	0.23 ± 0.02	0.23 ± 0.02	0.56 ± 0.07	0.67 ± 0.04	
parameters	10-11	11-12	12-13	13-14	14-15	15-16	16-17	17-20	
τ_1	0.32 ± 0.12	0.07 ± 0.04	1.59 ± 0.27	9.91 ± 2.24	1.14 ± 0.16	2.86 ± 1.50	0.03 ± 0.01	0.15 ± 5.68	
τ_2	1.90 ± 0.29	1.14 ± 0.11	0.22 ± 0.11	1.40 ± 0.28	2.20 ± 2.07	0.51 ± 0.22	1.03 ± 0.19	1.24 ± 0.20	
τ_3	0.07 ± 0.06	0.60 ± 0.29	4.98 ± 1.14	7.82 ± 3.47	9.83 ± 2.22	9.20 ± 2.28	3.72 ± 4.05	5.29 ± 4.19	
τ_4	0.30 ± 0.09	0.10 ± 0.06	0.07 ± 0.02	0.02 ± 0.06	0.35 ± 0.16	0.01 ± 0.01	0.12 ± 0.06	0.25 ± 0.14	
f_1	0.126 ± 0.039	0.141 ± 0.062	0.214 ± 0.042	0.026 ± 0.026	0.297 ± 0.036	0.112 ± 0.058	0.399 ± 0.090	0.000 ± 0.053	
f_2	0.149 ± 0.027	0.255 ± 0.026	0.166 ± 0.044	0.292 ± 0.038	0.000 ± 0.002	0.180 ± 0.059	0.300 ± 0.030	0.280 ± 0.039	
f_3	0.160 ± 0.063	0.034 ± 0.020	0.000 ± 0.004	0.000 ± 0.000	0.000 ± 0.005	0.000 ± 0.002	0.000 ± 0.000	0.000 ± 0.000	
f_4	0.058 ± 0.032	0.066 ± 0.048	0.192 ± 0.066	0.071 ± 0.120	0.037 ± 0.019	0.709 ± 0.330	0.056 ± 0.028	0.037 ± 0.024	
$1000 * \mu_{tzbk}$	-1.5 ± 1.6	-5.7 ± 2.8	7.1 ± 4.7	4.4 ± 4.8	-6.1 ± 3.0	6.0 ± 9.3	-11.8 ± 3.8	-3.6 ± 2.4	
$S1_{tzbk}$	1.38 ± 0.18	4.42 ± 3.78	19.47 ± 3.94	5.80 ± 1.01	1.07 ± 0.16	2.30 ± 0.46	3.66 ± 6.63	3.31 ± 0.80	
$S2_{tzbk}$	0.46 ± 0.13	1.10 ± 0.12	1.08 ± 0.18	1.40 ± 0.20	2.48 ± 0.69	0.64 ± 0.20	0.82 ± 0.13	0.91 ± 0.12	
β_{tzbk}	0.76 ± 0.10	0.13 ± 0.12	0.03 ± 0.02	0.25 ± 0.08	0.70 ± 0.15	0.43 ± 0.14	0.00 ± 0.06	0.24 ± 0.10	

Table B.9: The parameters of the t_z background fit for different p_T bins in the rapidity bin $3.5 < y < 4.0$.

parameters	p_T (GeV/c)							
	2-3	3-4	4-5	5-6	6-7	7-8	8-9	9-10
τ_1	0.96 ± 0.06	0.93 ± 0.08	1.29 ± 0.11	1.37 ± 0.21	1.24 ± 0.09	0.34 ± 0.09	0.38 ± 0.13	1.12 ± 0.17
τ_2	0.23 ± 0.01	0.22 ± 0.02	0.26 ± 0.02	0.32 ± 0.05	0.15 ± 0.04	1.65 ± 0.26	1.90 ± 0.29	5.00 ± 4.91
τ_3	3.37 ± 0.40	3.45 ± 0.28	2.71 ± 0.31	2.19 ± 0.44	3.07 ± 1.28	2.20 ± 1.63	1.61 ± 0.74	0.68 ± 0.25
τ_4	0.43 ± 0.02	0.42 ± 0.03	0.41 ± 0.04	0.39 ± 0.08	0.43 ± 0.09	0.38 ± 0.07	0.30 ± 0.09	0.02 ± 0.00
f_1	0.035 ± 0.003	0.037 ± 0.004	0.041 ± 0.005	0.053 ± 0.011	0.111 ± 0.009	0.150 ± 0.020	0.124 ± 0.027	0.218 ± 0.024
f_2	0.121 ± 0.003	0.102 ± 0.005	0.099 ± 0.006	0.099 ± 0.011	0.092 ± 0.019	0.102 ± 0.025	0.141 ± 0.030	0.018 ± 0.015
f_3	0.006 ± 0.001	0.019 ± 0.002	0.020 ± 0.003	0.023 ± 0.005	0.011 ± 0.005	0.006 ± 0.005	0.021 ± 0.013	0.047 ± 0.022
f_4	0.024 ± 0.001	0.032 ± 0.002	0.036 ± 0.003	0.030 ± 0.005	0.034 ± 0.007	0.040 ± 0.010	0.040 ± 0.014	0.400 ± 0.387
$1000 * \mu_{tzbk}$	0.9 ± 0.3	-0.5 ± 0.3	-0.7 ± 0.4	-1.9 ± 0.6	-3.3 ± 1.1	-0.8 ± 1.3	-2.8 ± 1.6	10.6 ± 2.3
$S1_{tzbk}$	2.70 ± 0.08	2.97 ± 0.11	3.12 ± 0.14	3.92 ± 0.25	4.20 ± 0.34	3.63 ± 0.41	3.48 ± 0.37	5.57 ± 1.13
$S2_{tzbk}$	1.05 ± 0.01	1.08 ± 0.01	1.10 ± 0.02	1.15 ± 0.02	1.15 ± 0.04	1.10 ± 0.06	1.03 ± 0.07	1.13 ± 0.09
β_{tzbk}	0.22 ± 0.01	0.24 ± 0.01	0.27 ± 0.01	0.26 ± 0.02	0.30 ± 0.03	0.34 ± 0.04	0.37 ± 0.05	0.24 ± 0.04
parameters	10-11	11-12	12-13	13-14	14-15	15-17	17-20	
τ_1	0.11 ± 0.03	10.00 ± 9.47	0.71 ± 0.24	1.12 ± 0.21	0.58 ± 0.37	0.05 ± 0.00	0.86 ± 0.27	
τ_2	1.50 ± 0.19	1.10 ± 0.17	2.66 ± 1.01	0.12 ± 0.18	1.80 ± 0.78	1.67 ± 0.10	0.86 ± 0.60	
τ_3	1.36 ± 9.06	0.04 ± 8.59	2.45 ± 6.20	9.76 ± 2.18	8.22 ± 3.21	0.72 ± 0.07	1.12 ± 1.75	
τ_4	0.07 ± 0.03	0.42 ± 0.18	0.46 ± 0.16	0.02 ± 0.01	3.69 ± 4.05	0.08 ± 0.01	0.00 ± 0.15	
f_1	0.189 ± 0.053	0.013 ± 0.012	0.191 ± 0.066	0.282 ± 0.050	0.158 ± 0.097	0.148 ± 0.014	0.229 ± 0.065	
f_2	0.217 ± 0.027	0.266 ± 0.032	0.136 ± 0.062	0.045 ± 0.038	0.147 ± 0.092	0.100 ± 0.000	0.078 ± 0.034	
f_3	0.000 ± 0.000	0.000 ± 0.000	0.000 ± 0.009	0.000 ± 0.000	0.000 ± 0.000	0.169 ± 0.010	0.000 ± 0.000	
f_4	0.112 ± 0.053	0.040 ± 0.021	0.055 ± 0.019	0.578 ± 0.253	0.000 ± 0.005	0.038 ± 0.009	0.579 ± 0.718	
$1000 * \mu_{tzbk}$	2.7 ± 4.1	-2.7 ± 3.5	-0.8 ± 3.6	13.9 ± 9.2	-0.8 ± 3.0	-1.4 ± 0.7	-4.2 ± 5.9	
$S1_{tzbk}$	10.00 ± 0.66	3.94 ± 1.13	2.19 ± 0.36	3.31 ± 0.69	4.64 ± 1.76	0.99 ± 5.73	1.08 ± 0.17	
$S2_{tzbk}$	1.01 ± 0.11	1.07 ± 0.15	0.91 ± 0.18	0.52 ± 0.17	0.92 ± 0.10	0.99 ± 0.08	7.53 ± 1.87	
β_{tzbk}	0.11 ± 0.04	0.28 ± 0.10	0.54 ± 0.16	0.34 ± 0.13	0.13 ± 0.07	0.07 ± 0.65	0.80 ± 0.03	

Table B.10: The parameters of the t_z background fit for different p_T bins in the rapidity bin $4.0 < y < 4.5$.

parameters	p_T (GeV/c)							
	2-3	3-4	4-5	5-6	6-7	7-8	8-9	
τ_1	1.05 ± 0.07	1.16 ± 0.14	1.26 ± 0.11	1.39 ± 0.39	0.31 ± 0.10	2.26 ± 1.14	0.26 ± 0.22	
τ_2	0.26 ± 0.02	0.30 ± 0.04	0.28 ± 0.05	0.34 ± 0.22	1.20 ± 0.25	0.78 ± 0.28	1.58 ± 0.31	
τ_3	6.10 ± 8.01	10.00 ± 9.24	5.00 ± 4.52	10.00 ± 8.25	9.90 ± 5.06	3.20 ± 6.53	0.88 ± 6.92	
τ_4	0.57 ± 0.06	0.55 ± 0.08	0.82 ± 0.11	0.73 ± 0.16	0.43 ± 0.10	0.58 ± 0.18	0.86 ± 0.43	
f_1	0.069 ± 0.008	0.058 ± 0.012	0.078 ± 0.011	0.089 ± 0.041	0.142 ± 0.034	0.055 ± 0.054	0.066 ± 0.042	
f_2	0.164 ± 0.010	0.127 ± 0.012	0.099 ± 0.062	0.093 ± 0.027	0.118 ± 0.037	0.140 ± 0.052	0.139 ± 0.039	
f_3	0.001 ± 0.001	0.002 ± 0.001	0.002 ± 0.001	0.006 ± 0.003	0.009 ± 0.004	0.000 ± 0.003	0.000 ± 0.003	
f_4	0.025 ± 0.004	0.023 ± 0.004	0.029 ± 0.004	0.025 ± 0.006	0.036 ± 0.009	0.025 ± 0.010	0.013 ± 0.033	
$1000 * \mu_{tzbkg}$	-0.3 ± 1.0	0.7 ± 1.1	3.9 ± 1.1	7.9 ± 1.8	-0.4 ± 2.2	6.6 ± 2.4	3.2 ± 3.2	
S^1_{tzbkg}	3.38 ± 0.26	3.38 ± 0.23	3.09 ± 0.22	4.97 ± 0.44	1.10 ± 0.08	3.58 ± 0.41	4.68 ± 0.52	
S^2_{tzbkg}	1.15 ± 0.02	1.15 ± 0.03	1.12 ± 0.04	1.31 ± 0.04	3.10 ± 0.36	1.08 ± 0.11	1.19 ± 0.09	
β_{tzbkg}	0.21 ± 0.02	0.25 ± 0.02	0.31 ± 0.03	0.18 ± 0.03	0.65 ± 0.07	0.41 ± 0.06	0.28 ± 0.05	
parameters	9-10	10-11	11-12	12-13	13-14	14-16	16-20	
τ_1	1.36 ± 0.23	2.81 ± 1.16	1.31 ± 0.36	1.22 ± 0.29	1.27 ± 0.37	2.27 ± 1.16	10.00 ± 2.18	
τ_2	0.05 ± 0.02	0.44 ± 0.17	0.11 ± 0.08	3.24 ± 2.00	0.38 ± 1.08	0.35 ± 0.17	0.55 ± 0.23	
τ_3	2.80 ± 3.76	9.88 ± 2.24	10.00 ± 8.63	7.18 ± 3.78	3.89 ± 4.09	3.49 ± 4.00	3.48 ± 4.00	
τ_4	0.36 ± 2.13	0.24 ± 0.09	0.09 ± 0.03	0.70 ± 0.40	0.02 ± 0.07	0.15 ± 0.08	0.02 ± 6.25	
f_1	0.177 ± 0.030	0.104 ± 0.042	0.187 ± 0.042	0.199 ± 0.043	0.197 ± 0.052	0.082 ± 0.044	0.067 ± 0.032	
f_2	0.269 ± 0.072	0.173 ± 0.044	0.091 ± 0.095	0.000 ± 0.023	0.000 ± 0.040	0.151 ± 0.052	0.129 ± 0.045	
f_3	0.000 ± 0.000	0.000 ± 0.000	0.002 ± 0.001	0.000 ± 0.000	0.000 ± 0.000	0.000 ± 0.000	0.000 ± 0.000	
f_4	0.000 ± 0.007	0.063 ± 0.027	0.179 ± 0.071	0.034 ± 0.019	0.372 ± 0.086	0.047 ± 0.032	0.000 ± 0.244	
$1000 * \mu_{tzbkg}$	-2.8 ± 4.8	3.9 ± 4.2	10.4 ± 1.4	2.6 ± 6.0	11.1 ± 8.0	1.2 ± 4.3	-1.6 ± 3.8	
S^1_{tzbkg}	1.06 ± 0.15	0.84 ± 0.20	0.10 ± 0.05	1.20 ± 0.29	1.60 ± 0.22	7.67 ± 3.52	10.00 ± 2.21	
S^2_{tzbkg}	5.86 ± 0.85	2.00 ± 0.31	1.19 ± 0.21	2.08 ± 0.45	8.16 ± 1.89	1.23 ± 0.14	1.10 ± 0.11	
β_{tzbkg}	0.72 ± 0.06	0.42 ± 0.16	0.13 ± 0.06	0.55 ± 0.26	0.80 ± 0.03	0.00 ± 0.14	0.04 ± 0.03	

⁷⁹¹ **C Efficiency tables**

Table C.1: The efficiency ϵ_{acc} in different bins of p_{T} and y for prompt $\psi(2S)$ mesons.

p_{T} (GeV/c)	$2 < y < 2.5$	$2.5 < y < 3$	$3 < y < 3.5$	$3.5 < y < 4$	$4 < y < 4.5$
2-3	0.638 ± 0.002	0.854 ± 0.001	0.926 ± 0.001	0.919 ± 0.001	0.828 ± 0.002
3-4	0.683 ± 0.002	0.882 ± 0.001	0.944 ± 0.001	0.940 ± 0.001	0.860 ± 0.002
4-5	0.723 ± 0.002	0.901 ± 0.002	0.955 ± 0.001	0.953 ± 0.001	0.886 ± 0.002
5-6	0.764 ± 0.003	0.929 ± 0.002	0.966 ± 0.001	0.966 ± 0.002	0.913 ± 0.003
6-7	0.805 ± 0.004	0.937 ± 0.003	0.973 ± 0.002	0.972 ± 0.002	0.919 ± 0.004
7-8	0.815 ± 0.005	0.948 ± 0.003	0.977 ± 0.002	0.982 ± 0.002	0.940 ± 0.005
8-9	0.837 ± 0.007	0.963 ± 0.004	0.983 ± 0.003	0.988 ± 0.003	0.947 ± 0.007
9-10	0.893 ± 0.009	0.972 ± 0.005	0.992 ± 0.003	0.987 ± 0.004	0.966 ± 0.008
10-11	0.879 ± 0.012	0.978 ± 0.006	0.986 ± 0.005	0.987 ± 0.006	0.984 ± 0.008
11-12	0.906 ± 0.015	0.976 ± 0.008	0.992 ± 0.005	0.986 ± 0.008	1.000 ± 0.000
12-13	0.901 ± 0.021	0.987 ± 0.009	0.993 ± 0.007	1.000 ± 0.000	0.986 ± 0.014
13-14	0.969 ± 0.015	0.989 ± 0.011	1.000 ± 0.000	1.000 ± 0.000	1.000 ± 0.000
14-15	0.941 ± 0.029	1.000 ± 0.000	1.000 ± 0.000	1.000 ± 0.000	1.000 ± 0.000
15-16	0.949 ± 0.035	1.000 ± 0.000	1.000 ± 0.000	1.000 ± 0.000	1.000 ± 0.000
16-17	0.903 ± 0.053	1.000 ± 0.000	1.000 ± 0.000	1.000 ± 0.000	1.000 ± 0.000
17-18	0.875 ± 0.083	1.000 ± 0.000			
18-19	1.000 ± 0.000	1.000 ± 0.000	1.000 ± 0.000	1.000 ± 0.000	0.917 ± 0.080
19-20					

Table C.2: The efficiency ϵ_{acc} in different bins of p_{T} and y for $\psi(2S)$ from b -decay.

p_{T} (GeV/c)	$2 < y < 2.5$	$2.5 < y < 3$	$3 < y < 3.5$	$3.5 < y < 4$	$4 < y < 4.5$
2-3	0.632 ± 0.001	0.852 ± 0.001	0.927 ± 0.001	0.920 ± 0.001	0.831 ± 0.001
3-4	0.679 ± 0.001	0.880 ± 0.001	0.944 ± 0.001	0.938 ± 0.001	0.863 ± 0.002
4-5	0.723 ± 0.001	0.906 ± 0.001	0.956 ± 0.001	0.953 ± 0.001	0.893 ± 0.002
5-6	0.767 ± 0.002	0.925 ± 0.001	0.966 ± 0.001	0.964 ± 0.001	0.907 ± 0.002
6-7	0.803 ± 0.002	0.941 ± 0.001	0.974 ± 0.001	0.972 ± 0.001	0.926 ± 0.002
7-8	0.830 ± 0.002	0.951 ± 0.001	0.981 ± 0.001	0.978 ± 0.001	0.945 ± 0.002
8-9	0.855 ± 0.002	0.962 ± 0.001	0.986 ± 0.001	0.984 ± 0.001	0.948 ± 0.003
9-10	0.875 ± 0.003	0.964 ± 0.002	0.988 ± 0.001	0.989 ± 0.001	0.962 ± 0.003
10-11	0.893 ± 0.003	0.975 ± 0.002	0.990 ± 0.001	0.992 ± 0.001	0.969 ± 0.003
11-12	0.903 ± 0.003	0.980 ± 0.002	0.992 ± 0.001	0.992 ± 0.002	0.970 ± 0.004
12-13	0.923 ± 0.004	0.990 ± 0.002	0.996 ± 0.001	0.990 ± 0.002	0.987 ± 0.003
13-14	0.923 ± 0.004	0.980 ± 0.002	0.994 ± 0.002	0.992 ± 0.002	0.984 ± 0.005
14-15	0.931 ± 0.005	0.984 ± 0.002	0.998 ± 0.001	0.999 ± 0.001	0.977 ± 0.005
15-16	0.937 ± 0.005	0.988 ± 0.003	0.997 ± 0.001	0.993 ± 0.002	0.990 ± 0.004
16-17	0.960 ± 0.005	0.990 ± 0.003	0.998 ± 0.001	0.999 ± 0.001	0.997 ± 0.002
17-18	0.941 ± 0.006	0.991 ± 0.003			
18-19	0.956 ± 0.005	0.998 ± 0.001	0.999 ± 0.001	0.997 ± 0.002	0.990 ± 0.004
19-20					

Table C.3: The efficiency ϵ_{acc} in different bins of p_{T} and y averaged over prompt $\psi(2S)$ and $\psi(2S)\text{-from-}b$

p_{T} (GeV/c)	$2 < y < 2.5$	$2.5 < y < 3$	$3 < y < 3.5$	$3.5 < y < 4$	$4 < y < 4.5$
2-3	0.633 ± 0.001	0.853 ± 0.001	0.927 ± 0.001	0.920 ± 0.001	0.830 ± 0.001
3-4	0.680 ± 0.001	0.880 ± 0.001	0.944 ± 0.001	0.939 ± 0.001	0.862 ± 0.001
4-5	0.723 ± 0.001	0.904 ± 0.001	0.956 ± 0.001	0.953 ± 0.001	0.891 ± 0.001
5-6	0.767 ± 0.001	0.926 ± 0.001	0.966 ± 0.001	0.965 ± 0.001	0.908 ± 0.002
6-7	0.803 ± 0.002	0.940 ± 0.001	0.973 ± 0.001	0.972 ± 0.001	0.924 ± 0.002
7-8	0.828 ± 0.002	0.951 ± 0.001	0.981 ± 0.001	0.979 ± 0.001	0.944 ± 0.002
8-9	0.853 ± 0.002	0.962 ± 0.001	0.986 ± 0.001	0.984 ± 0.001	0.948 ± 0.003
9-10	0.876 ± 0.003	0.965 ± 0.002	0.989 ± 0.001	0.988 ± 0.001	0.963 ± 0.003
10-11	0.892 ± 0.003	0.975 ± 0.002	0.990 ± 0.001	0.991 ± 0.001	0.971 ± 0.003
11-12	0.903 ± 0.003	0.980 ± 0.002	0.992 ± 0.001	0.991 ± 0.002	0.972 ± 0.004
12-13	0.922 ± 0.004	0.989 ± 0.001	0.996 ± 0.001	0.990 ± 0.002	0.987 ± 0.003
13-14	0.924 ± 0.004	0.980 ± 0.002	0.995 ± 0.001	0.993 ± 0.002	0.985 ± 0.004
14-15	0.932 ± 0.005	0.985 ± 0.002	0.998 ± 0.001	0.999 ± 0.001	0.978 ± 0.005
15-16	0.937 ± 0.005	0.988 ± 0.003	0.997 ± 0.001	0.993 ± 0.002	
16-17	0.959 ± 0.005	0.990 ± 0.003	0.998 ± 0.001		
17-18	0.940 ± 0.006	0.991 ± 0.003			
18-19	0.956 ± 0.005	0.998 ± 0.001	0.999 ± 0.001	0.997 ± 0.002	0.989 ± 0.004
19-20					

Table C.4: The efficiency $\epsilon_{\text{Reco\&Sel}}$ in different bins of p_{T} and y for prompt $\psi(2S)$ mesons.

p_{T} (GeV/c)	$2 < y < 2.5$	$2.5 < y < 3$	$3 < y < 3.5$	$3.5 < y < 4$	$4 < y < 4.5$
2-3	0.204 ± 0.001	0.359 ± 0.001	0.393 ± 0.001	0.377 ± 0.002	0.309 ± 0.002
3-4	0.199 ± 0.001	0.387 ± 0.002	0.443 ± 0.002	0.427 ± 0.002	0.327 ± 0.002
4-5	0.215 ± 0.002	0.440 ± 0.002	0.504 ± 0.002	0.480 ± 0.002	0.372 ± 0.003
5-6	0.241 ± 0.002	0.505 ± 0.003	0.544 ± 0.003	0.532 ± 0.003	0.436 ± 0.004
6-7	0.273 ± 0.003	0.550 ± 0.004	0.581 ± 0.004	0.570 ± 0.004	0.478 ± 0.005
7-8	0.305 ± 0.004	0.586 ± 0.005	0.611 ± 0.005	0.600 ± 0.005	0.524 ± 0.006
8-9	0.336 ± 0.005	0.617 ± 0.006	0.628 ± 0.006	0.624 ± 0.007	0.565 ± 0.008
9-10	0.366 ± 0.007	0.651 ± 0.007	0.651 ± 0.007	0.643 ± 0.010	0.582 ± 0.010
10-11	0.381 ± 0.008	0.662 ± 0.009	0.660 ± 0.009	0.669 ± 0.010	0.581 ± 0.013
11-12	0.405 ± 0.010	0.675 ± 0.010	0.672 ± 0.012	0.679 ± 0.013	0.603 ± 0.018
12-13	0.418 ± 0.013	0.688 ± 0.013	0.673 ± 0.015	0.687 ± 0.014	0.665 ± 0.019
13-14	0.465 ± 0.015	0.708 ± 0.015	0.715 ± 0.019	0.729 ± 0.017	0.640 ± 0.022
14-15	0.495 ± 0.019	0.705 ± 0.017	0.724 ± 0.020	0.717 ± 0.022	
15-16	0.453 ± 0.021	0.777 ± 0.017	0.716 ± 0.026		0.595 ± 0.026
16-17	0.466 ± 0.023	0.724 ± 0.022	0.699 ± 0.027		
17-18	0.528 ± 0.024	0.748 ± 0.035			
18-19	0.512 ± 0.028	0.704 ± 0.031	0.731 ± 0.021	0.679 ± 0.028	0.696 ± 0.024
19-20					

Table C.5: The efficiency $\epsilon_{\text{Reco\&Sel}}$ in different bins of p_{T} and y for $\psi(2S)$ from b -decay.

p_{T} (GeV/c)	$2 < y < 2.5$	$2.5 < y < 3$	$3 < y < 3.5$	$3.5 < y < 4$	$4 < y < 4.5$
2-3	0.200 ± 0.001	0.354 ± 0.002	0.388 ± 0.002	0.372 ± 0.002	0.302 ± 0.002
3-4	0.195 ± 0.001	0.379 ± 0.002	0.437 ± 0.002	0.420 ± 0.002	0.326 ± 0.002
4-5	0.210 ± 0.002	0.440 ± 0.002	0.492 ± 0.002	0.474 ± 0.002	0.374 ± 0.003
5-6	0.233 ± 0.002	0.497 ± 0.002	0.535 ± 0.003	0.526 ± 0.003	0.426 ± 0.004
6-7	0.269 ± 0.002	0.539 ± 0.003	0.572 ± 0.003	0.558 ± 0.004	0.478 ± 0.004
7-8	0.298 ± 0.003	0.587 ± 0.003	0.601 ± 0.004	0.579 ± 0.004	0.520 ± 0.005
8-9	0.317 ± 0.003	0.607 ± 0.004	0.623 ± 0.004	0.615 ± 0.005	0.556 ± 0.007
9-10	0.344 ± 0.004	0.630 ± 0.005	0.651 ± 0.005	0.630 ± 0.006	0.574 ± 0.009
10-11	0.376 ± 0.005	0.647 ± 0.006	0.645 ± 0.007	0.654 ± 0.008	0.597 ± 0.010
11-12	0.390 ± 0.006	0.667 ± 0.006	0.658 ± 0.008	0.669 ± 0.010	0.615 ± 0.011
12-13	0.410 ± 0.007	0.673 ± 0.008	0.656 ± 0.012	0.660 ± 0.011	0.612 ± 0.017
13-14	0.428 ± 0.008	0.680 ± 0.009	0.675 ± 0.010	0.650 ± 0.015	0.618 ± 0.019
14-15	0.454 ± 0.010	0.713 ± 0.009	0.710 ± 0.011	0.659 ± 0.014	0.659 ± 0.018
15-16	0.465 ± 0.011	0.669 ± 0.016	0.704 ± 0.013	0.675 ± 0.015	
16-17	0.467 ± 0.012	0.708 ± 0.013	0.683 ± 0.018		
17-18	0.480 ± 0.014	0.675 ± 0.018			
18-19	0.485 ± 0.013	0.699 ± 0.020			0.628 ± 0.019
19-20					

Table C.6: The efficiency $\epsilon_{\text{Reco\&Sel}}$ in different bins of p_{T} and y averaged over prompt $\psi(2S)$ and $\psi(2S)$ -from- b

p_{T} (GeV/c)	$2 < y < 2.5$	$2.5 < y < 3$	$3 < y < 3.5$	$3.5 < y < 4$	$4 < y < 4.5$
2-3	0.202 ± 0.001	0.356 ± 0.001	0.391 ± 0.001	0.375 ± 0.001	0.306 ± 0.001
3-4	0.197 ± 0.001	0.383 ± 0.001	0.440 ± 0.001	0.423 ± 0.001	0.326 ± 0.002
4-5	0.212 ± 0.001	0.440 ± 0.001	0.497 ± 0.002	0.477 ± 0.002	0.373 ± 0.002
5-6	0.236 ± 0.001	0.500 ± 0.002	0.539 ± 0.002	0.529 ± 0.002	0.431 ± 0.003
6-7	0.270 ± 0.002	0.543 ± 0.002	0.575 ± 0.002	0.563 ± 0.003	0.478 ± 0.003
7-8	0.300 ± 0.002	0.586 ± 0.003	0.605 ± 0.003	0.587 ± 0.003	0.522 ± 0.004
8-9	0.323 ± 0.003	0.610 ± 0.003	0.625 ± 0.004	0.619 ± 0.004	0.560 ± 0.005
9-10	0.350 ± 0.004	0.636 ± 0.004	0.651 ± 0.004	0.634 ± 0.005	0.577 ± 0.007
10-11	0.377 ± 0.004	0.651 ± 0.005	0.649 ± 0.006	0.659 ± 0.006	0.591 ± 0.008
11-12	0.394 ± 0.005	0.669 ± 0.005	0.662 ± 0.006	0.672 ± 0.008	0.611 ± 0.010
12-13	0.412 ± 0.006	0.677 ± 0.007	0.661 ± 0.010	0.667 ± 0.009	0.629 ± 0.013
13-14	0.437 ± 0.007	0.687 ± 0.008	0.685 ± 0.009	0.672 ± 0.012	0.625 ± 0.014
14-15	0.463 ± 0.008	0.711 ± 0.008	0.713 ± 0.009	0.675 ± 0.012	
15-16	0.462 ± 0.010	0.693 ± 0.014	0.707 ± 0.012		0.636 ± 0.015
16-17	0.467 ± 0.011	0.712 ± 0.011	0.687 ± 0.016		
17-18	0.490 ± 0.012	0.692 ± 0.016			
18-19	0.490 ± 0.012	0.700 ± 0.017			0.651 ± 0.015
19-20					

Table C.7: The efficiency ϵ_{MuonID} in different bins of p_T and y for prompt $\psi(2S)$ mesons.

p_T (GeV/c)	$2 < y < 2.5$	$2.5 < y < 3$	$3 < y < 3.5$	$3.5 < y < 4$	$4 < y < 4.5$
2-3	0.700 ± 0.004	0.727 ± 0.003	0.730 ± 0.003	0.678 ± 0.003	0.527 ± 0.003
3-4	0.708 ± 0.004	0.744 ± 0.003	0.747 ± 0.003	0.683 ± 0.003	0.525 ± 0.004
4-5	0.724 ± 0.005	0.764 ± 0.003	0.772 ± 0.003	0.700 ± 0.004	0.519 ± 0.004
5-6	0.747 ± 0.006	0.787 ± 0.004	0.796 ± 0.004	0.716 ± 0.004	0.517 ± 0.005
6-7	0.772 ± 0.007	0.808 ± 0.004	0.813 ± 0.005	0.731 ± 0.006	0.520 ± 0.006
7-8	0.792 ± 0.008	0.823 ± 0.006	0.823 ± 0.006	0.740 ± 0.007	0.522 ± 0.008
8-9	0.812 ± 0.009	0.837 ± 0.006	0.832 ± 0.007	0.749 ± 0.009	0.526 ± 0.011
9-10	0.824 ± 0.011	0.844 ± 0.009	0.837 ± 0.008	0.753 ± 0.011	0.536 ± 0.012
10-11	0.837 ± 0.013	0.848 ± 0.011	0.839 ± 0.011	0.748 ± 0.013	0.533 ± 0.016
11-12	0.844 ± 0.016	0.854 ± 0.011	0.839 ± 0.013	0.746 ± 0.017	0.547 ± 0.020
12-13	0.852 ± 0.020	0.855 ± 0.013	0.840 ± 0.015	0.743 ± 0.020	0.555 ± 0.024
13-14	0.861 ± 0.021	0.858 ± 0.016	0.841 ± 0.019	0.727 ± 0.024	0.552 ± 0.029
14-15	0.865 ± 0.020	0.858 ± 0.019	0.839 ± 0.024	0.724 ± 0.033	0.552 ± 0.027
15-16	0.869 ± 0.023	0.855 ± 0.026	0.835 ± 0.028		
16-17	0.873 ± 0.027	0.852 ± 0.029	0.834 ± 0.039		
17-18	0.873 ± 0.028	0.851 ± 0.033			
18-19	0.873 ± 0.035	0.849 ± 0.028			0.563 ± 0.034
19-20			0.818 ± 0.025	0.710 ± 0.034	

 Table C.8: The efficiency ϵ_{MuonID} in different bins of p_T and y for $\psi(2S)$ from b -decay.

p_T (GeV/c)	$2 < y < 2.5$	$2.5 < y < 3$	$3 < y < 3.5$	$3.5 < y < 4$	$4 < y < 4.5$
2-3	0.698 ± 0.004	0.725 ± 0.003	0.728 ± 0.003	0.675 ± 0.003	0.525 ± 0.004
3-4	0.707 ± 0.004	0.743 ± 0.003	0.745 ± 0.003	0.680 ± 0.003	0.523 ± 0.004
4-5	0.724 ± 0.005	0.762 ± 0.003	0.771 ± 0.003	0.700 ± 0.004	0.521 ± 0.005
5-6	0.747 ± 0.005	0.786 ± 0.003	0.794 ± 0.003	0.716 ± 0.004	0.517 ± 0.005
6-7	0.771 ± 0.005	0.807 ± 0.004	0.810 ± 0.004	0.730 ± 0.005	0.519 ± 0.006
7-8	0.792 ± 0.006	0.823 ± 0.004	0.822 ± 0.004	0.741 ± 0.006	0.526 ± 0.007
8-9	0.810 ± 0.006	0.835 ± 0.005	0.830 ± 0.005	0.750 ± 0.007	0.529 ± 0.008
9-10	0.823 ± 0.007	0.844 ± 0.005	0.832 ± 0.006	0.753 ± 0.009	0.535 ± 0.011
10-11	0.834 ± 0.008	0.850 ± 0.007	0.835 ± 0.007	0.750 ± 0.010	0.541 ± 0.014
11-12	0.845 ± 0.009	0.854 ± 0.007	0.838 ± 0.009	0.745 ± 0.012	0.545 ± 0.015
12-13	0.851 ± 0.010	0.856 ± 0.009	0.840 ± 0.010	0.737 ± 0.015	0.547 ± 0.019
13-14	0.859 ± 0.012	0.857 ± 0.009	0.840 ± 0.012	0.734 ± 0.018	0.551 ± 0.024
14-15	0.863 ± 0.013	0.857 ± 0.012	0.837 ± 0.015	0.719 ± 0.019	0.554 ± 0.020
15-16	0.869 ± 0.013	0.857 ± 0.013	0.836 ± 0.015		
16-17	0.870 ± 0.015	0.854 ± 0.015	0.830 ± 0.018		
17-18	0.874 ± 0.016	0.848 ± 0.019			
18-19	0.873 ± 0.015	0.848 ± 0.015	0.820 ± 0.016	0.705 ± 0.020	0.559 ± 0.024
19-20					

Table C.9: The efficiency ϵ_{MuonID} in different bins of p_T and y averaged over prompt $\psi(2S)$ and $\psi(2S)\text{-from-}b$

p_T (GeV/c)	$2 < y < 2.5$	$2.5 < y < 3$	$3 < y < 3.5$	$3.5 < y < 4$	$4 < y < 4.5$
2-3	0.699 ± 0.003	0.726 ± 0.002	0.729 ± 0.002	0.677 ± 0.002	0.526 ± 0.003
3-4	0.708 ± 0.003	0.744 ± 0.002	0.746 ± 0.002	0.682 ± 0.002	0.524 ± 0.003
4-5	0.724 ± 0.003	0.763 ± 0.002	0.772 ± 0.002	0.700 ± 0.003	0.520 ± 0.003
5-6	0.747 ± 0.004	0.787 ± 0.003	0.795 ± 0.003	0.716 ± 0.003	0.517 ± 0.004
6-7	0.771 ± 0.004	0.807 ± 0.003	0.811 ± 0.003	0.730 ± 0.004	0.519 ± 0.005
7-8	0.792 ± 0.005	0.823 ± 0.003	0.822 ± 0.004	0.741 ± 0.004	0.524 ± 0.005
8-9	0.810 ± 0.005	0.836 ± 0.004	0.831 ± 0.004	0.750 ± 0.005	0.528 ± 0.007
9-10	0.824 ± 0.006	0.844 ± 0.005	0.834 ± 0.005	0.753 ± 0.007	0.535 ± 0.008
10-11	0.835 ± 0.007	0.849 ± 0.006	0.836 ± 0.006	0.749 ± 0.008	0.538 ± 0.011
11-12	0.844 ± 0.008	0.854 ± 0.006	0.838 ± 0.007	0.746 ± 0.010	0.545 ± 0.012
12-13	0.851 ± 0.009	0.856 ± 0.008	0.840 ± 0.008	0.739 ± 0.012	0.550 ± 0.015
13-14	0.860 ± 0.010	0.857 ± 0.008	0.840 ± 0.010	0.732 ± 0.014	0.551 ± 0.018
14-15	0.864 ± 0.011	0.857 ± 0.010	0.838 ± 0.012	0.721 ± 0.017	0.553 ± 0.016
15-16	0.869 ± 0.012	0.856 ± 0.012	0.836 ± 0.013	0.715 ± 0.014	
16-17	0.871 ± 0.013	0.853 ± 0.013	0.831 ± 0.016		
17-18	0.874 ± 0.014	0.849 ± 0.016			
18-19	0.873 ± 0.014	0.848 ± 0.013	0.819 ± 0.013	0.706 ± 0.018	0.560 ± 0.020
19-20					

Table C.10: The efficiency $\epsilon_{\text{Trigger}}$ in different bins of p_T and y for prompt $\psi(2S)$ mesons.

p_T (GeV/c)	$2 < y < 2.5$	$2.5 < y < 3$	$3 < y < 3.5$	$3.5 < y < 4$	$4 < y < 4.5$
2-3	0.459 ± 0.003	0.504 ± 0.002	0.519 ± 0.002	0.540 ± 0.002	0.529 ± 0.004
3-4	0.512 ± 0.004	0.538 ± 0.002	0.554 ± 0.002	0.561 ± 0.003	0.545 ± 0.004
4-5	0.560 ± 0.004	0.588 ± 0.003	0.589 ± 0.003	0.592 ± 0.003	0.559 ± 0.005
5-6	0.601 ± 0.005	0.613 ± 0.003	0.619 ± 0.003	0.622 ± 0.003	0.579 ± 0.005
6-7	0.622 ± 0.005	0.641 ± 0.004	0.643 ± 0.004	0.646 ± 0.004	0.614 ± 0.007
7-8	0.639 ± 0.006	0.663 ± 0.004	0.666 ± 0.005	0.662 ± 0.005	0.611 ± 0.008
8-9	0.676 ± 0.007	0.669 ± 0.005	0.674 ± 0.006	0.662 ± 0.007	0.621 ± 0.010
9-10	0.673 ± 0.009	0.684 ± 0.006	0.678 ± 0.007	0.681 ± 0.008	0.622 ± 0.012
10-11	0.694 ± 0.010	0.693 ± 0.008	0.690 ± 0.009	0.675 ± 0.010	0.641 ± 0.015
11-12	0.720 ± 0.012	0.711 ± 0.009	0.693 ± 0.010	0.713 ± 0.012	0.658 ± 0.019
12-13	0.712 ± 0.014	0.721 ± 0.011	0.716 ± 0.012	0.703 ± 0.015	0.696 ± 0.022
13-14	0.740 ± 0.015	0.735 ± 0.013	0.707 ± 0.015	0.697 ± 0.018	0.662 ± 0.028
14-15	0.711 ± 0.018	0.723 ± 0.016	0.735 ± 0.017	0.761 ± 0.021	
15-16	0.683 ± 0.022	0.696 ± 0.019	0.710 ± 0.021		0.689 ± 0.025
16-17	0.761 ± 0.024	0.743 ± 0.021	0.718 ± 0.026		
17-18	0.763 ± 0.025	0.725 ± 0.024			
18-19	0.761 ± 0.024	0.742 ± 0.021	0.748 ± 0.018	0.726 ± 0.025	0.695 ± 0.028
19-20					

Table C.11: The efficiency $\epsilon_{\text{Trigger}}$ in different bins of p_{T} and y for $\psi(2S)$ from b -decay.

p_{T} (GeV/c)	$2 < y < 2.5$	$2.5 < y < 3$	$3 < y < 3.5$	$3.5 < y < 4$	$4 < y < 4.5$
2-3	0.466 ± 0.004	0.501 ± 0.002	0.518 ± 0.002	0.536 ± 0.003	0.523 ± 0.005
3-4	0.516 ± 0.004	0.546 ± 0.002	0.552 ± 0.002	0.558 ± 0.003	0.539 ± 0.005
4-5	0.564 ± 0.004	0.584 ± 0.002	0.592 ± 0.002	0.592 ± 0.003	0.566 ± 0.005
5-6	0.600 ± 0.004	0.611 ± 0.003	0.618 ± 0.003	0.621 ± 0.003	0.584 ± 0.006
6-7	0.625 ± 0.004	0.638 ± 0.003	0.643 ± 0.003	0.646 ± 0.004	0.614 ± 0.006
7-8	0.643 ± 0.005	0.664 ± 0.003	0.654 ± 0.004	0.664 ± 0.004	0.621 ± 0.007
8-9	0.663 ± 0.005	0.676 ± 0.004	0.670 ± 0.004	0.675 ± 0.005	0.618 ± 0.009
9-10	0.678 ± 0.006	0.688 ± 0.004	0.680 ± 0.005	0.686 ± 0.006	0.651 ± 0.010
10-11	0.701 ± 0.006	0.691 ± 0.005	0.686 ± 0.006	0.682 ± 0.008	0.652 ± 0.013
11-12	0.687 ± 0.007	0.697 ± 0.006	0.682 ± 0.007	0.701 ± 0.009	0.673 ± 0.014
12-13	0.723 ± 0.008	0.706 ± 0.007	0.691 ± 0.008	0.695 ± 0.011	0.637 ± 0.018
13-14	0.724 ± 0.009	0.705 ± 0.008	0.701 ± 0.009	0.683 ± 0.013	0.638 ± 0.022
14-15	0.748 ± 0.010	0.729 ± 0.009	0.694 ± 0.011	0.679 ± 0.016	0.659 ± 0.020
15-16	0.728 ± 0.011	0.735 ± 0.010	0.700 ± 0.013	0.724 ± 0.013	
16-17	0.727 ± 0.013	0.717 ± 0.012	0.683 ± 0.015		
17-18	0.718 ± 0.015	0.736 ± 0.014			
18-19	0.731 ± 0.013	0.736 ± 0.012	0.711 ± 0.011	0.709 ± 0.016	0.687 ± 0.023
19-20					

Table C.12: The efficiency $\epsilon_{\text{Trigger}}$ in different bins of p_{T} and y averaged over prompt $\psi(2S)$ and $\psi(2S)$ -from- b

p_{T} (GeV/c)	$2 < y < 2.5$	$2.5 < y < 3$	$3 < y < 3.5$	$3.5 < y < 4$	$4 < y < 4.5$
2-3	0.462 ± 0.002	0.502 ± 0.002	0.518 ± 0.002	0.538 ± 0.002	0.527 ± 0.003
3-4	0.514 ± 0.003	0.542 ± 0.002	0.553 ± 0.002	0.560 ± 0.002	0.542 ± 0.003
4-5	0.562 ± 0.003	0.586 ± 0.002	0.590 ± 0.002	0.592 ± 0.002	0.562 ± 0.003
5-6	0.600 ± 0.003	0.612 ± 0.002	0.619 ± 0.002	0.621 ± 0.002	0.581 ± 0.004
6-7	0.624 ± 0.003	0.639 ± 0.002	0.643 ± 0.002	0.646 ± 0.003	0.614 ± 0.005
7-8	0.642 ± 0.004	0.664 ± 0.003	0.659 ± 0.003	0.663 ± 0.003	0.617 ± 0.006
8-9	0.667 ± 0.004	0.674 ± 0.003	0.672 ± 0.003	0.670 ± 0.004	0.619 ± 0.007
9-10	0.676 ± 0.005	0.686 ± 0.004	0.680 ± 0.004	0.684 ± 0.005	0.639 ± 0.008
10-11	0.699 ± 0.005	0.691 ± 0.004	0.687 ± 0.005	0.679 ± 0.006	0.648 ± 0.010
11-12	0.696 ± 0.006	0.701 ± 0.005	0.686 ± 0.006	0.705 ± 0.007	0.667 ± 0.011
12-13	0.720 ± 0.007	0.711 ± 0.006	0.698 ± 0.007	0.697 ± 0.009	0.660 ± 0.014
13-14	0.728 ± 0.008	0.713 ± 0.007	0.703 ± 0.008	0.688 ± 0.011	0.647 ± 0.017
14-15	0.739 ± 0.009	0.727 ± 0.008	0.705 ± 0.009	0.705 ± 0.013	0.670 ± 0.016
15-16	0.718 ± 0.010	0.725 ± 0.009	0.702 ± 0.011	0.717 ± 0.011	
16-17	0.735 ± 0.012	0.723 ± 0.010	0.692 ± 0.013		
17-18	0.729 ± 0.013	0.733 ± 0.012			
18-19	0.737 ± 0.011	0.737 ± 0.010	0.720 ± 0.010	0.714 ± 0.013	0.690 ± 0.018
19-20					

Table C.13: The efficiency ϵ_{tot} in different bins of p_T and y for prompt $\psi(2S)$ mesons.

p_T (GeV/c)	$2 < y < 2.5$	$2.5 < y < 3$	$3 < y < 3.5$	$3.5 < y < 4$	$4 < y < 4.5$
2-3	0.042 ± 0.000	0.112 ± 0.001	0.138 ± 0.001	0.127 ± 0.001	0.071 ± 0.001
3-4	0.049 ± 0.001	0.136 ± 0.001	0.173 ± 0.001	0.154 ± 0.001	0.080 ± 0.001
4-5	0.063 ± 0.001	0.178 ± 0.001	0.219 ± 0.002	0.190 ± 0.002	0.096 ± 0.001
5-6	0.083 ± 0.001	0.226 ± 0.002	0.259 ± 0.002	0.229 ± 0.002	0.119 ± 0.002
6-7	0.105 ± 0.002	0.267 ± 0.003	0.295 ± 0.003	0.261 ± 0.003	0.140 ± 0.003
7-8	0.126 ± 0.003	0.303 ± 0.004	0.327 ± 0.004	0.289 ± 0.004	0.157 ± 0.004
8-9	0.154 ± 0.004	0.333 ± 0.005	0.347 ± 0.005	0.306 ± 0.006	0.175 ± 0.005
9-10	0.181 ± 0.005	0.365 ± 0.007	0.367 ± 0.007	0.325 ± 0.008	0.187 ± 0.007
10-11	0.194 ± 0.006	0.380 ± 0.009	0.376 ± 0.009	0.333 ± 0.009	0.195 ± 0.009
11-12	0.223 ± 0.009	0.400 ± 0.010	0.387 ± 0.011	0.356 ± 0.013	0.217 ± 0.012
12-13	0.229 ± 0.011	0.419 ± 0.013	0.402 ± 0.014	0.359 ± 0.014	0.254 ± 0.016
13-14	0.287 ± 0.014	0.442 ± 0.016	0.426 ± 0.018	0.369 ± 0.018	0.234 ± 0.018
14-15	0.286 ± 0.017	0.437 ± 0.017	0.446 ± 0.021	0.396 ± 0.024	0.226 ± 0.017
15-16	0.255 ± 0.019	0.462 ± 0.021	0.425 ± 0.024		
16-17	0.280 ± 0.025	0.458 ± 0.025	0.418 ± 0.029		
17-18	0.308 ± 0.035	0.461 ± 0.032			
18-19	0.340 ± 0.025	0.444 ± 0.027	0.448 ± 0.022	0.350 ± 0.025	0.250 ± 0.030
19-20					

 Table C.14: The efficiency ϵ_{tot} in different bins of p_T and y for $\psi(2S)$ from b -decay.

p_T (GeV/c)	$2 < y < 2.5$	$2.5 < y < 3$	$3 < y < 3.5$	$3.5 < y < 4$	$4 < y < 4.5$
2-3	0.041 ± 0.001	0.110 ± 0.001	0.136 ± 0.001	0.124 ± 0.001	0.069 ± 0.001
3-4	0.048 ± 0.001	0.135 ± 0.001	0.170 ± 0.001	0.149 ± 0.001	0.079 ± 0.001
4-5	0.062 ± 0.001	0.177 ± 0.001	0.215 ± 0.002	0.187 ± 0.002	0.098 ± 0.001
5-6	0.080 ± 0.001	0.221 ± 0.002	0.254 ± 0.002	0.225 ± 0.002	0.117 ± 0.002
6-7	0.104 ± 0.001	0.261 ± 0.002	0.290 ± 0.003	0.256 ± 0.003	0.141 ± 0.003
7-8	0.126 ± 0.002	0.305 ± 0.003	0.317 ± 0.003	0.279 ± 0.004	0.160 ± 0.003
8-9	0.145 ± 0.002	0.330 ± 0.003	0.342 ± 0.004	0.306 ± 0.005	0.172 ± 0.004
9-10	0.168 ± 0.003	0.353 ± 0.004	0.364 ± 0.005	0.322 ± 0.006	0.192 ± 0.006
10-11	0.196 ± 0.004	0.370 ± 0.005	0.366 ± 0.006	0.332 ± 0.007	0.204 ± 0.007
11-12	0.204 ± 0.004	0.389 ± 0.006	0.373 ± 0.007	0.347 ± 0.009	0.219 ± 0.009
12-13	0.233 ± 0.005	0.403 ± 0.008	0.380 ± 0.009	0.334 ± 0.010	0.210 ± 0.011
13-14	0.246 ± 0.007	0.402 ± 0.008	0.395 ± 0.010	0.323 ± 0.012	0.214 ± 0.013
14-15	0.273 ± 0.008	0.438 ± 0.010	0.411 ± 0.012	0.322 ± 0.013	0.235 ± 0.013
15-16	0.275 ± 0.009	0.416 ± 0.013	0.411 ± 0.013		
16-17	0.284 ± 0.010	0.429 ± 0.013	0.386 ± 0.016		
17-18	0.284 ± 0.011	0.417 ± 0.016			
18-19	0.296 ± 0.011	0.435 ± 0.016	0.407 ± 0.012	0.328 ± 0.015	0.239 ± 0.015
19-20					

⁷⁹² **D Fitting plots in each kinematic bin**

⁷⁹³ For each kinematic bin of $\psi(2S)$ candidates, the two-dimensional fit to the invariant mass
⁷⁹⁴ and the lifetime are shown in Fig. D.1-Fig. D.79.

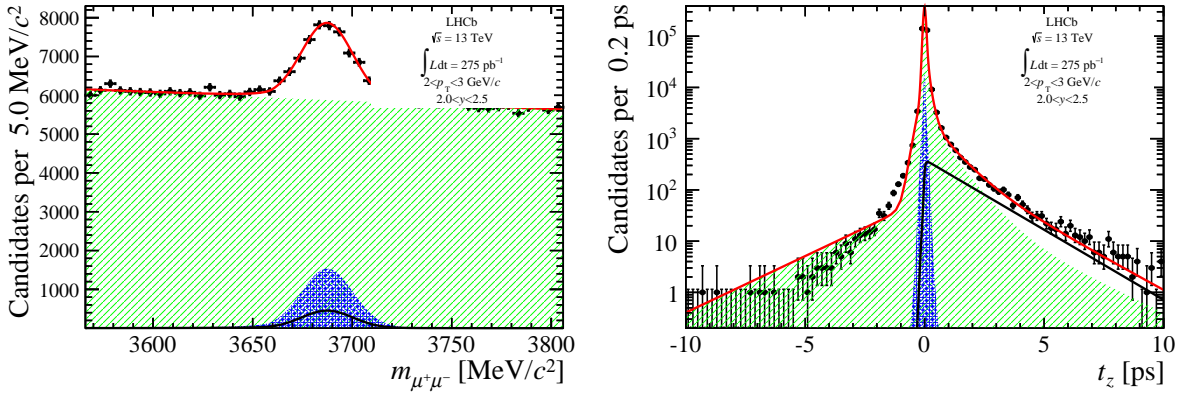


Figure D.1: (Left) Invariant mass and (Right) pseudo-proper decay time fit results of $\psi(2S)$ candidates with $p_T \in [2, 3]$ GeV/ c and $y \in [2.0, 2.5]$.

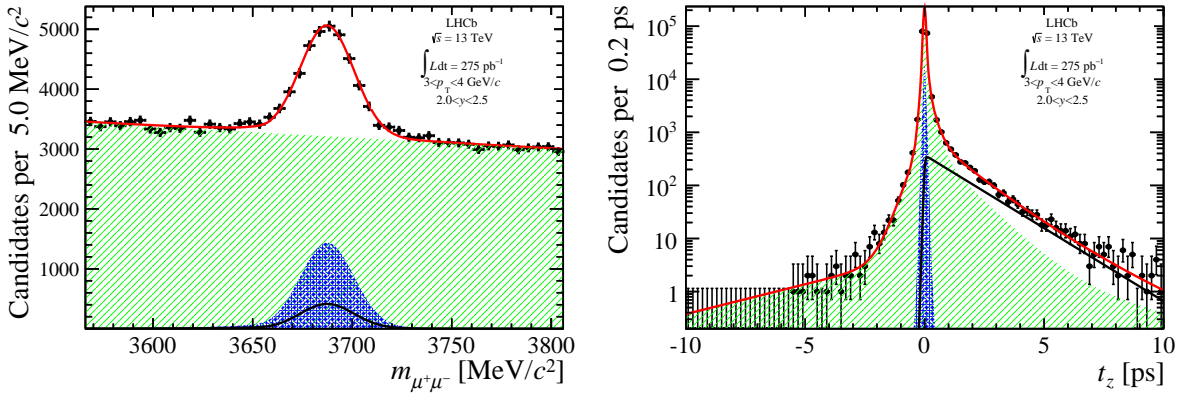


Figure D.2: (Left) Invariant mass and (Right) pseudo-proper decay time fit results of $\psi(2S)$ candidates with $p_T \in [3, 4]$ GeV/ c and $y \in [2.0, 2.5]$.

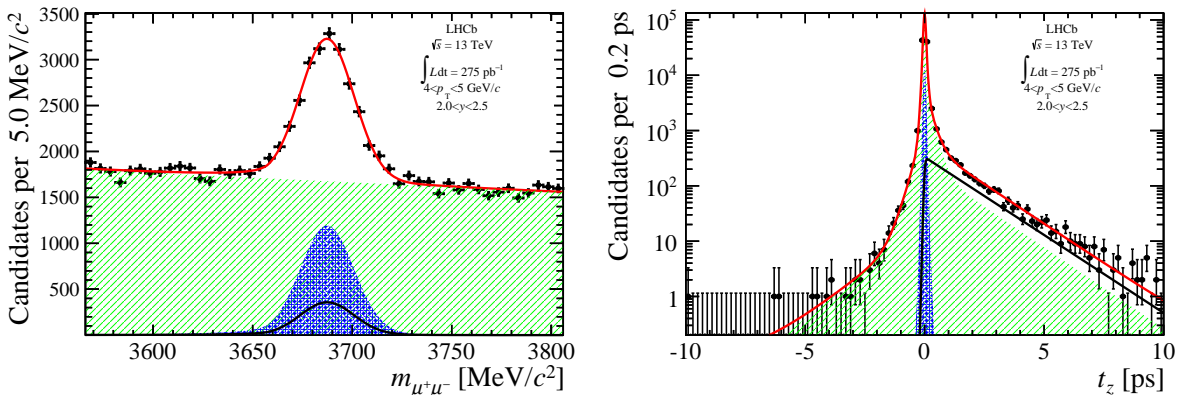


Figure D.3: (Left) Invariant mass and (Right) pseudo-proper decay time fit results of $\psi(2S)$ candidates with $p_T \in [4, 5]$ GeV/ c and $y \in [2.0, 2.5]$.

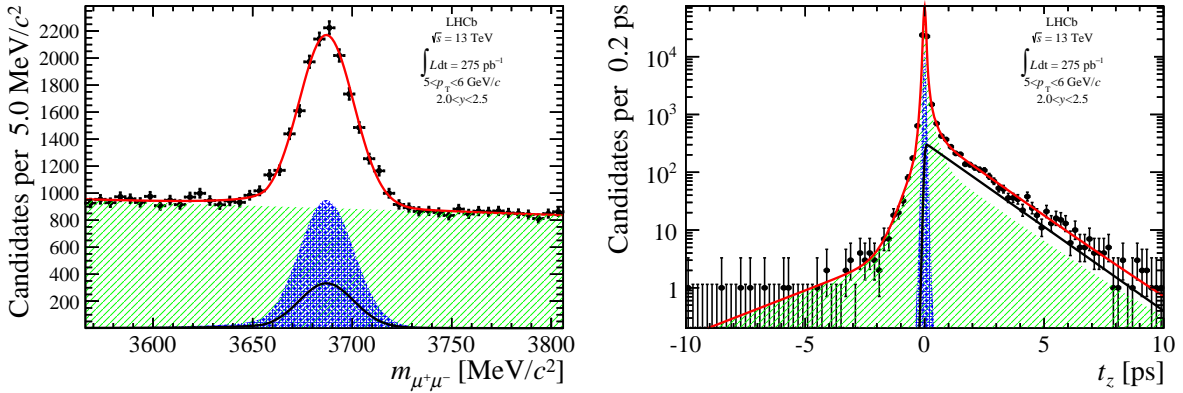


Figure D.4: (Left) Invariant mass and (Right) pseudo-proper decay time fit results of $\psi(2S)$ candidates with $p_T \in [5, 6]$ GeV/ c and $y \in [2.0, 2.5]$.

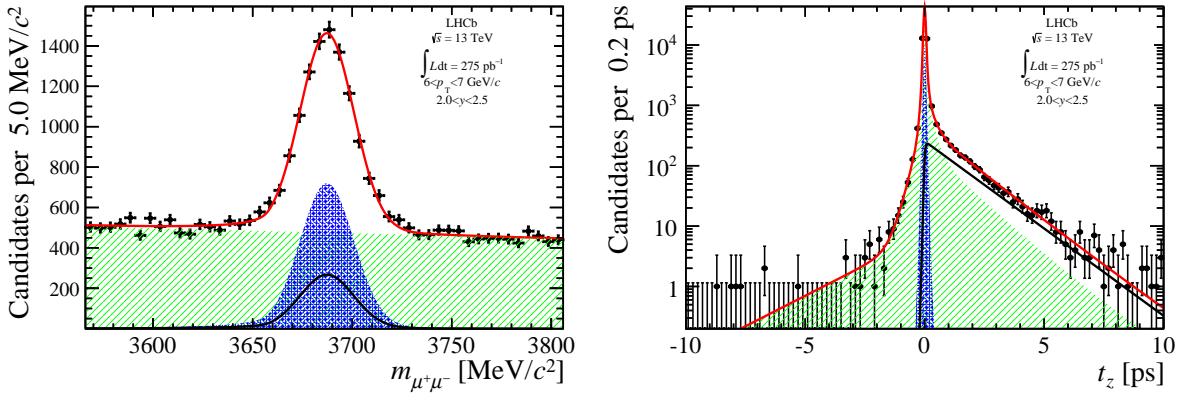


Figure D.5: (Left) Invariant mass and (Right) pseudo-proper decay time fit results of $\psi(2S)$ candidates with $p_T \in [6, 7]$ GeV/ c and $y \in [2.0, 2.5]$.

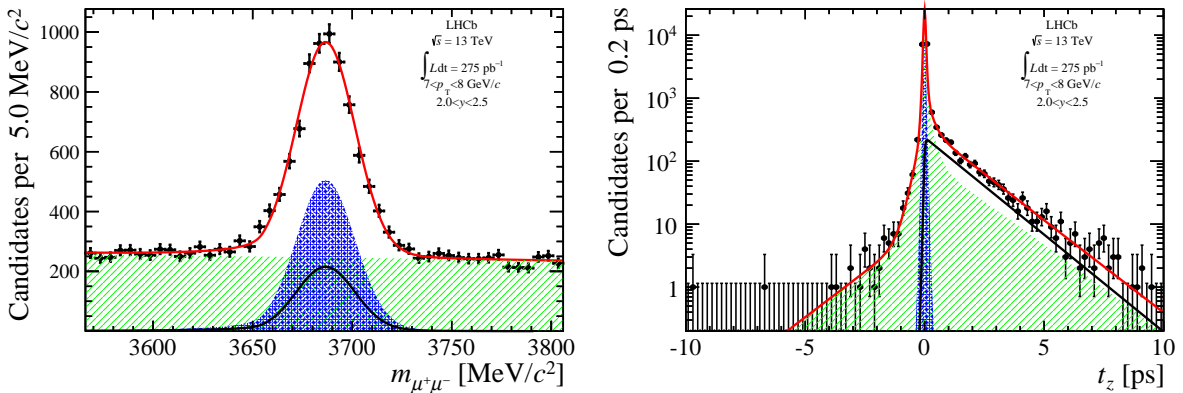


Figure D.6: (Left) Invariant mass and (Right) pseudo-proper decay time fit results of $\psi(2S)$ candidates with $p_T \in [7, 8]$ GeV/ c and $y \in [2.0, 2.5]$.

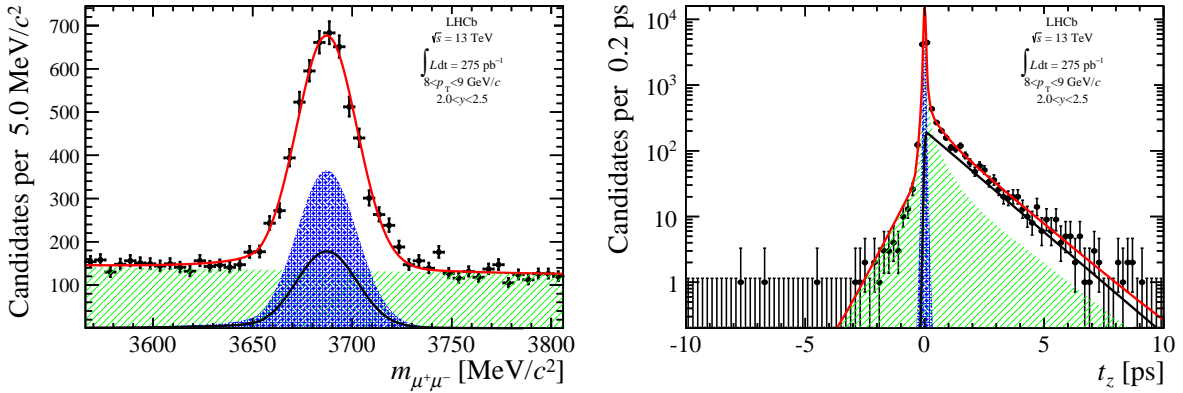


Figure D.7: (Left) Invariant mass and (Right) pseudo-proper decay time fit results of $\psi(2S)$ candidates with $p_T \in [8, 9]$ GeV/ c and $y \in [2.0, 2.5]$.

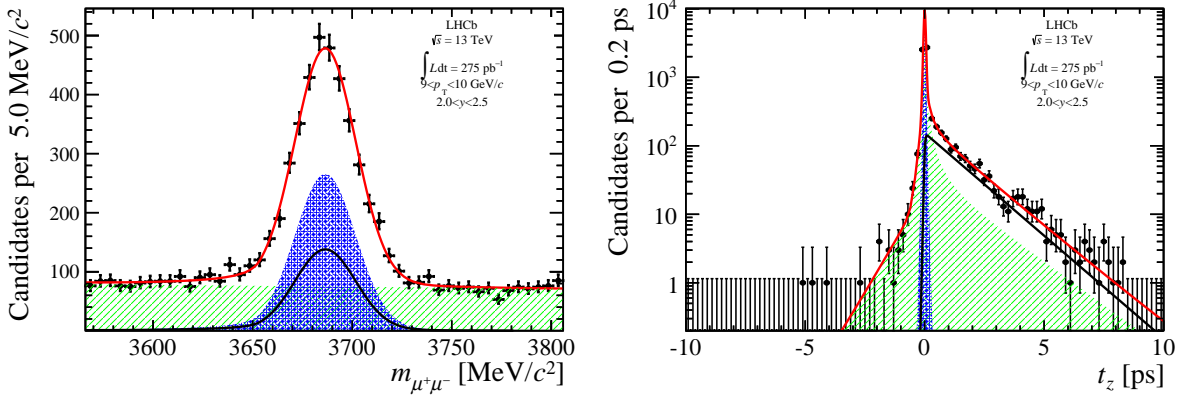


Figure D.8: (Left) Invariant mass and (Right) pseudo-proper decay time fit results of $\psi(2S)$ candidates with $p_T \in [9, 10]$ GeV/ c and $y \in [2.0, 2.5]$.

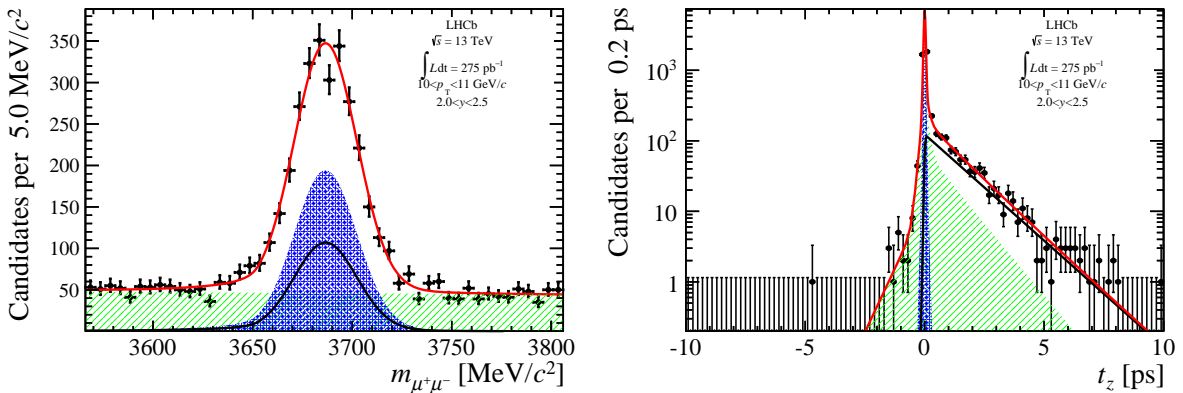


Figure D.9: (Left) Invariant mass and (Right) pseudo-proper decay time fit results of $\psi(2S)$ candidates with $p_T \in [10, 11]$ GeV/ c and $y \in [2.0, 2.5]$.

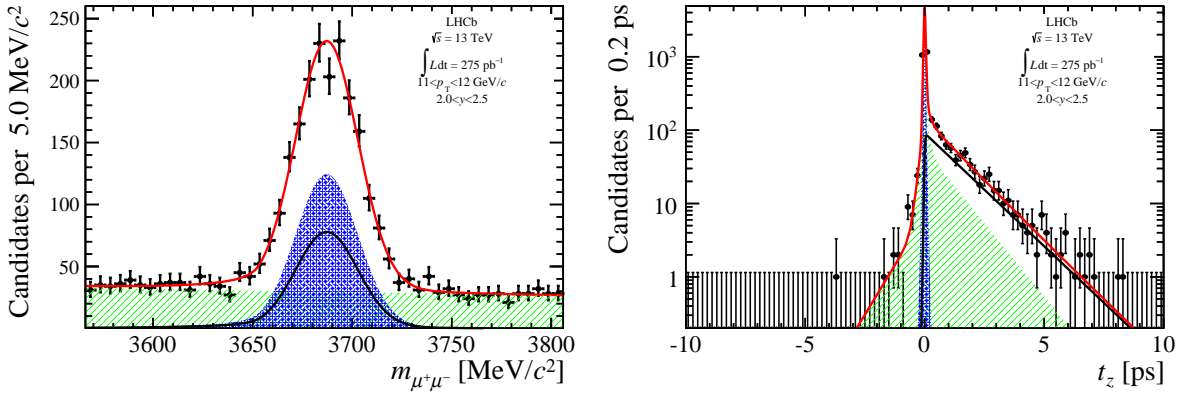


Figure D.10: (Left) Invariant mass and (Right) pseudo-proper decay time fit results of $\psi(2S)$ candidates with $p_T \in [11, 12]$ GeV/ c and $y \in [2.0, 2.5]$.

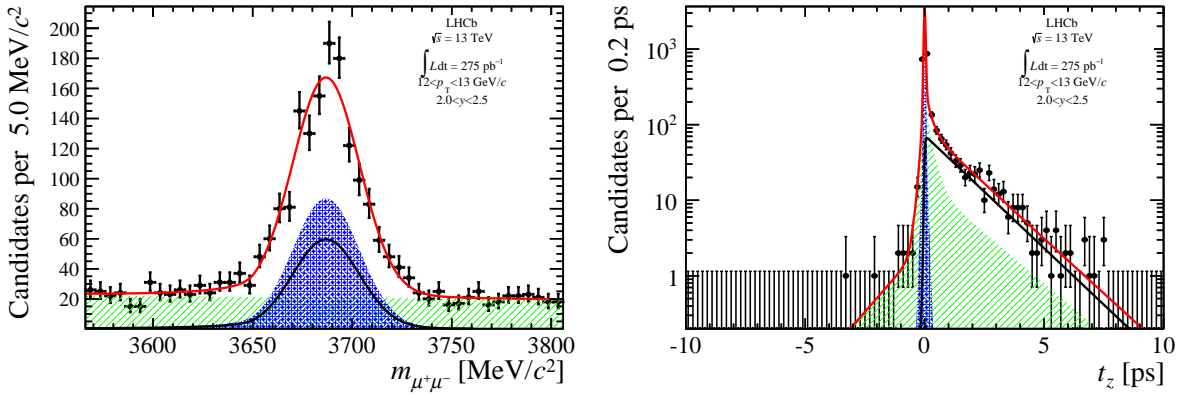


Figure D.11: (Left) Invariant mass and (Right) pseudo-proper decay time fit results of $\psi(2S)$ candidates with $p_T \in [12, 13]$ GeV/ c and $y \in [2.0, 2.5]$.

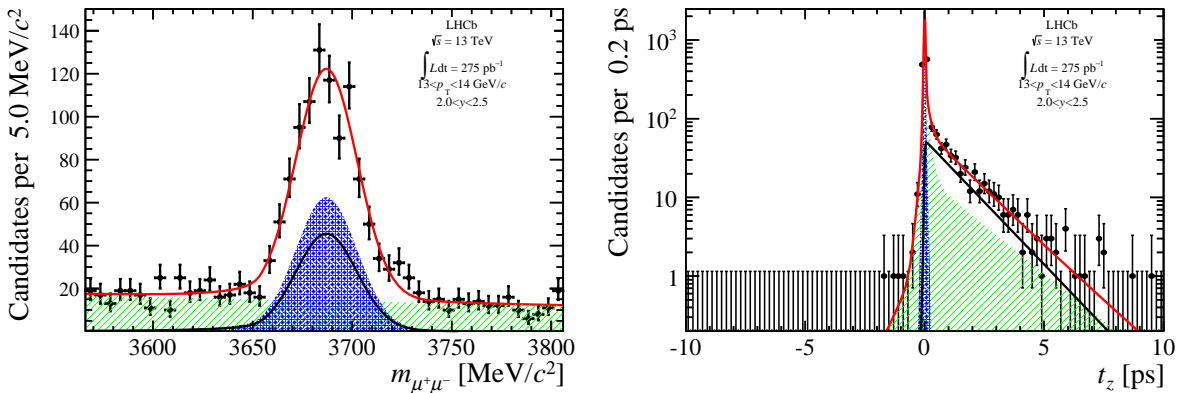


Figure D.12: (Left) Invariant mass and (Right) pseudo-proper decay time fit results of $\psi(2S)$ candidates with $p_T \in [13, 14]$ GeV/ c and $y \in [2.0, 2.5]$.

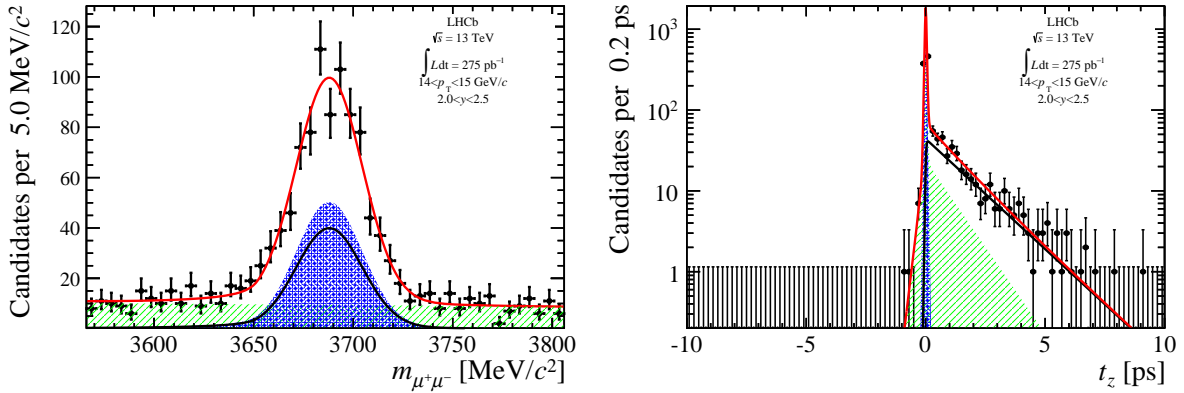


Figure D.13: (Left) Invariant mass and (Right) pseudo-proper decay time fit results of $\psi(2S)$ candidates with $p_T \in [14, 15]$ GeV/ c and $y \in [2.0, 2.5]$.

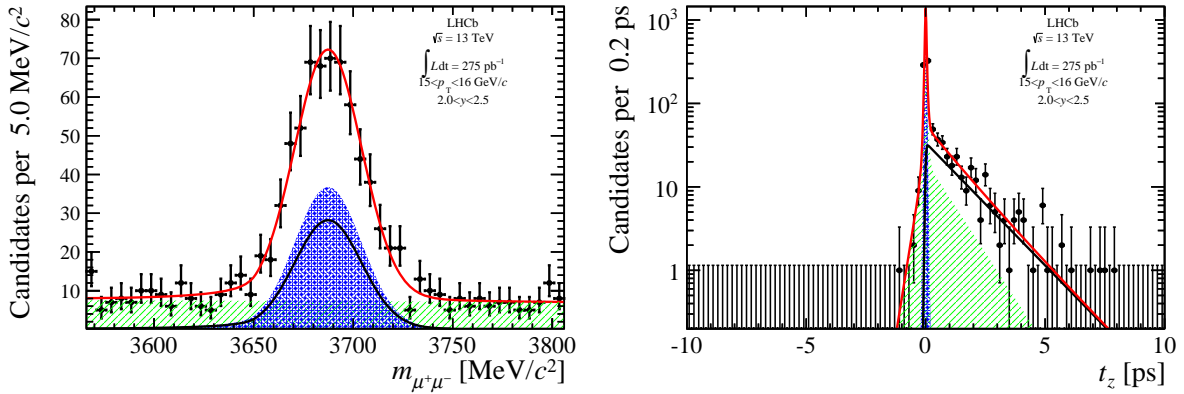


Figure D.14: (Left) Invariant mass and (Right) pseudo-proper decay time fit results of $\psi(2S)$ candidates with $p_T \in [15, 16]$ GeV/ c and $y \in [2.0, 2.5]$.

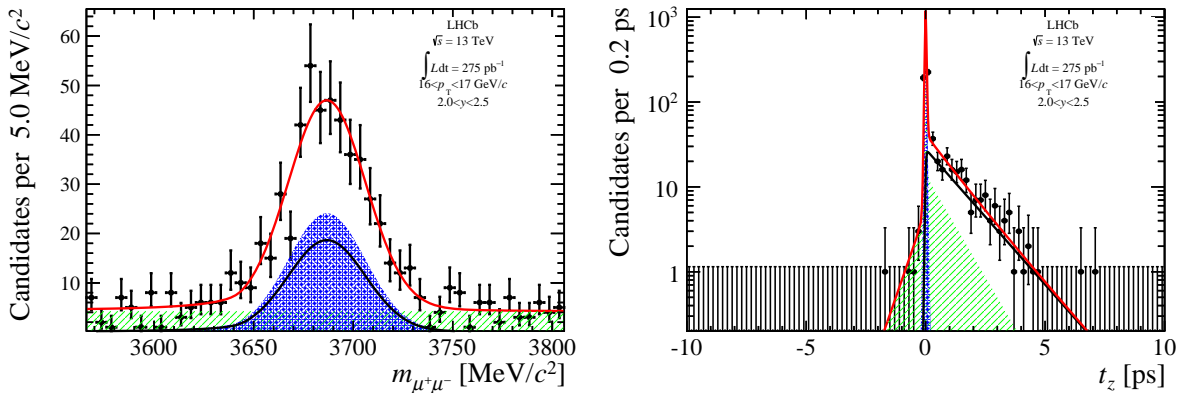


Figure D.15: (Left) Invariant mass and (Right) pseudo-proper decay time fit results of $\psi(2S)$ candidates with $p_T \in [16, 17]$ GeV/ c and $y \in [2.0, 2.5]$.

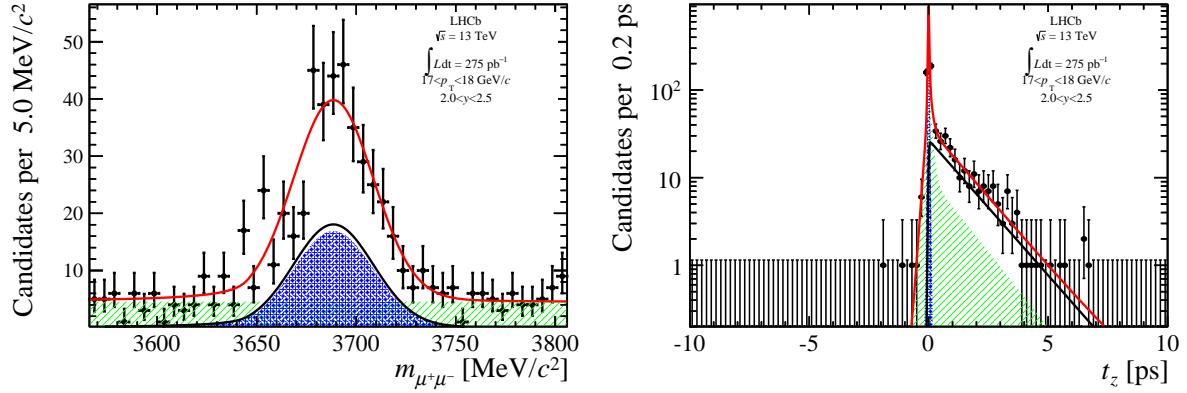


Figure D.16: (Left) Invariant mass and (Right) pseudo-proper decay time fit results of $\psi(2S)$ candidates with $p_T \in [17, 18] \text{ GeV}/c$ and $y \in [2.0, 2.5]$.

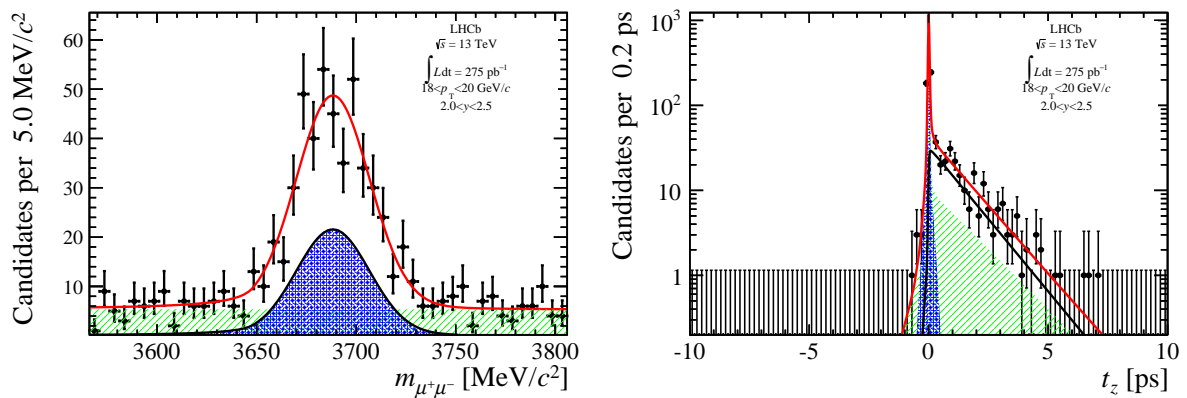


Figure D.17: (Left) Invariant mass and (Right) pseudo-proper decay time fit results of $\psi(2S)$ candidates with $p_T \in [18, 20] \text{ GeV}/c$ and $y \in [2.0, 2.5]$.

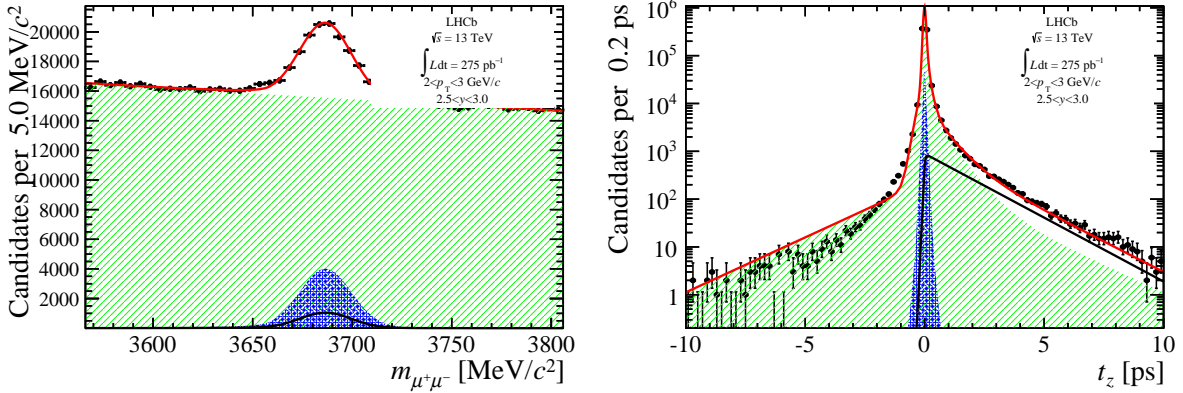


Figure D.18: (Left) Invariant mass and (Right) pseudo-proper decay time fit results of $\psi(2S)$ candidates with $p_T \in [2, 3]$ GeV/ c and $y \in [2.5, 3.0]$.

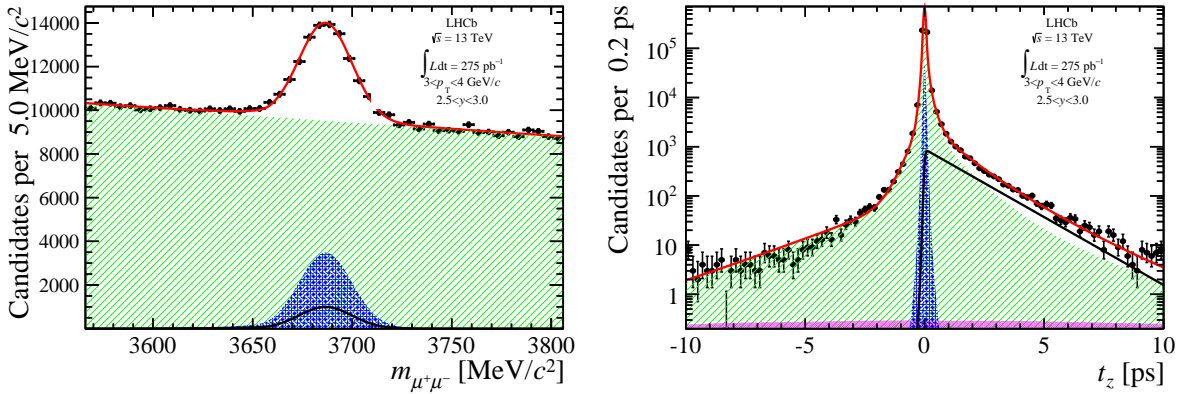


Figure D.19: (Left) Invariant mass and (Right) pseudo-proper decay time fit results of $\psi(2S)$ candidates with $p_T \in [3, 4]$ GeV/ c and $y \in [2.5, 3.0]$.

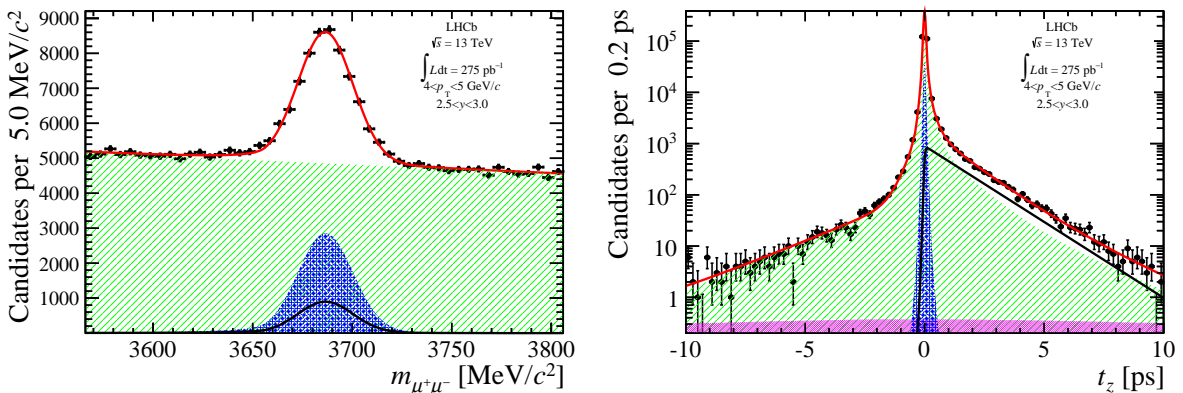


Figure D.20: (Left) Invariant mass and (Right) pseudo-proper decay time fit results of $\psi(2S)$ candidates with $p_T \in [4, 5]$ GeV/ c and $y \in [2.5, 3.0]$.

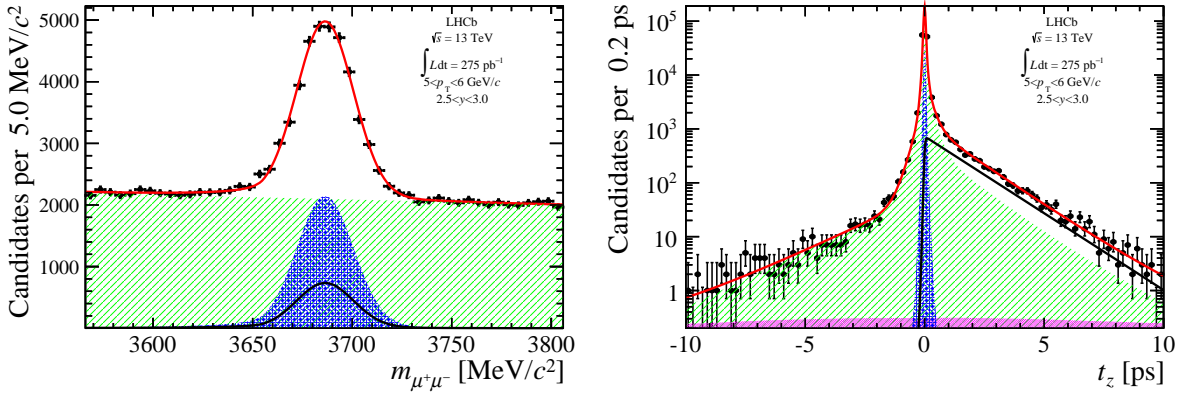


Figure D.21: (Left) Invariant mass and (Right) pseudo-proper decay time fit results of $\psi(2S)$ candidates with $p_T \in [5, 6]$ GeV/ c and $y \in [2.5, 3.0]$.

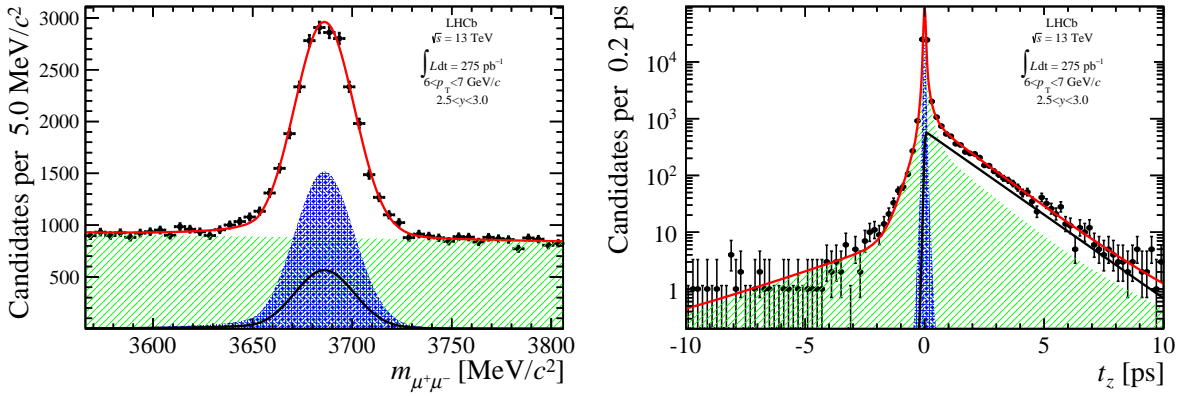


Figure D.22: (Left) Invariant mass and (Right) pseudo-proper decay time fit results of $\psi(2S)$ candidates with $p_T \in [6, 7]$ GeV/ c and $y \in [2.5, 3.0]$.

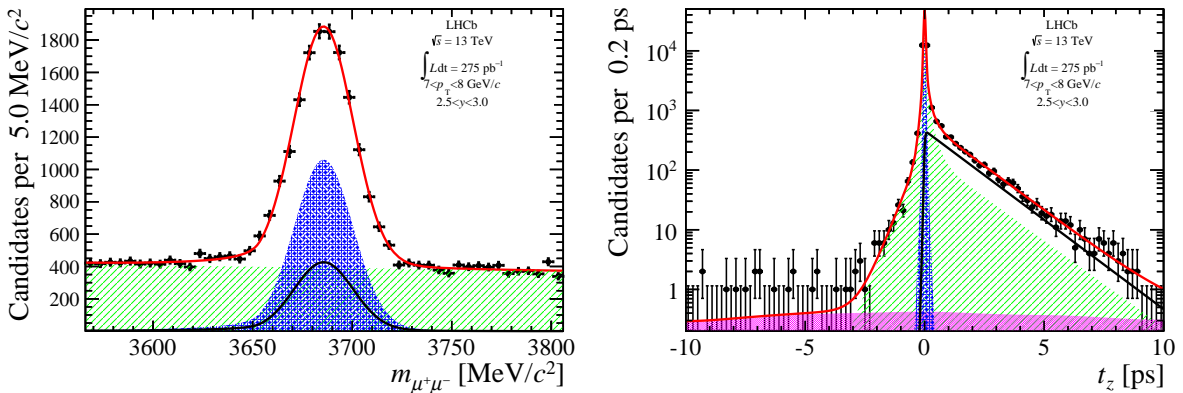


Figure D.23: (Left) Invariant mass and (Right) pseudo-proper decay time fit results of $\psi(2S)$ candidates with $p_T \in [7, 8]$ GeV/ c and $y \in [2.5, 3.0]$.

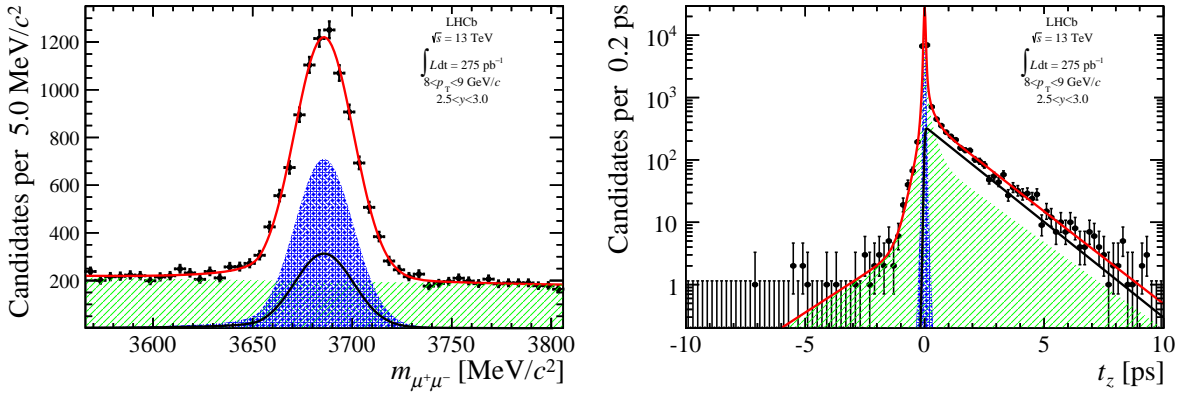


Figure D.24: (Left) Invariant mass and (Right) pseudo-proper decay time fit results of $\psi(2S)$ candidates with $p_T \in [8, 9]$ GeV/ c and $y \in [2.5, 3.0]$.

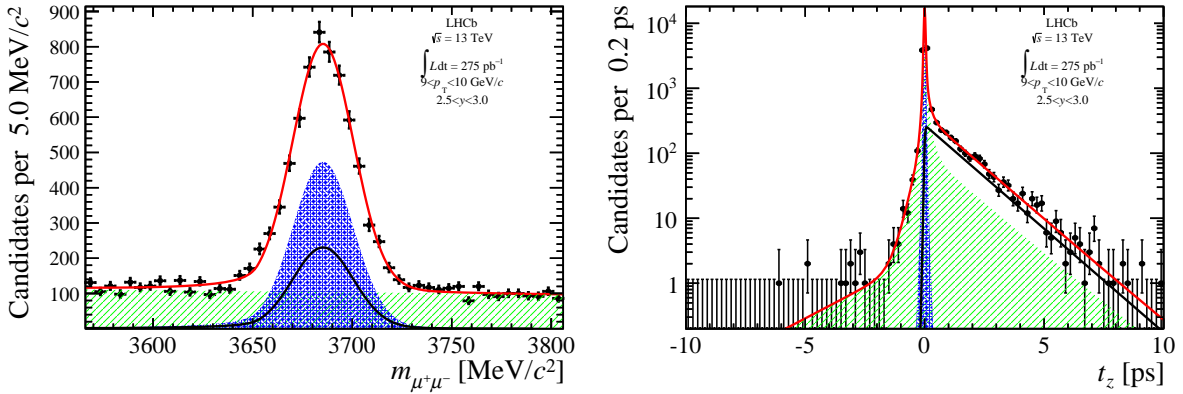


Figure D.25: (Left) Invariant mass and (Right) pseudo-proper decay time fit results of $\psi(2S)$ candidates with $p_T \in [9, 10]$ GeV/ c and $y \in [2.5, 3.0]$.

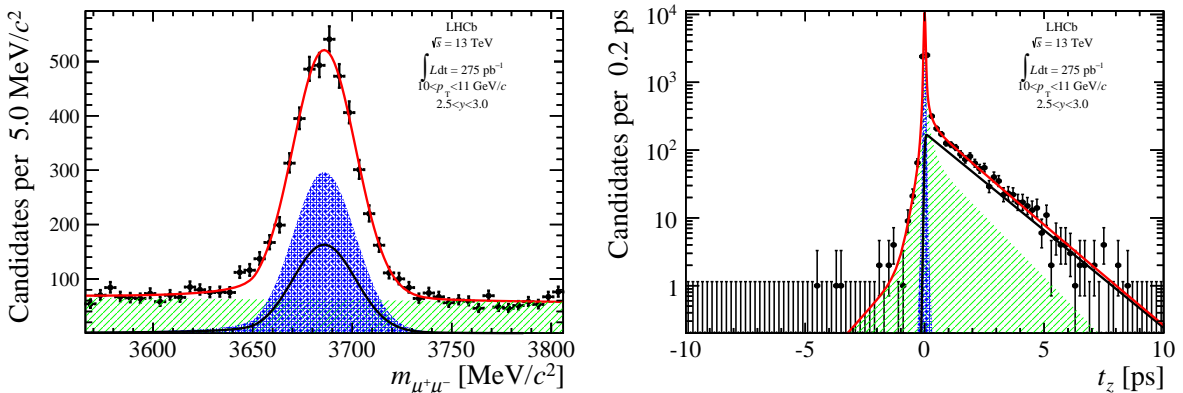


Figure D.26: (Left) Invariant mass and (Right) pseudo-proper decay time fit results of $\psi(2S)$ candidates with $p_T \in [10, 11]$ GeV/ c and $y \in [2.5, 3.0]$.

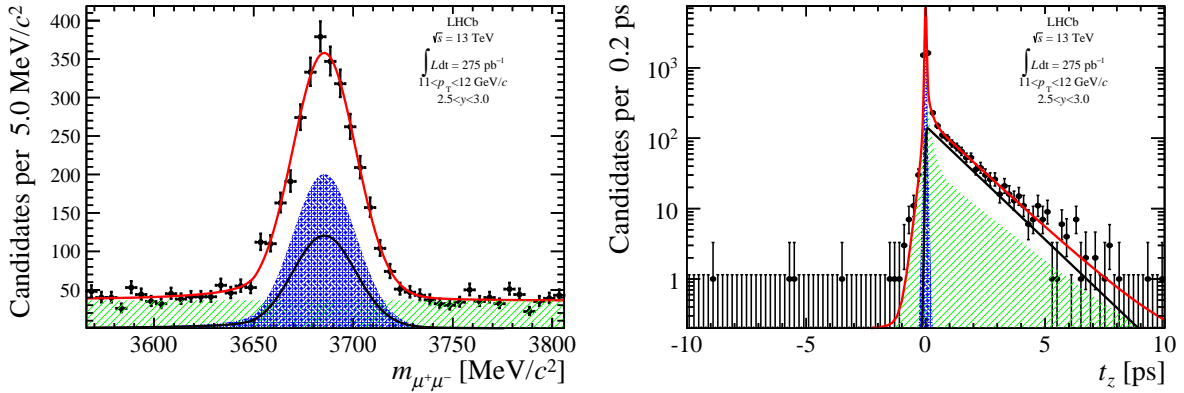


Figure D.27: (Left) Invariant mass and (Right) pseudo-proper decay time fit results of $\psi(2S)$ candidates with $p_T \in [11, 12]$ GeV/ c and $y \in [2.5, 3.0]$.

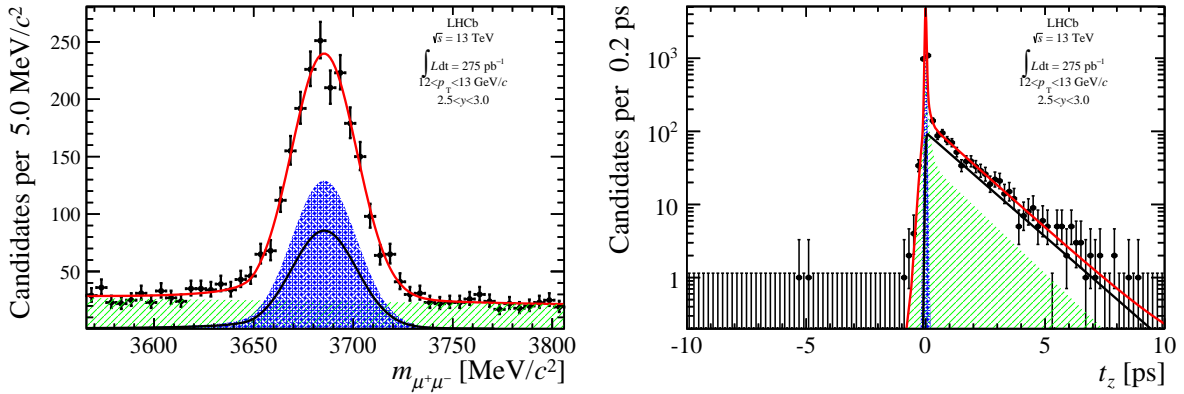


Figure D.28: (Left) Invariant mass and (Right) pseudo-proper decay time fit results of $\psi(2S)$ candidates with $p_T \in [12, 13]$ GeV/ c and $y \in [2.5, 3.0]$.

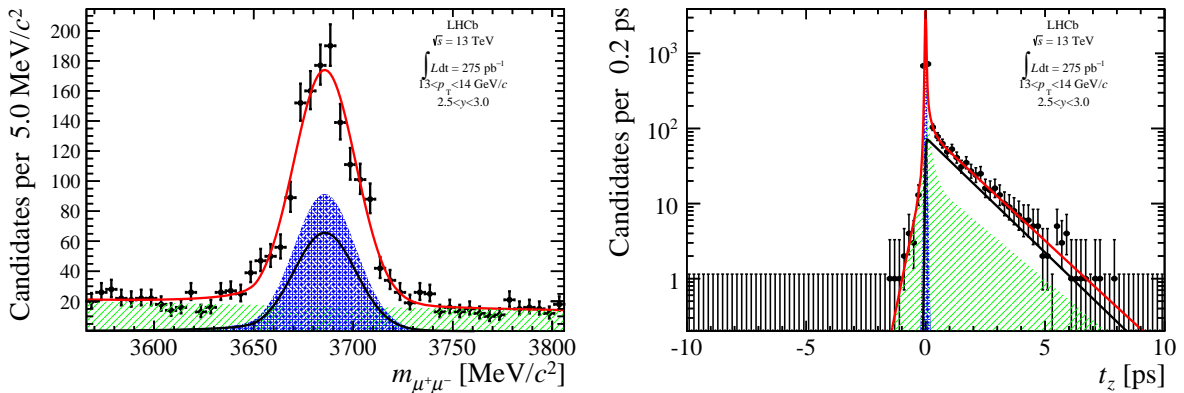


Figure D.29: (Left) Invariant mass and (Right) pseudo-proper decay time fit results of $\psi(2S)$ candidates with $p_T \in [13, 14]$ GeV/ c and $y \in [2.5, 3.0]$.

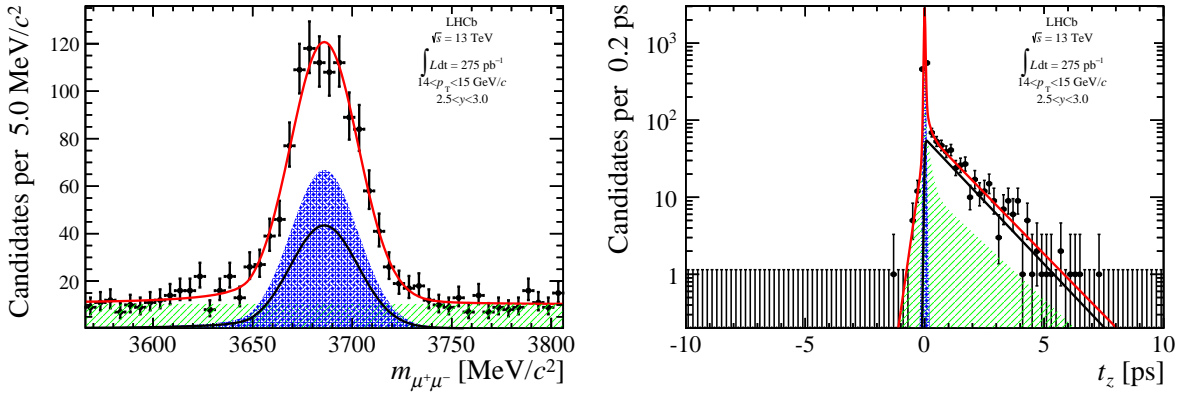


Figure D.30: (Left) Invariant mass and (Right) pseudo-proper decay time fit results of $\psi(2S)$ candidates with $p_T \in [14, 15]$ GeV/ c and $y \in [2.5, 3.0]$.

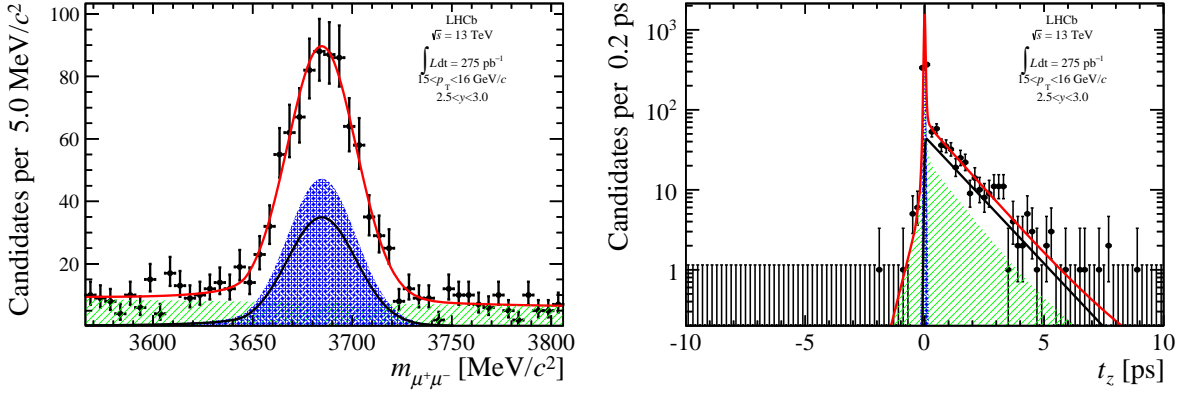


Figure D.31: (Left) Invariant mass and (Right) pseudo-proper decay time fit results of $\psi(2S)$ candidates with $p_T \in [15, 16]$ GeV/ c and $y \in [2.5, 3.0]$.

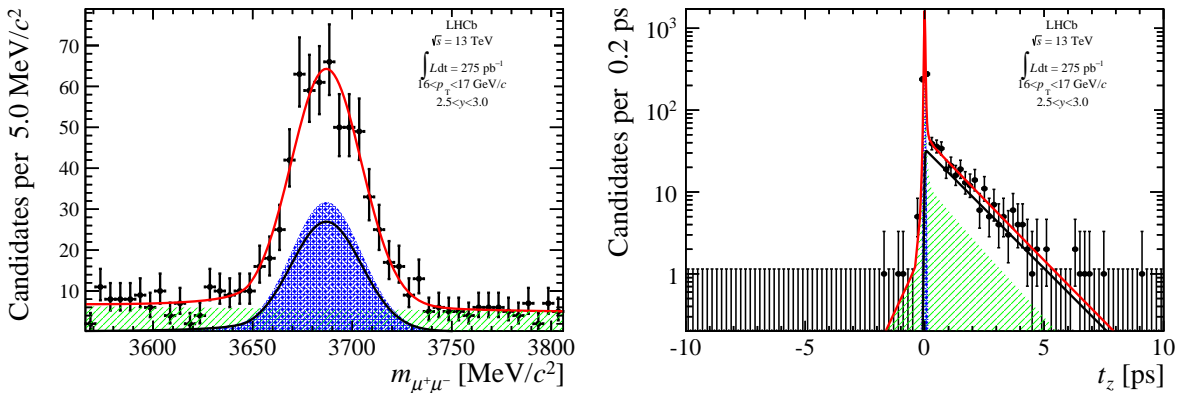


Figure D.32: (Left) Invariant mass and (Right) pseudo-proper decay time fit results of $\psi(2S)$ candidates with $p_T \in [16, 17]$ GeV/ c and $y \in [2.5, 3.0]$.

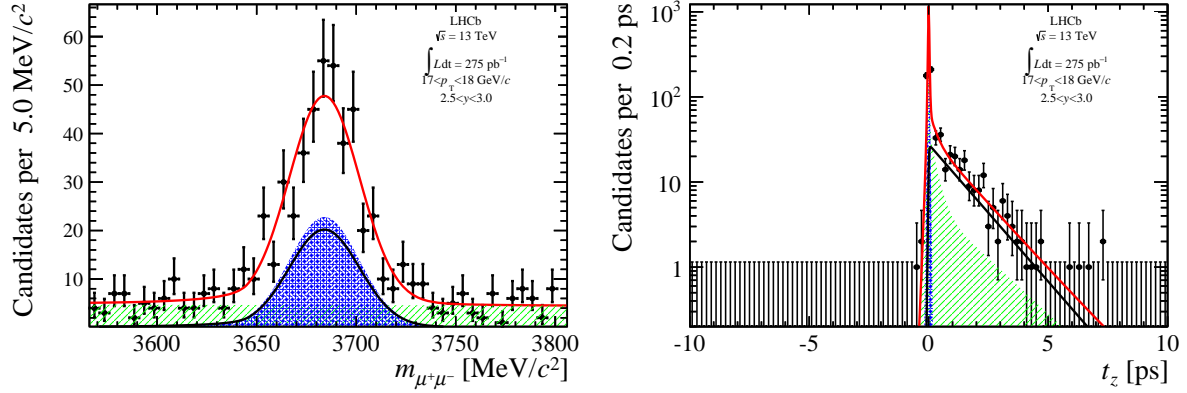


Figure D.33: (Left) Invariant mass and (Right) pseudo-proper decay time fit results of $\psi(2S)$ candidates with $p_T \in [17, 18]$ GeV/ c and $y \in [2.5, 3.0]$.

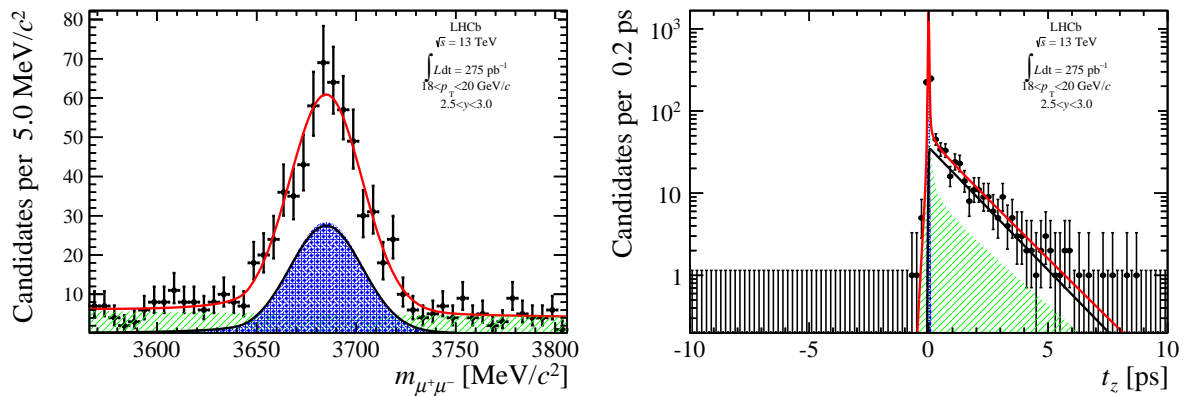


Figure D.34: (Left) Invariant mass and (Right) pseudo-proper decay time fit results of $\psi(2S)$ candidates with $p_T \in [18, 20]$ GeV/ c and $y \in [2.5, 3.0]$.

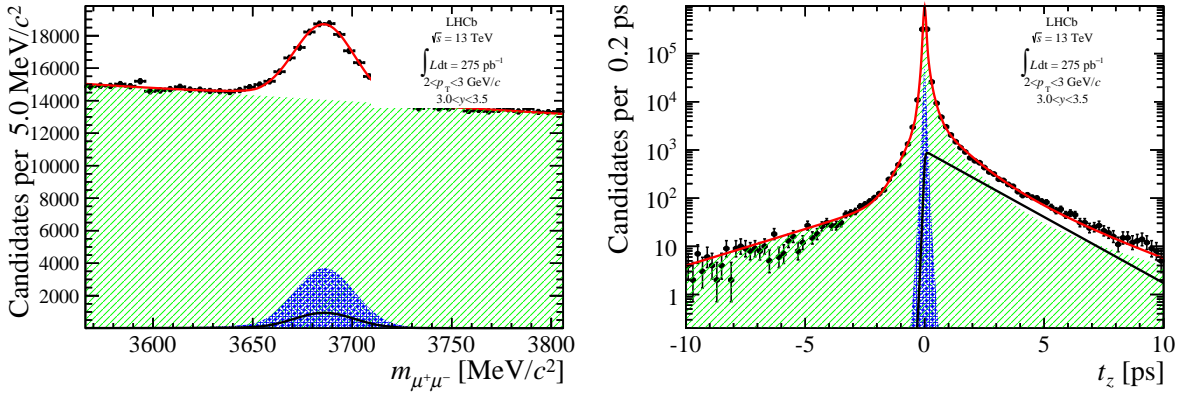


Figure D.35: (Left) Invariant mass and (Right) pseudo-proper decay time fit results of $\psi(2S)$ candidates with $p_T \in [2, 3]$ GeV/ c and $y \in [3.0, 3.5]$.

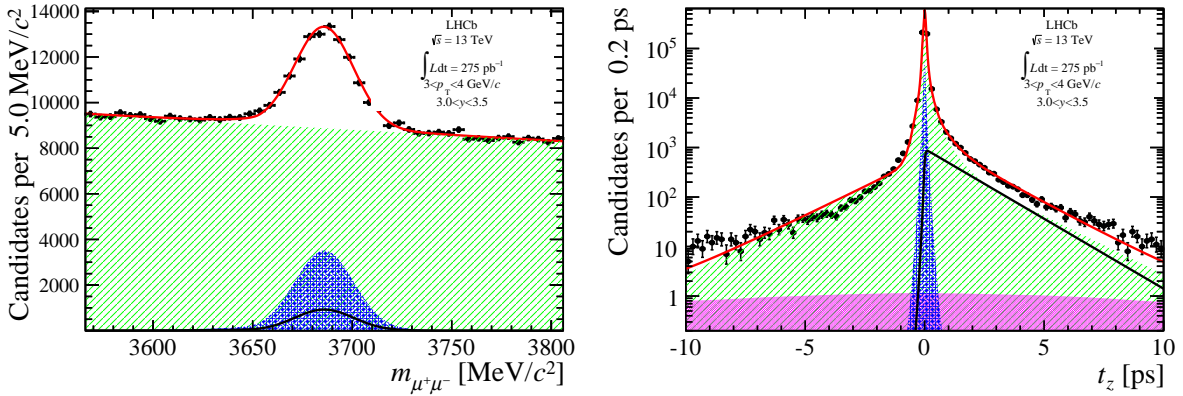


Figure D.36: (Left) Invariant mass and (Right) pseudo-proper decay time fit results of $\psi(2S)$ candidates with $p_T \in [3, 4]$ GeV/ c and $y \in [3.0, 3.5]$.

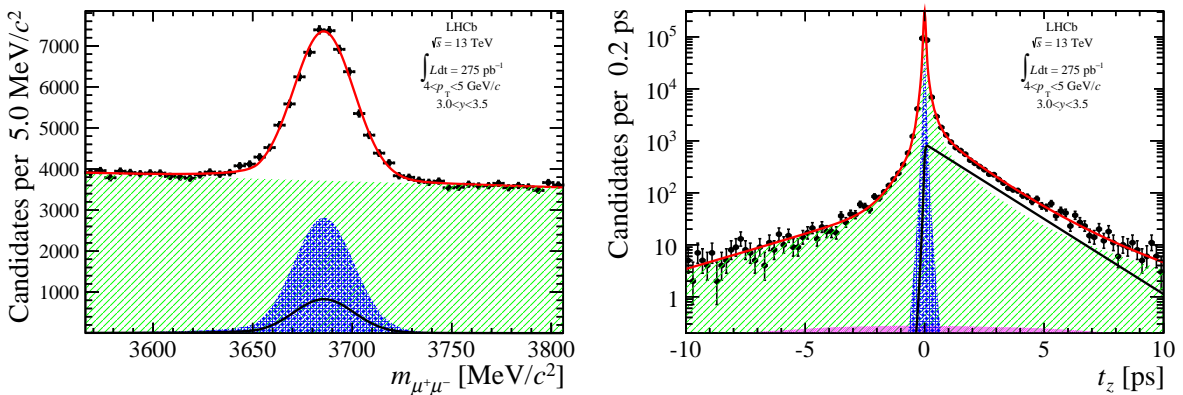


Figure D.37: (Left) Invariant mass and (Right) pseudo-proper decay time fit results of $\psi(2S)$ candidates with $p_T \in [4, 5]$ GeV/ c and $y \in [3.0, 3.5]$.

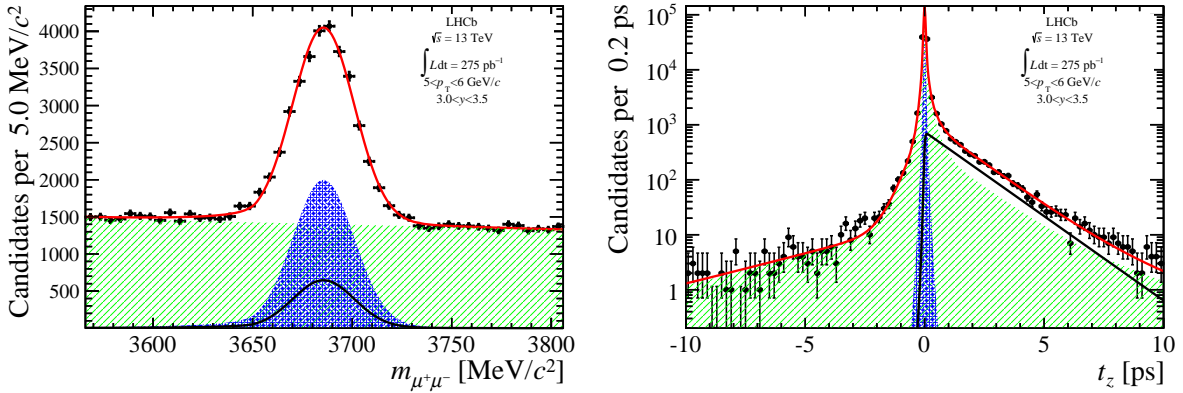


Figure D.38: (Left) Invariant mass and (Right) pseudo-proper decay time fit results of $\psi(2S)$ candidates with $p_T \in [5, 6]$ GeV/ c and $y \in [3.0, 3.5]$.

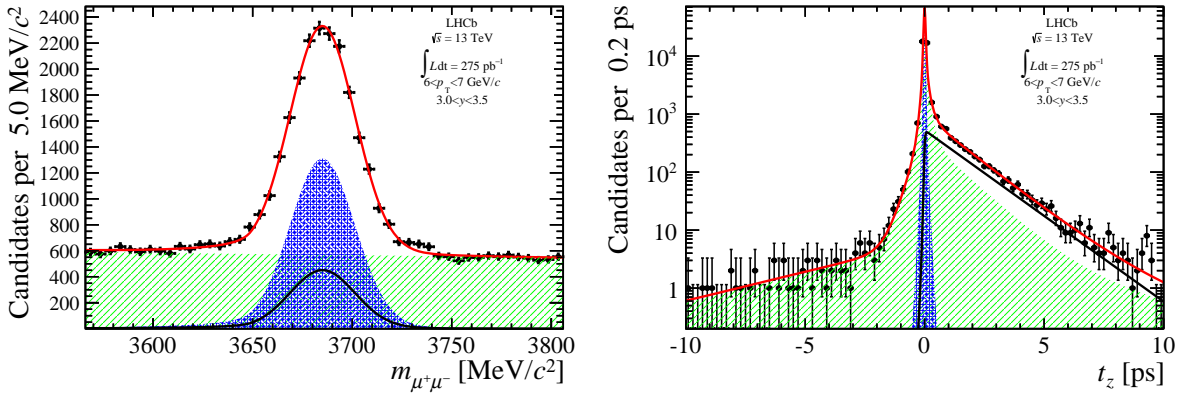


Figure D.39: (Left) Invariant mass and (Right) pseudo-proper decay time fit results of $\psi(2S)$ candidates with $p_T \in [6, 7]$ GeV/ c and $y \in [3.0, 3.5]$.

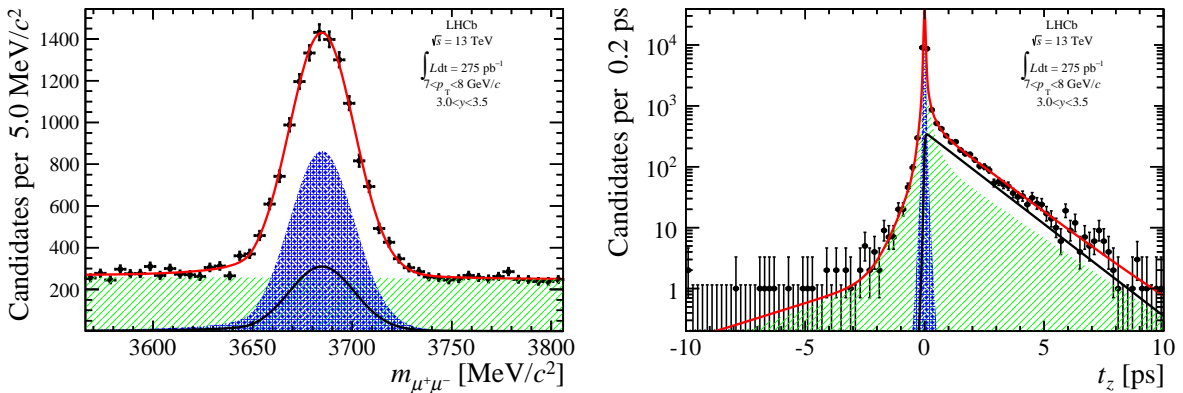


Figure D.40: (Left) Invariant mass and (Right) pseudo-proper decay time fit results of $\psi(2S)$ candidates with $p_T \in [7, 8]$ GeV/ c and $y \in [3.0, 3.5]$.

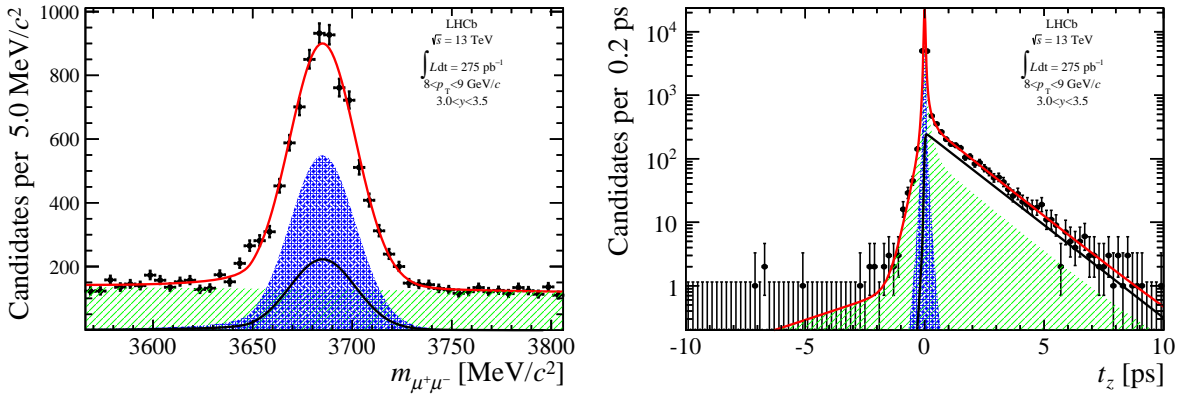


Figure D.41: (Left) Invariant mass and (Right) pseudo-proper decay time fit results of $\psi(2S)$ candidates with $p_T \in [8, 9]$ GeV/ c and $y \in [3.0, 3.5]$.

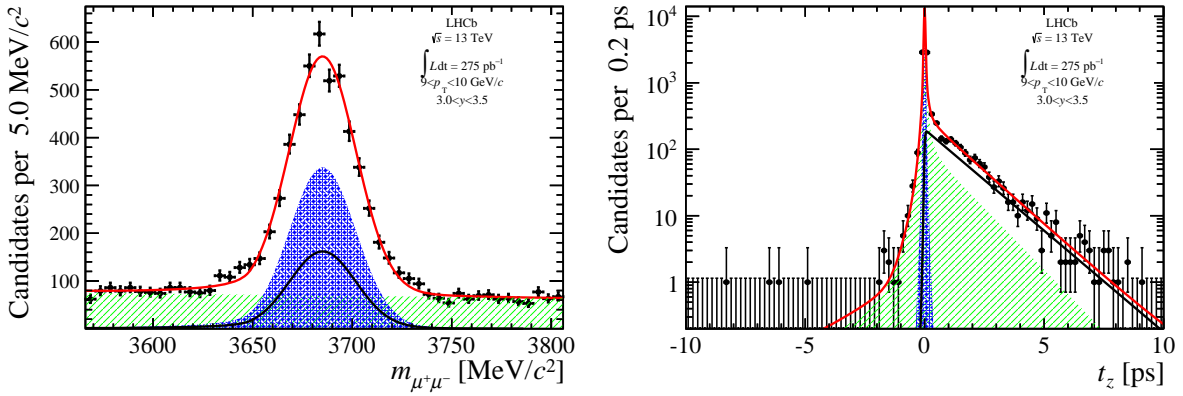


Figure D.42: (Left) Invariant mass and (Right) pseudo-proper decay time fit results of $\psi(2S)$ candidates with $p_T \in [9, 10]$ GeV/ c and $y \in [3.0, 3.5]$.

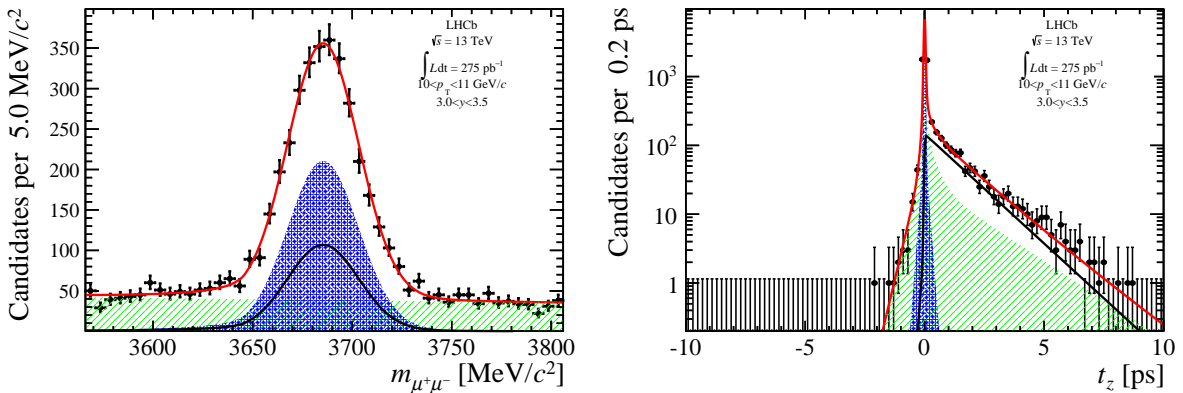


Figure D.43: (Left) Invariant mass and (Right) pseudo-proper decay time fit results of $\psi(2S)$ candidates with $p_T \in [10, 11]$ GeV/ c and $y \in [3.0, 3.5]$.

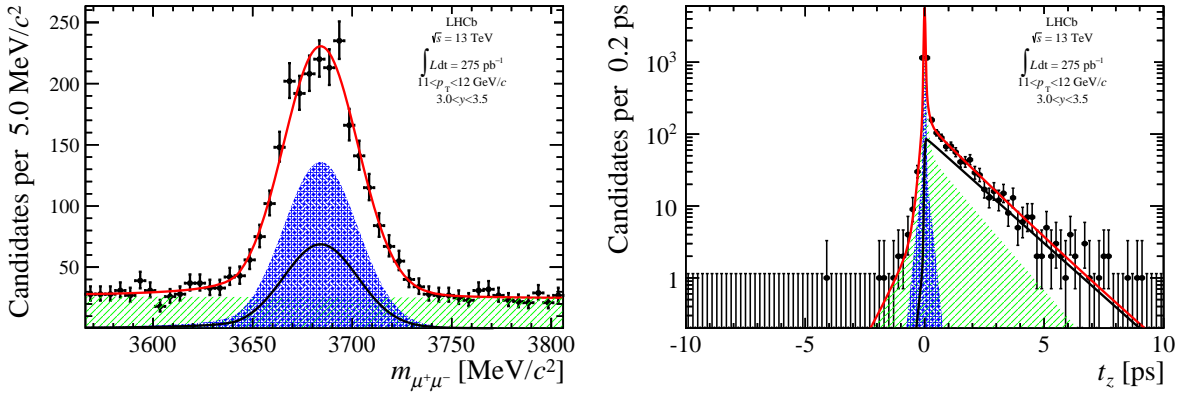


Figure D.44: (Left) Invariant mass and (Right) pseudo-proper decay time fit results of $\psi(2S)$ candidates with $p_T \in [11, 12]$ GeV/ c and $y \in [3.0, 3.5]$.

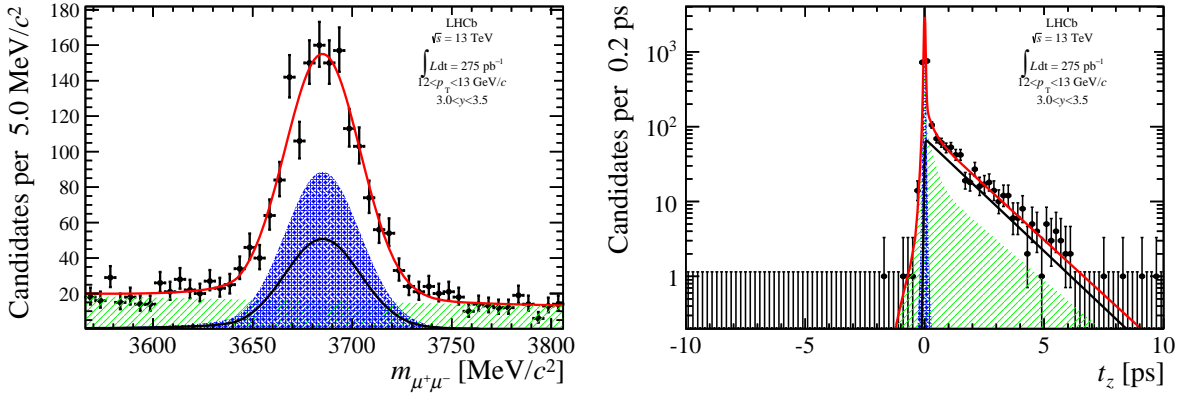


Figure D.45: (Left) Invariant mass and (Right) pseudo-proper decay time fit results of $\psi(2S)$ candidates with $p_T \in [12, 13]$ GeV/ c and $y \in [3.0, 3.5]$.

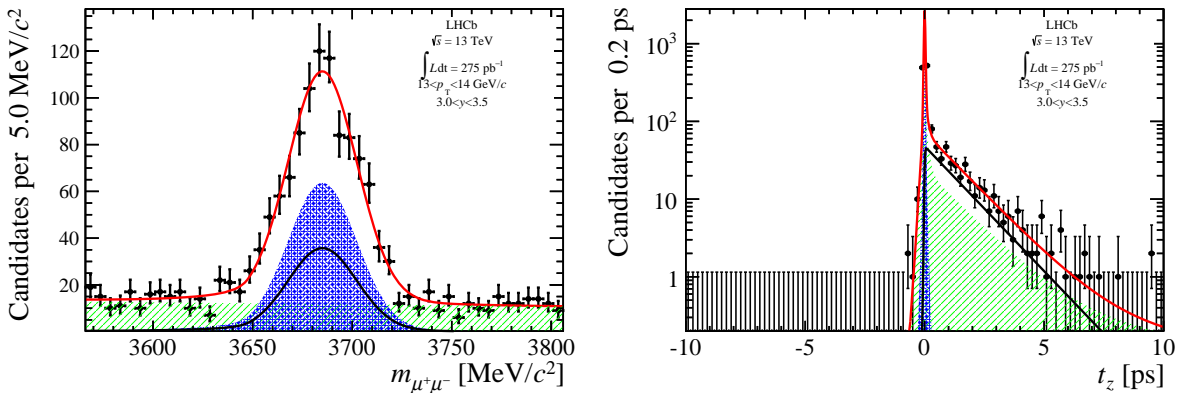


Figure D.46: (Left) Invariant mass and (Right) pseudo-proper decay time fit results of $\psi(2S)$ candidates with $p_T \in [13, 14]$ GeV/ c and $y \in [3.0, 3.5]$.

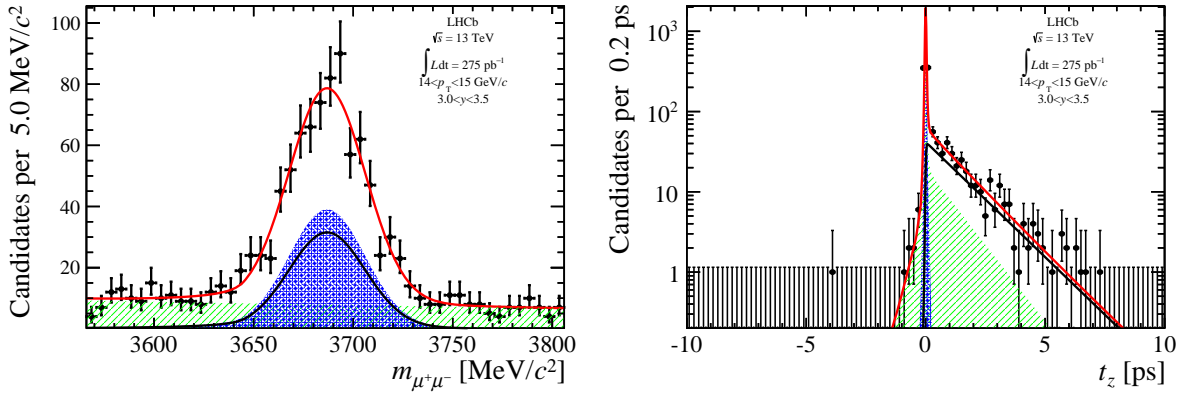


Figure D.47: (Left) Invariant mass and (Right) pseudo-proper decay time fit results of $\psi(2S)$ candidates with $p_T \in [14, 15]$ GeV/ c and $y \in [3.0, 3.5]$.

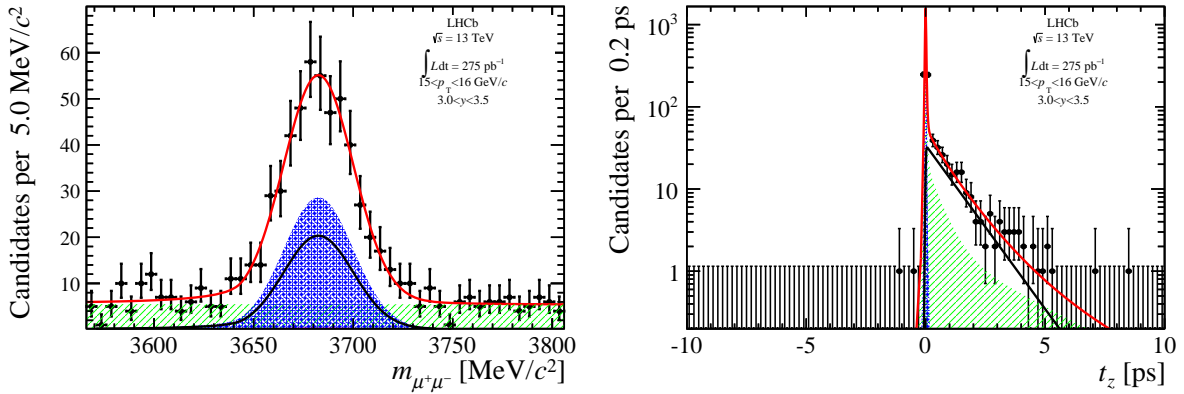


Figure D.48: (Left) Invariant mass and (Right) pseudo-proper decay time fit results of $\psi(2S)$ candidates with $p_T \in [15, 16]$ GeV/ c and $y \in [3.0, 3.5]$.

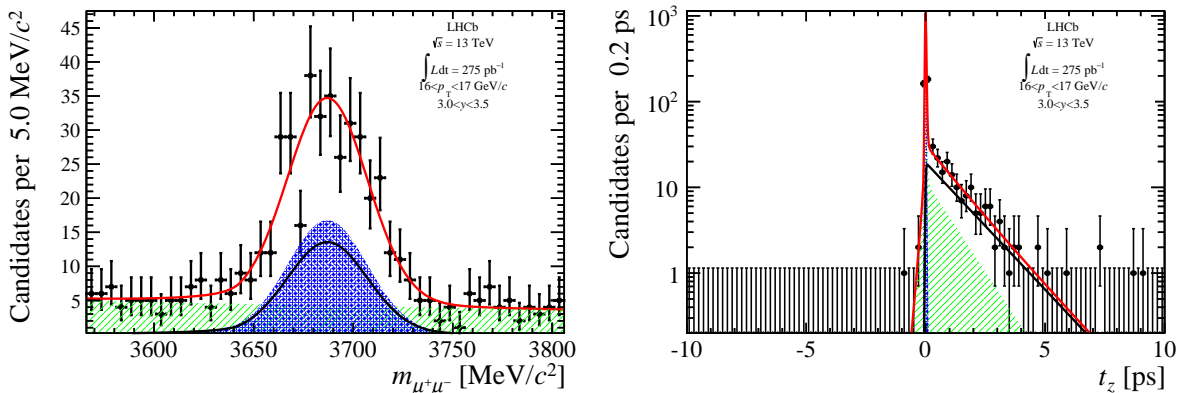


Figure D.49: (Left) Invariant mass and (Right) pseudo-proper decay time fit results of $\psi(2S)$ candidates with $p_T \in [16, 17]$ GeV/ c and $y \in [3.0, 3.5]$.

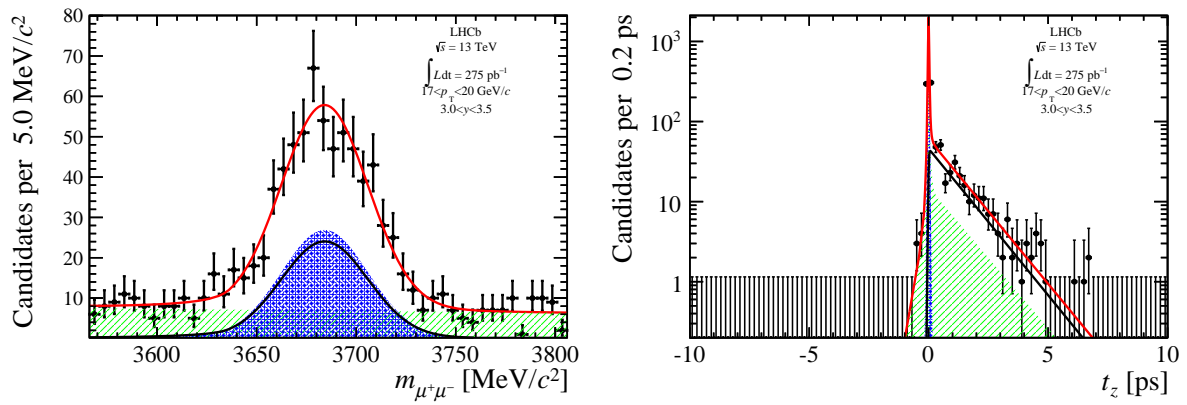


Figure D.50: (Left) Invariant mass and (Right) pseudo-proper decay time fit results of $\psi(2S)$ candidates with $p_T \in [17, 20]$ GeV/ c and $y \in [3.0, 3.5]$.

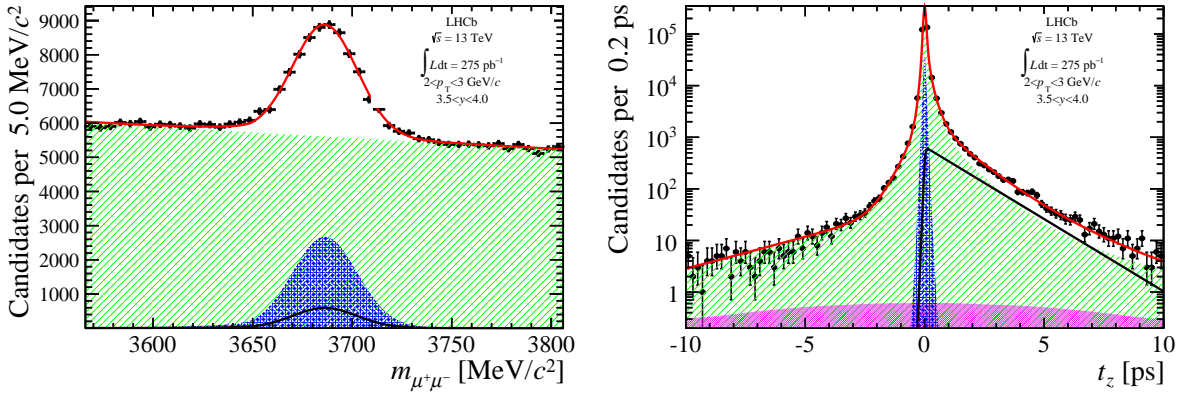


Figure D.51: (Left) Invariant mass and (Right) pseudo-proper decay time fit results of $\psi(2S)$ candidates with $p_T \in [2, 3]$ GeV/ c and $y \in [3.5, 4.0]$.

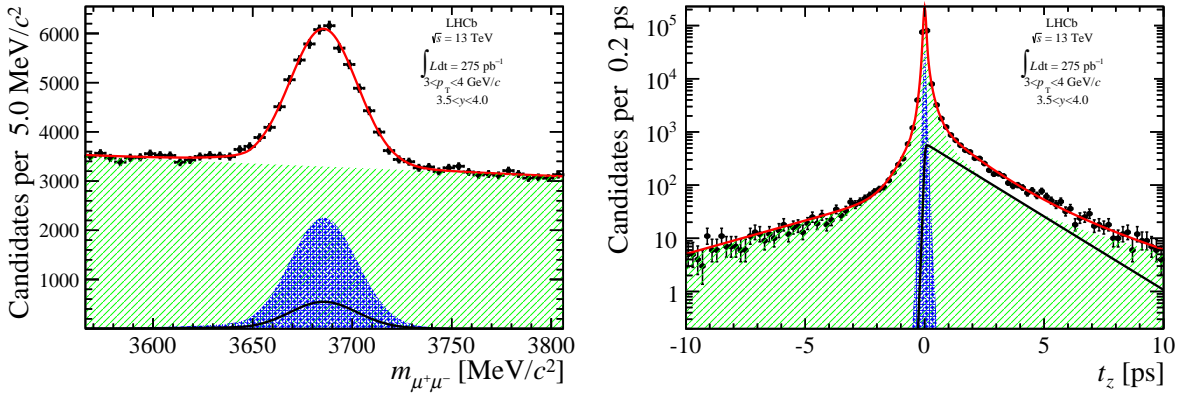


Figure D.52: (Left) Invariant mass and (Right) pseudo-proper decay time fit results of $\psi(2S)$ candidates with $p_T \in [3, 4]$ GeV/ c and $y \in [3.5, 4.0]$.

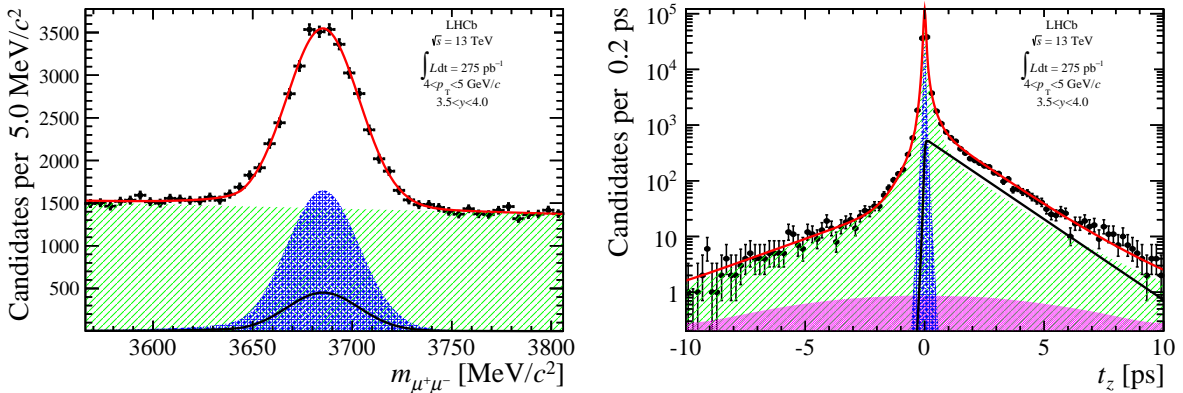


Figure D.53: (Left) Invariant mass and (Right) pseudo-proper decay time fit results of $\psi(2S)$ candidates with $p_T \in [4, 5]$ GeV/ c and $y \in [3.5, 4.0]$.

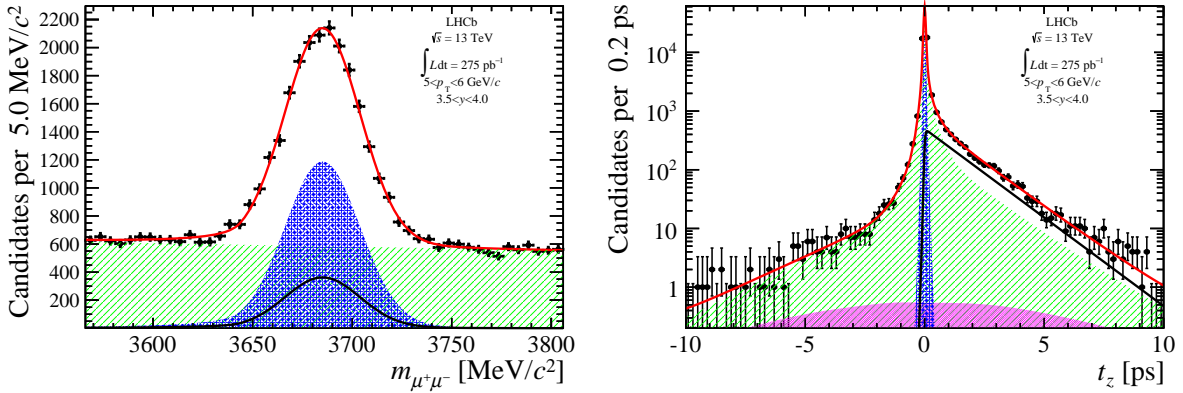


Figure D.54: (Left) Invariant mass and (Right) pseudo-proper decay time fit results of $\psi(2S)$ candidates with $p_T \in [5, 6]$ GeV/ c and $y \in [3.5, 4.0]$.

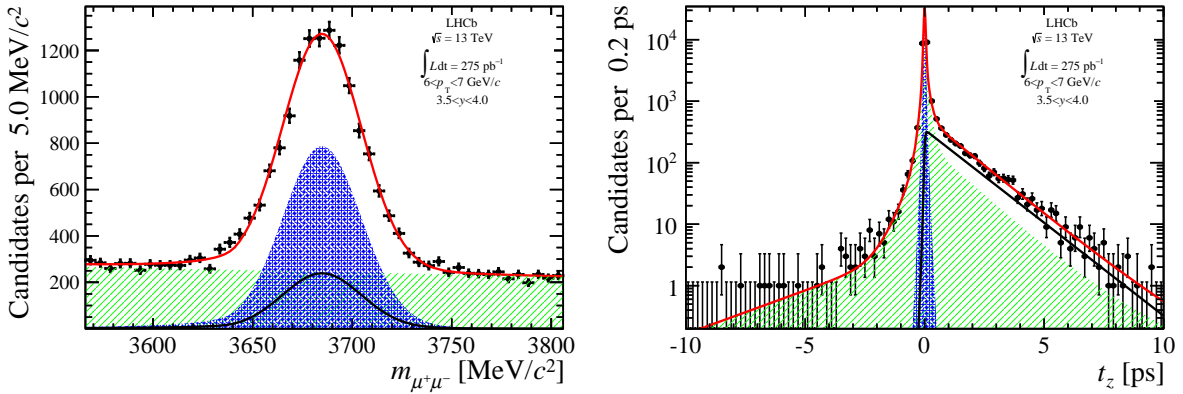


Figure D.55: (Left) Invariant mass and (Right) pseudo-proper decay time fit results of $\psi(2S)$ candidates with $p_T \in [6, 7]$ GeV/ c and $y \in [3.5, 4.0]$.

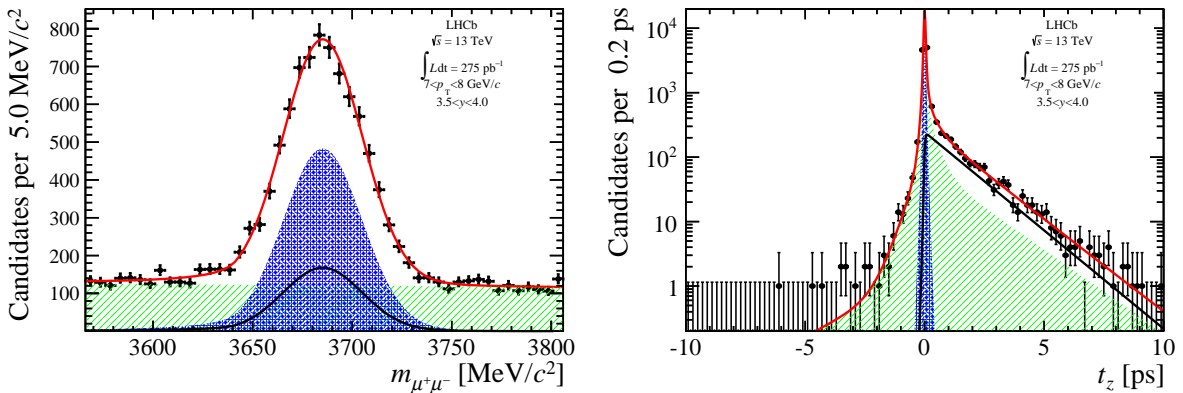


Figure D.56: (Left) Invariant mass and (Right) pseudo-proper decay time fit results of $\psi(2S)$ candidates with $p_T \in [7, 8]$ GeV/ c and $y \in [3.5, 4.0]$.

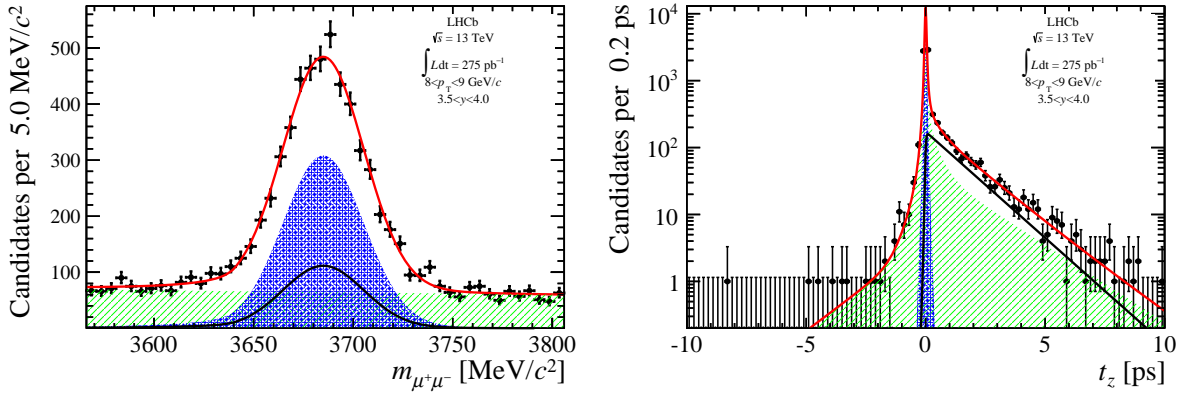


Figure D.57: (Left) Invariant mass and (Right) pseudo-proper decay time fit results of $\psi(2S)$ candidates with $p_T \in [8, 9]$ GeV/ c and $y \in [3.5, 4.0]$.

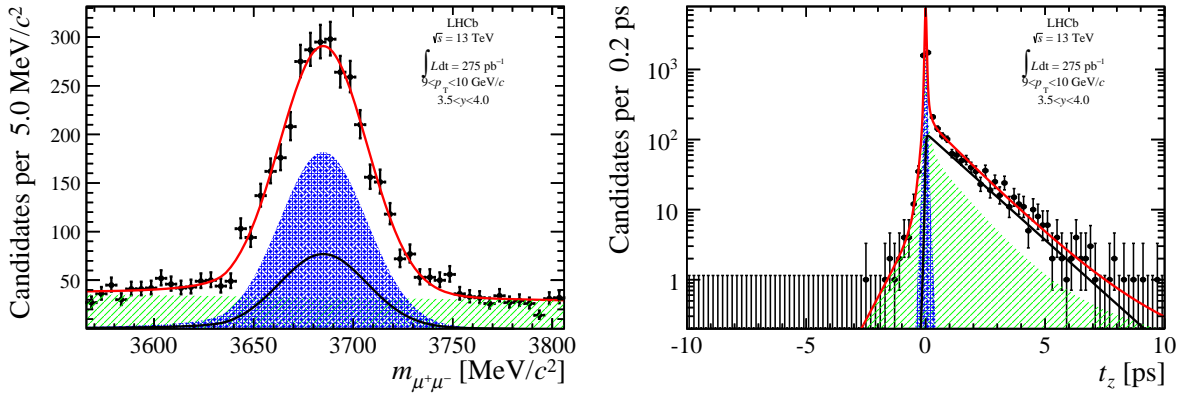


Figure D.58: (Left) Invariant mass and (Right) pseudo-proper decay time fit results of $\psi(2S)$ candidates with $p_T \in [9, 10]$ GeV/ c and $y \in [3.5, 4.0]$.

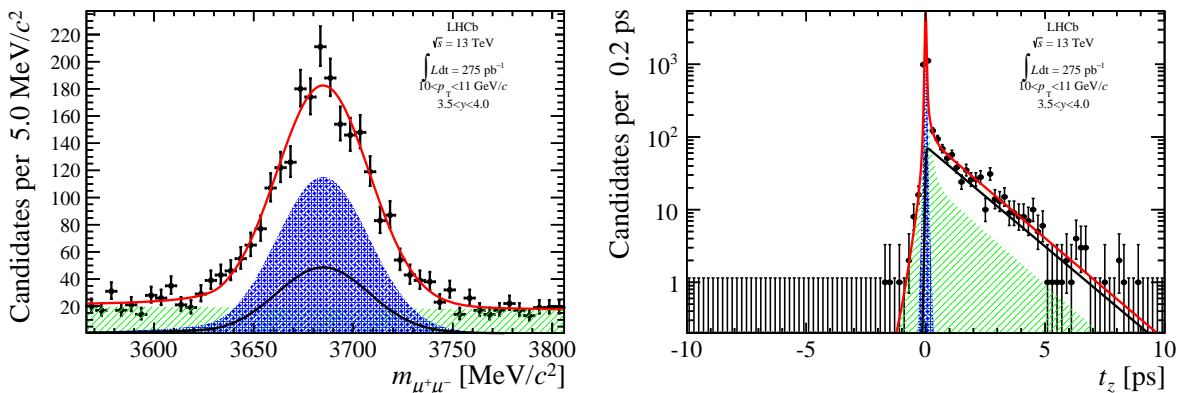


Figure D.59: (Left) Invariant mass and (Right) pseudo-proper decay time fit results of $\psi(2S)$ candidates with $p_T \in [10, 11]$ GeV/ c and $y \in [3.5, 4.0]$.

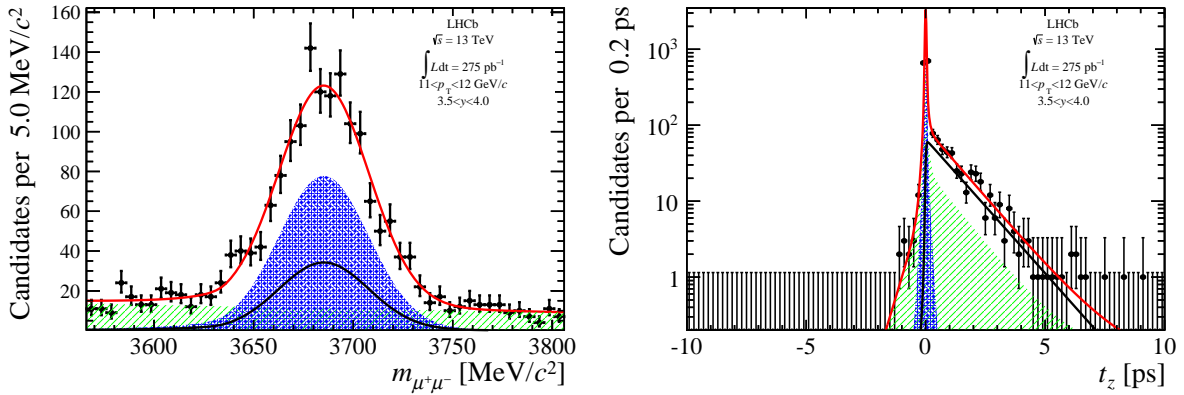


Figure D.60: (Left) Invariant mass and (Right) pseudo-proper decay time fit results of $\psi(2S)$ candidates with $p_T \in [11, 12]$ GeV/ c and $y \in [3.5, 4.0]$.

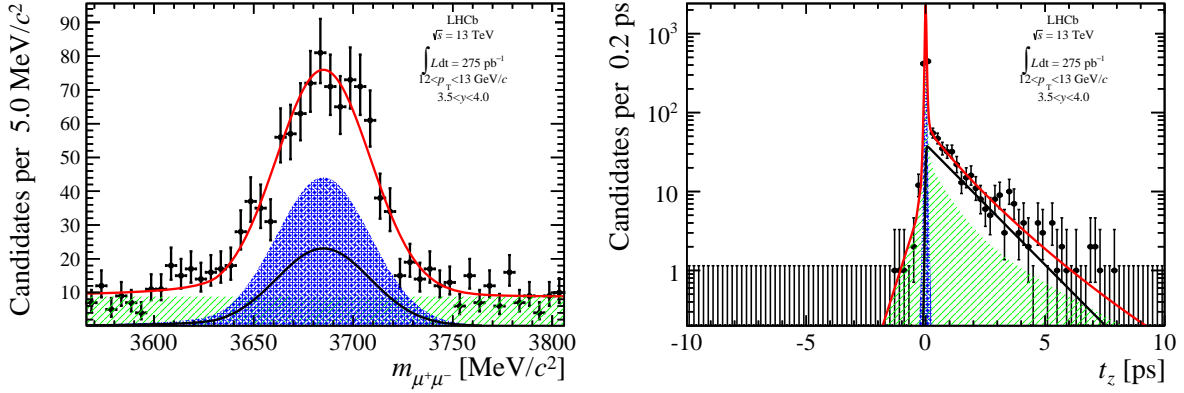


Figure D.61: (Left) Invariant mass and (Right) pseudo-proper decay time fit results of $\psi(2S)$ candidates with $p_T \in [12, 13]$ GeV/ c and $y \in [3.5, 4.0]$.

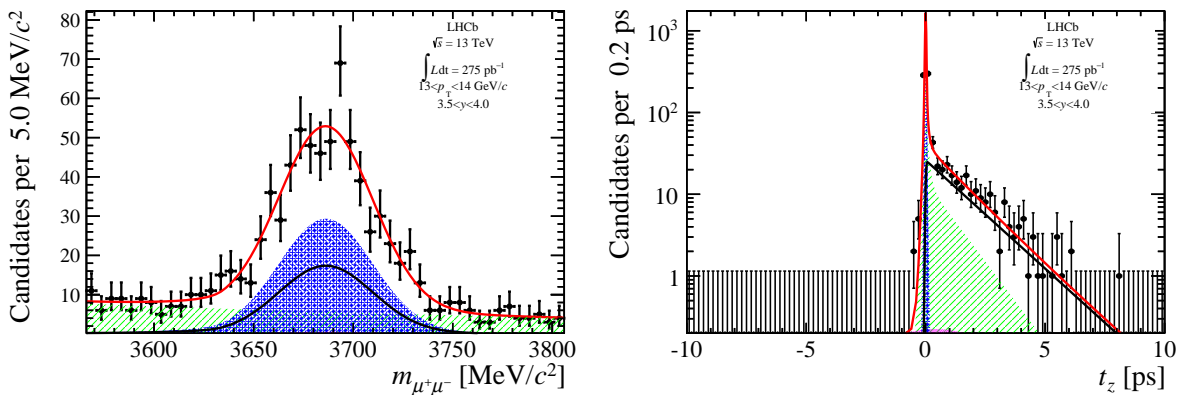


Figure D.62: (Left) Invariant mass and (Right) pseudo-proper decay time fit results of $\psi(2S)$ candidates with $p_T \in [13, 14]$ GeV/ c and $y \in [3.5, 4.0]$.

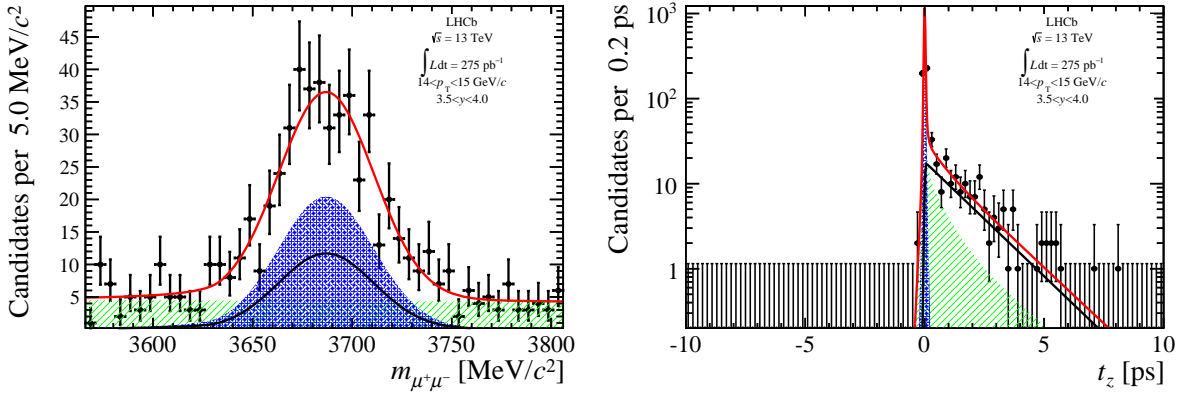


Figure D.63: (Left) Invariant mass and (Right) pseudo-proper decay time fit results of $\psi(2S)$ candidates with $p_T \in [14, 15]$ GeV/ c and $y \in [3.5, 4.0]$.

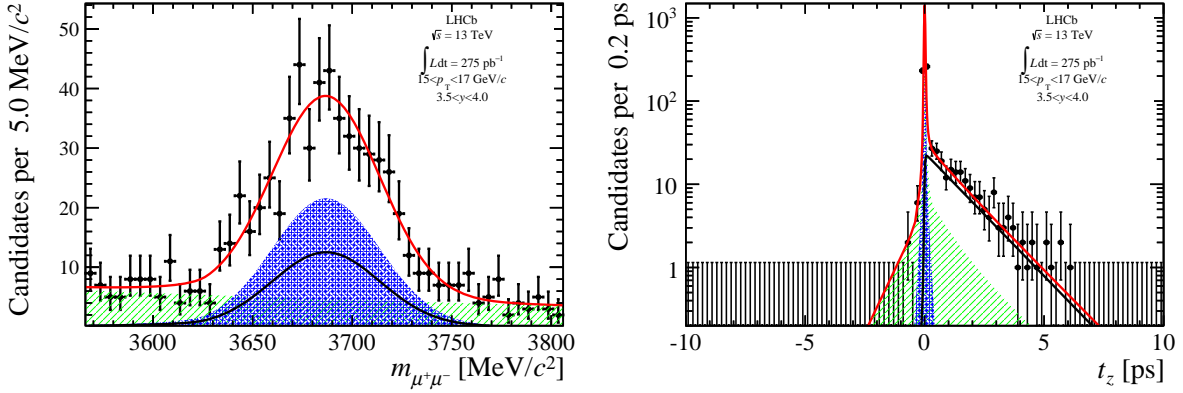


Figure D.64: (Left) Invariant mass and (Right) pseudo-proper decay time fit results of $\psi(2S)$ candidates with $p_T \in [15, 17]$ GeV/ c and $y \in [3.5, 4.0]$.

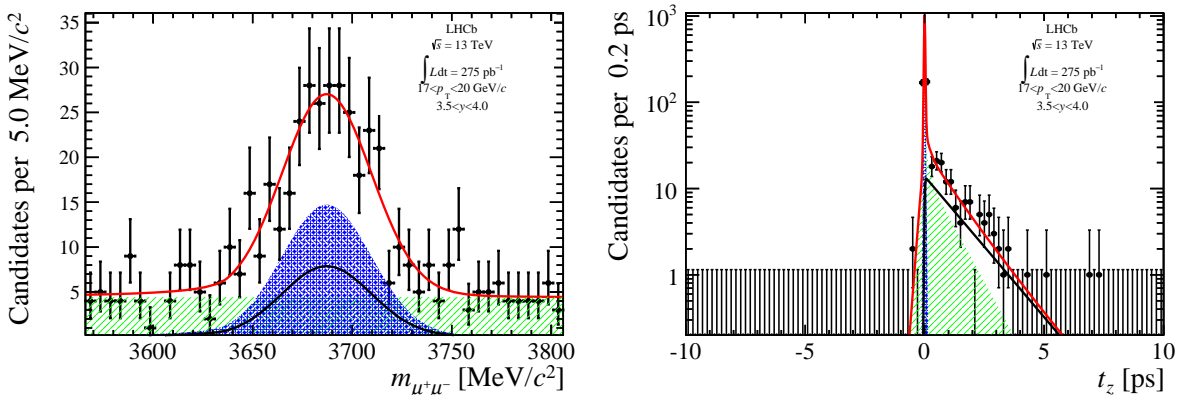


Figure D.65: (Left) Invariant mass and (Right) pseudo-proper decay time fit results of $\psi(2S)$ candidates with $p_T \in [17, 20]$ GeV/ c and $y \in [3.5, 4.0]$.

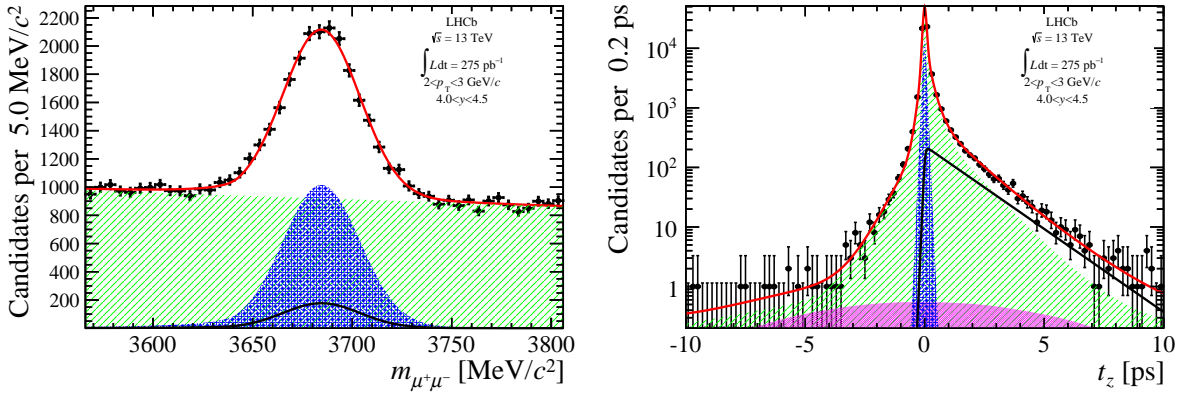


Figure D.66: (Left) Invariant mass and (Right) pseudo-proper decay time fit results of $\psi(2S)$ candidates with $p_T \in [2, 3]$ GeV/ c and $y \in [4.0, 4.5]$.

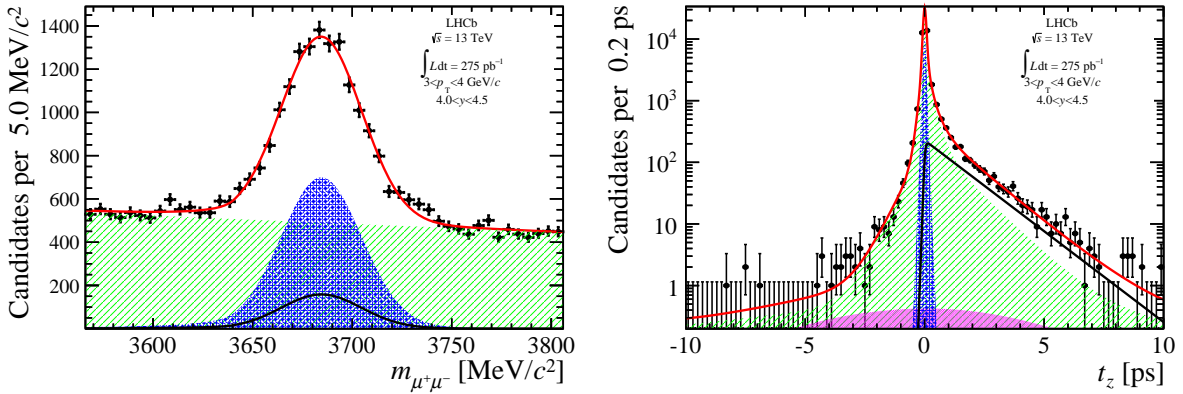


Figure D.67: (Left) Invariant mass and (Right) pseudo-proper decay time fit results of $\psi(2S)$ candidates with $p_T \in [3, 4]$ GeV/ c and $y \in [4.0, 4.5]$.

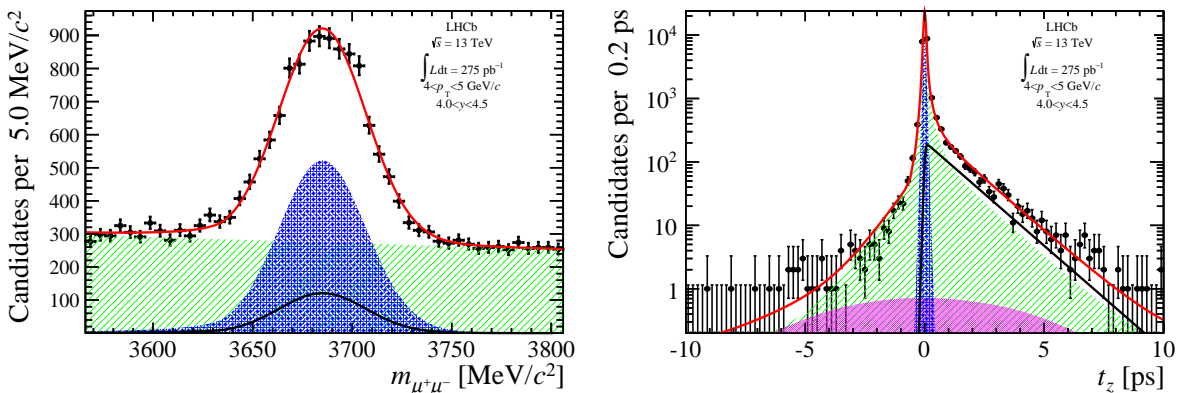


Figure D.68: (Left) Invariant mass and (Right) pseudo-proper decay time fit results of $\psi(2S)$ candidates with $p_T \in [4, 5]$ GeV/ c and $y \in [4.0, 4.5]$.

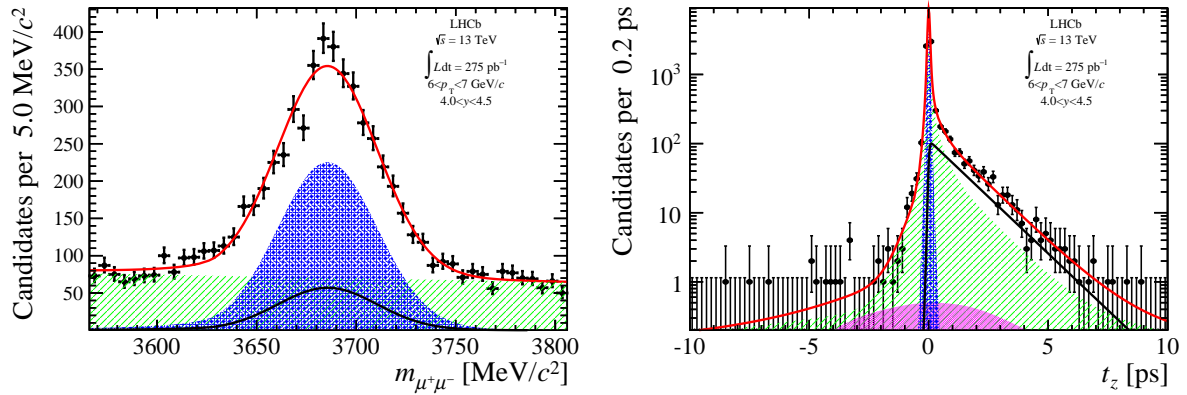


Figure D.69: (Left) Invariant mass and (Right) pseudo-proper decay time fit results of $\psi(2S)$ candidates with $p_T \in [5, 6]$ GeV/ c and $y \in [4.0, 4.5]$.

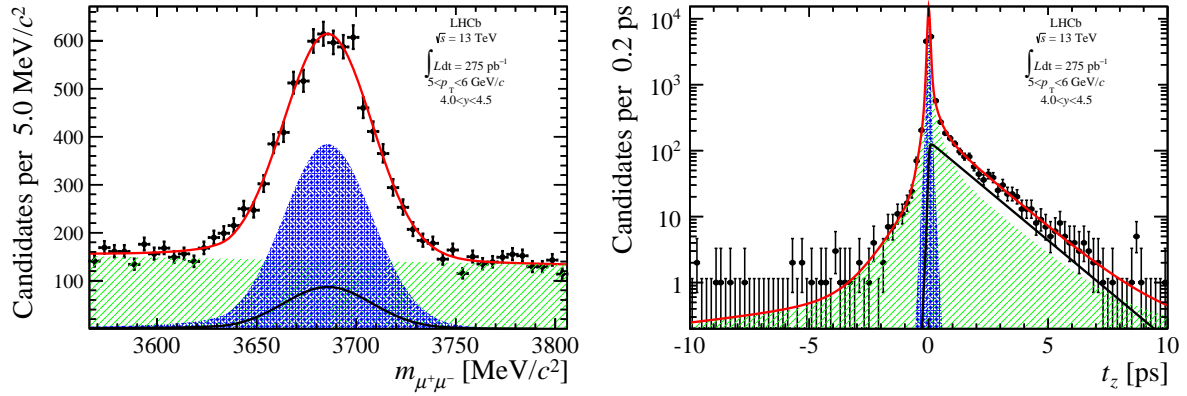


Figure D.70: (Left) Invariant mass and (Right) pseudo-proper decay time fit results of $\psi(2S)$ candidates with $p_T \in [6, 7]$ GeV/ c and $y \in [4.0, 4.5]$.

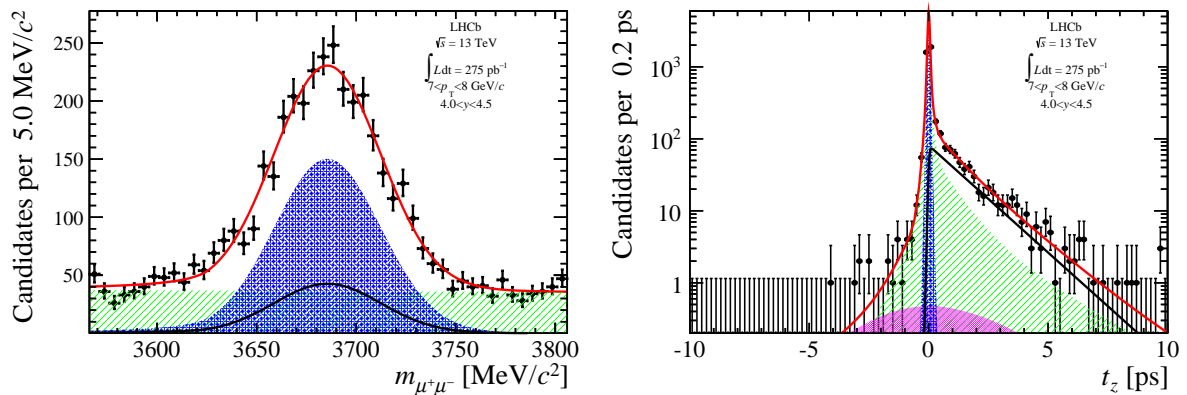


Figure D.71: (Left) Invariant mass and (Right) pseudo-proper decay time fit results of $\psi(2S)$ candidates with $p_T \in [7, 8]$ GeV/ c and $y \in [4.0, 4.5]$.

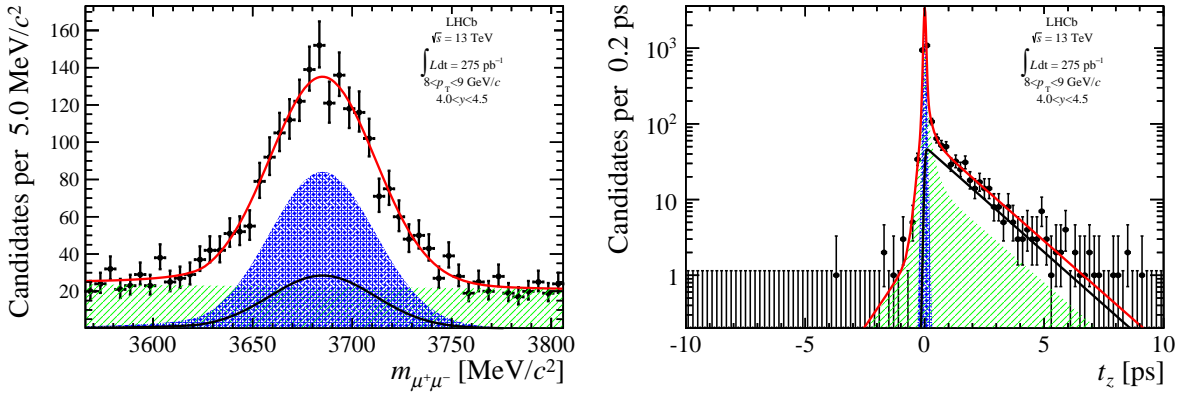


Figure D.72: (Left) Invariant mass and (Right) pseudo-proper decay time fit results of $\psi(2S)$ candidates with $p_T \in [8, 9]$ GeV/ c and $y \in [4.0, 4.5]$.

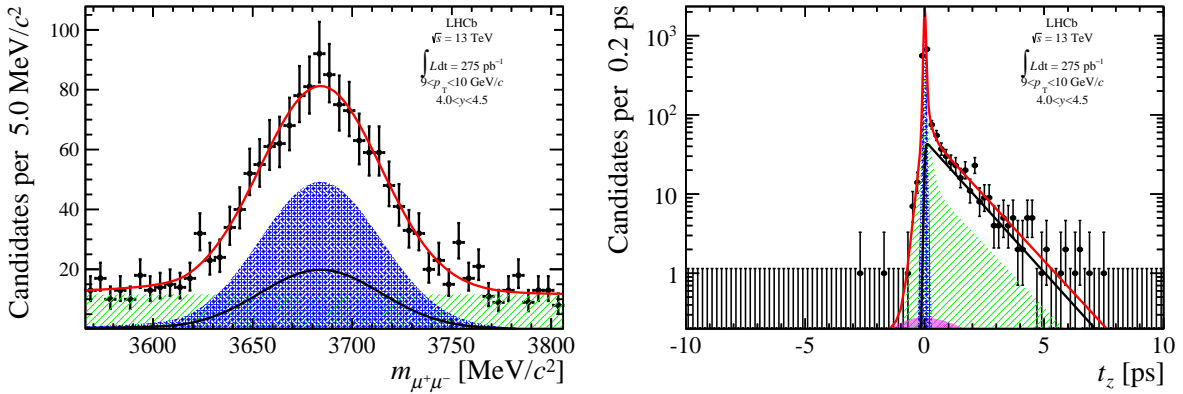


Figure D.73: (Left) Invariant mass and (Right) pseudo-proper decay time fit results of $\psi(2S)$ candidates with $p_T \in [9, 10]$ GeV/ c and $y \in [4.0, 4.5]$.

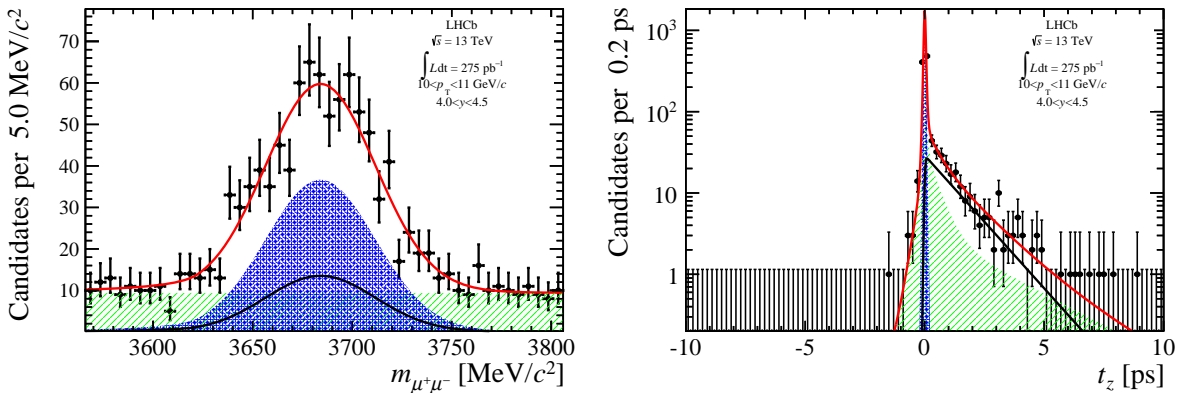


Figure D.74: (Left) Invariant mass and (Right) pseudo-proper decay time fit results of $\psi(2S)$ candidates with $p_T \in [10, 11]$ GeV/ c and $y \in [4.0, 4.5]$.

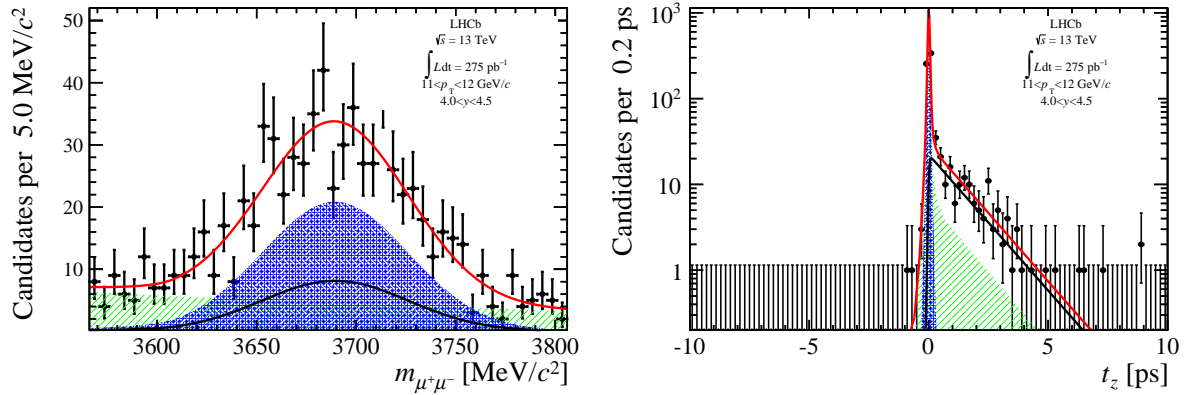


Figure D.75: (Left) Invariant mass and (Right) pseudo-proper decay time fit results of $\psi(2S)$ candidates with $p_T \in [11, 12] \text{ GeV}/c$ and $y \in [4.0, 4.5]$.

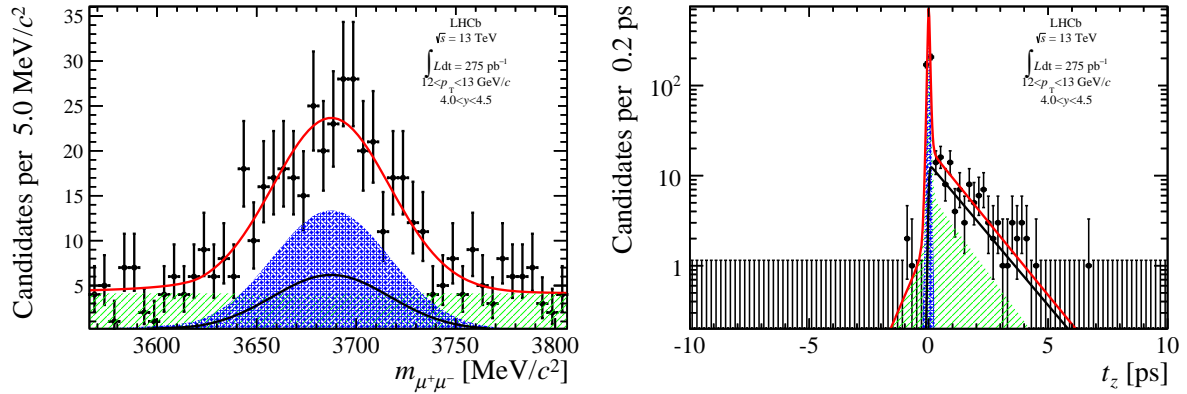


Figure D.76: (Left) Invariant mass and (Right) pseudo-proper decay time fit results of $\psi(2S)$ candidates with $p_T \in [12, 13] \text{ GeV}/c$ and $y \in [4.0, 4.5]$.

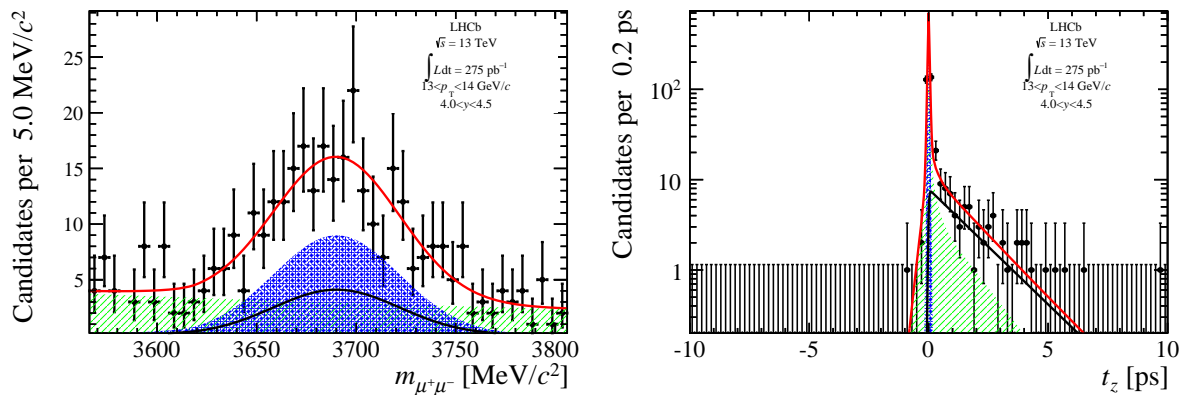


Figure D.77: (Left) Invariant mass and (Right) pseudo-proper decay time fit results of $\psi(2S)$ candidates with $p_T \in [13, 14] \text{ GeV}/c$ and $y \in [4.0, 4.5]$.

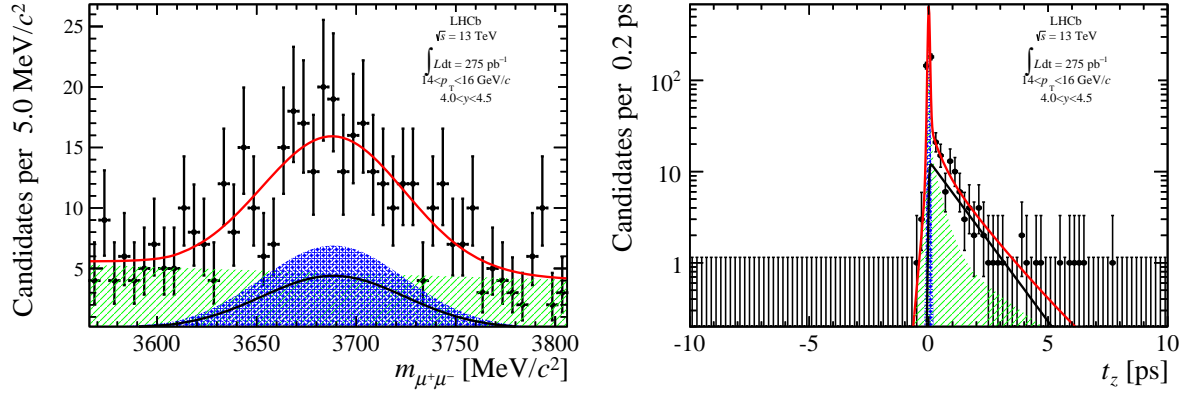


Figure D.78: (Left) Invariant mass and (Right) pseudo-proper decay time fit results of $\psi(2S)$ candidates with $p_T \in [14, 16]$ GeV/ c and $y \in [4.0, 4.5]$.

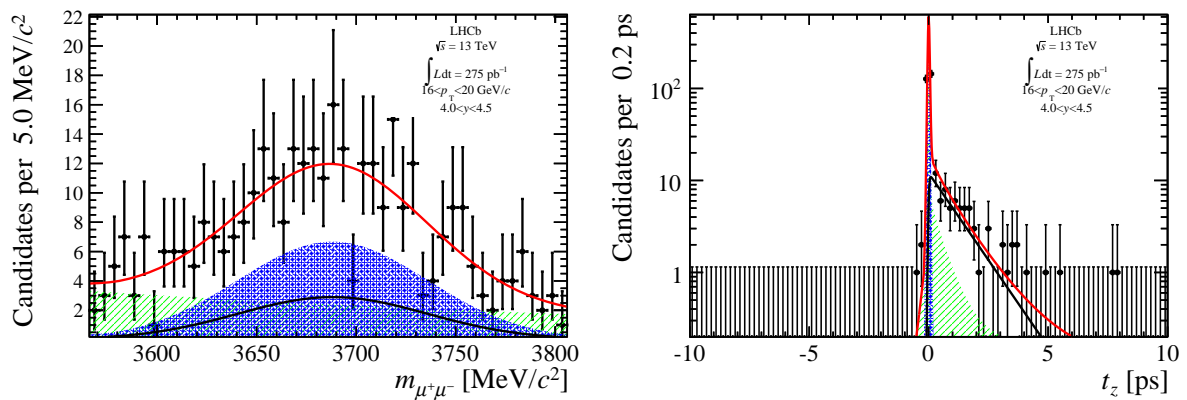


Figure D.79: (Left) Invariant mass and (Right) pseudo-proper decay time fit results of $\psi(2S)$ candidates with $p_T \in [16, 20]$ GeV/ c and $y \in [4.0, 4.5]$.

795 **E $\psi(2S)$ production cross-section measurement at**
796 **7 TeV with 2011 data.**

797 The fitting procedure, efficiency calculations and systematic estimations are exactly same
798 with 13 TeV measurement. All the relevant detailed information are described in the
799 following sections.

800 **E.1 Data and Monte Carlo samples**

801 This study reported here uses pp collision data collected by the LHCb detector at a
802 centre-of-mass energy of 7 TeV in 2011, corresponding to an integrated luminosity of
803 $614 \pm 11 \text{ pb}^{-1}$. The data used in this analysis were collected using four different trigger
804 configuration keys (TCKs).

- 805 • 185.49 pb^{-1} with TCK 0x790038 MagDown;
- 806 • 180.89 pb^{-1} with TCK 0x760037 MagDown;
- 807 • 37.96 pb^{-1} with TCK 0x790037 MagUp;
- 808 • 99.67 pb^{-1} with TCK 0x760037 MagUp;
- 809 • 110.06 pb^{-1} with TCK 0x790038 MagUp.

810 In this analysis only muon triggers are used, which are identical for the TCKs used.
811 To study the efficiency, simulated samples with about 10 M events are generated.
812 In the simulation, pp collisions are generated using PYTHIA [37] with a specific LHCb
813 configuration [38]. Decays of hadronic particles are described by EVTGEN [39], in
814 which final state radiation is generated using PHOTOS [40]. The interaction of the
815 generated particles with the detector and its response are implemented using the GEANT4
816 toolkit [41, 42] as described in Ref. [43]. The prompt charmonium production is simulated
817 in PYTHIA with contributions from both the leading order colour-singlet and colour-octet
818 mechanisms [38, 44], and the charmonium is generated without polarization.

819 **E.2 Trigger**

820 Our analysis is based on *L0Dimuon*, *Hlt1DiMuonHighMass* and *Hlt2DiMuonPsi2SHighPT*
821 and the selections are summarised in Table E.1.

822 **E.3 Offline selection**

823 The reconstruction and preselection of the $\psi(2S)$ candidates for real data were based
824 on the stripping line “FullDSTDiMuonPsi2MuMuTOSLine”. The offline selections are
825 applied to $\psi(2S)$ candidates to reduce the combinatorial background to a reasonable
826 level and ensure the good quality of the signal-extraction fit. We require the ghost
827 probability for each track (μ^+ and μ^-) to be less than 0.3. Both two tracks must have
828 full momentum p larger than $10 \text{ GeV}/c$ and transverse momentum p_T above $1 \text{ GeV}/c$,
829 pass muon identification and have a good quality of the track fit ($\chi^2/\text{ndf} < 3$). The
830 pseudorapidity of each muon is required to be in the range $2.0 < \eta < 4.9$. The PID is

Table E.1: Summary of the trigger lines used for the 7 TeV analysis.

trigger line	main cuts
<i>L0DiMuon</i>	$p_{\text{T}1} \times p_{\text{T}2} > 1.6(\text{GeV}/c)^2$, nSPDHits < 900
<i>Hlt1DiMuonHighMass</i>	$p > 6 \text{ GeV}/c$ $p_{\text{T}} > 0.5 \text{ GeV}/c$ Track $\chi^2/\text{ndf} < 3$ Muon ID: isMuon $m_{\mu^+\mu^-} > 2.7 \text{ GeV}/c^2$
<i>Hlt2DiMuonPsi2SHighPT</i>	$ m_{\mu^+\mu^-} - m_{\psi(2S)} < 120 \text{ MeV}/c^2$ $p_{\text{T}\psi(2S)} > 3500 \text{ MeV}/c$ Vertex fit $\chi^2/\text{ndf} < 25$

831 performed to identify muon candidates ($\text{DLLmu} > 2$). The two muons are required to
 832 form a good vertex by restricting the vertex fit quality $\text{Prob}(\chi^2/\text{ndf}) > 0.5\%$. , and have
 833 invariant mass within $100 \text{ MeV}/c^2$ of $\psi(2S)$ PDG mass value.

The full offline selection criteria are summarized in Table E.2.

Table E.2: Offline selection criteria for $\psi(2S) \rightarrow \mu^+\mu^-$.

Quantity	Requirement
Track ghost probability	< 0.3
μ : p_{T}	$> 1 \text{ GeV}/c$
μ : p	$> 10 \text{ GeV}/c$
μ : η	$2.0 < \eta < 4.9$
μ : track quality χ^2/ndf	< 3
μ : track PID	IsMuon and $\text{DLLmu} > 2$
$\psi(2S)$: Vertex $\text{Prob}(\chi^2/\text{ndf})$	> 0.5%
Pseudo proper time t_z	(−10, 10) ps
Uncertainty of t_z	< 0.3 ps
$\psi(2S)$: Mass Window	(3586, 3786) MeV/c^2
$\psi(2S)$: L0 Trigger On Signal	L0DiMuon
$\psi(2S)$: HLT1 Trigger On Signal	Hlt1DiMuonHighMass
$\psi(2S)$: HLT2 Trigger On Signal	Hlt1DiMuonPsi2SHighPT

834

835 E.4 Signal extraction

836 The two-dimensional fit to the invariant mass and the lifetime in the kinematic range
 837 $5 \text{ GeV}/c < p_{\text{T}} < 6 \text{ GeV}/c$ and $2.5 < y < 3.0$ is shown in Fig. E.1.

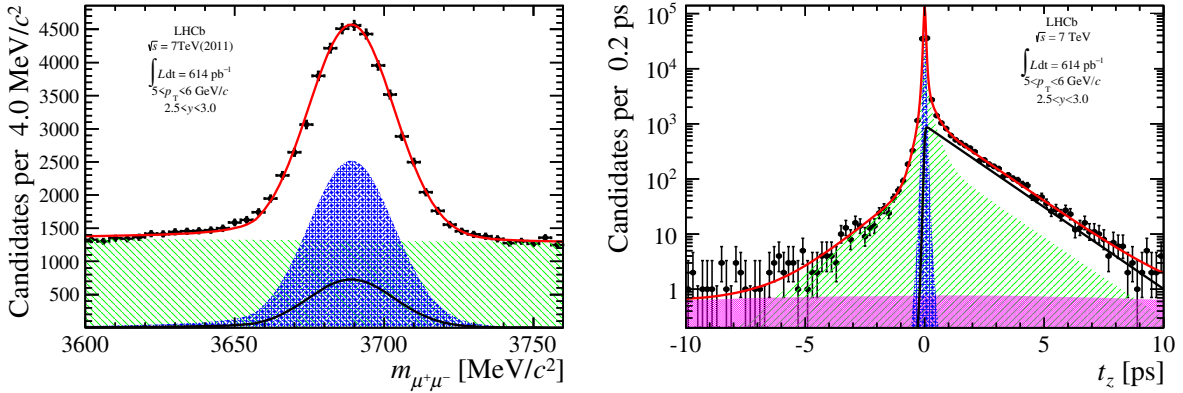


Figure E.1: Invariant mass (left) and pseudo decay time (right) distributions for the kinematic bin $5 < p_T < 6 \text{ GeV}/c$, $2.5 < y < 3.0$, with fit results superimposed. The solid (red) line is the total fit function, the shaded (green) area corresponds to the background component. The prompt $\psi(2S)$ contribution is shown in cross-hatched area (blue), $\psi(2S)$ -from- b in a solid (black) line and the tail contribution due to the association of $\psi(2S)$ with the wrong PV is shown in full filled (magenta) area. The tail contribution is not visible in the invariant mass plot.

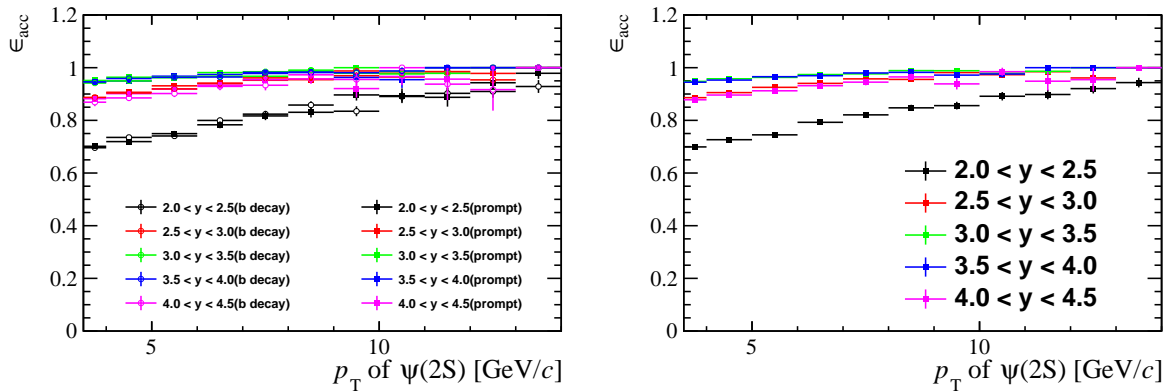


Figure E.2: Geometrical acceptance ϵ_{acc} calculated using simulated events as a function of p_T in bins of y . The right figure shows the average of both efficiencies of prompt $\psi(2S)$ and $\psi(2S)$ -from- b .

838 E.5 Efficiencies

839 The total efficiency ϵ_{tot} is expressed as the multiplication of the efficiencies of geometrical
840 acceptance, the reconstruction-selection, the muon identification and the trigger:

$$\epsilon_{\text{tot}} = \epsilon_{\text{acc}} \times \epsilon_{\text{Reco\&Sel}} \times \epsilon_{\text{MuonID}} \times \epsilon_{\text{Trigger}}, \quad (\text{E.1})$$

841 The total efficiency ϵ_{tot} is shown in Fig. E.6 for prompt $\psi(2S)$ and $\psi(2S)$ -from- b , and is
842 summarized in Tables E.3 and E.4. The average of the efficiency between prompt $\psi(2S)$
843 and $\psi(2S)$ -from- b in Fig. E.7 and table E.5. The separate efficiency for prompt $\psi(2S)$
844 and $\psi(2S)$ from b are used to calculate final cross-section.

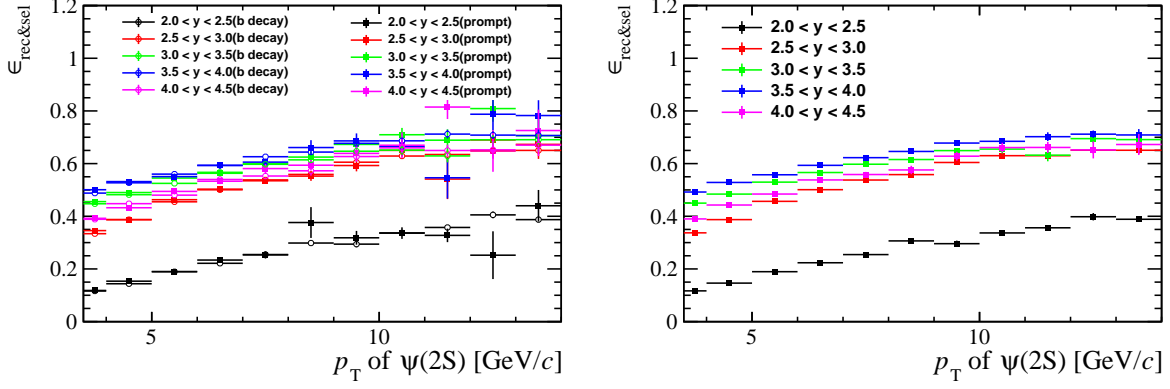


Figure E.3: Reconstruction-Selection efficiency $\epsilon_{\text{Reco\&Sel}}$ calculated using simulated events as a function of p_T in bins of y . The right figure shows the average between efficiency of prompt $\psi(2S)$ and $\psi(2S)$ -from- b .

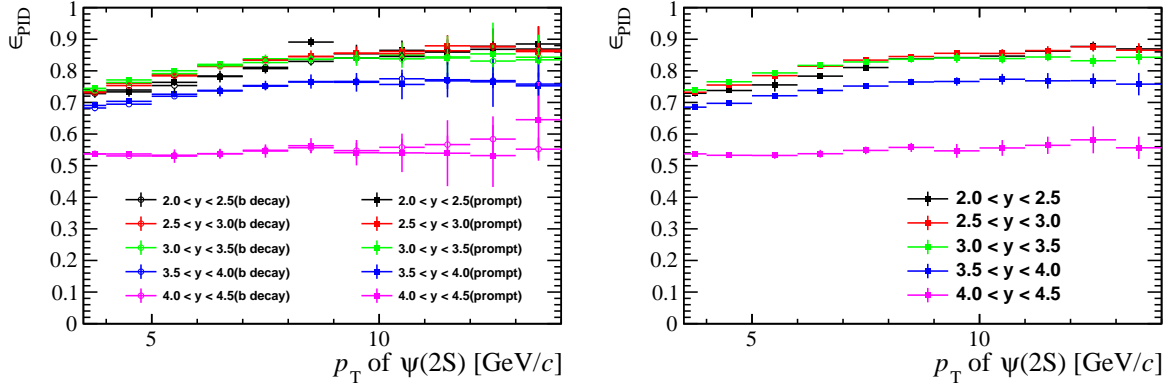


Figure E.4: MuonID efficiency ϵ_{MuonID} calculated using simulated events as a function of p_T in bins of y . The right figure shows the average between efficiency of prompt $\psi(2S)$ and $\psi(2S)$ -from- b .

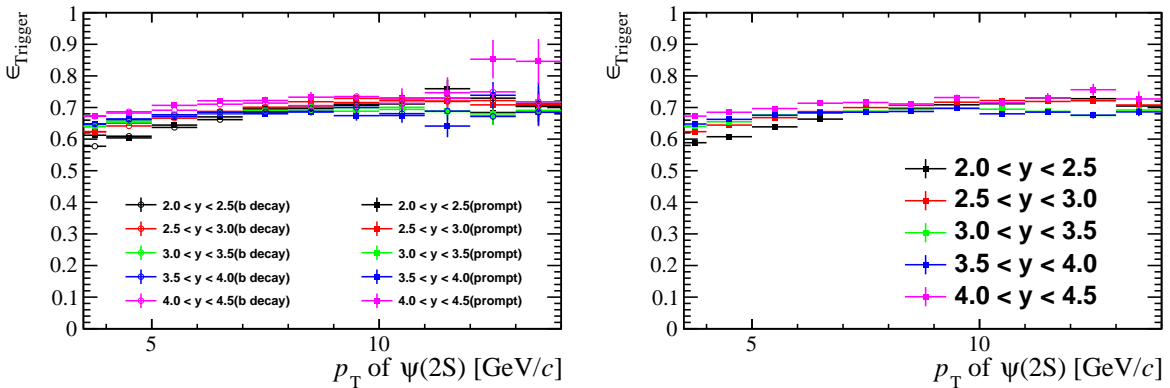


Figure E.5: Trigger efficiency $\epsilon_{\text{Trigger}}$ calculated using simulated events as a function of p_T in bins of y . The right figure shows the average between efficiency of prompt $\psi(2S)$ and $\psi(2S)$ -from- b .

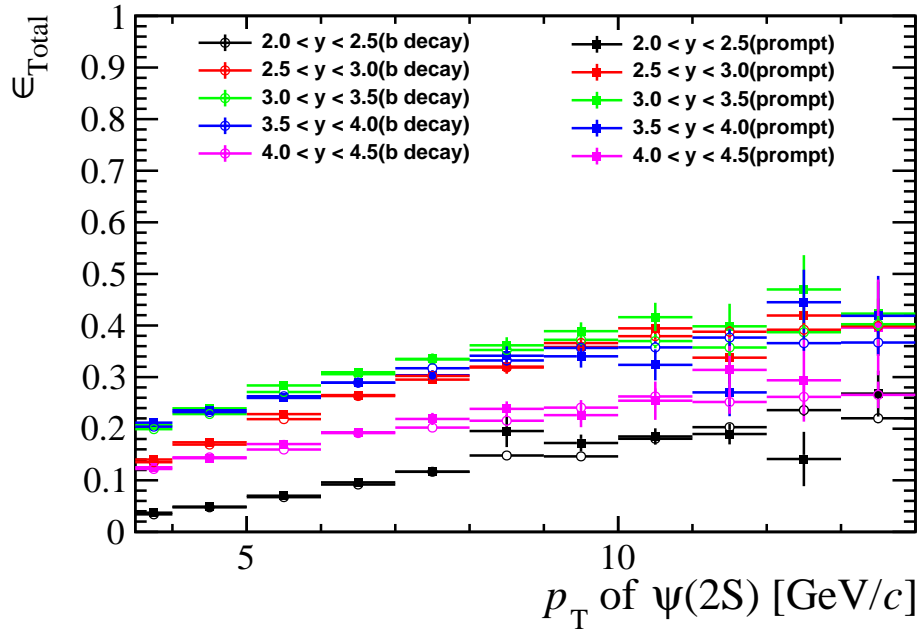


Figure E.6: Total efficiency ϵ_{tot} calculated using simulated events as a function of p_T in bins of y are shown in the plot.

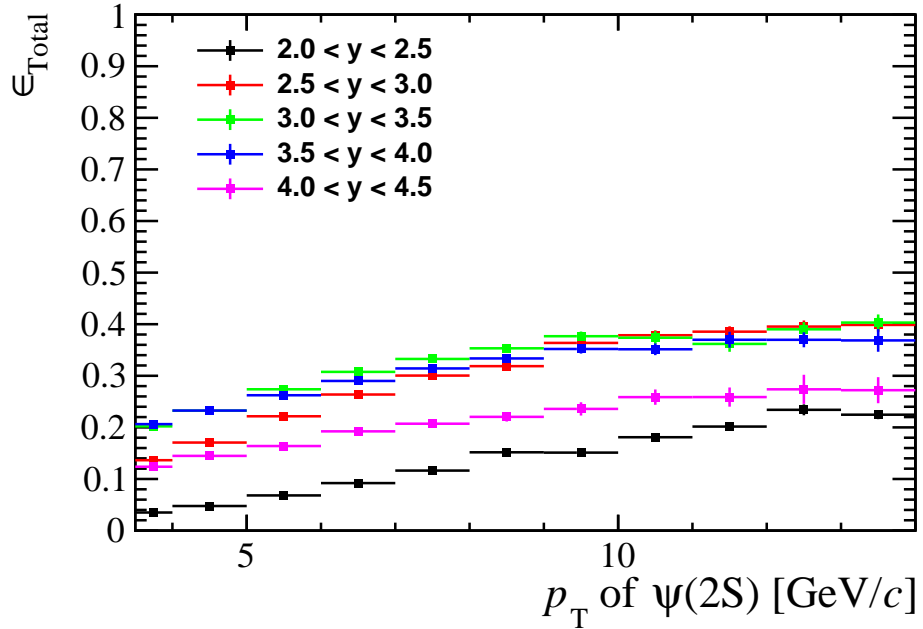


Figure E.7: Total efficiency ϵ_{tot} calculated using average between efficiency of prompt $\psi(2S)$ and $\psi(2S)$ -from- b .

845 E.6 Summary of systematic uncertainties

846 In Table E.6, the systematic uncertainties are summarized.

Table E.3: The efficiency ϵ_{tot} in different bins of p_{T} and y for prompt $\psi(2S)$ mesons.

p_{T} (GeV/c)	$2 < y < 2.5$	$2.5 < y < 3$	$3 < y < 3.5$	$3.5 < y < 4$	$4 < y < 4.5$
3.5-4	0.037 ± 0.001	0.140 ± 0.003	0.207 ± 0.004	0.212 ± 0.004	0.125 ± 0.003
4-5	0.049 ± 0.002	0.174 ± 0.003	0.239 ± 0.003	0.236 ± 0.004	0.143 ± 0.003
5-6	0.070 ± 0.002	0.228 ± 0.005	0.284 ± 0.004	0.260 ± 0.007	0.170 ± 0.008
6-7	0.096 ± 0.004	0.265 ± 0.007	0.309 ± 0.008	0.289 ± 0.010	0.193 ± 0.007
7-8	0.117 ± 0.007	0.295 ± 0.008	0.335 ± 0.011	0.304 ± 0.010	0.219 ± 0.012
8-9	0.195 ± 0.031	0.320 ± 0.014	0.362 ± 0.016	0.341 ± 0.019	0.238 ± 0.015
9-10	0.172 ± 0.016	0.358 ± 0.018	0.389 ± 0.017	0.340 ± 0.022	0.226 ± 0.023
10-11	0.185 ± 0.016	0.395 ± 0.022	0.416 ± 0.028	0.324 ± 0.030	0.254 ± 0.037
11-12	0.190 ± 0.020	0.338 ± 0.051	0.398 ± 0.044	0.270 ± 0.046	0.314 ± 0.068
12-13	0.141 ± 0.053	0.419 ± 0.033	0.470 ± 0.067	0.445 ± 0.063	0.294 ± 0.080
13-14	0.268 ± 0.044	0.397 ± 0.056	0.423 ± 0.062	0.419 ± 0.077	0.396 ± 0.093

Table E.4: The efficiency ϵ_{tot} in different bins of p_{T} and y for $\psi(2S)$ from b -decay.

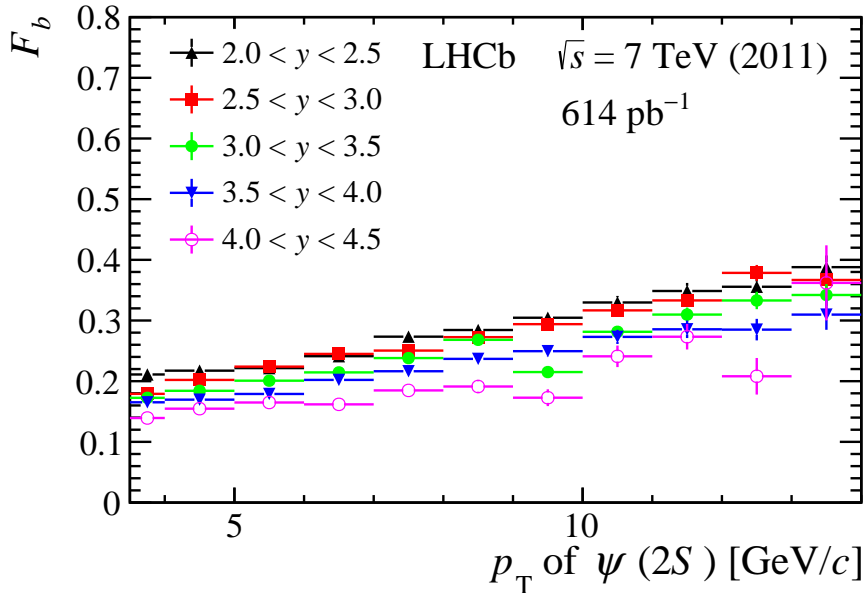
p_{T} (GeV/c)	$2 < y < 2.5$	$2.5 < y < 3$	$3 < y < 3.5$	$3.5 < y < 4$	$4 < y < 4.5$
3.5-4	0.034 ± 0.001	0.135 ± 0.002	0.199 ± 0.003	0.204 ± 0.005	0.122 ± 0.004
4-5	0.048 ± 0.001	0.169 ± 0.002	0.228 ± 0.003	0.232 ± 0.004	0.144 ± 0.004
5-6	0.067 ± 0.004	0.219 ± 0.003	0.271 ± 0.003	0.263 ± 0.004	0.160 ± 0.005
6-7	0.092 ± 0.002	0.263 ± 0.004	0.306 ± 0.004	0.289 ± 0.005	0.192 ± 0.007
7-8	0.117 ± 0.004	0.302 ± 0.005	0.334 ± 0.006	0.317 ± 0.006	0.202 ± 0.008
8-9	0.148 ± 0.005	0.319 ± 0.006	0.353 ± 0.007	0.332 ± 0.008	0.215 ± 0.011
9-10	0.146 ± 0.007	0.366 ± 0.006	0.372 ± 0.010	0.357 ± 0.010	0.241 ± 0.015
10-11	0.181 ± 0.008	0.379 ± 0.010	0.370 ± 0.014	0.358 ± 0.012	0.262 ± 0.016
11-12	0.203 ± 0.007	0.388 ± 0.011	0.357 ± 0.016	0.377 ± 0.016	0.252 ± 0.023
12-13	0.236 ± 0.011	0.392 ± 0.013	0.387 ± 0.014	0.366 ± 0.015	0.262 ± 0.034
13-14	0.220 ± 0.009	0.399 ± 0.014	0.402 ± 0.016	0.367 ± 0.023	0.266 ± 0.026

Table E.5: The efficiency ϵ_{tot} in different bins of p_{T} and y averaged over prompt $\psi(2S)$ and $\psi(2S)$ -from- b

p_{T} (GeV/c)	$2 < y < 2.5$	$2.5 < y < 3$	$3 < y < 3.5$	$3.5 < y < 4$	$4 < y < 4.5$
3.5-4	0.035 ± 0.001	0.136 ± 0.002	0.202 ± 0.003	0.206 ± 0.004	0.124 ± 0.003
4-5	0.048 ± 0.001	0.171 ± 0.002	0.232 ± 0.002	0.233 ± 0.003	0.145 ± 0.003
5-6	0.068 ± 0.003	0.222 ± 0.003	0.274 ± 0.003	0.262 ± 0.004	0.164 ± 0.004
6-7	0.092 ± 0.002	0.264 ± 0.003	0.308 ± 0.004	0.290 ± 0.005	0.192 ± 0.006
7-8	0.116 ± 0.003	0.300 ± 0.004	0.333 ± 0.005	0.314 ± 0.005	0.207 ± 0.007
8-9	0.152 ± 0.005	0.319 ± 0.005	0.353 ± 0.006	0.334 ± 0.007	0.220 ± 0.009
9-10	0.151 ± 0.007	0.364 ± 0.006	0.377 ± 0.009	0.352 ± 0.009	0.236 ± 0.013
10-11	0.181 ± 0.008	0.379 ± 0.009	0.374 ± 0.013	0.351 ± 0.011	0.259 ± 0.015
11-12	0.202 ± 0.006	0.386 ± 0.010	0.362 ± 0.015	0.370 ± 0.015	0.259 ± 0.019
12-13	0.234 ± 0.011	0.395 ± 0.012	0.390 ± 0.014	0.370 ± 0.014	0.274 ± 0.028
13-14	0.225 ± 0.009	0.399 ± 0.014	0.403 ± 0.016	0.369 ± 0.022	0.272 ± 0.025

Table E.6: Summary of the relative systematic uncertainties (%)

Quantity	Systematic uncertainty	Comment
Signal shape	0.0-8.5	Correlated between bins
Global event cuts(GECs)	0.45	Correlated between bins
Trigger	0.0-4.4	Correlated between bins
Tracking	(0.7-3.0) \oplus (2 \times 0.4)	Correlated between bins
Muon ID	(0.7-8.9) \oplus (0.4-5.4)	Correlated between bins
p_T - y -spectrum	0.0-4.9	Bin dependent
$\psi(2S)$ vertex fit	0.1	Correlated between bins
Radiative tail	1.0	Correlated between bins
Luminosity	1.7	Correlated between bins
$\mathcal{B}(\psi(2S) \rightarrow e^+e^-)$	2.2	Correlated between bins
Simulated sample size	1.3-13.1(prompt $\psi(2S)$) 1.2-9.5($\psi(2S)$ -from- b)	Bin dependent
t_z fits	0.1-9.2	Only affects $\psi(2S)$ -from- b


 Figure E.8: Fractions of $\psi(2S)$ -from- b in bins of p_T and y for 7 TeV. The uncertainties are mainly from statistical ones and systematic uncertainties are negligible.

847 E.7 Tables of cross-section results

848 E.8 Fraction of $\psi(2S)$ -from- b mesons

849 The fraction of $\psi(2S)$ -from- b , F_b , in each kinematic bin is calculated by the
 850 efficiency-corrected signal yield of prompt $\psi(2S)$, N_p , and that of $\psi(2S)$ -from- b , N_b :
 851 $F_b \equiv N_b/(N_b + N_p)$. The fractions F_b as functions of p_T and y for 7 TeV data are shown
 852 in Fig. E.8. The corresponding values are presented in Table E.9. Only statistical uncer-
 853 tainties are shown as the systematic uncertainties are negligible owing to the cancellation
 854 of most systematic uncertainties.

855 **E.9 Systematic uncertainties between $\psi(2S)$ and J/ψ at 7 TeV**

856 To be able to do any comparison between reported results and J/ψ results at 7 TeV,
857 possible correlations of systematic uncertainties between channels must be investigated.
858 As in the case of 13 TeV results, all sources of systematic uncertainties can be divided
859 into the following classes:

- 860 • $m_{\mu^+\mu^-}$ signal shape. Double CB functions are used to describe the $m_{\mu^+\mu^-}$ signal
861 shape both in $\psi(2S)$ measurement, J/ψ using single CB function. We can expect
862 some correlation as the basic shape is similar, but for a conservative estimation, we
863 assume no correlation.
- 864 • Luminosity. Same methods were used for luminosity determination between both
865 works, we are assuming correlation for this source of systematic uncertainty.
- 866 • Tracking. As the data are taken at different years (2010 and 2011) under a slightly
867 different conditions, we are assuming no correlations.
- 868 • Vertexing Due to different conditions we are assuming no correlations.
- 869 • MuonID. Due to different conditions we are assuming no correlations.
- 870 • Trigger efficiency. Due to differences between used triggers, to be conservative, we
871 assume no correlations.
- 872 • MC statistics. Fully uncorrelated variable.
- 873 • Radiative tail. Both two analyses used similar models to describe radiative $\psi(2S)$
874 decays, so this effect totally cancels (100% correlated) between different analysis.
- 875 • p_T - y -spectrum. Different MC samples produced under different conditions are used
876 for evaluation for $\psi(2S)$ and J/ψ . We are assuming no correlation.
- 877 • Global event cuts (GEC). This uncertainty for $\psi(2S)$ is 0.45%, while for J/ψ is 2%.
878 As we are not sure about the treatment at J/ψ analysis, we take this source as
879 uncorrelated.
- 880 • t_z fit. Same as for 13 TeV analysis, there exist partial correlations between the
881 different analyses, since the tail effects should behave with some similarity. However,
882 we also acknowledge they are not fully correlated. To be conservative, its correlation
883 is assumed to be 0.

884 Since the nominal results of both analyses take zero polarization assumption, the
885 polarization effect in the ratio is neglected.

886 **E.10 Measurement of the $\mathcal{B}(b \rightarrow \psi(2S)X)$ at 7 TeV**

887 The measurement of branching fraction $\frac{\mathcal{B}(b \rightarrow \psi(2S)X)}{\mathcal{B}(b \rightarrow J/\psi X)}$ was also done for 7 TeV data as a
888 cross-check with results at 13 TeV, using exactly same method.

889 The factors $\alpha_{4\pi}(\psi(2S))$ and $\alpha_{4\pi}(J/\psi)$ for 7 TeV data are found to be 12.05 (Pythia 8)
890 and 5.88 (Pythia 6 to be consistent with J/ψ analysis at RUN-I), respectively. Values of

⁸⁹¹ $\alpha_{4\pi}$ parameters obtained using different theoretical models can be found at Table. E.10.
⁸⁹² Using the ratio of the two factors, $\xi = \frac{\alpha_{4\pi}(\psi(2S))}{\alpha_{4\pi}(J/\psi)} = 2.049$, cancellation of the majority
⁸⁹³ of theoretical uncertainties is expected. However even after this cancellation, additional
⁸⁹⁴ uncertainty, arising from model uncertainties, equal to 3 % can be assigned to the ξ
⁸⁹⁵ parameter. Equation for $\mathcal{B}(b \rightarrow \psi(2S)X)$ is then written as:

$$\frac{\mathcal{B}(b \rightarrow \psi(2S)X)}{\mathcal{B}(b \rightarrow J/\psi X)} = \xi \frac{\sigma(\psi(2S)\text{-from-}b, 13 \text{ TeV})}{\sigma(J/\psi\text{-from-}b, 13 \text{ TeV})}. \quad (\text{E.2})$$

⁸⁹⁶ Using the value $\sigma(J/\psi\text{-from-}b, 13 \text{ TeV}) = 2.25 \pm 0.01(\text{stat}) \pm 0.14(\text{syst})$ we obtain:

$$\frac{\mathcal{B}(b \rightarrow \psi(2S)X)}{\mathcal{B}(b \rightarrow J/\psi X)} = 0.239 \pm 0.002(\text{stat}) \pm 0.019(\text{syst}) \pm 0.006(\text{BF}), \quad (\text{E.3})$$

⁸⁹⁷ where possible correlations between uncertainties originates from $\psi(2S)\text{-from-}b$ and
⁸⁹⁸ $J/\psi\text{-from-}b$, respectively, are taken into account. The last uncertainty originates from the
⁸⁹⁹ uncertainty of the branching fractions $\mathcal{B}(\psi(2S) \rightarrow e^+e^-)$ and $\mathcal{B}(J/\psi \rightarrow \mu^+\mu^-)$. Using
⁹⁰⁰ Particle Data Group (PDG) [31] value $\mathcal{B}(b \rightarrow J/\psi X) = (1.16 \pm 0.10) \times 10^{-2}$ we obtain

$$\mathcal{B}(b \rightarrow \psi(2S)X) = (2.77 \pm 0.02(\text{stat}) \pm 0.22(\text{syst}) \pm 0.27(\text{BF})) \times 10^{-3}. \quad (\text{E.4})$$

⁹⁰¹ The $\mathcal{B}(b \rightarrow J/\psi X)$ uncertainty dominates the total uncertainty originates from branching
⁹⁰² fractions.

⁹⁰³ Both results, ratio and BF $\mathcal{B}(b \rightarrow J/\psi X)$, are consistent within uncertainties between
⁹⁰⁴ 7 TeV and 13 TeV.

⁹⁰⁵ E.11 Comparison with polarised results at 7 TeV

⁹⁰⁶ In order to further studies about possible polarisation of $\psi(2S)$, cross-section measure-
⁹⁰⁷ ment was done also with polarisation based on polarisation measurements at 7 TeV [35].
⁹⁰⁸ Polarisation factor, based on aforementioned measurement, was calculated for every bin,
⁹⁰⁹ no global factor was assigned. Results, single differential cross-section as function of p_T
⁹¹⁰ (y) is shown at the Table E.11 (E.12). Only the polarisation parameter λ_{theta} is taken as
⁹¹¹ non-zero. The single largest deviation was found to be 6 % for low- y /high p_T bin, still
⁹¹² smaller than total systematic uncertainty, 16 %.

⁹¹³ Results are compatible with the results obtained under the assumption of no po-
⁹¹⁴ larisation, double-differential results for prompt $\psi(2S)$ are show at the Table E.13, for
⁹¹⁵ $\psi(2S)\text{-from-}b$ at the Table E.14, single-differential cross-section as function p_T and y is
⁹¹⁶ shown at the Table E.11 and E.12), respectively.

Table E.7: Double differential production cross-section in nb (GeV/c) for prompt $\psi(2S)$ mesons in bins of (p_T, y) . The first uncertainties are statistical, the second are the uncorrelated systematic uncertainties shared between bins and the last are the correlated systematic uncertainties.

p_T (GeV/c)	$2 < y < 2.5$	$2.5 < y < 3$	$3 < y < 3.5$	$3.5 < y < 4$	$4 < y < 4.5$
3.5-4	94.34 ± 2.49 ± 5.59 ± 8.65	109.85 ± 1.38 ± 2.50 ± 5.04	97.07 ± 0.99 ± 1.90 ± 4.33	77.87 ± 0.78 ± 1.51 ± 3.11	57.90 ± 0.80 ± 1.57 ± 2.09
4-5	73.08 ± 1.21 ± 4.35 ± 4.40	75.42 ± 0.66 ± 1.32 ± 3.53	65.66 ± 0.47 ± 0.85 ± 2.64	53.33 ± 0.40 ± 0.88 ± 2.23	36.34 ± 0.40 ± 0.80 ± 1.30
5-6	44.86 ± 0.71 ± 2.47 ± 2.24	43.26 ± 0.38 ± 1.04 ± 4.14	37.21 ± 0.30 ± 0.58 ± 1.54	31.96 ± 0.27 ± 0.86 ± 1.31	18.98 ± 0.26 ± 0.93 ± 0.65
6-7	25.99 ± 0.45 ± 1.64 ± 2.58	24.94 ± 0.25 ± 0.63 ± 1.20	22.42 ± 0.21 ± 0.58 ± 0.86	17.86 ± 0.19 ± 0.61 ± 0.69	10.33 ± 0.17 ± 0.39 ± 0.50
7-8	16.58 ± 0.30 ± 1.26 ± 1.04	15.21 ± 0.17 ± 0.41 ± 0.66	12.82 ± 0.14 ± 0.40 ± 0.50	9.98 ± 0.13 ± 0.33 ± 0.44	5.61 ± 0.12 ± 0.30 ± 0.26
8-9	7.03 ± 0.14 ± 1.16 ± 0.35	9.02 ± 0.12 ± 0.39 ± 0.41	7.16 ± 0.10 ± 0.31 ± 0.33	5.05 ± 0.09 ± 0.28 ± 0.23	2.92 ± 0.08 ± 0.18 ± 0.15
9-10	6.10 ± 0.14 ± 0.63 ± 0.28	5.26 ± 0.09 ± 0.26 ± 0.23	4.63 ± 0.08 ± 0.20 ± 0.18	3.16 ± 0.07 ± 0.20 ± 0.13	1.89 ± 0.07 ± 0.20 ± 0.12
10-11	3.89 ± 0.11 ± 0.36 ± 0.23	3.03 ± 0.06 ± 0.17 ± 0.14	2.50 ± 0.05 ± 0.17 ± 0.11	1.93 ± 0.06 ± 0.18 ± 0.07	1.04 ± 0.05 ± 0.15 ± 0.06
11-12	2.56 ± 0.08 ± 0.29 ± 0.13	2.30 ± 0.06 ± 0.35 ± 0.10	1.50 ± 0.04 ± 0.16 ± 0.13	1.46 ± 0.05 ± 0.25 ± 0.10	0.38 ± 0.02 ± 0.08 ± 0.02
12-13	2.42 ± 0.10 ± 0.90 ± 0.11	1.12 ± 0.04 ± 0.09 ± 0.05	0.84 ± 0.03 ± 0.12 ± 0.04	0.58 ± 0.03 ± 0.08 ± 0.05	0.35 ± 0.03 ± 0.10 ± 0.04
13-14	0.85 ± 0.04 ± 0.16 ± 0.04	0.88 ± 0.03 ± 0.12 ± 0.11	0.60 ± 0.03 ± 0.09 ± 0.04	0.33 ± 0.02 ± 0.06 ± 0.02	0.07 ± 0.01 ± 0.02 ± 0.01

Table E.8: Double differential production cross-section in nb (GeV/ c) for $\psi(2S)$ -from- b mesons in bins of (p_T, y). The first uncertainties are statistical, the second are the uncorrelated systematic uncertainties shared between bins and the last are the correlated systematic uncertainties.

p_T (GeV/ c)	2 < y < 2.5	2.5 < y < 3	3 < y < 3.5	3.5 < y < 4	4 < y < 4.5
3.5-4	27.65 ± 1.10 ± 1.64 ± 2.86	24.88 ± 0.55 ± 0.44 ± 1.66	21.06 ± 0.42 ± 0.35 ± 0.98	16.01 ± 0.36 ± 0.43 ± 0.65	9.62 ± 0.36 ± 0.32 ± 0.53
4-5	20.85 ± 0.54 ± 1.12 ± 1.36	19.60 ± 0.29 ± 0.26 ± 1.14	15.58 ± 0.22 ± 0.19 ± 0.74	11.05 ± 0.19 ± 0.18 ± 0.46	6.58 ± 0.18 ± 0.18 ± 0.23
5-6	13.31 ± 0.36 ± 0.96 ± 0.93	13.04 ± 0.19 ± 0.19 ± 1.31	9.80 ± 0.15 ± 0.13 ± 0.43	6.90 ± 0.13 ± 0.12 ± 0.28	4.00 ± 0.13 ± 0.14 ± 0.14
6-7	8.77 ± 0.24 ± 0.45 ± 0.93	8.15 ± 0.14 ± 0.12 ± 0.40	6.20 ± 0.11 ± 0.09 ± 0.26	4.53 ± 0.10 ± 0.08 ± 0.18	2.01 ± 0.09 ± 0.08 ± 0.14
7-8	6.24 ± 0.18 ± 0.33 ± 0.41	4.96 ± 0.10 ± 0.08 ± 0.25	4.02 ± 0.08 ± 0.07 ± 0.16	2.64 ± 0.07 ± 0.05 ± 0.15	1.38 ± 0.07 ± 0.06 ± 0.07
8-9	3.68 ± 0.12 ± 0.19 ± 0.23	3.40 ± 0.08 ± 0.07 ± 0.16	2.69 ± 0.07 ± 0.05 ± 0.14	1.61 ± 0.05 ± 0.04 ± 0.08	0.76 ± 0.05 ± 0.04 ± 0.04
9-10	3.14 ± 0.11 ± 0.21 ± 0.19	2.15 ± 0.06 ± 0.04 ± 0.09	1.33 ± 0.05 ± 0.04 ± 0.12	1.00 ± 0.04 ± 0.03 ± 0.04	0.37 ± 0.03 ± 0.02 ± 0.04
10-11	1.96 ± 0.08 ± 0.12 ± 0.12	1.46 ± 0.05 ± 0.04 ± 0.07	1.11 ± 0.04 ± 0.04 ± 0.07	0.66 ± 0.03 ± 0.02 ± 0.03	0.32 ± 0.03 ± 0.02 ± 0.02
11-12	1.28 ± 0.06 ± 0.07 ± 0.07	1.00 ± 0.04 ± 0.03 ± 0.05	0.75 ± 0.03 ± 0.03 ± 0.07	0.42 ± 0.02 ± 0.02 ± 0.03	0.18 ± 0.02 ± 0.02 ± 0.01
12-13	0.80 ± 0.04 ± 0.05 ± 0.05	0.73 ± 0.03 ± 0.02 ± 0.04	0.51 ± 0.03 ± 0.02 ± 0.02	0.28 ± 0.02 ± 0.01 ± 0.03	0.09 ± 0.02 ± 0.01 ± 0.01
13-14	0.66 ± 0.04 ± 0.07 ± 0.04	0.51 ± 0.03 ± 0.02 ± 0.06	0.33 ± 0.02 ± 0.01 ± 0.02	0.17 ± 0.02 ± 0.01 ± 0.01	0.06 ± 0.01 ± 0.01 ± 0.01

Table E.9: Fractions of $\psi(2S)$ -from- b (in %) at 7 TeV in bins of (p_T, y) of $\psi(2S)$ mesons. The uncertainties are statistical only. The systematic uncertainties are negligible.

p_T (GeV/ c)	$2.0 < y < 2.5$	$2.5 < y < 3.0$	$3.0 < y < 3.5$	$3.5 < y < 4.0$	$4.0 < y < 4.5$
3.5–4	21.11 ± 0.79	17.91 ± 0.37	17.26 ± 0.33	16.52 ± 0.34	13.93 ± 0.50
4–5	21.73 ± 0.53	20.21 ± 0.28	18.42 ± 0.25	16.95 ± 0.27	15.47 ± 0.40
5–6	22.15 ± 0.55	22.40 ± 0.31	20.08 ± 0.29	17.89 ± 0.32	16.49 ± 0.50
6–7	24.12 ± 0.61	24.49 ± 0.37	21.45 ± 0.35	20.21 ± 0.41	16.18 ± 0.65
7–8	27.34 ± 0.68	25.04 ± 0.44	23.81 ± 0.44	21.64 ± 0.52	18.48 ± 0.83
8–9	28.44 ± 0.80	27.26 ± 0.54	26.81 ± 0.57	23.68 ± 0.70	19.12 ± 1.10
9–10	30.46 ± 0.08	29.40 ± 0.68	21.50 ± 0.69	24.95 ± 0.88	17.28 ± 1.38
10–11	32.97 ± 1.08	31.67 ± 0.83	28.14 ± 0.87	27.30 ± 1.17	24.10 ± 1.77
11–12	34.86 ± 1.33	33.31 ± 1.02	30.98 ± 1.16	28.55 ± 1.44	27.33 ± 2.10
12–13	35.56 ± 1.62	37.85 ± 1.31	33.30 ± 1.44	28.50 ± 1.78	20.81 ± 3.01
13–14	38.79 ± 1.93	36.68 ± 1.51	34.21 ± 1.80	30.97 ± 2.50	36.20 ± 6.19

	$\psi(2S)$	J/ψ	ξ
Pythia 8	12.05	5.34	2.257
Pythia 6	N/A	5.88	2.049*
FONLL CTEQ6.6	13.48	4.96	2.718
NNPDF30_nlo_as_0118	13.477	5.099	2.643
FONLL MSTW	13.646	5.163	2.643

Table E.10: List of $\alpha_{4\pi}$ parameters obtained from Pythia, FONLL using for 7 TeV. * Ratio is done with respect to $\alpha_{4\pi}(\psi(2S))$ obtained via Pythia 8.

Table E.11: Differential cross-sections $d\sigma/dp_T$ (in nb/(GeV/ c)) of prompt $\psi(2S)$ and $\psi(2S)$ -from- b mesons, integrated over y between 2.0 and 4.5. The first uncertainties are statistical and the second (third) are uncorrelated (correlated) systematic uncertainties amongst bins.

p_T (GeV/ c)	Prompt $\psi(2S)$	$\psi(2S)$ -from- b
3.5–4	$218.19 \pm 1.60 \pm 3.38 \pm 11.59$	$49.53 \pm 0.69 \pm 0.91 \pm 3.33$
4–5	$151.70 \pm 0.78 \pm 2.38 \pm 7.03$	$36.77 \pm 0.35 \pm 0.60 \pm 1.96$
5–6	$88.23 \pm 0.47 \pm 1.52 \pm 4.95$	$23.55 \pm 0.24 \pm 0.50 \pm 1.55$
6–7	$50.85 \pm 0.30 \pm 1.00 \pm 2.92$	$14.85 \pm 0.16 \pm 0.25 \pm 0.95$
7–8	$30.51 \pm 0.21 \pm 0.75 \pm 1.47$	$9.75 \pm 0.12 \pm 0.18 \pm 0.52$
8–9	$15.79 \pm 0.13 \pm 0.67 \pm 0.75$	$6.15 \pm 0.09 \pm 0.11 \pm 0.33$
9–10	$10.65 \pm 0.10 \pm 0.39 \pm 0.48$	$4.05 \pm 0.07 \pm 0.11 \pm 0.24$
10–11	$5.91 \pm 0.07 \pm 0.23 \pm 0.29$	$2.62 \pm 0.05 \pm 0.06 \pm 0.15$
11–12	$3.91 \pm 0.06 \pm 0.26 \pm 0.23$	$1.73 \pm 0.04 \pm 0.04 \pm 0.11$
12–13	$2.57 \pm 0.05 \pm 0.46 \pm 0.14$	$1.15 \pm 0.03 \pm 0.03 \pm 0.07$
13–14	$1.31 \pm 0.03 \pm 0.11 \pm 0.10$	$0.82 \pm 0.03 \pm 0.03 \pm 0.07$

Table E.12: Differential cross-sections $d\sigma/dy$ (in nb) of prompt $\psi(2S)$ and $\psi(2S)$ -from- b mesons, integrated over p_T between 2 and 20 GeV/ c . The first uncertainties are statistical and the second (third) are uncorrelated (correlated) systematic uncertainties amongst bins.

y	Prompt $\psi(2S)$	$\psi(2S)$ -from- b
2.0-2.5	$230.2 \pm 2.0 \pm 6.3 \pm 15.7$	$74.4 \pm 0.9 \pm 1.8 \pm 5.8$
2.5-3.0	$235.5 \pm 1.1 \pm 2.3 \pm 13.1$	$67.4 \pm 0.5 \pm 0.4 \pm 4.4$
3.0-3.5	$204.0 \pm 0.8 \pm 1.6 \pm 8.5$	$52.8 \pm 0.4 \pm 0.3 \pm 2.5$
3.5-4.0	$164.6 \pm 0.7 \pm 1.7 \pm 6.8$	$37.2 \pm 0.3 \pm 0.3 \pm 1.6$
4.0-4.5	$106.9 \pm 0.7 \pm 1.6 \pm 4.2$	$20.5 \pm 0.3 \pm 0.3 \pm 1.0$

Table E.13: Double differential production cross-section in nb (GeV/c) for prompt $\psi(2S)$ mesons in bins of (p_{T}, y) . The first uncertainties are statistical, the second are the uncorrelated systematic uncertainties shared between bins and the last are the correlated systematic uncertainties. Results under the assumption of polarisation.

p_{T} (GeV/c)	$2 < y < 2.5$	$2.5 < y < 3$	$3 < y < 3.5$	$3.5 < y < 4$	$4 < y < 4.5$
3.5-4	$93.97 \pm 2.48 \pm 5.58 \pm 8.62$	$109.76 \pm 1.38 \pm 2.51 \pm 5.04$	$97.00 \pm 0.99 \pm 1.91 \pm 4.32$	$77.79 \pm 0.78 \pm 1.51 \pm 3.11$	$57.87 \pm 0.80 \pm 1.57 \pm 2.09$
4-5	$72.83 \pm 1.20 \pm 4.33 \pm 4.39$	$75.35 \pm 0.66 \pm 1.32 \pm 3.53$	$65.61 \pm 0.47 \pm 0.85 \pm 2.63$	$53.28 \pm 0.40 \pm 0.88 \pm 2.23$	$36.32 \pm 0.40 \pm 0.80 \pm 1.30$
5-6	$44.91 \pm 0.72 \pm 2.47 \pm 2.24$	$43.33 \pm 0.38 \pm 1.05 \pm 4.15$	$37.25 \pm 0.30 \pm 0.58 \pm 1.54$	$31.98 \pm 0.27 \pm 0.86 \pm 1.31$	$18.99 \pm 0.26 \pm 0.94 \pm 0.65$
6-7	$26.04 \pm 0.45 \pm 1.65 \pm 2.58$	$24.99 \pm 0.25 \pm 0.63 \pm 1.20$	$22.45 \pm 0.21 \pm 0.58 \pm 0.87$	$17.88 \pm 0.19 \pm 0.61 \pm 0.69$	$10.34 \pm 0.17 \pm 0.40 \pm 0.50$
7-8	$16.90 \pm 0.30 \pm 1.29 \pm 1.06$	$15.42 \pm 0.17 \pm 0.42 \pm 0.67$	$12.97 \pm 0.15 \pm 0.41 \pm 0.50$	$10.08 \pm 0.13 \pm 0.33 \pm 0.44$	$5.65 \pm 0.12 \pm 0.31 \pm 0.26$
8-9	$7.13 \pm 0.15 \pm 1.19 \pm 0.36$	$9.16 \pm 0.13 \pm 0.40 \pm 0.42$	$7.25 \pm 0.10 \pm 0.32 \pm 0.33$	$5.10 \pm 0.09 \pm 0.28 \pm 0.23$	$2.93 \pm 0.08 \pm 0.18 \pm 0.15$
9-10	$6.20 \pm 0.14 \pm 0.65 \pm 0.28$	$5.33 \pm 0.09 \pm 0.27 \pm 0.23$	$4.68 \pm 0.08 \pm 0.21 \pm 0.18$	$3.19 \pm 0.07 \pm 0.21 \pm 0.13$	$1.91 \pm 0.07 \pm 0.20 \pm 0.12$
10-11	$3.64 \pm 0.10 \pm 0.34 \pm 0.22$	$2.89 \pm 0.06 \pm 0.16 \pm 0.13$	$2.41 \pm 0.05 \pm 0.16 \pm 0.10$	$1.86 \pm 0.05 \pm 0.17 \pm 0.06$	$1.01 \pm 0.05 \pm 0.15 \pm 0.06$
11-12	$2.39 \pm 0.08 \pm 0.26 \pm 0.12$	$2.19 \pm 0.06 \pm 0.33 \pm 0.09$	$1.45 \pm 0.04 \pm 0.15 \pm 0.13$	$1.41 \pm 0.05 \pm 0.24 \pm 0.09$	$0.38 \pm 0.02 \pm 0.08 \pm 0.02$
12-13	$2.34 \pm 0.09 \pm 0.91 \pm 0.11$	$1.07 \pm 0.04 \pm 0.08 \pm 0.05$	$0.82 \pm 0.03 \pm 0.11 \pm 0.04$	$0.57 \pm 0.03 \pm 0.08 \pm 0.05$	$0.34 \pm 0.03 \pm 0.09 \pm 0.04$
13-14	$0.81 \pm 0.04 \pm 0.15 \pm 0.04$	$0.85 \pm 0.03 \pm 0.12 \pm 0.10$	$0.58 \pm 0.03 \pm 0.08 \pm 0.04$	$0.32 \pm 0.02 \pm 0.06 \pm 0.02$	$0.07 \pm 0.01 \pm 0.02 \pm 0.01$

Table E.14: Double differential production cross-section in nb (GeV/c) for $\psi(2S)$ -from- b mesons in bins of (p_T, y) . The first uncertainties are statistical, the second are the uncorrelated systematic uncertainties shared between bins and the last are the correlated systematic uncertainties. Results under the assumption of polarisation.

p_T (GeV/c)	$2 < y < 2.5$	$2.5 < y < 3$	$3 < y < 3.5$	$3.5 < y < 4$	$4 < y < 4.5$
3.5-4	$27.54 \pm 1.09 \pm 1.64 \pm 2.85$	$24.86 \pm 0.54 \pm 0.45 \pm 1.66$	$21.05 \pm 0.42 \pm 0.35 \pm 0.98$	$16.00 \pm 0.35 \pm 0.43 \pm 0.65$	$9.62 \pm 0.36 \pm 0.32 \pm 0.53$
4-5	$20.79 \pm 0.54 \pm 1.12 \pm 1.36$	$19.58 \pm 0.29 \pm 0.26 \pm 1.14$	$15.57 \pm 0.22 \pm 0.19 \pm 0.74$	$11.04 \pm 0.19 \pm 0.18 \pm 0.46$	$6.57 \pm 0.18 \pm 0.18 \pm 0.23$
5-6	$13.32 \pm 0.36 \pm 0.96 \pm 0.93$	$13.07 \pm 0.20 \pm 0.19 \pm 1.31$	$9.81 \pm 0.15 \pm 0.13 \pm 0.43$	$6.91 \pm 0.13 \pm 0.12 \pm 0.28$	$4.00 \pm 0.13 \pm 0.14 \pm 0.14$
6-7	$8.79 \pm 0.24 \pm 0.45 \pm 0.94$	$8.17 \pm 0.14 \pm 0.12 \pm 0.40$	$6.20 \pm 0.11 \pm 0.09 \pm 0.26$	$4.53 \pm 0.10 \pm 0.09 \pm 0.18$	$2.01 \pm 0.09 \pm 0.08 \pm 0.14$
7-8	$6.36 \pm 0.18 \pm 0.34 \pm 0.42$	$5.03 \pm 0.10 \pm 0.08 \pm 0.25$	$4.06 \pm 0.08 \pm 0.07 \pm 0.16$	$2.66 \pm 0.07 \pm 0.05 \pm 0.15$	$1.38 \pm 0.07 \pm 0.06 \pm 0.07$
8-9	$3.75 \pm 0.12 \pm 0.20 \pm 0.24$	$3.45 \pm 0.08 \pm 0.07 \pm 0.16$	$2.72 \pm 0.07 \pm 0.05 \pm 0.14$	$1.62 \pm 0.05 \pm 0.04 \pm 0.08$	$0.77 \pm 0.05 \pm 0.04 \pm 0.04$
9-10	$3.19 \pm 0.11 \pm 0.21 \pm 0.19$	$2.17 \pm 0.06 \pm 0.04 \pm 0.09$	$1.35 \pm 0.05 \pm 0.04 \pm 0.12$	$1.01 \pm 0.04 \pm 0.03 \pm 0.04$	$0.37 \pm 0.03 \pm 0.02 \pm 0.04$
10-11	$1.85 \pm 0.07 \pm 0.11 \pm 0.11$	$1.39 \pm 0.04 \pm 0.04 \pm 0.07$	$1.06 \pm 0.04 \pm 0.04 \pm 0.07$	$0.63 \pm 0.03 \pm 0.02 \pm 0.03$	$0.31 \pm 0.03 \pm 0.02 \pm 0.02$
11-12	$1.21 \pm 0.06 \pm 0.06 \pm 0.07$	$0.96 \pm 0.04 \pm 0.03 \pm 0.04$	$0.72 \pm 0.03 \pm 0.03 \pm 0.07$	$0.41 \pm 0.02 \pm 0.02 \pm 0.03$	$0.17 \pm 0.02 \pm 0.02 \pm 0.01$
12-13	$0.75 \pm 0.04 \pm 0.04 \pm 0.05$	$0.69 \pm 0.03 \pm 0.02 \pm 0.04$	$0.49 \pm 0.03 \pm 0.02 \pm 0.02$	$0.27 \pm 0.02 \pm 0.01 \pm 0.02$	$0.09 \pm 0.02 \pm 0.01 \pm 0.01$
13-14	$0.62 \pm 0.04 \pm 0.06 \pm 0.04$	$0.49 \pm 0.02 \pm 0.02 \pm 0.06$	$0.31 \pm 0.02 \pm 0.01 \pm 0.02$	$0.16 \pm 0.02 \pm 0.01 \pm 0.01$	$0.06 \pm 0.01 \pm 0.01 \pm 0.01$

917 F Checks and comparisons with the 2010 results

918 Figure F.1 shows the ratios of the production cross-sections in bins of p_T between the
 919 2015 result and the 2010 result, which was published in Ref. [34]. The left plot is the
 920 ratio as a function of p_T for prompt $\psi(2S)$, and the agreement between the data and the
 921 NRQCD calculation [55] is reasonable. The right plot is the ratio as function of p_T for
 922 $\psi(2S)$ -from- b , and the discrepancy between the data and the FONLL calculation [36] is
 923 significant. We noticed this large discrepancy during the review, but found nothing wrong
 924 in our code. During the approval to go to paper, Vicenzo commented that it is unlikely
 925 that the FONLL calculation could have such discrepancy from data, and it is unlikely
 926 that $b\bar{b}$ cross-section at 13 TeV could be three to four times larger than that at 7 TeV. He
 927 suggested us to check both results at 13 TeV and 7 TeV and also to contact the FONLL
 928 authors to check if we misused their calculations.

929 We checked all the details of the 13 TeV analysis, including cross-checks with indepen-
 930 dent codes and methods, and checks with the 13 TeV J/ψ sample. Everything looks OK.
 931 The FONLL authors also confirmed that the theoretical calculation is correctly used.

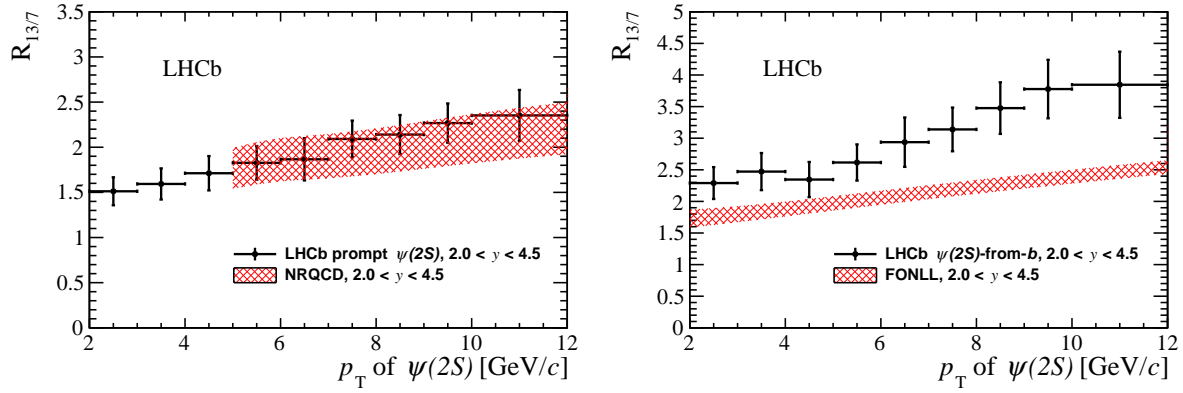


Figure F.1: Ratios of $\psi(2S)$ production cross-sections between 2015 and 2010. (Left) The prompt $\psi(2S)$ result is compared with the NRQCD calculation, while (right) the $\psi(2S)$ -from- b result is compared with the FONLL calculation.

932 We then decided to check the 7 TeV result using the 2010 data sample. However, we
 933 found that what we can do for the previous analysis is very limited due to various reasons.
 934 All the scripts and the original ntuples of the data and the simulated samples for the
 935 2010 analysis are missing. The information in the analysis note is limited. We consulted
 936 the proponents for the information. The 2010 results were based on Stripping12b, but
 937 this stripping is obsolete and was already removed from the disk at the time of this
 938 analysis. With the great helps from the computing group and the B&Q working group,
 939 the Stripping12b data is restored to the bookkeeping, but the simulated samples cannot
 940 be recovered. Due to these issues, the decision to look at the 2011 data sample was made.
 941 Details of the analysis with the 2011 sample can be found in Sect. E). The results of the
 942 2011 data are compared with the 2010 result, as shown in Figs. F.2, F.3 and F.4.

943 Figure F.2 shows the comparison between the 2010 results, the 2011 results and
 944 the theoretical calculations [36, 55]. Figures F.3 and F.4 shows the ratios between the
 945 2010 and 2011 results.⁵ For the systematic uncertainty cancellation, the uncertainty

⁵For the 2010 results, the branching fraction of $\psi(2S)$ decays has been corrected by using the value in

due to the branching fraction $\mathcal{B}(\psi(2S) \rightarrow e^+e^-)$ is considered to be fully cancelled, the uncertainty due to the luminosity determination is considered to be partially correlated with a correlation coefficient of 0.35, and all other systematic uncertainties are considered to be uncorrelated.⁶ Although both results from the 2010 and 2011 data samples agree with the theoretical calculations whose uncertainties are very large, the ratios reveals some interesting features. The ratio of prompt $\psi(2S)$ production cross-sections as a function of p_T indicates reasonable agreement between the 2010 and 2011 results, as shown in Fig. F.3; while the ratio of the production cross-sections of $\psi(2S)$ -from- b indicates significant discrepancies between the 2010 and the 2011 results, as shown in Fig. F.4. The significance of the discrepancy in each bin is naively defined as $(1 - R_{2010/2011})/\sigma_R$, where $R_{2010/2011}$ is the ratio of the cross-sections between 2010 and 2011, and σ_R is the uncertainty of the ratio. The discrepancies are found to vary from 2.2σ to 5.1σ in various bins. Since the uncertainty of the ratio in each bin is dominated by the systematic uncertainty, and they are mostly correlated between bins, the overall discrepancy almost equals to the value of the bin with the largest discrepancy. Besides, we found that the systematic uncertainty to account for the t_z fit was wrongly calculated in the 2010 result. It needs to be corrected by a factor F_p/F_b , where F_p is the fraction of prompt $\psi(2S)$, $F_p \equiv 1 - F_b$. This factor varies from 3 to 9 between the p_T bins. As shown in Fig. F.4, the discrepancies are still significant even if this underestimated uncertainty is taken into account. The discrepancies vary from 1.5σ to 4.2σ in various p_T bins.

Due to the issues mentioned above, it is difficult, if not impossible, for us to fully understand the reason(s) that causes this significant discrepancy. Nevertheless, we made some additional checks. The reasonable agreement between the 2010 and 2011 prompt $\psi(2S)$ production cross-sections does not definitely mean that these two results are correct. However, we assume that the the results of prompt $\psi(2S)$ are OK. Since the efficiencies of prompt $\psi(2S)$ and $\psi(2S)$ -from- b are very close to each other, we then suspected that the significant discrepancies of $\psi(2S)$ -from- b might mostly originate from the determination of the yields of $\psi(2S)$ -from- b . We noticed in the analysis note [58] of the published $\psi(2S)$ analysis using the 2010 data sample that the parameters τ_b obtained from the 2D fits to the $M_{\mu^+\mu^-}$ and t_z distributions are averagely smaller than expected and the values of F_p looks larger than expected (see Fig. F.5 or Fig. 36 in the note). Wenbin Qian studied in his PhD thesis [59] that the variable t_z is a good approximation of the b -hadron lifetime, and the value of the parameter τ_b is around 1.5 ps. This was well confirmed in many other analyses using the same method. We made the 2D fits to the $M_{\mu^+\mu^-}$ and t_z distributions in each p_T bin using the Psi2MuMuLINE of STRIPPING12B. The top (bottom) plot of Fig. F.6 shows the τ_b values in various kinematic bins from the fits to the 2010 (2011) data sample. These distributions are significantly different to the corresponding distribution in the ANA note of the previous $\psi(2S)$ analysis [58]. Unfortunately, these are almost the best checks we can make. The simulated sample is and will not be available, and the data sample used for the previous $\psi(2S)$ analysis cannot be reproduced in the available dataset (STRIPPING12B). We tried all possible available stripping lines in the available dataset, and neither has the same selection as described in the previous ANA note [58].

Figure F.7 shows a comparison of the fraction of prompt $\psi(2S)$ at 7 TeV. The 2010 old result is obtained from the published $\psi(2S)$ measurement [34]. The 2010 new result

PDG2016 [47].

⁶ The numerical results remain the same if we assume that the uncertainty due to the luminosity determination is uncorrelated.

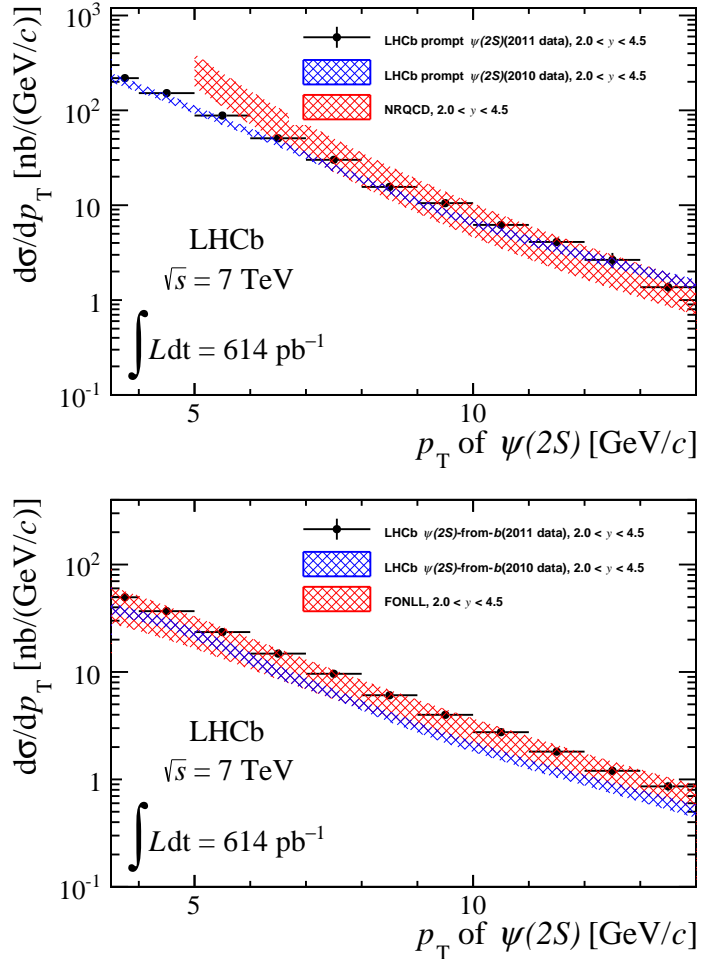


Figure F.2: Comparison of the 2010 and 2011 differential cross-sections as functions of p_T for (top) prompt $\psi(2S)$ and (bottom) $\psi(2S)$ -from- b . Only statistical uncertainty is considered for the 2011 results.

990 is obtained from the 2D fits to the 2010 data sample we obtained with the help of the
 991 computing group and the B&Q WG. Here, we assumed that the efficiencies are the same
 992 for prompt $\psi(2S)$ and $\psi(2S)$ -from- b . Only statistical uncertainty is considered.

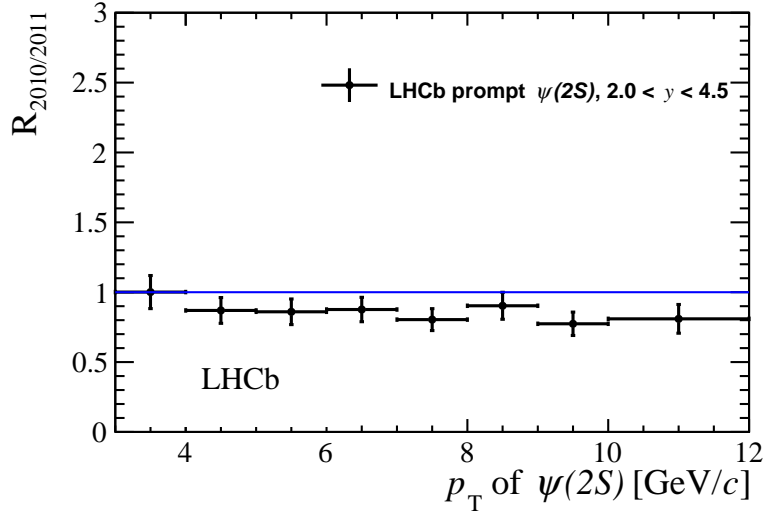


Figure F.3: Ratio of the prompt $\psi(2S)$ production cross-sections between 2010 and 2011.

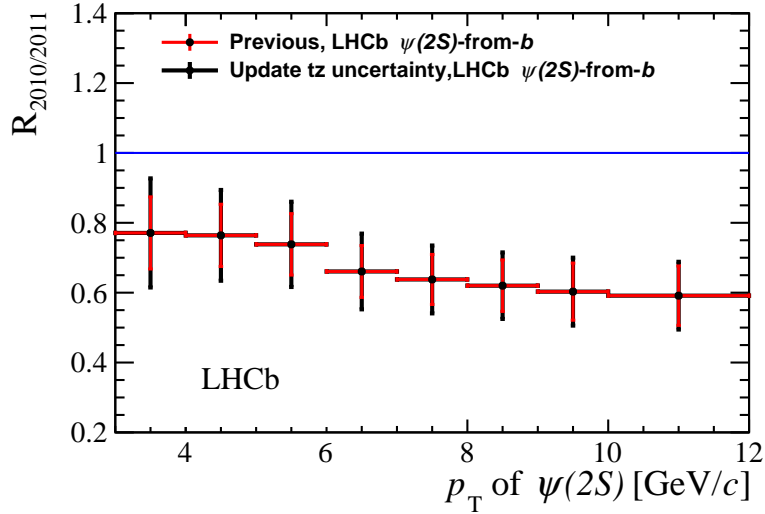


Figure F.4: Ratio of the production cross-sections of $\psi(2S)$ -from- b between 2010 and 2011. Both the original uncertainties and the updated uncertainties are shown.

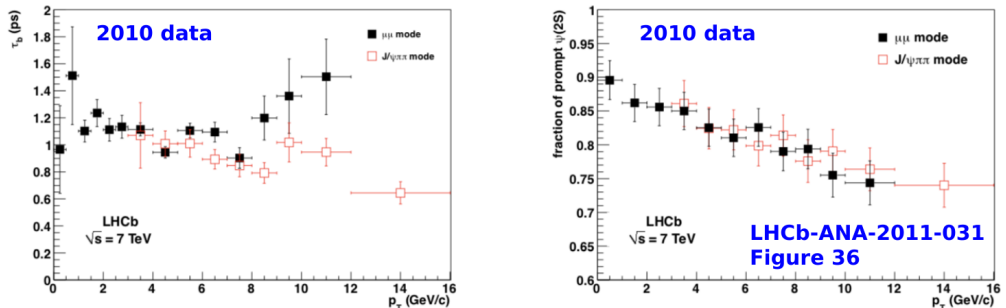


Figure F.5: Distributions of (left) the parameter τ_b from the 2D fits and (right) the fraction $\psi(2S)$ F_p of prompt $\psi(2S)$. Taken from the ANA note [58].

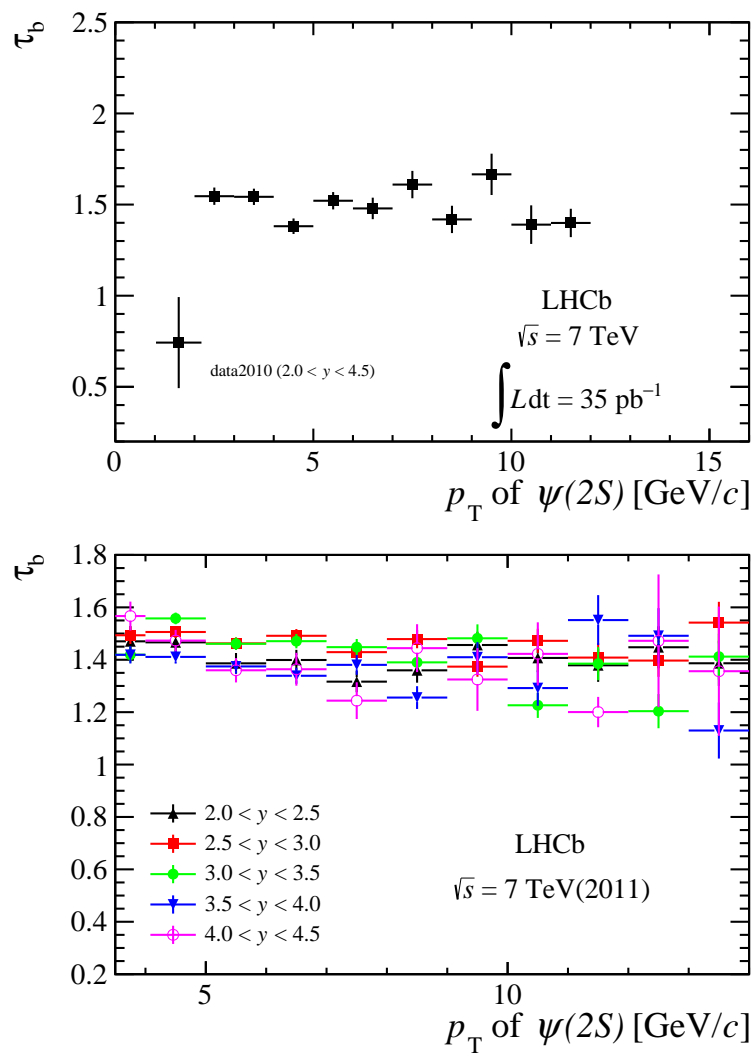


Figure F.6: Distributions of the values of the parameter τ_b from the 2D fits for (top) the re-analysed 2010 data and (bottom) the 2011 data.

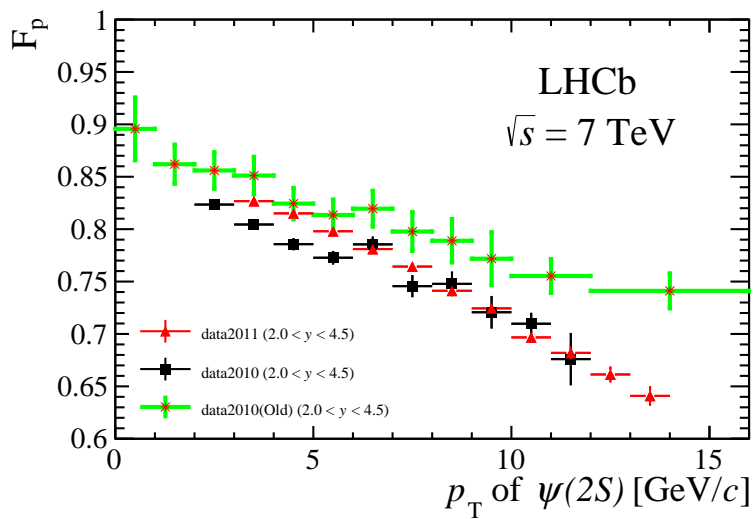


Figure F.7: Comparison of the fraction of prompt $\psi(2S)$ at 7 TeV. The 2010 old result is taken from the previous $\psi(2S)$ measurement [34]. Only statistical uncertainties are considered in the 2010 new result and the 2011 result.

993 G Checks and corrections done for 2010 erratum

994 Previously described issues with the 2010 results on the $\psi(2S)$ production and incompatibility
 995 with the analysis of 2011 data culminated into the need of official correction of
 996 published results in the form of erratum. This chapter will describe all checks and steps
 997 done to provide an erratum to the 2010 data using $\psi(2S)$ production paper [34]. For
 998 the rest of this chapter, published results will be denoted as '2010 old', corrected results
 999 as '2010 new'. Results obtained using 2010 partially reanalysed data (as mentioned at
 1000 section F), will be denoted as '2010 part'.

1001 Basic assumption for how the 2010 old results should be corrected is based on the
 1002 observed large discrepancy between 2010 old F_p and results obtained via partially reanal-
 1003 ysed 2010 data and 2011 data F.7. After the discussion with RC and PCs, the following
 1004 approach was suggested:

- 1005 1. Made a ratio $R_{F_b} = \frac{F_b \text{ (2010 part)}}{F_b \text{ (2010 old)}}$ for the common p_T range
- 1006 2. Use ratio from point 1 to obtain values of F_p for full p_T range 0-16 GeV, and correct
 1007 production cross-section of prompt $\psi(2S)$ and $\psi(2S)$ -from- b .
- 1008 3. Evaluate additional systematic uncertainties

1009 Ratio R_{F_p} between 2010 partially reanalysed and 2010 old F_p can be seen on Fig. G.1.
 1010 The linear fit shows the best agreement with the obtained R_{F_b} and thus is used as the
 1011 baseline for obtaining all new results. For the control fits, two another functions were
 1012 used: polynomial function of 2nd order and exponential function. Both control fits are
 1013 shown on Fig. G.3. After extrapolating fitting function from the common p_T range 2-10
 1014 GeV/ c to the full range of 2010 old data, 0-16 GeV, new results of F_p were obtained from
 1015 the R_{F_b} . Comparison of F_p values for 2010 old, 2010 part, 2011 and results based on the
 1016 2nd order polynomial fit is shown on Fig. G.4. Results obtained using control fits are
 1017 fully consistent with average deviation less than 3 %.

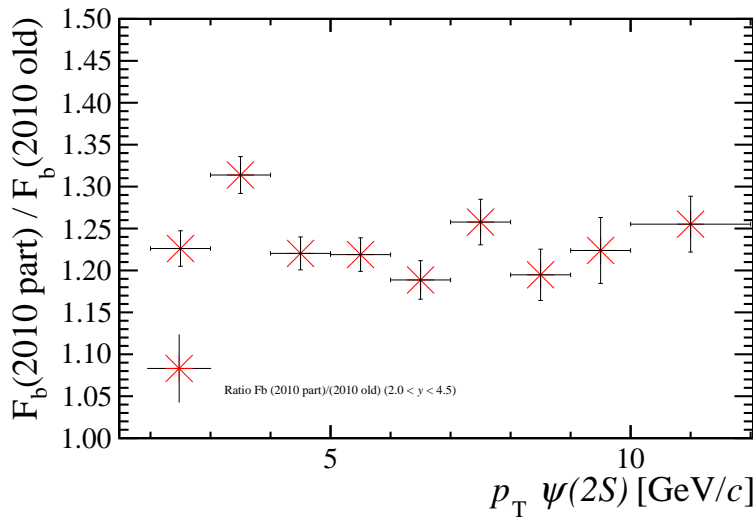


Figure G.1: Ratio $R_{F_b} = \frac{F_b \text{ (2010 part)}}{F_b \text{ (2010 old)}}$ for the common p_T range 2-10 GeV/ c .

1018 Next step is to evaluate additional systematic uncertainty due to corrections mentioned
 1019 above. Following new sources were taken into account:

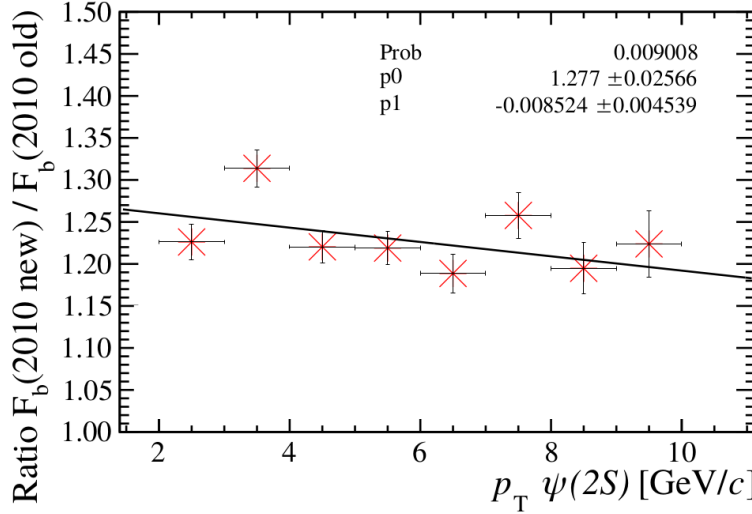


Figure G.2: Ratio $R_{F_b} = \frac{F_b \text{ (2010 part)}}{F_b \text{ (2010 old)}}$ for the common p_T range 2-10 GeV/ c , nominal fit using linear function.

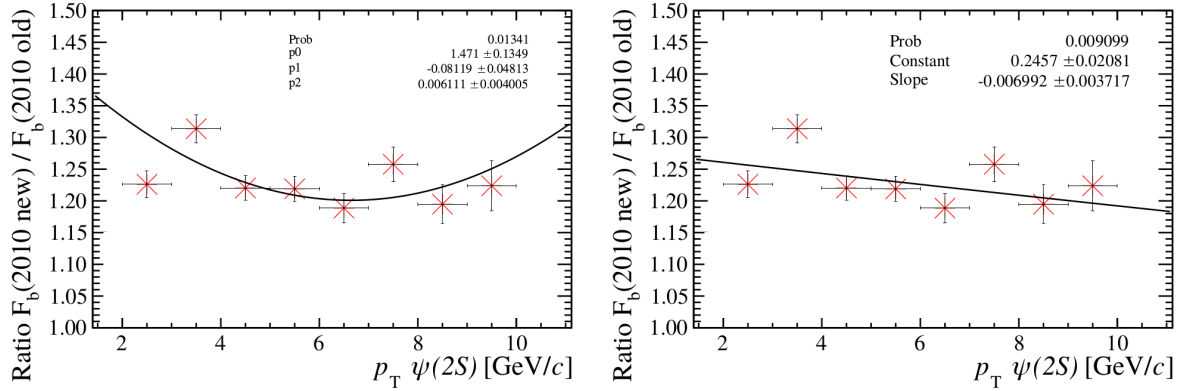


Figure G.3: Ratio $R_{F_b} = \frac{F_b \text{ (2010 part)}}{F_b \text{ (2010 old)}}$ for the common p_T range 2-10 GeV/ c , control fits using 2nd order polynomial fit (left) and exponential function (right).

- 1020 1. Difference between 2010 part results and results using parametrized F_p . For points
- 1021 outside common p_T range the same relative uncertainty as for the nearest point in
- 1022 p_T range was taken in account.
- 1023 2. Difference between results using two different parametrization of F_p (linear and 2nd
- 1024 order polynomial).

1025 New total systematic uncertainty is then combination of original systematic uncertainty
 1026 of 2010 old results corrected for incorrect uncertainty due to t_z fit (as described at Sec.
 1027 F) and new sources mentioned above.

1028 Final corrected results for $\psi(2S)$ -from- b production cross section are shown on Fig.

1029 G.5 together with 2011 results. Numerical results are then summarised at Table G.1.

1030 However, due to nature of previous analysis, where F_p been used for separation of
 1031 prompt and from- b production from the total inclusive cross-section, also the prompt
 1032 $\psi(2S)$ results must be corrected, although the effect is smaller than for $\psi(2S)$ -from- b .

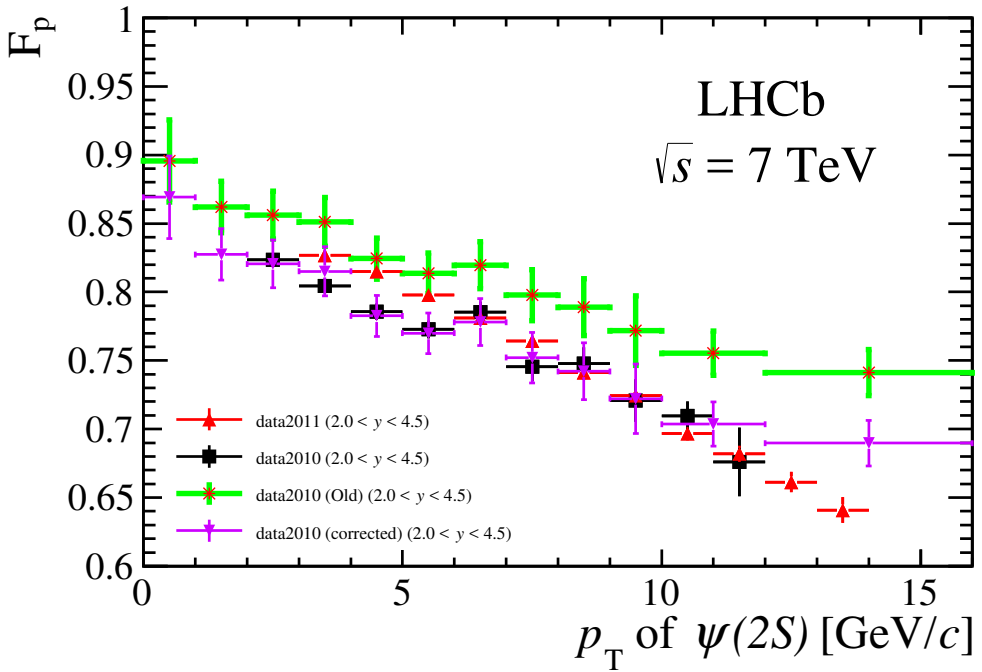


Figure G.4: Comparison of the fraction of prompt $\psi(2S)$ at 7 TeV for 2011, 2010 old, 2010 part and 2010 results corrected by linear fit. Only statistical uncertainties are considered in the 2010 new result and the 2011 result.

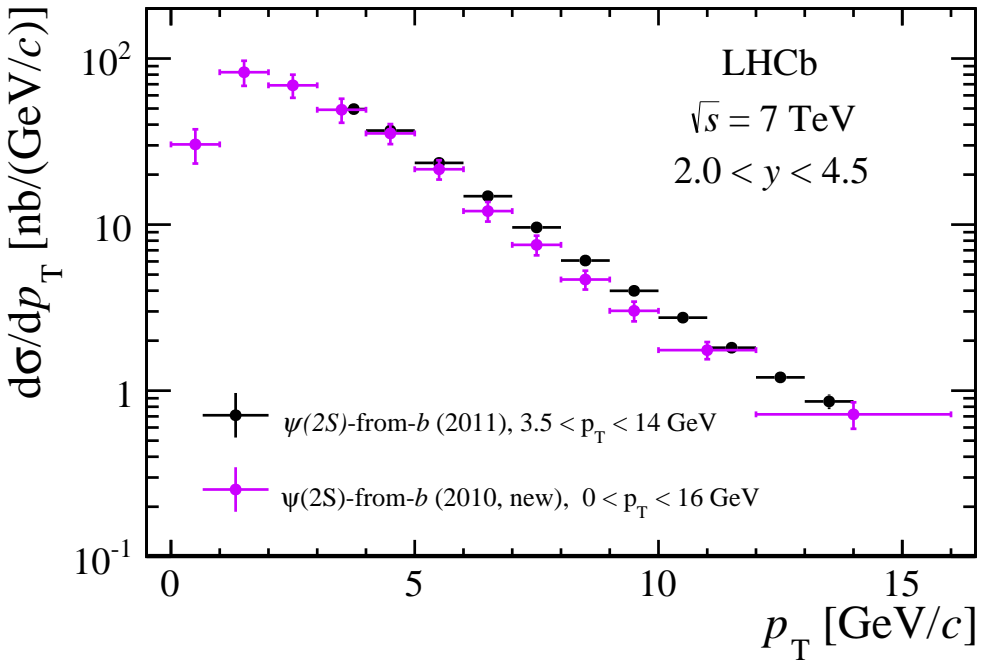


Figure G.5: Comparison of 2010 new differential cross-sections as functions of p_T with 2011 results for $\psi(2S)$ -from- b .

¹⁰³³ Corrected results are shown on Fig. G.7, together with 2010 old, 2011 results and NRQCD calculations. Numerical values are summarised at Table G.1.

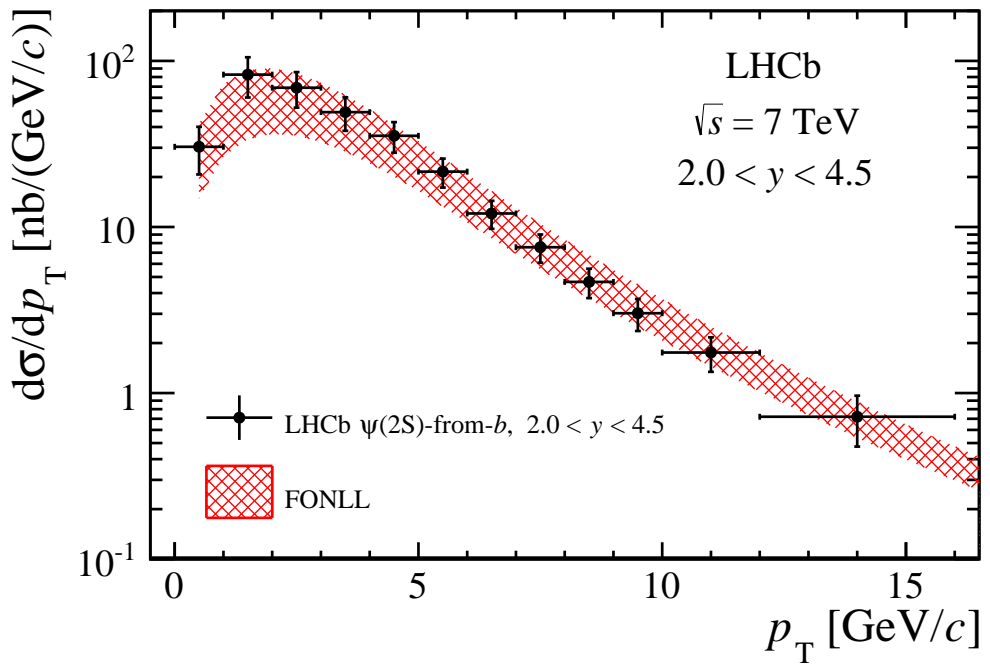


Figure G.6: Differential production cross-section of $\psi(2S)$ -from- b as a function of p_T in the range $2.0 < y < 4.5$. Results are compared with the FONLL calculations [36]. Error bars include statistical and systematic uncertainties added in quadrature.

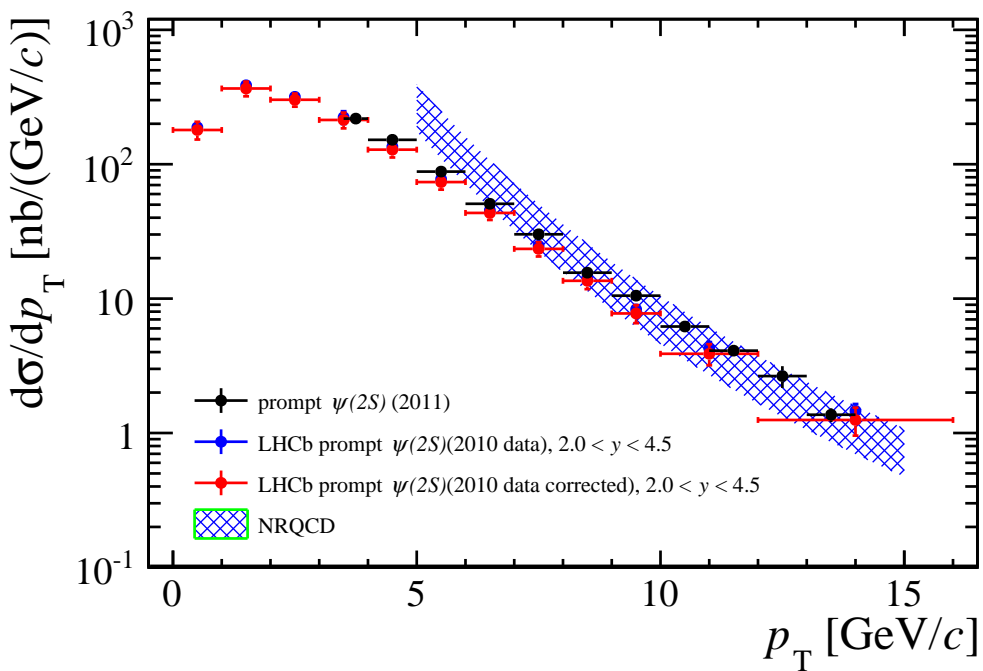


Figure G.7: Comparison of the 2010 new differential cross-sections as functions of p_T with 2010 old, 2011 results for $\psi(2S)$ -from- b . NRQCD prediction is also shown.

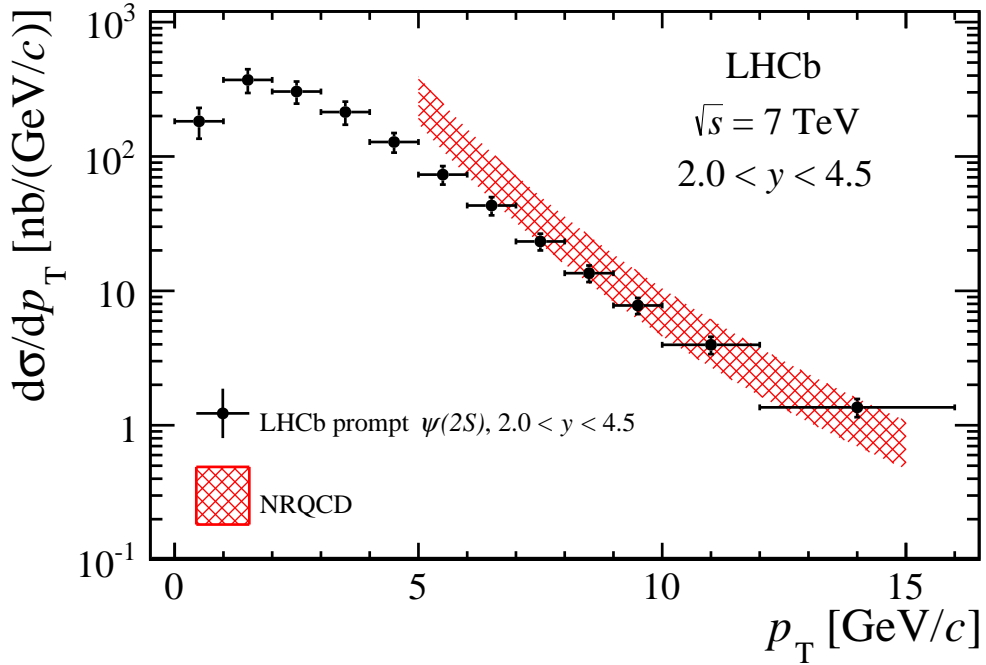


Figure G.8: Differential production cross-section of prompt $\psi(2S)$ as a function of p_T in the range $2.0 < y < 4.5$. Results are compared with the NRQCD calculations [55]. Error bars include statistical and systematic uncertainties added in quadrature.

Table G.1: Differential cross-sections $d\sigma/dp_T$ (in $\text{nb}/(\text{GeV}/c)$) of prompt $\psi(2S)$ and $\psi(2S)$ -from- b mesons at $\sqrt{s} = 7 \text{ TeV}$, integrated over y between 2.0 and 4.5. The first error is statistical and the second error is systematic. The third asymmetric uncertainty for the prompt $\psi(2S)$ mesons is due to the unknown polarisation.

p_T (GeV/c)	Prompt $\psi(2S)$	$\psi(2S)$ -from- b
0–1	$182.70 \pm 5.52 \pm 46.83^{+31}_{-65}$	$27.51 \pm 2.76 \pm 5.63$
1–2	$371.31 \pm 7.44 \pm 74.15^{+58}_{-114}$	$77.47 \pm 3.50 \pm 12.51$
2–3	$304.23 \pm 6.28 \pm 56.61^{+42}_{-84}$	$66.54 \pm 2.95 \pm 10.10$
3–4	$214.08 \pm 6.00 \pm 41.39^{+26}_{-51}$	$48.56 \pm 2.56 \pm 7.58$
4–5	$128.15 \pm 3.50 \pm 21.04^{+15}_{-29}$	$35.61 \pm 1.76 \pm 4.49$
5–6	$73.30 \pm 1.87 \pm 11.37^{+9}_{-17}$	$21.90 \pm 1.05 \pm 2.61$
6–7	$43.16 \pm 1.14 \pm 6.60^{+5}_{-9}$	$12.31 \pm 0.64 \pm 1.46$
7–8	$23.32 \pm 0.74 \pm 3.24^{+3}_{-6}$	$7.68 \pm 0.47 \pm 0.89$
8–9	$13.54 \pm 0.50 \pm 1.84^{+2}_{-3}$	$4.70 \pm 0.33 \pm 0.50$
9–10	$7.79 \pm 0.36 \pm 1.01^{+0.8}_{-1.6}$	$2.99 \pm 0.27 \pm 0.30$
10–12	$3.97 \pm 0.23 \pm 0.54^{+0.5}_{-0.7}$	$1.67 \pm 0.15 \pm 0.18$
12–16	$1.36 \pm 0.07 \pm 0.20^{+0.2}_{-0.3}$	$0.61 \pm 0.05 \pm 0.07$

1035 **References**

- 1036 [1] C. E. Carlson and R. Suaya, *Hadronic production of J/ψ mesons*, Phys. Rev. **D14**
1037 (1976) 3115.
- 1038 [2] A. Donnachie and P. V. Landshoff, *Production of lepton pairs, J/ψ and charm with*
1039 *hadron beams*, Nucl. Phys. **B112** (1976) 233.
- 1040 [3] S. D. Ellis, M. B. Einhorn, and C. Quigg, *Comment on hadronic production of psions*,
1041 Phys. Rev. Lett. **36** (1976) 1263.
- 1042 [4] H. Fritzsch, *Producing heavy quark flavors in hadronic collisions: A test of quantum*
1043 *chromodynamics*, Phys. Lett. **B67** (1977) 217.
- 1044 [5] M. Glück, J. F. Owens, and E. Reya, *Gluon contribution to hadronic J/ψ production*,
1045 Phys. Rev. **D17** (1978) 2324.
- 1046 [6] C.-H. Chang, *Hadronic production of J/ψ associated with a gluon*, Nucl. Phys. **B172**
1047 (1980) 425.
- 1048 [7] R. Baier and R. Rückl, *Hadronic production of J/ψ and Υ : Transverse momentum*
1049 *distributions*, Phys. Lett. **B102** (1981) 364.
- 1050 [8] G. T. Bodwin, E. Braaten, and G. P. Lepage, *Rigorous QCD analysis of inclusive*
1051 *annihilation and production of heavy quarkonium*, Phys. Rev. **D51** (1995) 1125,
1052 arXiv:hep-ph/9407339.
- 1053 [9] P. L. Cho and A. K. Leibovich, *Color octet quarkonia production*, Phys. Rev. **D53**
1054 (1996) 150, arXiv:hep-ph/9505329.
- 1055 [10] P. L. Cho and A. K. Leibovich, *Color octet quarkonia production. 2.*, Phys. Rev. **D53**
1056 (1996) 6203, arXiv:hep-ph/9511315.
- 1057 [11] CDF collaboration, F. Abe *et al.*, *J/ψ and $\psi(2S)$ production in $p\bar{p}$ collisions at*
1058 *$\sqrt{s} = 1.8 \text{ TeV}$* , Phys. Rev. Lett. **79** (1997) 572.
- 1059 [12] J. M. Campbell, F. Maltoni, and F. Tramontano, *QCD corrections to J/ψ*
1060 *and Υ production at hadron colliders*, Phys. Rev. Lett. **98** (2007) 252002,
1061 arXiv:hep-ph/0703113.
- 1062 [13] J. P. Lansberg, *J/ψ production at $\sqrt{s} = 1.96$ and 7 TeV : colour-singlet model*,
1063 *NNLO** and polarization, J. Phys. **G38** (2011) 124110, arXiv:1107.0292.
- 1064 [14] B. Gong and J.-X. Wang, *Next-to-leading-order QCD corrections to J/ψ polarization*
1065 *at Tevatron and Large-Hadron-Collider energies*, Phys. Rev. Lett. **100** (2008) 232001,
1066 arXiv:0802.3727.
- 1067 [15] M. Cacciari, M. Greco, M. L. Mangano, and A. Petrelli, *Charmonium production at*
1068 *the Tevatron*, Phys. Lett. **B356** (1995) 553, arXiv:hep-ph/9505379.
- 1069 [16] E. Braaten and S. Fleming, *Color octet fragmentation and the psi-prime surplus at*
1070 *the Tevatron*, Phys. Rev. Lett. **74** (1995) 3327, arXiv:hep-ph/9411365.

- [17] Y.-Q. Ma, K. Wang, and K.-T. Chao, *Complete next-to-leading order calculation of the J/ψ and ψ' production at hadron colliders*, Phys. Rev. **D84** (2011) 114001, arXiv:1012.1030.
- [18] B. Gong, X. Q. Li, and J.-X. Wang, *QCD corrections to J/ψ production via color-octet states at the Tevatron and LHC*, Phys. Lett. **B673** (2009) 197, arXiv:0805.4751.
- [19] M. Butenschoen and B. A. Kniehl, *Reconciling J/ψ production at HERA, RHIC, Tevatron, and LHC with NRQCD factorization at next-to-leading order*, Phys. Rev. Lett. **106** (2011) 022003, arXiv:1009.5662.
- [20] M. Beneke and I. Z. Rothstein, *ψ' polarization as a test of color octet quarkonium production*, Phys. Lett. **B372** (1996) 157, arXiv:hep-ph/9509375.
- [21] K.-T. Chao *et al.*, *J/ψ polarization at hadron colliders in nonrelativistic QCD*, Phys. Rev. Lett. **108** (2012) 242004, arXiv:1201.2675.
- [22] B. Gong, L.-P. Wan, J.-X. Wang, and H.-F. Zhang, *Polarization for prompt J/ψ and $\psi(2S)$ production at the Tevatron and LHC*, Phys. Rev. Lett. **110** (2013), no. 4 042002, arXiv:1205.6682.
- [23] M. Butenschoen and B. A. Kniehl, *J/ψ polarization at the Tevatron and the LHC: Nonrelativistic-QCD factorization at the crossroads*, Phys. Rev. Lett. **108** (2012) 172002, arXiv:1201.1872.
- [24] CDF collaboration, A. Abulencia *et al.*, *Polarizations of J/ψ and $\psi(2S)$ mesons produced in $p\bar{p}$ collisions at $\sqrt{s} = 1.96$ TeV*, Phys. Rev. Lett. **99** (2007) 132001, arXiv:0704.0638.
- [25] D0 collaboration, V. M. Abazov *et al.*, *Measurement of the polarization of the v_{1S} and v_{2S} states in $p\bar{p}$ collisions at $\sqrt{s} = 1.96$ -TeV*, Phys. Rev. Lett. **101** (2008) 182004, arXiv:0804.2799.
- [26] ALICE collaboration, B. Abelev *et al.*, *J/ψ polarization in pp collisions at $\sqrt{s} = 7$ TeV*, Phys. Rev. Lett. **108** (2012) 082001, arXiv:1111.1630.
- [27] CMS collaboration, S. Chatrchyan *et al.*, *Measurement of the prompt J/ψ and $\psi(2S)$ polarizations in pp collisions at $\sqrt{s} = 7$ TeV*, Phys. Lett. **B727** (2013) 381, arXiv:1307.6070.
- [28] CMS collaboration, S. Chatrchyan *et al.*, *Measurement of the $\Upsilon(1S)$, $\Upsilon(2S)$ and $\Upsilon(3S)$ polarizations in pp collisions at $\sqrt{s}=7$ TeV*, Phys. Rev. Lett. **110** (2013) 081802, arXiv:1209.2922.
- [29] LHCb, R. Aaij *et al.*, *Measurement of J/ψ polarization in pp collisions at $\sqrt{s} = 7$ TeV*, Eur. Phys. J. **C73** (2013), no. 11 2631, arXiv:1307.6379.
- [30] LHCb, R. Aaij *et al.*, *Measurement of $\psi(2S)$ polarisation in pp collisions at $\sqrt{s} = 7$ TeV*, Eur. Phys. J. **C74** (2014), no. 5 2872, arXiv:1403.1339.
- [31] Particle Data Group, M. Tanabashi *et al.*, *Review of particle physics*, Phys. Rev. **D98** (2018) 030001.

- 1109 [32] CDF collaboration, T. Aaltonen *et al.*, *Production of $\psi(2S)$ mesons in $p\bar{p}$ collisions*
 1110 *at 1.96 TeV*, Phys. Rev. **D80** (2009) 031103, [arXiv:0905.1982](#).
- 1111 [33] CMS collaboration, S. Chatrchyan *et al.*, *J/ψ and $\psi(2S)$ production in pp collisions*
 1112 *at $\sqrt{s} = 7$ TeV*, JHEP **02** (2012) 011, [arXiv:1111.1557](#).
- 1113 [34] LHCb collaboration, R. Aaij *et al.*, *Measurement of $\psi(2S)$ meson production in pp*
 1114 *collisions at $\sqrt{s} = 7$ TeV*, Eur. Phys. J. **C72** (2012) 2100, [arXiv:1204.1258](#).
- 1115 [35] LHCb collaboration, R. Aaij *et al.*, *Measurement of $\psi(2S)$ polarisation in pp collisions*
 1116 *at $\sqrt{s} = 7$ TeV*, Eur. Phys. J. **C74** (2014) 2872, [arXiv:1403.1339](#).
- 1117 [36] M. Cacciari, M. Greco, and P. Nason, *The $P(T)$ spectrum in heavy flavor hadropro-*
 1118 *duction*, JHEP **9805** (1998) 007, [arXiv:hep-ph/9803400](#).
- 1119 [37] T. Sjöstrand, S. Mrenna, and P. Skands, *PYTHIA 6.4 physics and manual*, JHEP **05**
 1120 (2006) 026, [arXiv:hep-ph/0603175](#).
- 1121 [38] I. Belyaev *et al.*, *Handling of the generation of primary events in Gauss, the LHCb*
 1122 *simulation framework*, J. Phys. Conf. Ser. **331** (2011) 032047.
- 1123 [39] D. J. Lange, *The EvtGen particle decay simulation package*, Nucl. Instrum. Meth.
 1124 **A462** (2001) 152.
- 1125 [40] P. Golonka and Z. Was, *PHOTOS Monte Carlo: A precision tool for QED corrections*
 1126 *in Z and W decays*, Eur. Phys. J. **C45** (2006) 97, [arXiv:hep-ph/0506026](#).
- 1127 [41] Geant4 collaboration, J. Allison *et al.*, *Geant4 developments and applications*, IEEE
 1128 Trans. Nucl. Sci. **53** (2006) 270.
- 1129 [42] Geant4 collaboration, S. Agostinelli *et al.*, *Geant4: A simulation toolkit*, Nucl. Instrum.
 1130 Meth. **A506** (2003) 250.
- 1131 [43] M. Clemencic *et al.*, *The LHCb simulation application, Gauss: Design, evolution and*
 1132 *experience*, J. Phys. Conf. Ser. **331** (2011) 032023.
- 1133 [44] M. Bargiotti and V. Vagnoni, *Heavy quarkonia sector in PYTHIA 6.324: Tuning,*
 1134 *validation and perspectives at LHC(b)*, CERN-LHCB-2007-042.
- 1135 [45] S. Kullback and R. A. Leibler, *On information and sufficiency*, Ann. Math. Statist. **22**
 1136 (1951) 79; S. Kullback, *Letter to editor: The Kullback-Leibler distance*, The American
 1137 Statistician **41** (1987) 340; the use of the Kullback-Leibler distance is described in M.
 1138 Needham, *Clone track identification using the Kullback-Leibler distance*, LHCb-2008-
 1139 002.
- 1140 [46] Particle Data Group, K. A. Olive *et al.*, *Review of particle physics*, Chin. Phys. **C38**
 1141 (2014) 090001, and 2015 update.
- 1142 [47] Particle Data Group, C. Patrignani *et al.*, *Review of particle physics*, Chin. Phys. **C40**
 1143 (2016) 100001.

- 1144 [48] T. Skwarnicki, *A study of the radiative cascade transitions between the Upsilon-prime*
 1145 *and Upsilon resonances*, PhD thesis, Institute of Nuclear Physics, Krakow, 1986,
 1146 DESY-F31-86-02.
- 1147 [49] LHCb collaboration, R. Aaij *et al.*, *Measurement of forward J/ψ production cross-*
 1148 *sections in pp collisions at $\sqrt{s} = 13 \text{ TeV}$* , JHEP **10** (2015) 172, Erratum *ibid.* **05**
 1149 (2017) 063, [arXiv:1509.00771](https://arxiv.org/abs/1509.00771).
- 1150 [50] J. Lefrancous, *Crystal ball fits*, link.
- 1151 [51] LHCb collaboration, R. Aaij *et al.*, *Measurement of the track reconstruction efficiency*
 1152 *at LHCb*, JINST **10** (2015) P02007, [arXiv:1408.1251](https://arxiv.org/abs/1408.1251).
- 1153 [52] V. Belyav *et al.*, *Production of J/ψ and $\Upsilon(nS)$ mesons in pp collisions at $\sqrt{s} = 8$*
 1154 *TeV*, LHCb-ANA-2012-058.
- 1155 [53] M. Pivk and F. R. Le Diberder, *sPlot: A statistical tool to unfold data distributions*,
 1156 Nucl. Instrum. Meth. **A555** (2005) 356, [arXiv:physics/0402083](https://arxiv.org/abs/physics/0402083).
- 1157 [54] *Tracking correction table*, <https://twiki.cern.ch/twiki/bin/view/LHCb/LHCbTrackingEfficiencies>.
- 1158 [55] H.-S. Shao *et al.*, *Yields and polarizations of prompt J/ψ and $\psi(2S)$ production in*
 1159 *hadronic collisions*, JHEP **05** (2015) 103, [arXiv:1411.3300](https://arxiv.org/abs/1411.3300).
- 1160 [56] M. Cacciari, M. L. Mangano, and P. Nason, *Gluon PDF constraints from the ratio of*
 1161 *forward heavy-quark production at the LHC at $\sqrt{S} = 7$ and 13 TeV* , Eur. Phys. J.
 1162 **C75** (2015), no. 12 610, [arXiv:1507.06197](https://arxiv.org/abs/1507.06197).
- 1163 [57] T. Sjöstrand, S. Mrenna, and P. Skands, *A brief introduction to PYTHIA 8.1*, Comput.
 1164 Phys. Commun. **178** (2008) 852, [arXiv:0710.3820](https://arxiv.org/abs/0710.3820).
- 1165 [58] G. Carboni, S. De Capua, and G. Sabatino, *Measurement of the $\psi(2S)$ production*
 1166 *cross-section in LHCb*, , LHCb-PAPER-2011-045.
- 1167 [59] W. Qian, *J/ψ production study at the LHCb experiment*, PhD thesis, Tsinghua
 1168 University, Beijing, 2010, CERN-THESIS-2010-307.